

**U.S. Department of Energy
Office of FreedomCAR and Vehicle Technologies
1000 Independence Avenue S.W.
Washington, DC 20585-0121**

FY 2004

Progress Report for High Strength Weight Reduction Materials

Energy Efficiency and Renewable Energy
Office of FreedomCAR and Vehicle Technologies
Advanced Materials Technologies

Edward Wall	Program Manager, OFCVT
Rogelio Sullivan	Advanced Materials Technologies Team Leader
Sidney Diamond	Technology Development Area Specialist

April 2005

CONTENTS

1	INTRODUCTION	1
2	MATERIALS DEVELOPMENT	7
A	Integrated Approach for Development of Energy-Efficient Steel Components for Heavy Vehicle and Transportation Applications.....	7
3	MATERIALS PROCESSING TECHNOLOGIES	19
A	Oxidative Stabilization of PAN Fiber Precursor	19
B	Wrought Magnesium Alloy/Process Development	25
C	Equal Channel Angular Extrusion of Soft Ferromagnetic Materials.....	33
D	Equal Channel Angular Extrusion Processing of Alloys for Improved Mechanical Properties.....	39
E	Development of an Advanced Squeeze Casting Process for the Production of High-Integrity Truck Components	49
F	Thermomechanical Processing of Ti and Ti-6Al-4V Sheet and Plate.....	53
4	ENABLING TECHNOLOGIES.....	61
A	Improved Friction Tests for Engine Materials.....	61
B	Laser Glazing of Railroad Rails to Reduce Friction.....	66
C	Laser Texturing of Materials	71
D	Joining of Advanced Materials by Plastic Deformation.....	77
E	Friction Stir Joining and Processing of Advanced Materials Including Metal Matrix Composites	85
F	Friction-Stir-Joined Aluminum Sheet Materials for Heavy Vehicle Cab Structures	95
G	Friction Stir Welding and Processing of Advanced Materials	101
H	Basic Studies of Ultrasonic Welding for Advanced Transportation Systems	109
I	Attachment Techniques for Heavy Truck Composite Chassis Members	119
J	Rapid, Low-Cost Tooling Development	129
K	Inventory of Heavy-duty Truck Lightweighting Candidates.....	35
L	Truck-to-Auto Technology Transfer for Lightweight Materials	141
5	LIGHTWEIGHT VEHICLE STRUCTURES	143
A	Lightweight Stainless Steel Bus Frame—Phase III.....	143
B	Stainless Steel Bus Structure—Manufacturing Cost Analysis	149
C	Side Impact Analysis of a Lightweight Stainless Steel Bus Structure	153
D	New-Generation Frame for Pickup/Sport Utility Vehicle Application	159
E	Lightweight Trailer—Liburndas Project	163
6	APPLICATION OF INNOVATIVE MATERIALS.....	169
A	Advanced Materials for Friction Brakes	169
B	Advanced Composite Structural Cab Components	175
C	Advanced Composite Structural Chassis Components.....	181
D	Carbon Fiber SMC for Class 8 Vehicle Hoods	185
E	Advanced Composite Support Structures.....	189
F	Hybrid Composite Materials for Weight-Critical Structures.....	199
G	Application of Carbon Fiber for Large Structural Components.....	203

1. INTRODUCTION

As a major component of the U.S. Department of Energy's (DOE's) Office of FreedomCAR and Vehicle Technologies (OFCVT), the High-Strength Weight Reduction (HSWR) Materials Technology Development Area seeks to reduce parasitic energy losses due to the weight of heavy vehicles without reducing vehicle functionality, durability, reliability, or safety and to do so cost-effectively. The development area is focused on the development of materials and materials processing technologies that can contribute to weight reduction. In addition, it is recognized that improved materials may enable the implementation of other technologies that can further improve the fuel efficiency of the vehicles. Through many of its technology development programs, DOE supports the government/industry 21st Century Truck Partnership.

The specific goals of the HSWR Materials Technology Development Area are

- By 2010, reduce the weight of an unloaded tractor-trailer combination from the current 23,000 pounds to 18,000 pounds, a 22% reduction in weight.
- By 2010, develop and validate advanced material technologies needed to meet OFCVT goals.
- Enable significant reductions in the weight of other classes of heavy vehicles (10–33% reduction in vehicle weight, depending on performance requirements and duty cycles).
- Develop materials that exhibit performance, durability, reliability, and safety characteristics comparable to those of conventional vehicle materials and that are cost-competitive on a life-cycle basis.
- Be consistent with the materials regulation requirements to maintain environmental responsibility.

To reach the stated goals, the HSWR Materials Technology Development Area has been developing a broad spectrum of advanced materials technologies that can be applied to a wide array of body, chassis, and suspension components. The research required to develop these technologies is too high-risk to be pursued independently by the heavy vehicle industry because of substantial return-on-investment uncertainties. Research is focused on overcoming barriers to the widespread introduction of lightweight materials in the heavy vehicle industry. Major barriers exist in the following areas: cost; design and simulation technologies; manufacturability; prototyping and tooling; joining and assembly; and maintenance, repair, durability, and recycling. Priority materials include advanced high-strength steels, aluminum, magnesium, titanium, and composites such as metal matrix materials and glass- and carbon-fiber-reinforced thermosets and thermoplastics.

Research and development (R&D) activities are being conducted through a variety of contractual mechanisms, including cooperative research and development agreements (CRADAs), university grants, R&D subcontracts, and directed research. Research partners include heavy vehicle manufacturers (including member companies of the 21st Century Truck Partnership), first-tier and materials suppliers, national laboratories, and other non-profit technology organizations. Laboratories include Argonne National Laboratory (ANL), Idaho National Engineering and Environmental Laboratory (INEEL), Los Alamos National Laboratory (LANL), Oak Ridge National Laboratory (ORNL), and Pacific Northwest National Laboratory (PNNL). Research is coordinated with various organizations—both government and private—as shown in the following table.

Research Coordination

Technology area	Organization
Production and fabrication of aluminum	The Aluminum Association, DOE-Industrial Technologies Program (ITP), Natural Resources of Canada (NRCAN), Automotive Lightweighting Materials (ALM) Technology Development Area
Production and fabrication of magnesium	International Magnesium Association, NRCAN, ALM Technology Development Area
Fabrication of steel and cast iron	American Iron and Steel Institute, the Auto/Steel Partnership, ALM Technology Development Area
Fundamental materials research	DOE Office of Energy Research, National Science Foundation
High-volume composite processing	Department of Commerce—National Institute of Standards and Technology's Advanced Technology Program, ALM Technology Development Area
Materials research for defense applications	Department of Defense
Materials research for space applications	National Aeronautics and Space Administration
Crashworthiness	Department of Transportation, ALM Technology Development Area
International vehicle material R&D	International Energy Association
Production and fabrication of titanium	The International Titanium Association, ALM Technology Development Area
Production and fabrication of composites	American Plastics Council

FY 2004 Accomplishments

Carbon-fiber-reinforced polymer composites have a great potential to reduce the weight of heavy vehicles. However, a number of technical and economic barriers prevent their widespread implementation. The National Composites Center is leading a team focused on enhancing the rapid implementation of lightweight composite materials in Class 7/Class 8 vehicles via the development of advanced composite support structures, specifically lateral braces. Mass reductions are targeted for 50%.

The effort is focused in four areas: modeling, prototyping, molding, and materials characterization. Integration of progressive failure analysis using the Genoa software has successfully predicted fatigue behavior and elastic constants of test composite materials. In addition, the Genesis software was used to successfully develop an optimized design based on weight savings, cost, and manufacturing. A prototype lateral brace was successfully designed and fabricated by resin transfer molding and aluminum tooling in less than 4 weeks.

A collaborative effort between ORNL and PNNL is focused on overcoming the technical issues associated with joining composite materials in heavy vehicles. The project supports the industry-led effort to develop advanced composite support structures, including chassis lateral braces and primary beams for Class 7 and 8 vehicles (Figure 1). The initial focus of research is development and validation of one or more joint designs for a composite structural member attached to a metal member that together satisfy the truck chassis structural requirements both economically and reliably and with requisite durability.



Figure 1. Optimized geometry for lateral brace smoothed and drafted for manufacturability.

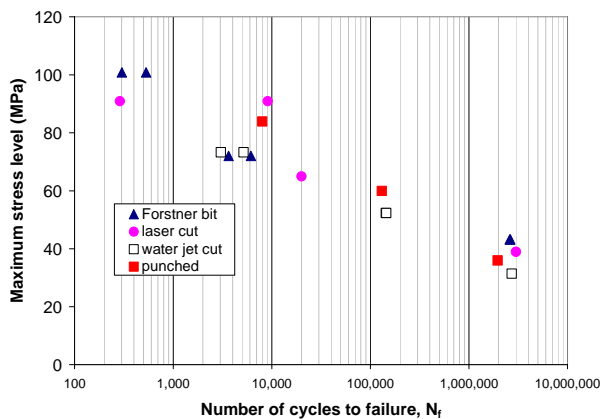


Figure 2. Fatigue testing results for specimens with holes fabricated with different methods.

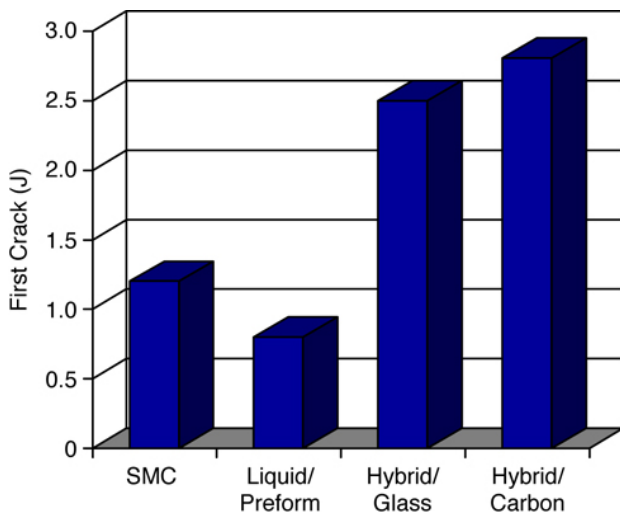


Figure 3. Resin system allowing excellent impact energy.

The multi-pronged approach includes evaluating a variety of hole fabrication techniques and their effects on subsequent performance (Figure 2); developing methods for detection of flaws and damage development during testing; static and fatigue testing under various environmental conditions; analyzing the effects of pre-load and bolt torque; and developing models for predicting the performance of joints. The results will be used to develop the first prototype composite component and joint for durability track testing in the latter part of 2005.

Selective reinforcement of large truck cab components with higher-stiffness carbon fibers has the potential to reduce both cost and weight simultaneously while maintaining structural functionality. PNNL is leading a collaborative project to develop robust methods of forming glass and carbon fiber materials together, while meeting Class A surface finish requirements and meeting thermal and structural performance requirements. A series of factors associated with optimizing details of the process

technology are being addressed, and the CRADA partner is developing an approach to molding full-scale parts that will ultimately be tested in over-the-road trials. To date, the team has been successful in molding structural carbon fiber Class A components with a cost-effective hybrid fiber system that has demonstrated significant structural performance in fatigue and impact tests (Figure 3). In addition, it has achieved molding of very thin section panels, which resulted in attractive weight savings.

Magnesium alloys that have high specific strength (strength per unit of mass) are attractive materials for weight reduction. Presently, most magnesium use is limited to die-cast parts. Wrought magnesium alloys hold great promise for use in such components as hoods and doors. However, the need for a large number of processing steps and associated lengthy annealing times contributes to the high cost of sheet materials and presents one of the greatest barriers to the application of magnesium in these components. Researchers at ORNL, in collaboration with industry and universities, are applying infrared processing technology to reduce this barrier. A successful demonstration run made at a commercial rolling mill equipped with a bank of infrared lamps (Figure 4) produced materials with properties identical to those of materials produced with conventional techniques, but with much shorter annealing times and the potential for considerable cost savings. Future efforts will attempt to incorporate this technology with continuous twin roll casting to further reduce costs.



Figure 4. Infrared lamp rolling mill at Manufacturing Sciences, Inc., and close-up of magnesium alloy sheet exiting the roll gap.

As a result of a competitive solicitation, Heil Trailer International is working on a project to reduce the weight of an aluminum semi-trailer tanker by 20% through innovative design and the assimilation of composite materials into select components. Excellent progress has been made on the vessel design and finite element analysis (Figure 5). Analysis, testing, and manufacturing studies have been completed successfully for the vessel and for the run gear/ fifth wheel/bumper/underride. It is anticipated that the first full-scale prototype will be completed in early 2005.

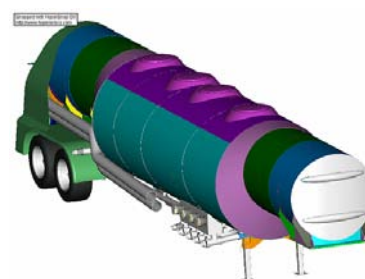


Figure 5. New-concept petroleum trailer

Future Direction

The HSWR Materials Technology Development Area, for the most part, has addressed the near- and intermediate-term energy efficiency and safety technical needs of the heavy-duty transport sector (primarily class 7 and 8 trucks) in conjunction with the original equipment manufacturers and their suppliers. Metals and their alloys still dominate the material usage in these arenas, but over the longer term, composites of many types are expected to receive wider and significant applications. The makeup of the research portfolio of this technology development area reflects the current industry needs and these future expectations.

As noted last year, several materials thrust areas have been identified, and exploratory efforts have been initiated within them. They are

1. Advanced joining technologies
2. Titanium use in heavy-duty structural and component applications
3. Advanced surface modification technologies to tailor friction and wear characteristics and other surface-sensitive properties of materials.

In area 1, advanced joining, DOE seeks to develop effective joining technologies that can enable the increased use of attractive advanced materials such as metal matrix composites without the severe alteration of microstructure and degradation of properties that are attendant upon conventional joining methods. The latter generally involve heating the materials adjacent to the joint into the liquid state. This technique results in significant phase redistribution, among other modifications that are deleterious to the properties of the resulting joint. Several promising joining techniques are in the early phases of evaluation to determine if they

can achieve the desired technical results. Economic assessment will follow to determine their cost competitiveness.

In area 2, vigorous efforts are under way around the world that may result in the delivery of titanium feedstock at considerably lower costs than have prevailed up to this time. Anticipating this achievement, DOE has initiated activities to identify and develop applications of titanium and titanium alloys in various structural, engine, and transmission components for heavy vehicles because of their attractive lightweighting, high-strength, and high-temperature characteristics. In some of these applications, the significantly lower thermal conductivity of titanium may be an additional advantage for certain components.

In area 3, advanced surface modification, a number of innovative technologies have been identified that can significantly reduce the friction coefficients and wear rates of many engine and transmission components of heavy vehicles. These can contribute to appreciable increases in the energy efficiency of the vehicles. In addition, optimizing lubricant-surface interaction through formulation modification may enable a total increase in energy efficiency of up to 5% in addition to improvements that may be gained in the combustion process. These technologies have been ranked in terms of their projected relative salubrious effects and are currently being systematically characterized and tested. Data from this work are being prepared for presentation via oral presentations at professional society meetings and in published papers.

It is anticipated that collaborative efforts with the Automotive Lightweighting Materials Technology Development Area will be continued so that energy-efficient technologies may be developed expeditiously without duplication and introduced into both the heavy-duty and light-duty sectors to maximize the impact on reducing fuel consumption. The conventional near-term and intermediate-term R&D activities performed in conjunction with DOE's industrial partners will, however, continue to make up the bulk of the project portfolio, with a modest number of projects of longer-term and more speculative nature.

It is interesting and probably significant to note that just when an experienced, knowledgeable practitioner in the field of technology conception and development feels that he has seen all the major advances that he might reasonably expect to encounter, his superbly motivated technical colleagues, young and old alike, discover and share new and remarkable technologies that promise greater efficiency gains, improved properties, and even lower costs than the conventional materials of current use. This wonderfully innovative and exhilarating process is more than influential enough to keep old workhorses in harness, vying with and eventually winning over a harried and unreceptive user public and a generally otherwise directed political bureaucracy.



Sidney Diamond
Technology Development Area Specialist
Office of FreedomCAR and Vehicle
Technologies
Energy Efficiency and Renewable Energy

2. MATERIALS DEVELOPMENT

A. Integrated Approach for Development of Energy-Efficient Steel Components for Heavy Vehicle and Transportation Applications

Co-Principal Investigator: Leo Chuzhoy

Caterpillar, Inc.

P.O. Box 1875, Peoria, IL 61656-1875

(309) 578-6621; fax: (309) 578-2953; e-mail: chuzhoy_leo@cat.com

Co-Principal Investigator: Gerard Ludtka

Oak Ridge National Laboratory

P.O. Box 2008, Oak Ridge, TN 37831-6064

(865) 574-5098; fax: (865) 574-3940; e-mail: ludtkagm1@ornl.gov

Co-Principal Investigator: Clyde Briant

Brown University

Box D, Brown University, Providence, RI 02912-D

(401) 863-1422; fax: 401-863-1157; e-mail : clyde_briant@brown.edu

Technology Development Area Specialist: Sidney Diamond

(202) 586-8032; fax: (202) 586-1600; e-mail: sid.diamond@ee.doe.gov

Field Technical Manager: Philip S. Sklad

(865) 574-5069; fax: (865) 576-4963; e-mail: skladps@ornl.gov

Contractor: Caterpillar Inc.

Contract No.: DE-AC05-00OR22726

Objective

- Develop methods and tools to achieve energy-efficient and environmentally benign steel components.
- Develop microstructure-level (often called mesoscale) simulation tools to capture the formation and influence of non-homogeneous (real-life) microstructures in steel processing. The tools will be used to understand and predict microstructure evolution during processing and ultimately to predict the resultant component performance.
- Use the information from the simulations to design steel microstructures and develop process roadmaps.
- Demonstrate the developed techniques on a pilot project at Caterpillar involving a defined structural component, namely a track roller shaft, that represents a steel component with high production volume that can potentially benefit from microstructure-level improvements.

Approach

- Develop microstructure-level models to accurately predict the evolution and behavior of steel microstructures during component processing and performance.
- Characterize thermomechanical properties of microstructural constituents as a function of temperature and composition for exact chemistries.

- Develop the tools to assess required environmental resources and integrate them into the modeling simulation endeavor.

Accomplishments

- Acquired 1045 and 15V45 steel material.
- Distributed the two alloys to be investigated to the project team members so that machining of the test specimens required for the tasks of microstructural characterization, machining experiments, and determination of strain-rate-dependent mechanical properties could be initiated during the first quarter of FY 2004.
- Acquired two track roller shafts and distributed segments of these to the project team members.
- Completed machining testing (round 1).
- Completed mechanical testing for 1045.
- Assessed resources for machining of track roller shafts.
- Assessed resources for processing of track roller shafts.
- Characterized ferrite and pearlite for the 1045 alloy.
- Received three ultra-pure materials from CRIM.
- Initiated simulation of heat treatment and machining operations.
- Compared machining model predictions for different microstructures and machining parameters with experimental results from precision-controlled machining experiments.
- Demonstrated that the machining model qualitatively predicts the adiabatic shear band formation and chip morphology observed in the machining chips obtained from the machining experiments.

Future Direction

- Develop and demonstrate a microstructure-level model incorporating phase transformation kinetics, but without chemical and microstructural inhomogeneities (to be implemented in year 3), for the heat treatment processes used by Caterpillar for the SAE 1045 and SAE 15V45 steel alloys (9/2005).
- For both types of steel, produce in the laboratory the microstructures that evolve during these heat treatment processes and thoroughly characterize them to provide quantitative input data for the heat treatment simulation models.
- Perform all mechanical tests on these microstructures that are required for inputs and validation of the heat treatment models.
- Characterize the influence of mill thermomechanical processing (TMP) variables on deformation and recrystallization behavior for incorporation into coupled polycrystalline and recrystallization models developed during years 2 and 3 of this project.
- Initiate development of coupled polycrystalline plasticity and recrystallization models to simulate mill TMP variable effects on austenite grain evolution behavior and characteristics.

Introduction

Product cost and performance are two major pressures influencing the acceptance of energy-saving technologies by manufacturers, suppliers, and users in the heavy vehicle and transportation industries. Energy cost has become a significant portion

of total product cost for steel applications. Major reductions in energy use are potentially achievable for the transportation and heavy vehicle industries through development and optimization of cost-effective fabrication processes and enhanced product performance. The key enabling technologies to achieve these benefits are improved materials and

realistic, microstructure-level simulations to predict manufacturability and life-cycle performance. Over the past two decades, steel mills and forge shops have successfully implemented numerous energy-efficient processes. The next logical step is to focus on the development of steel microstructures that are produced in such a way that they are energy efficient and environmentally benign over the entire manufacturing cycle.

Structural materials used in critical steel components of machines have evolved to the point where further improvements in performance can be achieved only through a fundamental understanding of the mechanisms driving material behavior during processing and service. Microstructural elements such as grain size, inclusion and precipitate distributions, and chemistry control the performance of engineering materials. Variation in these microstructural elements leads to variation in such critical properties as fatigue life, toughness, and wear resistance. Therefore, understanding and developing the capability to control the formation of steel microstructures, and predicting their functional and environmental performance, are critical to moving the industry closer to its energy-efficiency, resource-efficiency, and pollution-prevention goals. The full realization of these benefits, however, requires a design tool that optimizes the micro-structure with respect to the mechanical and environmental performance throughout the life cycle of a particular steel component.

To apply an integrated approach to development of energy-efficient steel components, the development of three major areas of research needs to be completed:

- Micro-structure-level models to accurately predict evolution and behavior of steel microstructures during component processing and performance
- thermomechanical properties of microstructural constituents as a function of temperature and composition for exact chemistries
- tools to assess required environmental resources

This project addresses activities required for the first of these three areas. The second and third tasks are either supported by current funding through the National Science Foundation (NSF) or are expected to be funded through the DOE Initiative for Proliferation Prevention. Through these integrated efforts, a design tool will be developed that optimizes the

microstructure, manufacturability, and performance of components with respect to the mechanical and environmental performance required throughout the components' life cycles. The overall benefit of this research will be the development and demonstration of a design methodology that will enable the domestic transportation and heavy vehicle industries to compete effectively in future worldwide markets through improved product performance and energy savings. Furthermore, the proposed design tool can be extended to other materials—i.e., cast iron, aluminum, titanium, magnesium, nickel-based alloys, ceramics, and composites—thus impacting virtually all industries.

In addition to the significant energy and cost savings benefits that the transportation and steel industries will realize from microstructure-level modeling, virtually all industries will be impacted. Examples include aerospace (engines, transmissions, structural), marine (engines and drives), agricultural and construction equipment, oil and chemical processing (pumps and gear boxes), military vehicles, mining machinery, appliances (compressors, motors, gear boxes, shafts), power tools, and automotive aftermarket.

Project Deliverables

The deliverables for the project will be

- Microstructure-level methods for simulating the manufacturing cycle of steel products, coupled with material performance computations (Tasks 1, 2, and 3)
- A specific chemical composition and processing map for a 1500-series steel and a microalloyed steel suitable for the application under consideration (Task 4)
- A determination of the energy and environmental resources required to produce the selected steel component using at least two steels and processing schemes (Task 4)

Project tasks will focus on three critical areas in the development of these models: heat treatment processing, machining, and materials performance in specific applications. These three processes have been chosen because they are critical steps toward the goal of developing a specific steel for a particular application, with a heavy reliance on modeling and with energy requirements optimized as an integral part of the development process. Casting and

forming processing have been modeled under other programs, and Caterpillar has shown successful application and commercialization of these models. These existing models will be used, along with the heat treatment, machining, and specific applications models described in this report, to complete a suite of models for the manufacture of microalloyed steels.

To accomplish the project objectives, a multi-disciplinary team consisting of a national laboratory, a university, and a steel end-user has been assembled. The team will be supported by an international research institute for material characterization and by experts in environmental impact assessment.

Technical Tasks

Task 1: Heat Treating Process

This task will quantify the influence of chemical and microstructural inhomogeneities in the austenite phase on the final heat-treatment response. The microstructure-level models incorporating phase transformation kinetics, polycrystalline plasticity, and recrystallization dynamics will be developed collaboratively by the Oak Ridge National Laboratory (ORNL), Brown University, and Caterpillar. Validation will be accomplished using the unique experimental capabilities and expertise at ORNL for conducting kinetic and metallurgical characterization and using Caterpillar's capability to produce heat-treated specimens in precisely specified and controlled conditions. The modeling effort will draw on the programs at Brown and Caterpillar that have developed microstructural modeling capabilities.

The coupled mesoscale deformation and recrystallization models developed cooperatively by the three team members will be implemented to study the influence of mill TMP variables and mesoscale composition variation on the grain size, grain-size distribution, and austenite grain-boundary character prior to the decomposition of austenite. The coupled deformation and recrystallization models will be used to predict the evolution of austenite grain structure and grain-boundary character distribution during the TMP steps involved during secondary fabrication. The output of these simulations will feed directly into an austenite decomposition code that predicts phase transformation during the heat-treatment operation.

Task 2: Machining Processing

A microstructure-level model will be applied to machining simulation of steels to determine their machinability and material state after TMP. The model will consist of four main elements integrated into the finite element structure: microstructure simulation, material modeling, material characterization, and material flow and fracture. The microstructure simulation module will assemble individual constituents into a composite material based on microstructural composition, grain size, and grain-size distribution. This information, along with residual stress predictions for individual grains, will be obtained from Task 1.

The material modeling module will account for the response of each constituent to high strains, strain rates, temperature, damage, and effects of loading paths associated with machining. The material characterization module will provide the material modeling module with parameters to define strain rate and temperature-dependent behavior of individual phases. The material flow and fracture module will periodically examine each grain for damage, locate deformed grain boundaries, and generate new boundaries. This module will compute stress, strain, temperature, and damage in each phase based on initial microstructure, material state, tool geometry, and process parameters.

A concerted effort will be made to review and leverage all current developments in this materials and process-simulation field that is the scope of this project. Microstructure, residual stress, and cutting force measurements obtained by various research groups (e.g., ongoing research at Purdue University by S. Chandrasekar) will be used for model development and validation.

Task 2 and Task 1 will be augmented by a parallel project among Caterpillar, Brown, and the Central Research Institute for Materials in St. Petersburg, Russia, in which a detailed examination is being performed of the relationship between composition, microstructure, and mechanical properties of steels of highly controlled purity and microstructure.

Task 3: Material Performance and Application

After the materials have been processed and machined, the next concern is to predict their subsequent performance, that is, their strength and resistance to fracture. Thus the models for material performance need to be developed and validated. These models will explicitly include such microstructural elements as inclusions, precipitates, and grain boundaries and will be based on several finite element methods developed at Brown University.

The first step will be to develop predictive models of damage initiation by either cracking or debonding of second-phase inclusions and precipitates. This modeling will be performed using a cohesive surface framework to model the interface between the inclusion (or precipitate) and the matrix and to model the initiation and growth of cracks within the second phase. Parameter studies will be undertaken to identify measurable and controllable features of the microstructure that are key for damage initiation. The results for damage initiation will be used in a modified Gurson model¹ to predict material performance. Of initial interest will be the prediction of performance in a suite of test specimens that give rise to different plastic strain-stress triaxiality histories so that the predictive capabilities of this modeling can be compared with experimental observations. Three-dimensional calculations of more complex geometries will also be performed to demonstrate the capability of predicting failure in component-like geometries.

At the same time, experiments will be performed using specimens that have been carefully designed so that their mechanical response can be fully modeled. These specimens will be pulled in tension to various loads and then sectioned so that the microstructure can be observed. Particular attention will be given to identifying the second-phase particles that are present in the material and participate in crack nucleation.

Task 4: Pilot Project

The proposed research will focus on track roller shafts as a pilot component. The track roller shaft represents a component with high-production-volume steel at Caterpillar. It transmits the weight of a tractor through the undercarriage (see Figure 1) and can be produced from either conventional steel

(heat-treated for strength) or microstructurally improved microalloy steel. The use of microalloy steel has been demonstrated to reduce the cost and environmental impact of the heat-treatment stage, making it currently the preferred material in regions with high energy costs (such as Japan). The use of microstructure-level simulation and sustainability metrics to evaluate and optimize its environmental performance throughout the entire life cycle may lead to further improvements and serve as an example of the effectiveness of integrated methodology.



Figure 1. The tractor undercarriage receives the weight of the tractor (a) through a track roller shaft (b).

First, the entire life cycle of a track roller shaft made with a conventional 1500-series steel will be modeled, and the environmental resources needed throughout a component life cycle will be assessed. The chemical composition and processing map will be optimized to minimize the environmental impact and cost of the component. Then the modeling process will be repeated for using a microalloyed steel, which will be optimized for the same requirements. This study aims to provide optimum chemical compositions and processing road maps for a track roller shaft made with a conventional 1500-series steel and a microalloyed steel. In addition, the pilot project will quantify energy and environmental resources required for the entire life cycle of a track roller shaft made with the steels and processes mentioned above.

A critical component in this task, as well as in the others, will be the quantification of energy use during production of a part, and optimization of the proposed process to minimize energy usage. Caterpillar has already established a project called “Bridges to Sustainability,” and NSF interns at

Brown worked in the summer of 2003 on this project. The tools developed by the NSF-sponsored project will be applied in this project to assess energy usage and savings for the processes used here.

Current Period Progress

Microstructure-Level Modeling of Machining

At the microstructural level, steel can no longer be treated as a homogeneous material. Different types of microstructures due to chemical composition and heat treatment cause the material to appear as a composite on the microscale. Thus material heterogeneity must be considered. Different microstructures—namely ferrite, pearlite, martensite, bainite, and tempered martensite—as well as inclusions, porosity, and precipitates, will have combined effects on the material behavior. By looking at deformation at the microstructural level, much detailed information can be obtained. Thus microstructure grains or colonies will be built into the model explicitly. A plasticity model based on dislocation interaction and evolution called the BCJ model will be used to describe the single-phase behavior of each microstructure. Owing to the nature of local high temperatures caused by mechanical deformation and high strain rate near the contact between tool and part, a material model should also be a function of temperature and strain rate.

Since material behavior is a function of temperature, the thermal field also turns out to be very important for this current simulation. A coupled thermal-mechanical scheme is adopted in the analysis methodology. It shows significant impact on chip formation. Friction-generated heat is assumed to be important traditionally; therefore friction-generated heat and heat transferred between the contact interfaces of the tool and part are also included in the model.

Machining test modeling input. Several orthogonal cutting tests have been done on different microstructures generated by different heat treatment operations. Microstructures before the machining operation have been recorded as modeling input. Microstructures in the chips and the machined surface after machining have also been checked for validation purposes. (These results were shown in this project's prior semiannual report.)

Microstructure evolution results. During the machining operation, individual microstructure grains and colonies will change significantly as a result of large shear deformation and even be broken into smaller grains or colony size. This microstructural change will affect the cutting process and the material properties after machining. The simulation results show steel with a ferrite/pearlite microstructure. The volume fraction of ferrite is about 30%, and the rest is pearlite. In an optical micrograph image, pearlite colonies are shown in black and ferrite grains are shown in white. Cutting was simulated for two speeds, 2m/s and 3.33m/s. Results for microstructure in the chip and the machining part from the simulation and test are shown in Figure 2 for the first speed. In the chip, grains are deformed in the direction of shear localization. Similar patterns of this deformation can be seen in both the simulation and the actual machining test. On the machined surface of the part, grains are separated by the cutting process and form a thin-layer shear zone. The simulation shows good agreement with testing.

Chip morphology. Different chip shapes can have an impact on the machining operation. Figures 2 and 3 show the chip shape under two different cutting speeds, for simulation and test. For the higher cutting speed, the chip appears to be more segmented. Also, chip thickness is reduced compared with the low cutting speed. Those changes are mainly due to different shear localization behaviors at the different cutting speeds. At high speed, the temperature increases locally because of the short transit time, which causes large local softening and a segmented chip. At low speed, heat generated by deformation will spread out and cause a more uniform temperature field. At the same time, the local temperature cannot go very high. A larger amount of material is softened to form the chip; this will cause the chip thickness to increase.

Temperature field. Material response during machining is highly dependent on the temperature. The temperature field is also very important for cooling during machining. In some cases, material can become welded onto the tool, a behavior that can be related to the temperature field. Simulation results for the temperature field are shown in Figure 4 for the two different cutting speeds. It can

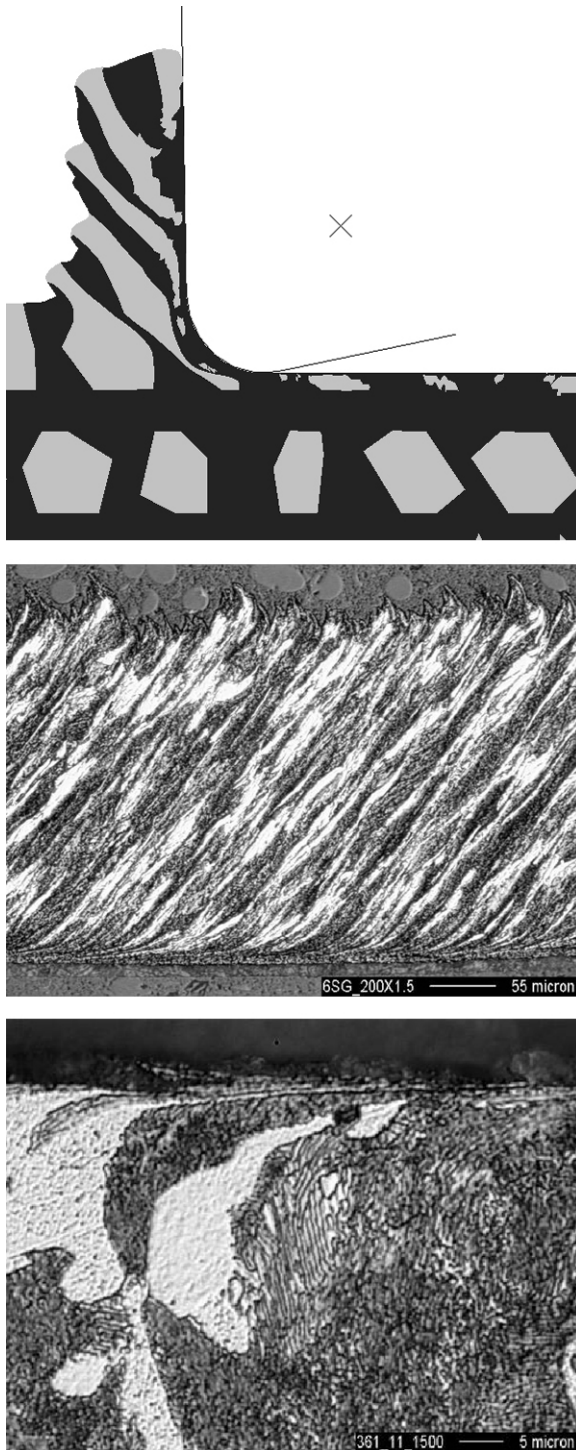


Figure 2. Microstructure evolution during cutting at 2 m/s: (top) simulation shows microstructure in chip and part; (middle) microstructure in chip after testing; (bottom) microstructure for part after testing.

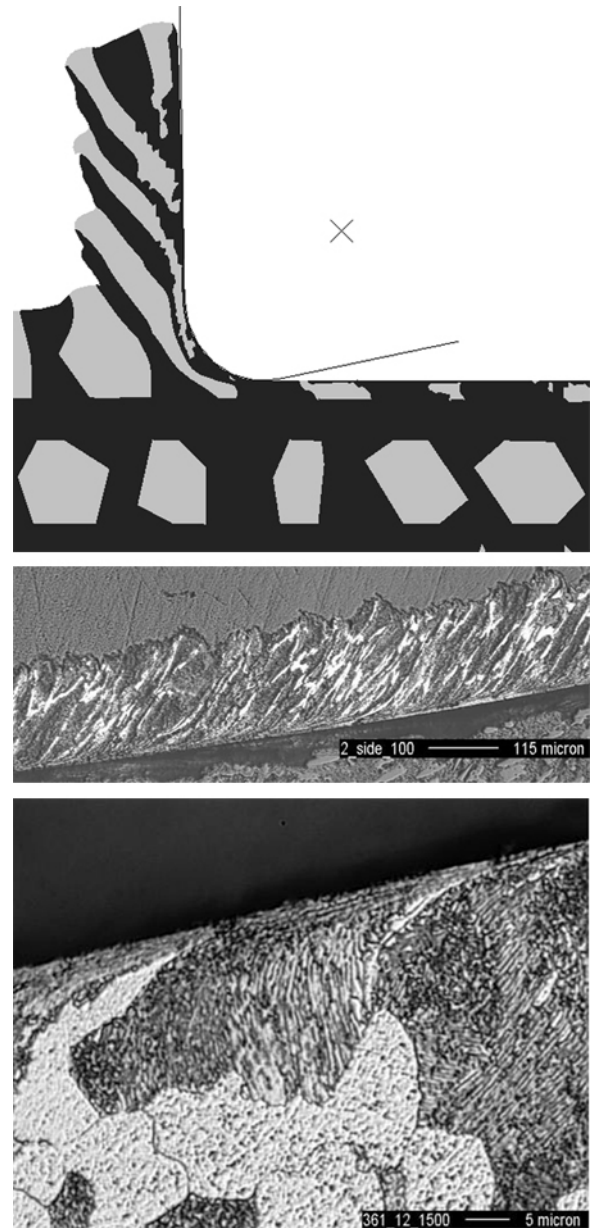


Figure 3. Microstructure evolution during cutting at 3.33 m/s: (top) simulation shows microstructure in chip and part; (middle) microstructure in chip after testing; (bottom) microstructure for part after testing.

be seen that the maximum temperature occurs slightly above the tool nose. This is normally where welding of material onto the tool can occur. For high-speed machining, temperature is more localized and has a higher maximum value.

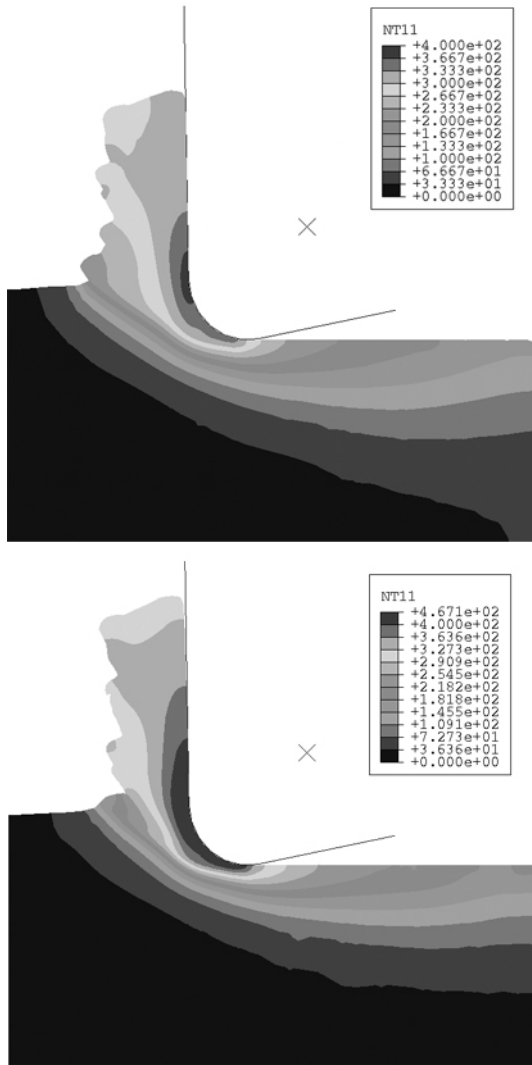


Figure 4. Temperature field for two different cutting speeds: 2 m/s (top) and 3.33 m/s (bottom).

By comparison, chip shape is shown in Figure 5 for an adiabatic situation. It shows a significant difference from the case with heat conduction. The segmented chip shape shows an indication of adiabatic shear band formation. It can be concluded that at this cutting speed, heat conduction must be considered.

Friction heat generation. Friction is another source of heat generation. A model was set up to account for heat generation by friction and account for the heat conduction between tool and part. A temperature field is shown in Figure 6 for cases with friction-generated heat and without. It can be seen that temperature increases directly as a result of the friction-generated heat.

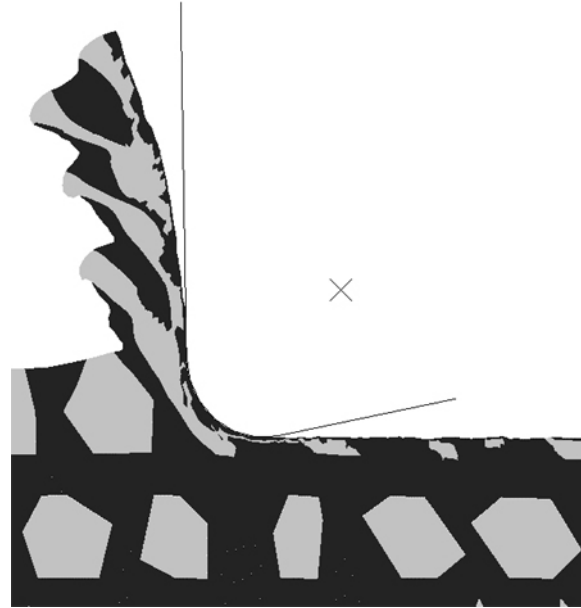


Figure 5. Chip formation for adiabatic condition at a cutting speed of 2 m/s.

Effects on cutting force. Figure 7 shows several cutting force predictions and testing results resulting from different conditions of cutting speed and friction.

The cutting force predicted in the simulation with a friction coefficient of 1.2 is in good agreement with testing results. In machining operations, the friction coefficient can vary from 0.6 to 2.0. Here, a constant value is assumed throughout the whole cutting time. Higher friction will increase the cutting force. At the extreme case of infinite friction, the cutting force goes up by about 10% compared with the friction coefficient of 1.2. The cutting force will also be affected by cutting speed; higher cutting speed results in a lower cutting force for the same material.

Conclusions. A simulation model of the machining process at the mesoscale microstructure level has been set up. The model includes microstructural features such as grains and colonies. The material model is related to dislocation motion and interaction. A fully coupled thermal mechanical setup gives more realistic thermal field and chip formation. This model shows its capabilities in accurate prediction of chip shape, temperature field, and cutting force directly based on material microstructure. This simulation tool can also be extended

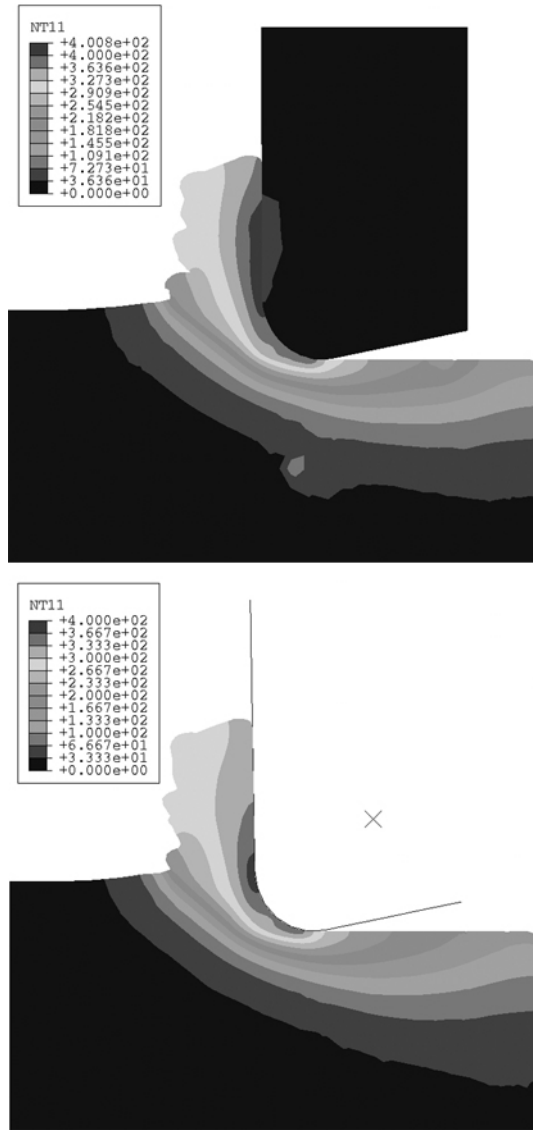


Figure 6. Temperature field with friction-generated heat (top) and without (bottom).

to simulation of other manufacturing processes fairly easily.

Future work. Currently, material properties have been characterized for only two types of microstructures, ferrite and pearlite. More material characterizations are needed; they are already included in another parallel material characterization project. A proper model for friction is needed for accurate predictions.

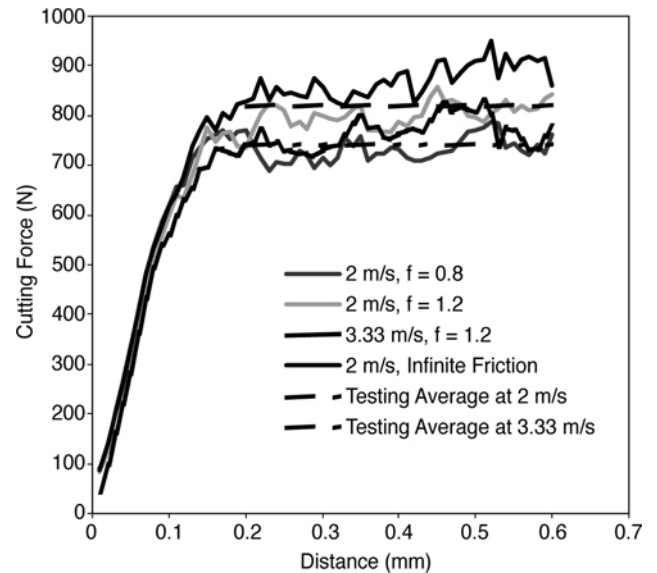


Figure 7. Cutting force vs. distance.

Development of Microstructure Evolution Module Using Cellular Automata

As the first step in developing a robust microstructure evolution module for simulation of heat treatment, a single austenite grain transforming to multiple ferrite grains upon cooling was studied using cellular automata (CA) techniques coupled with a Monte Carlo approach. The cellular automation used in this study has been developed in two dimensions on a square grid, representing an austenite grain. The computation domain is one austenite grain with an 'average' grain size. The general approach is to calculate the total energy for a given cell in the austenite phase and the ferrite phase first. Then a probability is determined for that given volume to change from austenite to ferrite. The probability is calculated using Boltzmann statistics. Initial results (Figure 8) have shown that the CA modeling technique can be successfully used for phase transformation modeling that will provide information on microstructure evolution. This information can be combined with an MLS model to provide explicit microstructure information for material properties calculation in the heat treatment simulation.

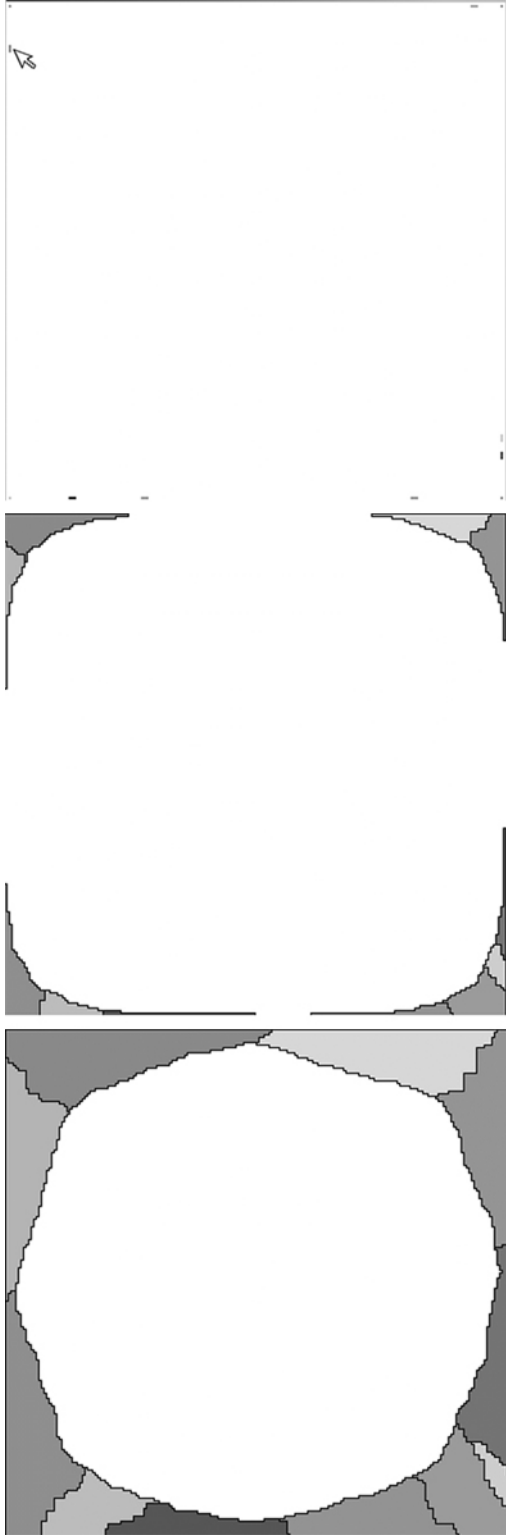


Figure 8. Initial nuclei site of ferrite in austenite grain (top); ferrite grain growth (middle); ferrite grains when eutectoid temperature is reached (bottom).

Material responses during quenching of steel.

The most critical issue in modeling heat treatment is the multiphase material constitutive relationship on a highly heterogeneous material found in a heat treatment process. The traditional approach has been to use an elastic-plastic or elastic-viscoplastic model based on a linear rule of mixtures (RM) or an average material property model. For microscale-level simulation, material properties for each individual phase can be accurately described according to the result of each individual phase characterized in a parallel project. Explicit microstructural descriptions can also be obtained from a microstructure evolution simulation based on stochastic modeling of microstructure. Using a macro/micro modeling technique, material properties for the multiphase structure during heat treatment can be calculated according to the MLS model. As an initial step, effective yield strength for 1045 steel with different constituent fractions of martensite and austenite phases was evaluated. These material properties for the martensite and austenite phases are given in Table 1.

Table 1. Material properties for martensite and austenite

Phase	E(GPa)	ν	σ_y @ $\epsilon=0$ (MPa)	σ_y @ $\epsilon=0.04$ (MPa)
Martensite	214	0.3	1550	2339
Austenite	196	0.3	189	289

A 2-dimensional finite element model (FEM) with random shape and orientation was created for the martensite and austenite phases. The mesh for 31% martensite (dark grey) + 69% austenite (light grey) is shown in Figure 9. Periodic boundary conditions were prescribed at the edges by considering (1) symmetry along the left and bottom edge, (2) constraint of the nodes on the top edge to exhibit the same Y-displacement, and (3) constraint of the right-edge nodes to exhibit the same X-displacement. Displacement loading was applied to the right edge. The mechanical analysis was performed at room temperature using plane stress quadrilateral elements in ABAQUS.

Figure 10 shows the stress-strain plot for different fractions of martensite and austenite. The solid line depicts the results from the FEM study, and the dotted line represents the yield strength values calculated using the linear RM. Figure 10 shows clearly that the composite of martensite and austen-

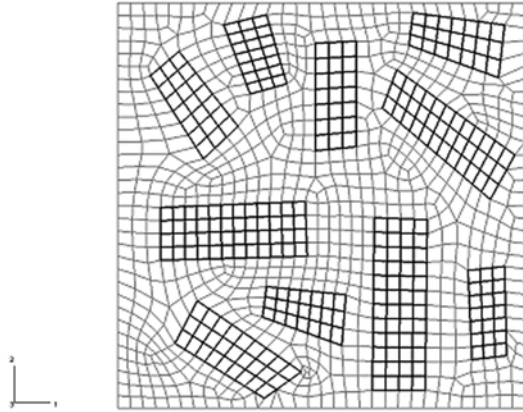


Figure 9. Finite element mesh.

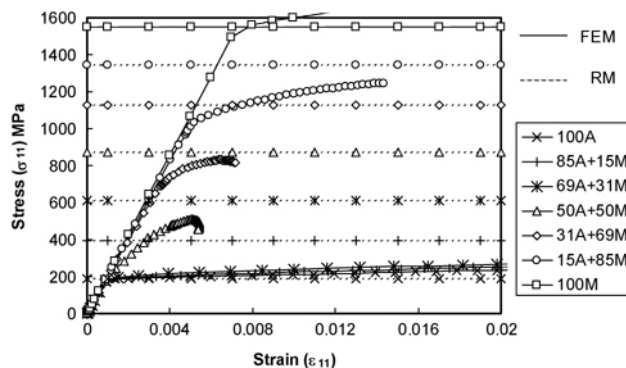


Figure 10. Stress-strain plot for different fractions of martensite (M) and austenite (A) phases. FEM results are represented by the solid line and dotted line shows the yield strength calculated using rule of mixtures (RM).

ite shows considerably lower values of yield strength from FEM than the RM values. The difference is significant (200 to 300%) at higher fractions of austenite (85% A, 69% A and 50% A). At higher fractions of martensite (85% and 69% M), the difference between the yield strength values is around 50%. This difference decreases at higher fractions of martensite, primarily because of the high yield strength of 100% martensite compared with 100% austenite.

With this MLS approach to describe each individual phase explicitly, transformation-induced plasticity, a concept generally used in continuum models, can be explicitly modeled with great accuracy. The next step would be to incorporate material characterization results with the microstructure evolution model to implement an MLS scheme to provide material properties for a heat treatment simulation with a macro/micro model approach.

Integrated heat treat model development.

Heat treatment simulation tool development is a key enabling part of the road map for resource-efficient steel components, as heat treatment provides the necessary material properties for many steel parts with great efficiency and minimum resource costs. In the case of the track roller shaft, quenching and tempering is applied after the forging process. Then induction heat treatment is applied again after the quenching and tempering process to create material properties that meet roller shaft design performance requirements. The manufacturing process is completed with a finish grinding after the induction process. To provide the final microstructure and predict roller shaft performance, an integrated computation method was developed to simulate the quenching/tempering process and the following induction hardening process. Microstructure and residual stress predicted from the quenching/tempering process were fed into an induction-hardening simulation model as input. The final microstructure, residual stress, and distortion could be predicted after the induction hardening process.

Conclusions

This research has successfully accomplished its first-year goals. The microstructural characterization and mechanical property tasks are proceeding on schedule. These efforts have been completed for the initial microstructures of the SAE 1045 and 15V45 steels in support of the heat treatment and machining simulation code development activities. In addition, the machining tests at two machining speeds for both alloys were accomplished. Finally, preliminary machining modeling results have been shown to qualitatively predict the chip morphology, including adiabatic shear band formation, for the as-quenched microstructure of the 15V45 steel alloy.

References

1. A.L. Gurson, "Continuum Theory of Ductile Rupture, Void Nucleation and Growth," *Journal of Engineering Materials Technology*, **99**(2) (1977).

3. MATERIALS PROCESSING TECHNOLOGIES

A. Oxidative Stabilization of PAN Fiber Precursor

Principal Investigator: Felix L. Paulauskas

Oak Ridge National Laboratory

Oak Ridge, TN 37831-8048

(865) 576-3785; fax: (865) 574-8257; e-mail: paulauskasfl@ornl.gov

Project Manager, Composites: C. David Warren

Oak Ridge National Laboratory

P.O. Box 2008, Oak Ridge, TN 37831-6065

(865) 574-9693; fax: (865) 576-4963; e-mail: warrencd@ornl.gov

Technology Development Area Specialist: Sidney Diamond

(202) 586-8032; fax (202) 586-2476; e-mail: sid.diamond@hq.doe.gov

Field Technical Manager: Philip S. Sklad

(865) 574-5069; fax: (865) 576-4963; e-mail: skladsps@ornl.gov

Participants

Terry L. White and Kenneth D. Yarborough, Oak Ridge National Laboratory

Professor Joseph Spruiell, University of Tennessee

Daniel Sherman, Atmospheric Glow Technologies

Contractor: Oak Ridge National Laboratory

Contract No.: DE-AC05-00OR22725

Objectives

- Develop an improved technique for oxidizing carbon fiber precursor with increased line speed, reduced carbon fiber cost, and reduced equipment footprint.
- Verify that produced fiber properties satisfy automotive and heavy vehicle manufacturers' requirements.
- Conduct a preliminary evaluation of the cost impact of the new oxidation technique.

Approach

- Develop a plasma process for oxidation in an atmospheric-pressure plasma reactor.
- Develop fiber handling protocols for continuous processing.
- Conduct parametric studies to correlate processing parameters and fiber properties.
- Characterize fibers to confirm that they satisfy program requirements.

Accomplishments

- Demonstrated the ability to oxidize fiber in atmospheric-pressure plasma in stages equivalent to those used in conventional oxidation furnaces.
- Identified key process parameters and critical operating range and modified the reactor to achieve stable operation in the required parametric space.

- Identified the preferred range of feed gas compositions.
- Improved dielectric properties monitoring technology and presented a conference paper on that topic.

Future Direction

- Continue refining the reactor design and processing protocols to achieve rapid, single-stage fiber oxidation.
 - Develop “pre-stabilization” technique.
 - Develop continuous processing protocols.
 - Conduct parametric studies and fiber characterization to better understand process effects and the processing window and to quantify fiber properties.
 - Conduct rate-effect studies and update cost analysis.
-

Introduction

The purpose of this project is to investigate and develop a plasma processing technique to rapidly and inexpensively oxidize a polyacrylonitrile (PAN) precursor. Oxidative stabilization is a slow thermal process that typically consumes 70% or more of the processing time in a conventional carbon fiber conversion line. A rapid oxidation process could dramatically increase the conversion line throughput and appreciably lower the fiber cost. A related project has already demonstrated the potential for greatly increasing line speed in the carbonization and graphitization stages, but the oxidation time must be greatly reduced to fully exploit faster carbonization and graphitization. This project intends to develop a plasma oxidation module that integrates with other advanced fiber processing modules to produce inexpensive carbon fiber with properties suitable for use by the automotive industry. Critical technical criteria include (1) 25 Msi tensile modulus, 250 ksi ultimate strength, and 1.0% ultimate strain in the finished fiber; (2) acceptably uniform properties over the length of the fiber tow; (3) repeatable and controllable processing; (4) and significant unit cost reduction compared with conventional processing.

Project Deliverable

At the end of this project, we will have demonstrated satisfactory fiber oxidation in a multiple-tow plasma oxidation module operating at line speed exceeding that typical of conventional carbon fiber conversion lines.

Technical Approach

We are investigating PAN precursor fiber oxidation by “direct exposure” in a nonequilibrium, nonthermal plasma at atmospheric pressure, with the fiber transported through the plasma. Plasma processing is believed to enhance oxygen diffusion and chemistry in the PAN oxidation process. Atmospheric-pressure plasma provides better control over the thermal environment and reaction rates than does evacuated plasma, in addition to eliminating the sealing problems accompanying evacuated plasma processing. Various fiber characterization tools and instruments are used to conduct parametric studies and physical, mechanical, and morphological evaluations of the fibers to optimize the process. An evacuated plasma reactor is useful for bench-scale studies, because it allows a greater degree of manipulation and control over reactive species and related parameters. Early in the project, processing tests were conducted in an evacuated plasma reactor, and that same reactor is now used for conducting the bench-scale parametric studies.

Atmospheric-Pressure Plasma Processing Results

Exposure in plasma at or near atmospheric pressure provides superior thermal control because the gas flow should convectively heat or cool the fibers. This is deemed particularly important to avoid fiber melting from the exothermic reactions associated with the PAN cross-linking that occurs during stabilization. However, the mean free path of the chemically reactive species is shorter by orders of magnitude than it is in an evacuated environment, and this makes it very difficult to find a combination

of process parameters that will oxidize the fibers with acceptable residence time.

Conventional PAN oxidation is typically accomplished in three or four thermal stages (stages can be physically separate furnaces or zones in a single physical furnace) in air, at temperatures increasing from about 200 to 250°C. In FY 2004, the researchers demonstrated the ability to reproduce the oxidation advancement in each of the conventional furnaces two, three, and four. The virgin PAN is chemically fragile; hence we have not yet discovered a satisfactory nonthermal processing protocol that reproduces the oxidation advancement in the first conventional furnace. Subsequent experiments have demonstrated the ability to advance the oxidation from the beginning of furnace two through the exit of furnace three in a single, uninterrupted process. These processing results are schematically illustrated in Figure 1.

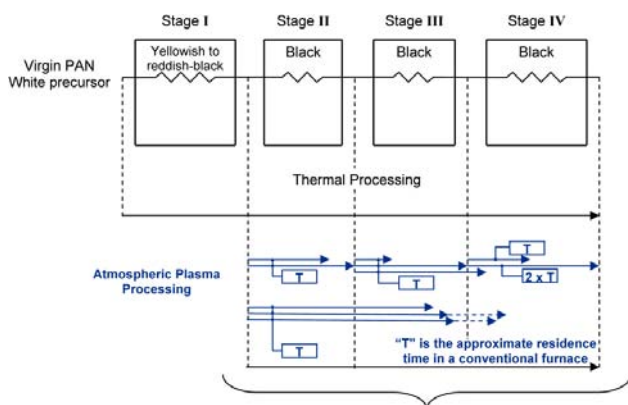


Figure 1. Schematic of conventional thermal oxidation process and progress in plasma oxidation process.

A potentially very important discovery was that the cores of plasma-oxidized fibers are more chemically stable than those of conventionally processed fibers. Figure 2 illustrates the advancement of oxidation and stabilization through a filament cross-section. Most of the fiber must be oxidized, as represented by the outer region, before it can withstand carbonization. In thermal oxidation, the outer stabilized and oxidized region grows inward slowly, purely by diffusion. However, in plasma oxidation, we have observed that oxidation over the filament cross-section is much more uniform; and the entire fiber becomes highly oxidized at a lower fiber density (fiber density is normally used as an indicator of

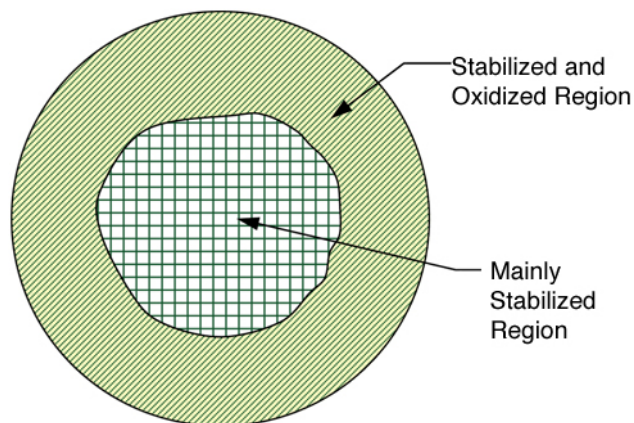


Figure 2. Illustration of advancing oxidation and stabilization through filament cross-section.

degree of oxidation advancement). This suggests that plasma oxidation may allow onset of carbonization at a lower fiber density, a thesis that will be experimentally tested in future work. If carbonization can indeed commence at a lower fiber density, this could significantly reduce the residence time required for oxidation.

The researchers have made good progress toward identifying the parameters that most affect the oxidation rate and optimizing those parameters within the reactor. For patent protection and export control reasons, the detailed results are not published, but they are periodically disclosed to the relevant program managers in oral briefings.

Feed Gas Composition

The researchers investigated the effects of plasma oxidation with various gas compositions. It was confirmed that the chemistry can be quite sensitive to feed gas composition, as illustrated in Figure 3. A wide range of feed gas compositions were investigated and the results recorded. Specific compositions and processing parameters are not published for patent protection and export control reasons.

Instrumentation

During this reporting period, the researchers continued developing techniques and hardware for measuring the fiber dielectric properties over a selected range of oxidation processing conditions. A dielectric measurement system, shown schematically in Figure 4, was validated. Several temperature



Figure 3. Plasma with two different feed gas compositions in evacuated plasma reactor.

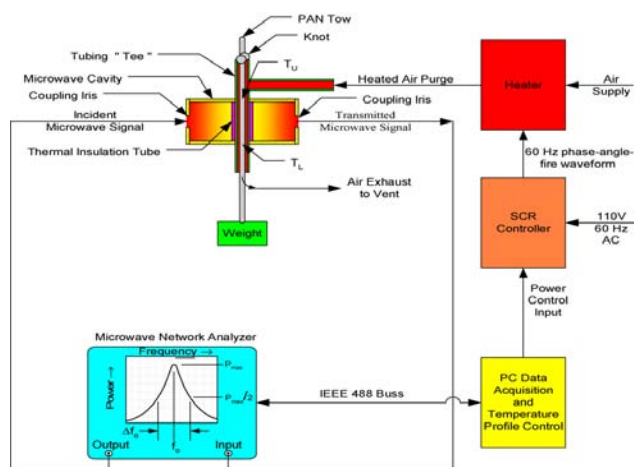


Figure 4. Dielectric measurement system schematic.

control problems were identified and corrected by adjusting control and operational parameters, modifying hardware, and changing the PAN cross-section in the instrument chamber. A large number of runs were conducted with PAN partially oxidized to differing degrees. The real and imaginary parts of the dielectric constant correlated well with the degree of PAN oxidation. A paper on this topic was presented at the 2004 SAMPE Symposium and Exposition in Long Beach CA.

The researchers began creating a dielectric properties database for 3-k and 80-k PAN fiber tows that were partially oxidized in varying degrees by conventional means. Plasma-oxidized fiber properties can later be compared against this database as a selector for fiber specimens that will be further characterized by more time-consuming spectroscopy techniques.

The researchers need a rapid turnaround technique for indicating oxidation trends, to quickly assess whether various parametric processing trials have successfully advanced the oxidation. Density measurements are frequently used by fiber manufacturers. In this project, dielectric measurement equipment and techniques have been successfully developed and validated, and morphology measurements are also used to characterize the fibers. However, density, dielectric, and morphology measurements all have turnaround times of hours to days because of measurement duration, instrument cost and location, required operator skill, and/or instrument time-sharing. The fiber changes color, starting from white and successively darkening until it turns completely black after it is about 10–20% oxidized. Therefore, color is a reasonable progress indicator in early oxidation, but another technique is needed for the remainder of oxidation.

The researchers investigated dc electrical resistance measurement as an oxidation progress indicator. The very high tow resistance ($10^{12} - 10^{15}$ ohms) is beyond the capability of most resistance meters and can be accurately measured only under exceedingly well-controlled environmental conditions. A high-resistance meter was purchased and tested. The PAN fiber must present the most conductive path between measurement terminals to achieve accurate resistance measurement. Since moisture, and even air, can provide a conductive “short,” the researchers concluded that dc resistance measurements are too unreliable, even with meters rated for ultra-high resistance. The researchers are still searching for a good, inexpensive, rapid turnaround technique for monitoring the relative oxidation progress.

Economics

During FY 2004, Kline and Company completed a cost study of DOE’s entire carbon fiber development program, estimating profitable selling prices for baseline technology and if various technologies under development were implemented. Kline’s estimates generally indicated that advanced oxidation techniques should reduce fiber selling price by about 6–8%. These estimates, however, were based on a line speed comparable to that of conventional conversion lines. Rough calculations suggest that if we can achieve much higher line speeds, the savings could increase dramatically. We have not discovered any inherent physics limits that would prevent us

from achieving a large increase in conversion line speed using plasma oxidation and microwave-assisted plasma carbonization.

Education

The materials characterization has been conducted in partnership with the University of Tennessee's (UT's) materials science department. Two UT graduate students were engaged to provide characterization support to the project.

Partners

ORNL gratefully acknowledges contributions to this project by Fortafil and Hexcel. Both have generously provided raw materials and offered technical consultation. An updated materials transfer agreement was executed with Hexcel during this reporting period. Additionally, technical and programmatic consultation has been provided by the Automotive Composites Consortium and by Delphi Corporation.

Conclusions

The development of plasma-based oxidation technology has achieved a major milestone by dem-

onstrating the feasibility of plasma processing to oxidize PAN precursor fibers. Preliminary data suggest that the plasma oxidation process may allow earlier onset of carbonization, thus reducing oxidation residence time. Understanding of the parametric processability space has grown substantially during this period. Preliminary economics studies support the value of research in advanced oxidation. The researchers expect to demonstrate continuous plasma processing, and continue growing our understanding of the plasma oxidation process and its benefits, in FY 2005.

Presentations

F. L. Paulauskas and T. L. White, "Temperature-Dependent Dielectric Measurements of Polyacrylonitrile Fibers during Air Oxidation," 49th International SAMPE Symposium 2004, Long Beach, CA. May 16–20, 2004. Published in the conference proceedings, 2004.

B. Wrought Magnesium Alloy/Process Development

Principal Investigator: J. A. Horton

Oak Ridge National Laboratory

P.O. Box 2008, Oak Ridge, TN 37831-6115

(865) 74-5575; fax: (865) 574-825; hortonja@ornl.gov

Principal Investigator: S. R. Agnew

University of Virginia

116 Engineer's Way

P.O. Box 400745, Charlottesville, VA 22904-4745

Technology Development Area Specialist: Sidney Diamond

(202) 586-8032; fax: (202) 586-1600; e-mail: sid.diamond@ee.doe.gov

Field Technical Manager: Philip S. Sklad

(865) 574-5069; fax: (865) 576-4963; e-mail: skladps@ornl.gov

Contractor: Oak Ridge National Laboratory

Contract No.: DE-AC05-00OR22725

Objectives

- Develop wrought magnesium alloys with better formability than current magnesium alloys.
- Investigate new processing techniques for cost reduction and formability improvement.
- Contribute to basic understanding of deformation, processing, and alloy behavior for this lightweight metal.

Approach

- Explore new processing schemes for magnesium alloy sheets.
- Evaluate the practical formability of new alloys and after new processes.
- Determine deformation mechanisms using experimentation and simulation.

Accomplishments

- Demonstrated feasibility of infrared sheet processing at a commercial facility, Manufacturing Sciences, Inc.
- Designed warm formability testing tool based upon the "OSU test."
- Experimentally validated the dislocation-based mechanism hypotheses developed through simulation.
- Collected data to determine if various dislocation-based mechanisms have distinct grain-size dependence.
- Completed assessment of texture evolution during equal channel angular extrusion.

Future Direction

- Interact with an industrial partner to advance commercialization of infrared processing for cost reductions.
- Define further correlations of microstructure, mechanisms, and anisotropy.

- Further explore superplastic-type behavior observed at warm forming temperatures.
- Investigate fundamental parameters affecting castability of the more creep-resistant alloys.

Introduction

The world market for magnesium has changed substantially in recent years with the emergence of China as the leading producer (~50% of the market.) For instance, some western competitors have been driven out of business (e.g., Noranda in Canada) or have uncertain futures (e.g., AMC in Australia). It is still unclear what the final outcome will be, since at least one major western supplier (Norsk Hydro) has formed an alliance with a Chinese partner. Magnesium sheet manufacturers face a number of technical issues that we continue to research:

- Rolling magnesium to thin-gage sheet currently leads to expensive solutions.
- Obtaining an excellent surface finish is difficult.
- Corrosion performance is poor vis-a-vis die-cast alloys.
- Sheet formability is limited at low temperatures.

During FY 2003, in addition to focusing on the sheet formability issues, we began addressing the concerns associated with the cost of sheet products.

Demonstration of Infrared Processing at A Commercial Rolling Facility

After lab studies of the relevant infrared parameters, microstructures, and mechanical properties involved with infrared processing of sheet magnesium, a demonstration was performed at Manufacturing Sciences under the direction of Tom Muth. This commercial rolling mill facility has a 3 × 8 ft bank of infrared lamps at 12 W/cm² installed on one side of a reversing mill (Figure 1). Starting material for this demonstration was commercial sheets of 6-mm-thick AZ31 tooling plate. Initial heatup required 5 min; subsequent heatups with thinner sheet required less time until the last pass required approximately 2 min. Newer designs of the infrared bank have an even higher output, promising even shorter anneal times.

Sets of rolling sequences were performed aiming at 15%, 20%, and 40% rolling reductions for each pass until 1-mm thickness was obtained. A fi-



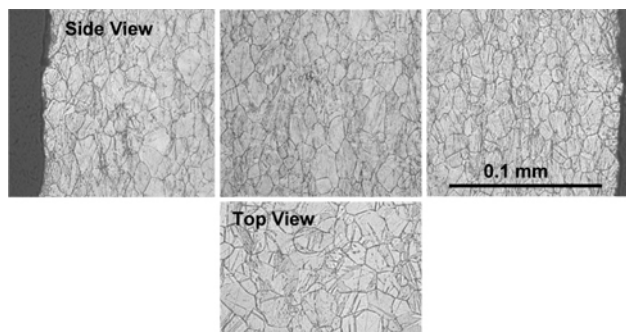
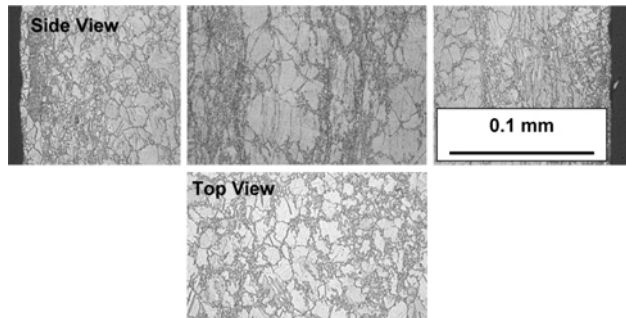
Figure 1. Commercial rolling mill facility has a 3 × 8 ft bank of infrared lamps at 12 W/cm² installed on one side of a reversing mill.

nal roll on a 6-mm plate was performed with as much reduction as we dared. Desired temperatures were 400°C and 500°C. However, 500°C could not be reached because of the large airflow. Specimens were collected at several points in the rolling sequence. Table 1 lists the as-rolled mechanical properties for five test runs at various points during the rolling. The amount of cold work saturated after few passes. However, the tensile strengths and ductilities indicate that the magnesium was essentially cold-rolled. Further experiments are under way to attempt to study actual rolling temperature effects on texture and properties.

Figure 2 shows that the microstructure in the near-surface regions was similar to that of the cen-

Table 1. As-rolled mechanical property data after infrared processing

T (°C)	Average reduction (%)	Thickness (mm)	Passes	UTS (MPa)	Elongation (%)
400	16.5	2.1	6	275	6
		1.3	9	285	5
		1.0	10	307	4
400	23	1.5	5	298	6
		1.0	7	404	7
~425	44	1.1	3	363	3
~425	66	2.1	1	265	5

**Figure 2.** Side and top views of the microstructure of 1mm thick sheets after the 10th pass at average of 16.5% reduction showing that the near surface regions were similar to the center.**Figure 3.** Side and top views of the microstructure sheets after a single pass of 66% reduction showing evidence of dynamic recrystallization in the form of fine grain necklaces.

ter. The largest reduction used, 66%, resulted in some dynamic recrystallization, as shown in Figure 3. Such an approach could be used to develop a very fine-grained structure appropriate for superplastic forming, as an example. In addition to microstructure, we examined the texture, since it is so significant for determining the properties of magnesium. The (0002) pole figure from the as-received 6-

mm tooling plate was little changed by the infrared rolling.

These results were presented at the Magnesium 2004 symposium at the TMS annual meeting and generated much interest. A member of the audience raised the concern that such large reductions could introduce microcracks or other defects during this processing, resulting in the low ductilities shown in Table 1. Subsequent annealing studies for 2 hours at 185°C and 345°C resulted in much higher ductilities, suggesting that normal commercial wrought properties, or better, can be obtained (see Table 2).

Table 2. Mechanical property data after 2-hour anneals

Anneal T (°C)	Yield (MPa)	UTS (MPa)	Elongation (%)
As-rolled	262±57	312±49	5±2
185	185±11	269±6	18±2
345	141±14	247±6	24±2

Design and Implementation of a Warm Formability Testing Apparatus

Throughout our research project, we have been continually pursuing the possibility of forming magnesium sheet metal at lower temperatures. Traditional wisdom states that the forming temperatures should be in the range of 250°C or higher. One problem is that there really is no standardized testing methodology for warm forming. In the past, we have used a high-temperature cylindrical cup drawing apparatus at Oak Ridge National Laboratory as an indicator of formability; and we have been able to make qualitative comparisons between alloys. However, there are a couple of problems with this ap-

proach: (1) Since our target applications are vehicles, the most important forming operations tend to be primarily stretching, as opposed to drawing. (2) The results of the cup drawing test are heavily influenced by thermal gradients. In our case, the die is heated, but the punch is not. While this actually leads to enhanced practical formability, it is not the best way to assess the intrinsic formability of the material at a given temperature and strain rate.

We studied the literature and found a new test developed at Ohio State University (the OSU test) that actually deforms the sheet metal in a condition very close to plane strain tension. This is significant, since studies of technological forming failures have indicated 80% of stamping failures are under conditions of plane strain. This is also the division between the drawing and stretching halves of the forming limit diagram (FLD); it yields a result known as FLD_0 , which is the lowest point on the FLD. This test requires a relatively small die set-up and thus can fit within one of the furnaces mounted on mechanical testing frames at the University of Virginia (Figure 4). A few trial runs on copper and aluminum alloy sheets have been performed at ambient temperatures. Once a protocol has been developed, warm formability tests on aluminum and magnesium alloys will be performed. These may be conventional alloy sheets, sheets subjected to novel processing schemes, or experimental alloys.

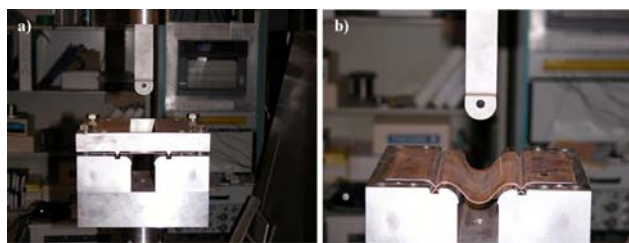


Figure 4. Warm formability testing apparatus based upon “the OSU test” shown (a) prior to deformation, as the metal is being clamped into the die, and (b) after deformation.

Validation of Anisotropy and Simulation Approach to Mechanism Determination

It is of interest to determine the deformation mechanisms that control the deformation behavior of wrought magnesium. For instance, if particular mechanisms can be determined to be responsible for the cold-formability problems or the excellent formability at elevated temperatures, improvements may

be made through targeted alloy or microstructure design. Our approach has been to probe the deformation mechanisms with the help of computer simulations based on polycrystal plasticity theory.

Information about the material’s structure (i.e., crystallographic texture) and deformation mechanisms (solved for iteratively) serves as input, and the mechanical behavior and texture evolution are outputs. Experimentally, the initial texture, the mechanical response, including anisotropy, and the final texture are measured. When the simulations predict the observed behavior, it is an indication that the deformation mechanisms used as inputs are reflective of the material’s mechanisms.

Last year it was demonstrated that alloy AZ31B sheet exhibits a strong correlation between the sharp increase in tensile ductility (and formability in general) at mildly elevated temperatures and a sharp decrease in anisotropy (Figure 5). Through the approach outlined, it was suggested that this strong decrease in anisotropy is associated with the activation of another deformation mechanism at elevated temperatures, pyramidal $\langle c+a \rangle$ slip. Of all the slip mechanisms known to operate within magnesium, this was the only one for which the simulations predicted the observed lowering of anisotropy. Provided the intrinsic assumptions of polycrystal plasticity are correct, this would represent a significant finding.

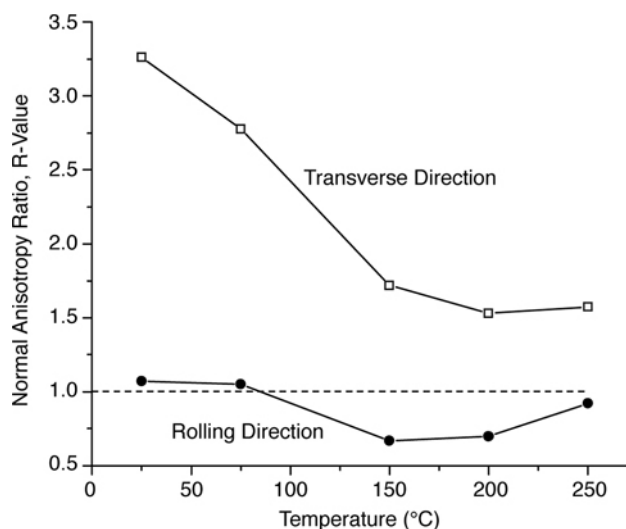


Figure 5. The r-value measurements over a range of temperatures show that the r-value drops strongly in all directions as the temperature is raised. This behavior has been linked to an increase in the activity of pyramidal $\langle c+a \rangle$ slip as the temperature is raised.

This year, efforts have been focused on demonstrating that the predictions of the approach are grounded in reality. Transmission electron microscope (TEM) dislocation analysis was used to examine deformed samples for evidence of mechanisms predicted to be operational by the modeling approach. As an initial step, samples deformed at room temperature were examined for evidence of non-basal $\langle a \rangle$ slip. The simulations suggested that up to 80% of strain is accommodated by non-basal slip. This is in stark contrast with magnesium single-crystal observations of the 1950s and 1960s, which showed no evidence of non-basal slip below $\sim 180^\circ\text{C}$, even under constraint. The TEM study did show evidence of extensive non-basal $\langle a \rangle$ dislocation slip (Figure 6), and a preliminary report was published in the *Proceedings of the Magnesium Technology 2004 Symposium of the TMS Annual Meeting*. A full journal paper in the *International Journal of Plasticity* is in-press.

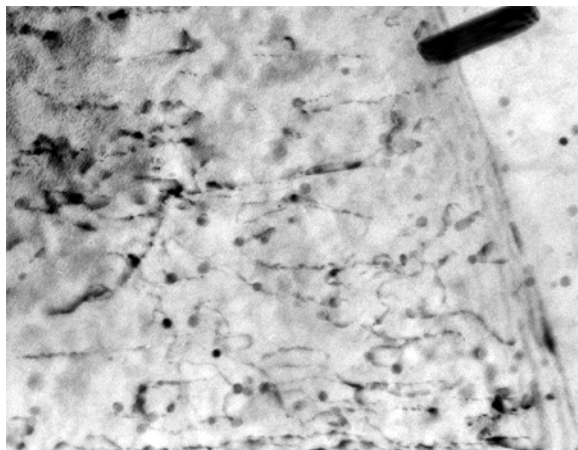


Figure 6. TEM image of magnesium alloy AZ31B deformed in tension shows curved dislocations when viewing from a basal plane edge-on perspective. Thus the dislocations are gliding on non-basal planes. A complete Burgers vector analysis shows the majority of dislocations to have $b = \frac{1}{3}[11\bar{2}0]$ or $[a3]$.

The same approach is being applied to determine (1) whether non-basal slip is strongly controlled by grain size and (2) whether our hypothesis that high-temperature formability is controlled by $\langle c+a \rangle$ slip is correct. Both of these findings would have significant practical implications, since processing can strongly affect the microstructure of magnesium (see following discussion), and secondary slip can be heavily influenced by alloying additions.

Samples of alloy AZ31 sheet with different linear intercept grain sizes (14–220 μm) have been produced through annealing for different times (1 h–1 week) and temperatures (345–525 $^\circ\text{C}$). To date, the grain size has been assessed and tensile tests along the rolling (RD) and transverse (TD) directions have been performed, since these were previously shown to exhibit distinct behaviors connected with varying ratios of basal : non-basal dislocation slip (Figure 7a). Plotting the results in the conventional Hall-Petch fashion (Figure 7b) reveals a grain size dependence of this alloy's yield strength similar to that published previously.^{1,2}

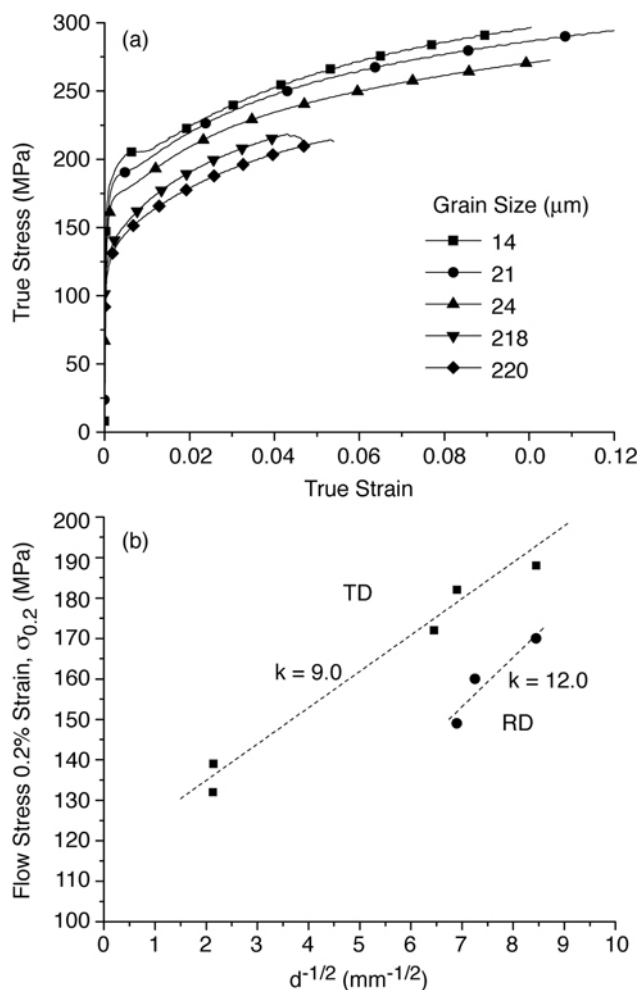


Figure 7. Grain size dependence of the (top) flow curves for transverse direction samples and (bottom) the yield stresses of both transverse and rolling direction samples of magnesium alloy AZ31 sheet.

More interesting are the differences in the anisotropy that are exhibited by samples of different

grain sizes (Figure 8). The as-received (not annealed) samples exhibit the lowest anisotropy. Annealing and grain growth actually appear to enhance the anisotropy, contrary to popular opinion. If the r -values are measured at a strain of 11%, as we have done previously, there appears to be only a slight change with annealing.

A special extensometer has been obtained that can measure the Poisson strain along the sample's width direction in-situ. The r -value evolution can be determined

$$r = \varepsilon_w / \varepsilon_t = -\varepsilon_w / (\varepsilon_l + \varepsilon_w)$$

by virtue of the incompressible nature of metal plasticity ($\varepsilon_w + \varepsilon_t + \varepsilon_l = 0$), where ε_w , ε_t , and ε_l are the strains along the sample's width, thickness and length directions. This new tool shows the evolution of anisotropy is strikingly different between the samples of different grain sizes (Figure 8).

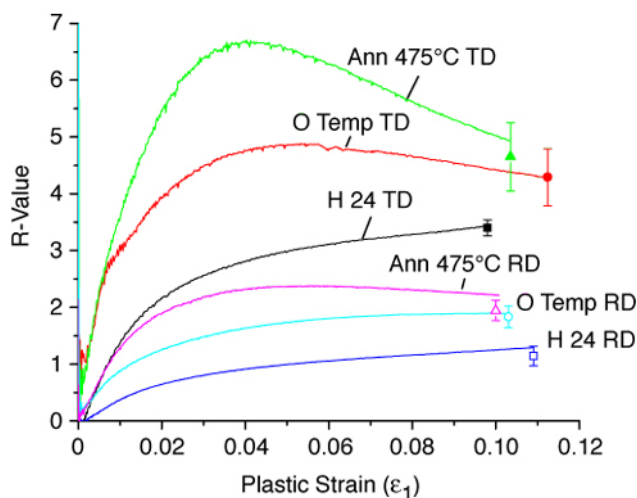


Figure 8. Evolution of the anisotropy (r -value) with strain for samples of different grain sizes (H24 temper $\sim 9 \mu\text{m}$, O temper $\sim 14 \mu\text{m}$, and annealed at $475^\circ\text{C} > 30 \mu\text{m}$).

It was anticipated that larger grain samples might exhibit less non-basal slip and therefore lower r -values (using modeling arguments discussed earlier.) However, the initial results show that all of the larger grain samples have higher r -values. This fact may not be linked to mechanistic changes, since the higher overall anisotropy may be connected with a change in the texture during annealing; so we are now measuring the textures of samples in addition to their grain size. The final results will be important

input for microstructure design of wrought magnesium.

Texture Evolution during Equal Channel Angular Processing

This project focused on wrought magnesium began with an investigation of the potential of equal channel angular (ECA) processing to improve the mechanical properties of magnesium alloys by modifying the microstructure (i.e., reducing the grain size and heterogeneity.) The grain structure of bulk magnesium alloys was successfully modified and the elevated temperature ductility (e.g., superplasticity) improved early in the project. Later, a report published by a Japanese group led us to consider the possibility that the room-temperature ductility could be improved by ECA processing by reducing the crystallographic texture. We were able to duplicate the improvement in ductility; however, we found that the crystallographic texture of the samples was stronger than the initial texture. This sparked a renewed interest in the potential to improve the properties of magnesium alloys through texture modification.

This year the possible texture evolutions of five different wrought alloys—AZ31, AZ80, ZK60, WE43—and an experimental alloy containing 4 wt% Li were cataloged. These alloys were processed at a range of temperatures, different starting microstructures and textures, and a range of processing routes. The result of the study is an extensive database of texture evolutions. For the purpose of this short report, the results are described in Table 3. A couple of examples of the textures are shown in Figure 9. Another finding was that the texture throughout a sample is a strong function of position, particularly after processing by so-called route B (where the samples are rotated 90° between subsequent passes through the ECA die.) Analysis of how the deformation is actually introduced into a representative billet (Figure 10) has begun, and the differences in the textures from different parts of the samples can now be rationalized.

References

1. F. E. Hauser, P. R. Langdon, J. E. Dorn, "Fracture of Magnesium Alloys at Low Temperature," *J Metals, Trans. AIME*, **206**, 589–93 (1956).

Table 3. Summary of texture evolution of 5 magnesium alloys during ECA processing

Alloy	Initial state	T (°C)	Route	Pass	Texture description	Peak (002)	Classification
AZ31	Plate	300	A	1	(002) tilted forward	~6	High temp, Al
				2	“	~8	“
				4	“	~8	“
				8	“	~8	“
“	Extru	200	A	1	(002) tilted backward	~6	Low temp, Al
				2	“	~6	“
				4	“	~6	“
“	As-cast	200	A	1	(002) tilted backward	~6	“
AZ80	Extru	200	A	1	(002) tilted backward	~6	“
ZK60	Extru	260	A	1	(002) vertical, FPN	~4	High temp, Zr
				2	(002) vertical	~6	“
				4	“	~6	“
				8	“	~8	“
WE43	Extru	325	A	2	(002) vertical, FPN	~4	“
				4	“	~4	“
Mg4Li	Extru	260	A	1	(002) vertical		Li alloy
				2	(002) vertical, FPN		“
				4	(002) FPN, vertical		“
ZK60	Extru	260	C	2	(002) tilted forw, back	~4	High temp, Zr
“	“	“	“	4	“	~6	“
ZK60	Extru	260	B	4	(002) tilted forw, back	~4	“
AZ31	Extru	200	B	2	(002) tilt back, vertical	~6	Low temp, Al
“	“	“	“	8	(002) tilted back	>10	“
“	Cast	“	“	2	“	>10	“
AZ80	Extru	200	B	2	(002) tilt back, vertical	~6	“
“	“	“	“	4	“	~6	“
“	“	“	“	8	“	>10	“

2. N. Ono, K. Nakamura, S. Miura, “Influence of Grain Boundaries on Plastic Deformation in Pure Mg and AZ31 Mg alloy Polycrystals,” *Mater. Sci. Forum*, **419–422**, 195–200 (2003).

Publications and Presentations

S. R. Agnew, “Wrought Magnesium: A 21st-Century Outlook,” *JOM* **56**(5), 20–21 (2004).

S. R. Agnew and O. Duygulu, “Plastic Anisotropy and the Role of Non-basal Slip in Magnesium Alloy AZ31,” accepted for publication in *Inter. J. Plasticity* in 2005.

S. R. Agnew, J. A. Horton, T. M. Lillo, and D. W. Brown, “Enhanced Ductility in Strongly Textured Magnesium Produced by Equal Channel Angular (ECA) Processing,” *Scripta Mater.* **50**, 377–381 (2004).

S. R. Agnew, C. N. Tomé, and D. W. Brown, “The Effect of Texture on the Deformation Mechanisms of AZ31B,” presented at Symposium on

Phase Transformations and Deformation in Magnesium Alloys, TMS Annual Meeting, Charlotte, NC, March 16, 2004.

A. L. Bowles, H. Dieringa, C. Blawert, N. Hort, K. U. Kainer, “Investigations in the Magnesium-Tin System,” in *Proceedings of the International Conference on Magnesium—Science, Technology and Applications*, Beijing, China.

A. L. Bowles, H. Dieringa, C. Blawert, N. Hort, K. U. Kainer, “Investigations in the Magnesium-Tin System,” presented at International Conference on Magnesium—Science, Technology and Applications, Beijing, China, September 20–24, 2004.

O. Duygulu and S. R. Agnew, “TEM Investigation of Dislocation Mechanisms in Mg Alloy AZ31B Sheet,” pp. 61–66 in *Magnesium Technology 2004*, Ed. A. A. Luo, TMS, Warrendale, PA, 2004.

O. Duygulu and S. R. Agnew, “TEM Investigation of Dislocation Mechanisms in Mg Alloy

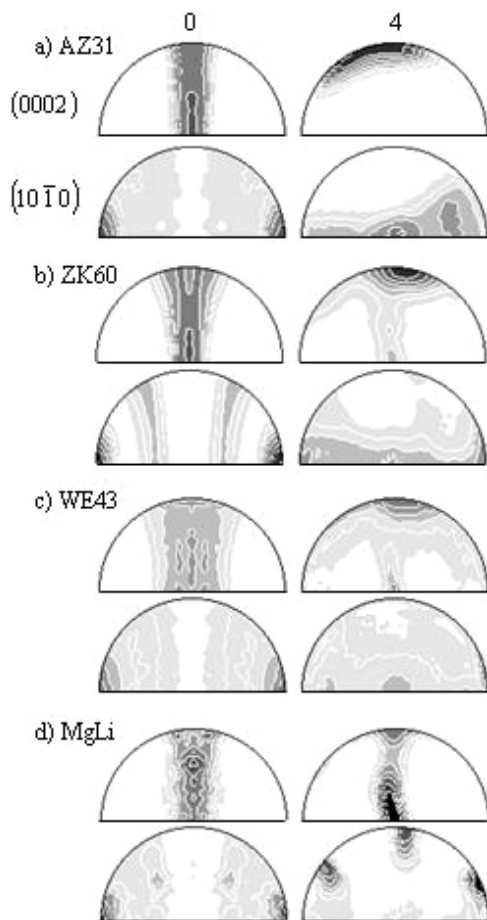


Figure 9. Representative textures from conventional extrusion, labeled 0, and the effect of 4 passes of ECA extrusion, labeled 4. Note strong differences between four of the alloys examined (a) AZ31, (b) ZK60, (c) WE43, and (d) Mg-4 wt % Li despite similarity of initial extrusion textures. Contours are on a logarithmic scale with a maximum (black) of eight multiples of a random distribution.

AZ31B Sheet,” presented at Magnesium Technology 2004 Symposium, 2004 TMS Annual Meeting, Charlotte, NC, March 16, 2004.

J. A. Horton, C. A. Blue, S. R. Agnew, and T. Muth, “Infrared Processing of Wrought Magnesium Alloys,” presented at Magnesium Technology 2004, TMS Annual Meeting, Charlotte, NC, March 16, 2004.

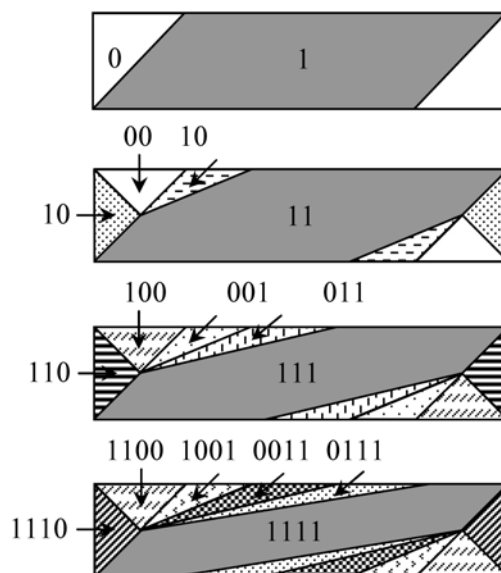


Figure 10. Schematics of the deformed regions of billets after 1, 2, 3, and 4 route A passes through the die, emphasizing the shrinking region, which is completely deformation. (1's and 0's indicate strained and unstrained portions during a given pass. For example, 1011 indicates the region was strained during the 1st, 3rd, and 4th passes, but not the 2nd.)

P. K. Liaw, G. M. Stoica, L. J. Chen, E. A. Payzant, C. Xu, T. G. Langdon, and D. E. Fielden, “Plastic Flow and Mechanical Behavior of Some Mg- and Al- Alloys Deformed by Equal Channel Angular Pressing,” presented at Third International Symposium on Ultrafine Grained Materials, TMS Annual Meeting, Charlotte, NC, March 16, 2004.

G. Song, A. L. Bowles, and D. H. StJohn, “Effect of Aging on Yield Stress and Corrosion Resistance of Die Cast Magnesium Alloy,” in *Proceedings of the International Conference on Magnesium—Science, Technology and Applications*, Beijing, China.

G. Song, A. L. Bowles, and D. H. StJohn, “Effect of Aging on Yield Stress and Corrosion Resistance of Die Cast Magnesium alloy,” presented at International Conference on Magnesium—Science, Technology and Applications, Beijing, China, September 20–24, 2004.

C. Equal Channel Angular Extrusion of Soft Ferromagnetic Materials

Principal Investigator: R. B. Schwarz

Los Alamos National Laboratory

MST-8, Mail Stop G755, Los Alamos NM 87545

(505) 667-8454; e-mail: rxzs@lanl.gov

Co-Investigators: T. D. Shen, J. D. Thompson, J. I. Archuleta (LANL), and K. Mukherjee (UC-Davis)

Technology Development Area Specialist: Sidney Diamond

(202) 586-8032; fax: (202) 586-1600; e-mail: sid.diamond@ee.doe.gov

Field Technical Manager: Philip S. Sklad

(865) 574-5069; fax: (865) 576-4963; e-mail: skladps@ornl.gov

Contractor: Los Alamos National Laboratory

Contract No.: W-31-109-Eng-38

Objective

- Conduct research on the theory, synthesis, and properties of soft ferromagnetic alloys having the potential to improve the efficiency of energy conversion devices in the U.S. transportation industry.

Approach

- Use mechanical alloying (MA) (a high-energy ball milling technique) to prepare Fe-rich alloy powders.
- Characterize the powder by X-ray diffraction, scanning differential calorimetry, and magnetometry.
- Consolidate the mechanically alloyed powders by equal-channel angular extrusion and spark-plasma sintering.
- Characterize the compacted alloys by ac and dc magnetic measurements.

Accomplishments

- Prepared nanocrystalline Fe-Al-Si powders by MA. We used differential scanning calorimetry and X-ray diffraction to determine the optimal annealing parameters for reducing the residual stress in the Fe-Al-Si powders, while maintaining the crystallite size below 20 nm, as required for soft ferromagnetic properties.
- Demonstrated that minimizing the magnetic coercivity requires annealing within a narrow temperature window at which residual stresses are eliminated, yet grain growth is avoided.
- Analyzed the effects of crystallite size and residual stress on the magnetic properties.
- Studied the consolidation of our mechanically alloyed Fe-Al-Si powders by spark plasma sintering (collaboration with Professor A. K. Mukherjee at the University of California, Davis).
- Measured the magnetic properties of Fe-Al-Si alloys in both powder and consolidated form.

Introduction

There is continued interest in increasing the efficiency of electrical energy-conversion devices.¹ Here we are interested in ferromagnetic cores of motors and transformers and in magnetic material for

switched-mode power supplies. The challenge for low-loss transformer applications is to develop ferromagnetic materials that have low coercivity, H_C , and high magnetic saturation, M_s . The challenge for efficient switched-mode power supply inductors is

to develop ferromagnetic alloys with high saturation flux density, low permeability, and low losses at high frequencies.

For the first application, the best results have been obtained with two-phase alloys consisting of nanosized *bcc* Fe particles embedded in an amorphous alloy matrix. Two nanocrystalline alloys, known under the trade names Nanoperm² and Finemet,³ are prepared by the partial crystallization of 30- to 50- μm -thick rapidly quenched glassy ribbons. The saturation magnetization of these materials is approximately 1.4 T. Their main drawback is their thinness of gauge and brittleness, which are not optimal for the construction of power transformers.

For the second application, industry has relied extensively on gapped ferrite cores and on “distributed-gap” cores made from pressed ferromagnetic powder or powder cast into a polymer. The last method has the advantage of a low manufacturing cost.

In the present project, we are investigating the synthesis and magnetic properties of *nanocrystalline* ferromagnetic alloys. We prepare these alloys in powder form using mechanical alloying. We then consolidate them using a spark-plasma sintering technique.

Magnetic Properties of Nanocrystalline Ferromagnetic Fe₉₂Al₂Si₆ Alloy Powders

The synthesis of nanocrystalline alloy powders by MA was described in the FY 2003 report and thus will not be repeated here. In that earlier report, we also described the magnetic properties of Fe₈₀Cu₂₀ alloys prepared by MA. We then proposed to continue this work by studying the magnetic properties of Fe-Al-Si alloys. The reason for choosing this alloy was to raise the temperature at which one obtains optimal magnetic properties upon annealing, and to have an alloy of lower magnetostriction.

We used MA to prepare Fe₉₂Al₂Si₆ alloy powders. The as-prepared alloy powders have residual stresses, which have a detrimental effect on the magnetic properties of the alloy. The residual stresses must be eliminated through careful annealing.

In the present study, it is imperative to have accurate measures of the residual stresses and of the crystallite size (more accurately, the size of crystalline domain that diffracts coherently). Most research

to date has deduced these two quantities from an analysis of X-ray diffraction data using the Williamson-Hall method. In this method, for each Bragg reflection, the peak-width-at-half-maximum is plotted as a function of the scattering vector. The crystallite size and residual strain follow from the intercept and slope of a straight line plotted through the data. Figure 1(a) shows that the Williamson-Hall plot is inaccurate because the data have excessive scatter. The problem is that the Williamson-Hall method does not take into account the elastic anisotropy of the crystal, which affects each of the Bragg reflections differently. We used the recent methods of Ungar and co-workers⁴ to calculate the contrast factors, C , needed to take into account the anisotropy. Figure 1(b) shows the modified plot. Here, all the diffraction data fit nicely a straight line. We used this method to analyze the diffraction data as a function of annealing temperature.

Figure 2 shows the crystallite size D , square root of the dislocation density (proportional to the residual strain ε), and coercivity H_c as a function of annealing temperature T_a for 1-h anneals. Each datum is for a different powder aliquot annealed at the stated temperature. The coercivity was measured using a well-calibrated superconducting quantum-interference device (SQUID), which has an accuracy of approximately ± 0.1 Oe. Annealing causes a monotonic decrease in the residual strain and a monotonic increase in the crystallite size. The coercivity, however, first decreases, reaching a sharp minimum for $T_a \approx 450^\circ\text{C}$, and then increases for higher annealing temperatures. Notice the sharp minimum in the coercivity. We detected no phase separation on heating the Fe₉₂Al₂Si₆ alloy up to 600°C . Thus the increase in H_c after annealing above 450°C is due to the increase in D .

Our data demonstrate that in nanostructured materials, the coercivity H_c depends not only on the grain size D (as assumed by earlier theories) but also on the residual stress. This is a new result, as we explain next.

Previous research on the magnetic properties of nanocrystalline alloys addressed the dependence of coercivity on grain size. In an extensively quoted paper, Herzer⁵ proposed an explanation for the often observed decrease in the coercivity, $H_c \propto D^6$, for grain sizes below approximately 30 nm. Guided by this theory, researchers have studied nanostructured ferromagnetic alloys without paying attention to the residual stresses in the alloys. Although the residual

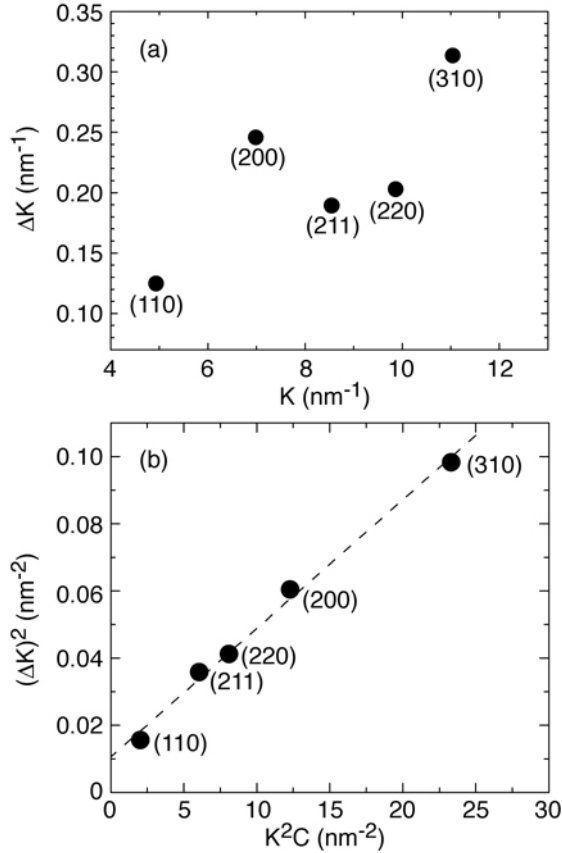


Figure 1. Peak width at half maximum, ΔK , as a function of wavenumber, K , for as-mechanically-alloyed $\text{Fe}_{92}\text{Al}_2\text{Si}_6$ powder: (a) using the Williamson-Hall method, and (b) using contrast-factors, C , according to Ungar [ref. 4].

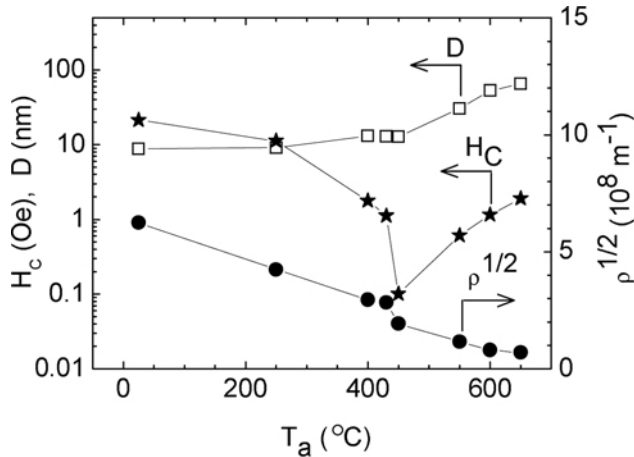


Figure 2. Crystallite size, D , coercivity, H_c , and residual strain, ε , (proportional to the square root of the dislocation density, ρ) in mechanically alloyed $\text{Fe}_{92}\text{Al}_2\text{Si}_6$ powder as a function of annealing temperature. The annealing time is 1 h.

stress is low in rapidly quenched ribbons, it cannot be neglected in alloy powders prepared by mechanical alloying.

The data in Figure 2 suggest two magnetic regimes. For $T_a < 450^\circ\text{C}$, the decrease in coercivity is dominated by the residual stress in the material; and for $T_a > 450^\circ\text{C}$, the increase in coercivity is due to the increase in the crystallite size D .

The residual stress in our nanocrystalline alloys is of two types, *microstress* and *macrostress*. The microstresses are generated by dislocation walls that delimit the crystallite size D . The macrostresses are present because the total stress must average to zero. Because the microstress distribution is dominated by compressive components, the macrostress is dilatational in nature, as we confirmed by X-ray diffraction. Annealing facilitates the motion of the dislocations, leading to dislocation polygonization and/or annihilation. This process decreases both the microstresses and macrostresses.

We have measured the residual microstress and macrostress independently. The *microstress* is proportional to the measured square root of the dislocation density and causes a broadening of the Bragg peaks. The *macrostress* is proportional to the overall lattice expansion, which causes a homogeneous shift of *all* the Bragg peaks versus diffracting angle. Figure 3 shows the macrostress in our Fe-Al-Si alloy powder as a function of annealing temperature. Notice that the macrostress vanishes at an annealing temperature of approximately 500°C . The microstress, deduced from the width of the Bragg peaks, shows a very similar dependence on annealing temperature.

An important result to emerge from this work is that the coercivity correlates with the macrostress and not with the microstress. The reason is that the first Fourier component of the microstress distribution (the most important component) is shorter than the magnetic exchange length, L_{ex} . This is to be expected because the crystallite size is less than 20 nm, whereas L_{ex} is about 30 nm. Thus the motion of the magnetic Bloch walls is impervious to the presence of the random short-range microstresses. The domain walls do interact with the long-ranged macrostresses. Therefore, to obtain a magnetically soft nanocrystalline material, one has to first and foremost anneal out the macrostresses. However, the annealing temperature cannot be increased too much. Indeed, the data in Figure 2 show that annealing above 450°C causes an increase in the crystallite

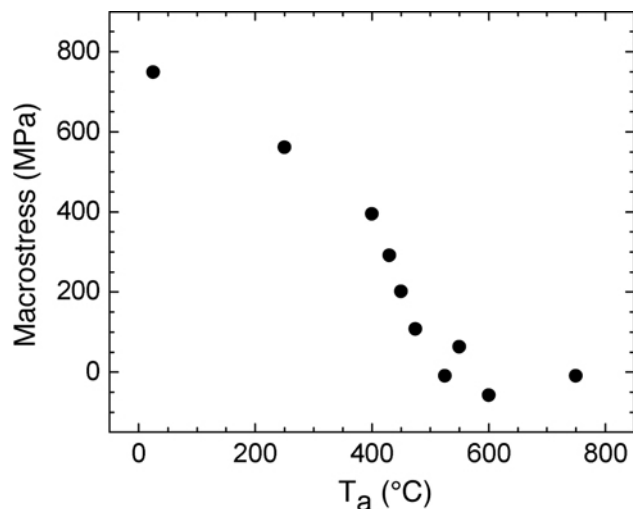


Figure 3. Macrostress in mechanically alloyed $\text{Fe}_{92}\text{Al}_2\text{Si}_6$ powder as a function of annealing temperature. The annealing time for each sample was 1 h.

size D . When D becomes comparable in size to L_{ex} , then the coercivity increases rapidly because now the range of the microstresses becomes comparable to L_{ex} . Then the coercivity increases proportionally to D^6 , as predicted by the random anisotropy model.^{5,6}

Magnetic Properties of Consolidated Nanocrystalline Ferromagnetic $\text{Fe}_{92}\text{Al}_2\text{Si}_6$ Alloy Powder

The mechanically alloyed $\text{Fe}_{92}\text{Al}_2\text{Si}_6$ powder was consolidated by spark-plasma-sintering at UC-Davis. In this technique, the powder is first cold pressed to about 300 MPa and heated to approximately 700°C. A series of current pulses are then sent through the compressed powder. The current heats preferentially the contact points between the particles, accelerating the sintering process. The consolidated disks were approximately 90% dense.

The consolidated disks were cut (at Los Alamos National Laboratory) to prepare small toroid-shaped specimens. Primary and secondary solenoids were added to the toroids to create small transformers on which to measure magnetic properties.

Figure 4 shows the B-H curve for such a toroid. The saturation magnetization is approximately 1.6 T, and the coercivity is approximately 4 Oe. The coercivity, although low compared with that of any ferromagnetic powder prepared by MA, is still too high for it to be used in ferromagnetic cores of low-loss transformers and motors. We attribute the finite co-

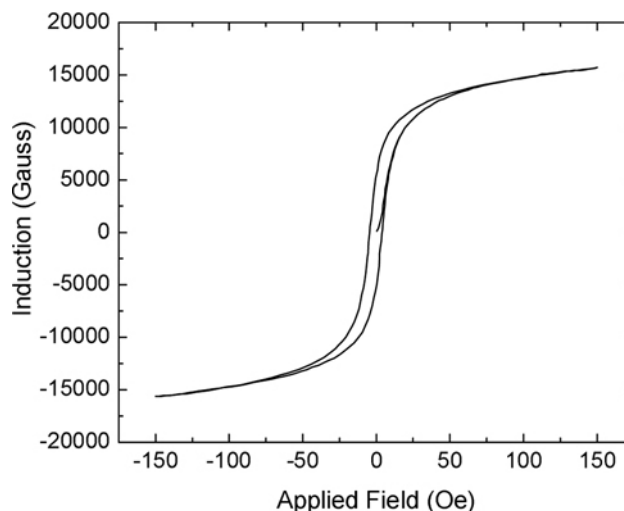


Figure 4. Induction, B , as a function of applied field, H , in a toroid-shaped sample made from $\text{Fe}_{92}\text{Al}_2\text{Si}_6$ powder. The toroid was cut from a bulk disk made by consolidating the powder using spark-plasma-sintering at UC-Davis.

ercivity to the presence of macrostresses introduced during the consolidation process. These macrostresses have not been reduced by annealing. In addition, during the consolidation at 700°C, the grain size grows to above 100 nm.

Future Research

1. Optimize the temperature used during the spark-plasma-sintering consolidation to minimize the grain growth.
2. Study the influence of post-annealing on reducing the macrostresses introduced during consolidation.
3. Optimize the composition of the Fe-Al-Si to minimize the magnetostriction and magneto-crystalline anisotropy.
4. Study the magnetic properties of two-phase materials consisting of $\text{Fe}_{92}\text{Al}_2\text{Si}_6$ powder with nanosize grains and a ferromagnetic “glue” consisting of an amorphous ferromagnetic alloy with a glass transition temperature lower than 450°C. The $\text{Fe}_{92}\text{Al}_2\text{Si}_6$ alloy should provide a high saturation magnetization, whereas the amorphous phase will deform during sintering, closing the gaps and producing a fully dense ferromagnetic alloy.

Acknowledgment

This work was supported by the DOE Office of FreedomCAR and Vehicle Technologies.

References

1. U.S. Department of Energy, "Annual Energy Review 2001," from www.eia.doe.gov.
2. A. Kojima, H. Horikiri, Y. Kamamura, A. Makino, A. Inoue, and T. Matsumoto, "Production of Nanocrystalline bcc Fe-Nb-B Bulk Alloys by Warm Extrusion and Their Magnetic Properties," *Mater. Sci. Eng. A* **179/180**, 511 (1994).
3. Y. Yoshizawa, S. Oguma, and K. Yamauchi, "New Fe-based Soft Magnetic Alloys Composed of Ultrafine Grain Structure," *J. Appl. Phys.* **64**, 6044 (1988).
4. T. Ungar, I. Dragomir, A. Revesz, and A. Borbely, "The Contrast Factors of Dislocations in Cubic Crystals: The Dislocation Model of Strain Anisotropy in Practice," *J. Appl. Cryst.* **32**, 992 (1999).
5. G. Herzer, in *Handbook of Magnetic Materials*, vol. 10, ed. K. H. J. Buschow, Elsevier Science B. V., Amsterdam, 1997, chap. 3.
6. G. Herzer, "Grain Size Dependence of Coercivity and Permeability in Nanocrystalline Ferromagnets," *IEEE Trans. Magn.* **26**, 1397 (1990).

Publications and Presentations

T. Li, F. Grignon, D. J. Benson, K. S. Vecchio, E. A. Olevsky, F. Jiang, A. Rohatgi, R. B. Schwarz, and M. A. Meyers, "Modeling the Elastic Properties and Damage Evolution in Ti-Al₃Ti Metal-Intermetallic Laminate (MIL) Composites," *Mater. Sci. and Eng. A* **374**, 10–26 (2004).

R. B. Schwarz, "Synthesis and Properties of Ferromagnetic Bulk Metallic Glasses," MST Division Seminar, Argonne National Laboratory, November 7, 2003.

R. B. Schwarz and T. Lillo, "Metal-Intermetallic Composites Prepared by Melt Reaction Synthesis," presented at the Workshop on Ceramics Ductilization, Los Alamos National Laboratory, November 15–18, 2004.

R. B. Schwarz and T. D. Shen, "High-Strength, High Conductivity Bulk Nanostructured Alloys," invited presentation at the Symposium on Processing and Properties of Structural Nanomaterials, 2003 TMS Fall Meeting, Chicago, November 9–12, 2003.

R. B. Schwarz, T. D. Shen, U. Harms, and T. Lillo, "Soft Ferromagnetism in Amorphous and Nanocrystalline Alloys," *Journal of Magnetism and Magnetic Materials* **283**, 223–230 (2004).

R. B. Schwarz, T. D. Shen, T. Lillo, G. D. Zhan, and A. K. Mukherjee, "Soft Ferromagnetism in Nanocrystalline Alloys," invited presentation at the 10th International Symposium on Metastable, Mechanically Alloyed and Nanocrystalline Materials (ISMANAM 2003), Foz do Iguacu, Brazil, August 22–26, 2003.

T. D. Shen, U. Harms, and R. B. Schwarz, "Bulk Fe-based Metallic Glass with Extremely Soft Ferromagnetic Properties," *Materials Science Forum* **386–388**, pp. 441–446 (2002).

Awards

R. B. Schwarz was awarded the Von Humboldt Research Award for Senior U.S. Scientists for his research and teaching and was awarded the ISMANAM Medal for research in amorphous and nanocrystalline crystals at the International Symposium on Metastable, Mechanically Alloyed, and Nanocrystalline Materials.

D. Equal Channel Angular Extrusion Processing of Alloys for Improved Mechanical Properties

Principal Investigator: Thomas M. Lillo

Idaho National Engineering and Environmental Laboratory

MS2218, P.O. Box 1625, Idaho Falls, ID 83415-2218

(208) 526-9746; fax: (208) 526-4822; e-mail: tml@inel.gov

Technology Development Area Specialist: Sidney Diamond

(202) 586-8032; fax: (202) 586-1600; e-mail: sid.diamond@ee.doe.gov

Field Technical Manager: Philip S. Sklad

(865) 574-5069; fax: (865) 576-4963; e-mail: skladps@ornl.gov

Contractor: Idaho National Engineering and Environmental Laboratory

Contract No.: DE-AC07-99ID13727

Objective

- Investigate equal channel angular extrusion (ECAE) as a deformation processing technique to improve material properties such as strength, formability, fatigue, and corrosion.
 - Apply ECAE processing to produce advanced, lightweight materials with enhanced formability, higher strength-to-weight ratio, and higher stiffness, ultimately leading to reductions in vehicle weight and thus more fuel-efficient vehicles.

Approach

- Assess the effects of ECAE processing parameters on the mechanical properties of a magnesium alloy (ZK60A) and an aluminum metal matrix composite (MMC) (AL6061+B₄C). Both are lightweight alloys with potential for use in lightweight structural applications in vehicles.
- Determine the optimum ECAE processing schedule for the maximum increase in mechanical properties.
- Characterize the microstructure and mechanical properties of the ECAE-processed material.
- Use microstructure and mechanical properties data to model the flow stress of materials processed with ECAE.

Accomplishments

- ECAE-processed five billets of ZK60A using new ECAE processing schedules and temperatures.
 - CAE-processed eight billets of AL6061 + 10 wt% B₄C using new ECAE processing schedules and temperatures.
- Characterized microstructure and mechanical properties of ECAE-processed AL6061+10 wt% B₄C.
 - Improved ductility (>10% in some cases) and increased the modulus of elasticity from 70 GPa to over 85 GPa, and in some cases >100 GPa, of AL6061+10 wt% B₄C.
- Performed strain rate jump tests on ECAE-processed ZK60A to determine superplastic behavior.
 - Characterized the microstructure of various ECAE-processed and annealed brasses using orientation imaging microscopy (OIM) in support of flow-stress modeling work.

Future Direction

- Complete the superplastic behavior study of ECAE-processed ZK60A.
 - Understand the variation in elastic modulus and tensile strength of MMCs with ECAE processing parameters through further ECAE processing, microstructural characterization, and mechanical testing.
 - ECAE process an AL6061+ 20wt% B₄C MMC, as well as other MMCs, and evaluate mechanical properties to demonstrate the universal improvement in the mechanical properties associated with ECAE processing.
 - Determine the modifications in ECAE die design and ECAE furnace design to ECAE process titanium-based MMCs.
 - Continue ECAE processing, characterization of microstructure, and characterization of mechanical properties in support of flow-stress modeling.

Introduction

Over the past years, this ECAE program has studied ECAE processing (Figure 1) of a wide variety of materials, from pure metals to alloys and MMCs. Initially it was surmised that ECAE processing might be a method of producing bulk nano-crystalline materials through grain refinement

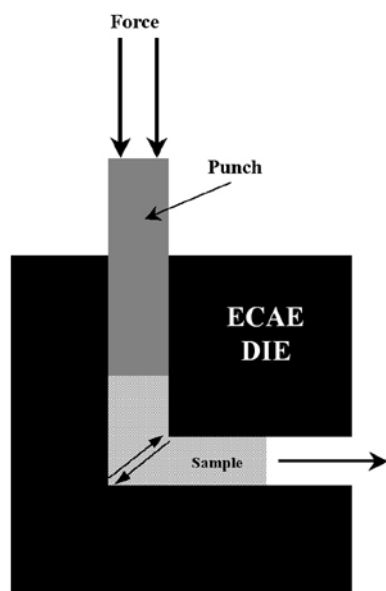


Figure 1. Schematic of ECAE processing.

associated with intense plastic deformation. Microstructural development and mechanical properties were tracked as a function of ECAE processing parameters such as processing route (Figure 2), number of passes through the ECAE die, processing temperature, and the level of back

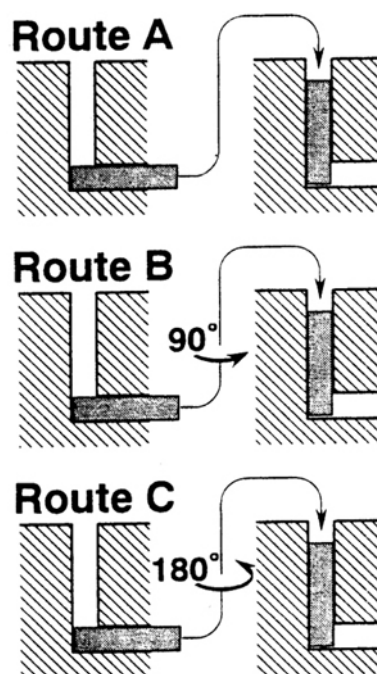


Figure 2. Schematic illustrating sample rotation between subsequent passes through the ECAE die.

stress during processing. A nano-crystalline grain size was difficult to obtain in most materials. Typically, the grain size stabilized after relatively few (4–10) passes through the ECAE die at a value determined by the metal or alloy being processed and the ECAE processing temperature. Although this grain size was generally sub-micron, it was not nano-crystalline (≤ 100 nm). Furthermore, the grain boundary structures were not in stable equilibrium; and the property improvements exhibited by ultra-fine-grain materials made by other methods were not realized in ECAE-processed materials.

However, most materials exhibited significant improvements in their mechanical properties as a result of ECAE processing with a subsequent annealing procedure. One example with potential lightweight vehicle applications was a commercial magnesium alloy ZK60A (Mg-5% Zn-0.5% Zr). During FY 2003, it was found that, with the appropriate combination of ECAE parameters, ZK60A could be ECAE-processed to a final grain size of 1–2 μm . Alloys in this grain size range have been known to exhibit superplastic behavior. A subsequent superplastic study of this ECAE-processed material showed elongations of >200% at 200°C and a strain rate of $10^{-3}/\text{sec}$. Since this was a first attempt, part of the focus during FY 2004 was to optimize the ECAE-processing schedule to obtain superplasticity at higher strain rates.

Another material found to benefit from ECAE processing was an experimental MMC, AL6061 with 10 wt% B_4C particles, obtained from Dynamet Technologies. Dynamet desires to develop lightweight materials with high stiffness for structural applications. The composite was made by powder metallurgy techniques and suffered from very low ductility (virtually zero) and little enhancement to the stiffness over commercial AL6061. However, elongations as high as 10% and improvements to the stiffness (>10%) were found after ECAE processing. The elastic modulus (~80 GPa) was still significantly below the theoretical value of ~110 GPa.

Again, since this was a first attempt, a portion of FY 2004 was devoted to exploring the optimization of ECAE processing to obtain greater improvements in the mechanical properties of this composite. Furthermore, work on this alloy will be useful in the processing of titanium MMCs that have greater application for lightweight, high-strength structural applications. Titanium MMCs will require modifications to the ECAE die and furnace, so the AL6061 composite is used to demonstrate proof-of-principle.

Work in support of the effort to model the flow stress of metals and alloys also continued during FY 2004. ECAE processing produces very fine-grain-size materials—finer than previously obtained by rolling, for instance. Determination of the relationship between flow stress and grain size at very small grain sizes aids in the elucidation of flow stress behavior. The data will eventually be integrated into a model capable of predicting grain size development and the resulting mechanical

properties of thermomechanically-processed materials.

Previous flow stress modeling work raised issues of the effect of stacking fault energy on the flow stress behavior. To answer these questions, various brasses, ranging from 30 to 5% Zn, with widely varying stacking fault energies, were ECAE-processed and annealed to obtain a wide range of grain sizes. The microstructure was analyzed during FY 2004, and the flow stress behavior of these materials was determined and related back to the developing flow stress model.

ECAE Processing of Magnesium Alloys

Previously, commercial-grade ZK60A (Mg-5% Zn-0.5% Zr) was ECAE-processed using three different sets of parameters:

- Four passes by the B-route at 260°C and no applied back stress
- Four passes by the B-route at 150°C and 18.3 ksi back stress
- Six passes by the B-route at 150°C and 18.3 ksi back stress

The results of the superplastic study on these samples seemed to indicate that lower ECAE temperatures and more passes through the die correlated with improvements in superplastic behavior. Therefore, new ECAE processing schedules, incorporating these insights, were devised. Specifically, billets were processed according to Table 1.

Table 1. ZK60A ECAE processing schedules

Sample	Initial billet condition	ECAE temperature (°C)	ECAE route	Back stress level, ksi
1	T5	150	8B	15.1
2	T5	150	2B	15.1
		135	1B	15.1
		120	1B	19.7
3	T5	150	2B	15.1
		130	4B	15.1
4	Solution treated	200	2B	10.6
		150	6B	21.2
5	T5	150	2A	15.1

Sample 1 explored the effect of the number of passes through the ECAE die on superplastic behavior; Sample 2 looked at ECAE processing temperature; and Sample 3 was processed with a combination of both variables. Sample 4 attempted

to look at the effect of precipitation from solid solution *during* ECAE processing, and Sample 5 was to evaluate the uniformity of strain in the billet.

At this time, tensile bars have been made and strain rate jump tests performed at 180, 225, 250 and 275°C on Samples 1–4. The strain rate sensitivity factor, m , was calculated from:

$$m = \log(\sigma_2/\sigma_1)/\log(\dot{\epsilon}_2/\dot{\epsilon}_1), \quad (1)$$

where $\dot{\epsilon}$ was the strain rate, σ was the flow stress and the subscripts 1 and 2 referred to the values before and after the strain rate jump, respectively. The m factors are plotted in Figure 3 as a function of strain rate for the test temperatures. (The strain rates in the plots are taken as the average of the strain rate before and after the strain rate jump.) Superplastic behavior is associated with m values near 0.5. At 250 and 275°C, all samples behaved similarly, and presumably rapid grain growth out of the superplastic regime was occurring. At the two lower temperatures (180 and 225°C), only sample 4 showed significantly different behavior across the strain rates investigated. Sample 4 exhibited $m \approx 0.5$ around a strain rate of $\sim 10^{-2} \text{ sec}^{-1}$ at 225°C. The other samples exhibited $m \approx 0.5$ only at very low strain rates at all temperatures studied. Sample 4 was ECAE-processed in the solutionized state, and precipitation occurred during processing and possibly during testing to produce the different superplastic behavior. Microstructural examination of Sample 4 will be performed to try to assess the effect of ECAE processing on precipitation. Finally, samples will be tested using the most promising combination of temperature and strain rate to determine the maximum elongation possible.

It was also demonstrated during FY 2003 that a modified version of ZK60A (with additions of cerium and yttrium), provided by Daniel Schechtmen at NIST, demonstrated even better superplastic behavior than commercial ZK60A.

Once the optimum ECAE processing schedule is developed and superplastic parameters (temperature and strain rate) are determined for commercial ZK60A, they will be applied to the modified ZK60A and the resulting superplastic behavior documented.

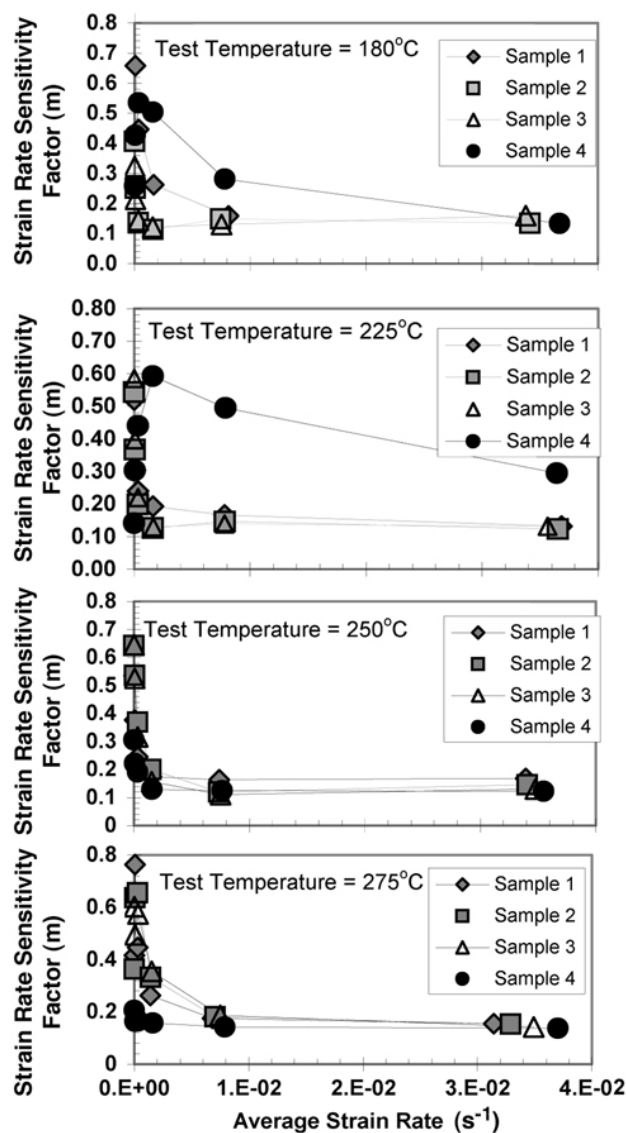


Figure 3. Strain rate sensitivity of ECAE-processed ZK60A at 180 and 225°C.

These preliminary results suggest that it might be possible to develop a high-strain-rate superplastic magnesium alloy. This would facilitate the use of magnesium alloys in automotive applications. Superplastic forming would minimize fabrication waste for this relatively expensive alloy, making it more economically competitive with traditional iron-based materials. High-strain-rate superplastic forming also offers the potential for rapid fabrication, resulting in higher productivity and making this alloy more competitive with conventional materials of construction. Ultimately, vehicles incorporating magnesium alloys would be lighter

than those that rely on traditional alloys, and therefore more fuel-efficient.

ECAE Processing of Aluminum Alloy Composites

Additional billets of prototype MMCs were purchased from Dynamet Technology. The material consisted of an AL6061 matrix with boron carbide particles (~50 μm in dia-meter on average) present at a level of either 10 or 20 wt %. Additions of B_4C particles increase the stiffness of the AL6061 matrix, making it more suitable for use in lightweight structural applications by reducing the deflection under load. The material was fabricated by powder metallurgy methods and contained agglomerates of boron carbide particles. During FY 2003, it was found that the B_4C particles appeared to be concentrated around prior aluminum alloy powder particles. The interface between adjacent B_4C particles was very weak and acted as a defect during tensile loading, causing premature fracture. The elongation/ductility of these composites was negligible in the as-received state.

During FY 2003, it was found that considerable increases in density, elongation, and elastic modulus could be realized through ECAE processing. Relatively high ECAE processing temperatures closed residual porosity, while lower ECAE processing temperatures eliminated poorly bonded particle/particle interfaces (i.e., dispersed the particles in the agglomerates). Therefore, during the first half of FY 2004, ECAE processing schedules were devised that incorporated initial passes at relatively high temperatures (~300°C) to close porosity, followed by subsequent passes at lower temperatures ($\leq 150^\circ\text{C}$) to disperse B_4C agglomerates.

The specific schedules used are shown in Table 2. The ECAE-processed billets remained intact and were free of cracks and other flaws commonly found in ECAE-processed materials of low ductility. Tensile bars were prepared from each billet and oriented parallel to the ECAE direction.

The density of each tensile bar was determined by the Archimedes principle, and the average density is shown in Table 3. ECAE processing significantly increased the density (~3.5%), but full density still was not achieved. There also is very little difference in density between the different ECAE processing routes.

Table 2. Processing schedules for AL6061+10wt% B_4C

Sample	Initial condition	ECAE temperature ($^\circ\text{C}$)	ECAE route	Back stress (ksi)
B3528-1	T0	300	2A	10.6
		150	4B	22.7
B3528-8	T0	300	2A	10.6
		150	4A	22.7
B3528-10	T0	300	2B	10.6
		150	4B	22.7

Table 3. Effect of ECAE processing on density

Sample	Average density (grams/cm ³)	Relative density ^a (%)
As-received	2.55	94.9
B3528-1	2.64	98.1
B3528-8	2.64	98.1
B3528-10	2.65	98.5

^aThe theoretical density was taken as 2.69 g/cm³, based on a rule-of-mixtures calculation

The tensile bars were heat treated to either the T4 (solid solution) or T6 (optimum aging treatment) condition. (The samples were heat treated to remove the grain size refinement due to ECAE processing. Only the effect of ECAE processing on the B_4C particulate was of interest at this time.) Two tensile tests for each heat treatment condition were run at room temperature for each billet. The results are shown in Table 4. Significant increases in all properties resulted from ECAE processing compared with the as-received material, B3528 AR. Generally, the ductility in the T4 condition is greater than in the T6 condition (~9% vs. ~3%, respectively); but both are much greater than in the as-received material, which exhibited virtually no ductility. The yield and ultimate tensile strength (UTS) increased by more than 30% and 50%, respectively, with the UTS in some cases almost doubling that of the as-received material. The ECAE-processed materials also showed an increase in the yield and ultimate strengths, ~15% and ~5%, respectively, over commercial AL6061 (without B_4C reinforcement). The elastic modulus also increased and, in one case, Sample B3528 1-2, approached the theoretical value (~110 GPa) as calculated by the rule-of-mixtures. Overall, billet B3528-10 exhibited slightly better mechanical properties than billets ECAE-processed by other schedules, although the differences were not great.

Table 4. Mechanical properties of ECAE-processed AL6061+10wt% B₄C

Heat treatment	Specimen ID	Modulus (GPa)	Yield strength (MPa)	UTS (MPa)	Elongation (%)	RA (%)
T4	B3528 1-2	115	158	248	9	10
	B3528 1-6	73	161	208	3	5
	B3528 8-2	59	140	198	3	4
	B3528 8-6	69	161	249	8	10
	B3528 10-2	94	163	260	9	11
	B3528 10-6	97	170	268	7	5
	B3528 AR	56	117	129	0.8	0
	B3528 1-1	75	326	337	2	4
	B3528 1-5	88	N/A	314	0.2	2
	B3528 8-1	59	279	298	1.6	1
T6	B3528 8-5	80	325	331	1.3	2
	B3528 10-1	73	333	351	3	6
	B3528 10-5	83	340	356	3.7	7
	B3528 AR	71	N/A	193	0	0

Although increases in the mechanical properties are observed *on average*, significant variability was observed in specimens from the same billet with the same heat treatment. This condition, most likely, arose from remaining B₄C particle/particle weak interfaces and residual porosity.

The ECAE-processed microstructures were significantly different from the as-received material. Figure 4 compares the microstructures of the as-received and sample B3528-1. The micrographs were taken from samples in the T4 condition and were perpendicular to the extrusion axis. The as-received material had more B₄C agglomerates and voids within the agglomerates (at the arrows in Figure 4a) compared with ECAE-processed material (Figure 4b). Smaller agglomerates and a reduced number of voids were found in the ECAE-processed material. The B₄C particles also were more evenly distributed throughout the material compared with the as-received sample. These factors undoubtedly contributed to the observed increase in mechanical properties. The microstructures of the other ECAE-processed samples showed similar results and indicated the ECAE processing route had little influence on the microstructure. Only the number of passes seemed to significantly affect the boron carbide particle distribution.

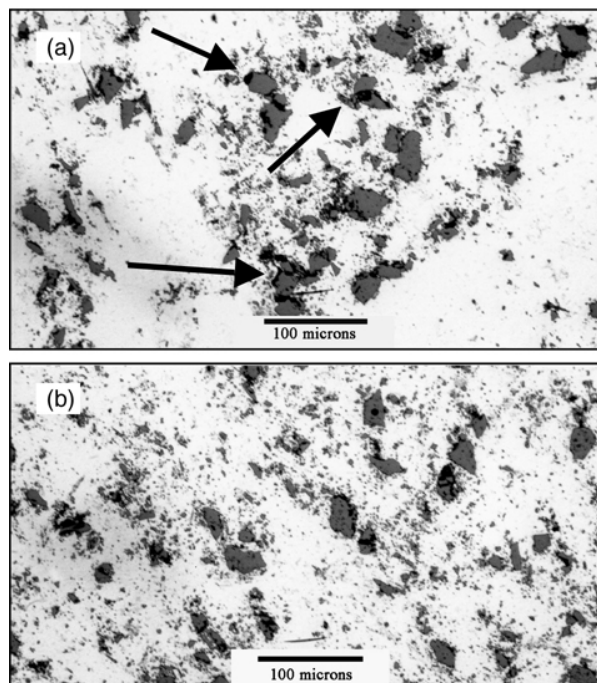


Figure 4. Microstructure of AL6061+ 10 wt% B₄C of the (a) as-received and (b) B3528-1 in the T-4 condition.

Overall, the tensile results in FY 2004 confirmed the preliminary findings obtained in FY 2003 that ECAE can be used to significantly increase the mechanical properties of these MMCs. However, resid-

ual porosity and weak particle/ particle interfaces still existed even after ECAE processing with the new processing schedules. These defects, although greatly reduced, are still thought to adversely affect the mechanical properties. Therefore, new schedules were developed to further reduce residual porosity and eliminate B₄C agglomerates and weak B₄C particle/particle interfaces. Specifically, additional passes were added to the end of those outlined in Table 2 to further redistribute the particles and close any porosity generated during the low-temperature passes through the ECAE die. The elastic modulus was evaluated after various passes using ultrasonic methods. After the fourth pass, very little change in the elastic modulus was observed even up to a total of 8 passes. The elastic modulus stabilized at ~ 80–85 GPa, which is still significantly lower than theoretical for this composite (~110 GPa). Tensile samples will be tested early in FY 2005. The mechanical properties of material processed by simplified ECAE processing schedules (only 4 passes through the ECAE die) also will be determined in early FY 2005 for comparison with previous results. Heat treatment of the ECAE-processed material to promote better bonding of the B₄C particles to the AL6061 matrix will be explored. The goal is to increase the elastic modulus to near theoretical values. Preliminary exploration of titanium MMCs will begin after these experiments and mechanical testing.

ECAE processing of MMCs still appears to have the greatest potential for improving mechanical properties. The improved fabricability of ECAE-processed MMCs may enable the use of these lightweight, high-stiffness materials in more transportation applications for increased fuel efficiency.

Modeling Flow Stress

Brasses with 5%, 10%, or 30% zinc were ECAE processed during FY 2003 and then analyzed during the first half of FY 2004 for microstructure and mechanical properties. The goal is to relate the difference in stacking fault energy with the flow stress behavior. Tensile samples were annealed for 1 hour at 300, 400, and 600°C. Obvious differences in the room-temperature flow stress behavior between the different brasses were found (Figure 5).

Samples were prepared from the failed tensile bars and sent out for OIM and analysis. Among other things, OIM analysis revealed that samples

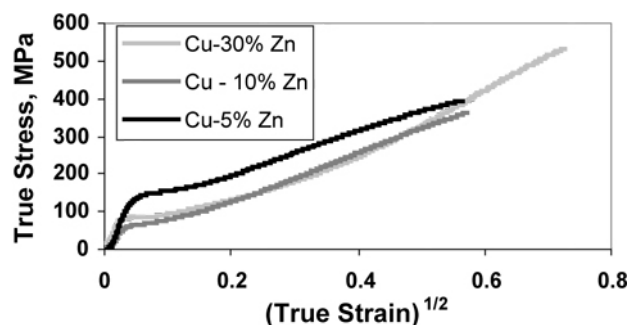


Figure 5. Flow stress behavior of various brasses ECAE-processed and annealed at 600°C for 1 hour.

BR16–1 and –2 were not fully recrystallized; the result was low $\Sigma 3$ (twin) grain boundary fraction for these samples (Table 5). OIM analysis also revealed that the grain size at a given annealing temperature is influenced by the zinc content—the grain size increases with increasing zinc content. All fully recrystallized samples have a high twin grain boundary fraction (>50%). The OIM data will be combined with the tensile data and analyzed for the flow stress model under development.

The OIM data also revealed one other noteworthy result. The $\Sigma 3$ grain boundary content for Br2C-14 (700°C, 1 hour) was significantly lower than expected (Table 5). A closer look at the OIM data revealed a fairly high fraction (~28%) of low-angle grain boundaries. Mapping of the low-angle grain boundaries revealed they were mainly associated

Table 5. OIM analysis results for ECAE-processed and annealed brasses

Sample	Description	Grain-size	$\Sigma 3$ fraction	Total CSL fraction
BR16	Cu-5Zn			
-1	300°C	0.46	0.210	0.240
-2	400°C	0.70	0.361	0.410
-3	600°C	1.44	0.699	0.752
BR17	Cu-10Zn			
-1	300°C	0.57	0.561	0.634
-2	400°C	0.89	0.574	0.621
-3	600°C	11.77	0.593	0.605
BR2C	Cu-30Zn			
-7	400°C	1.73	0.488	0.526
-12	500°C	7.63	0.514	0.529
-8	600°C	20.83	0.592	0.611
-14	700°C	53.24	0.398	0.406

with twin grain boundaries (Figure 6). Three low-angle boundaries associated with twins are shown at the arrows, as examples. The low-angle grain boundaries ($<10^\circ$) are shown in white. The grain boundaries near these low-angle grain boundaries no longer have a twin orientation. Therefore, it would appear that annealing at 700°C leads to the breakup of twin boundaries in this material. This also is shown by Figure 7, where the tolerance for what is considered a twin grain boundary has been varied. Twin boundaries in black represent deviations of up to about 8.7° , while those in white are within 2.9° of the exact twin orientation. For Br2C-8 (600°C , 1 hour), nearly all of the twin boundaries are within 2.9° of the exact twin orientation (Figure 7b), while the twin grain boundaries in the sample annealed at 700°C show relatively large deviations from the exact twin orientation (Figure 7a).

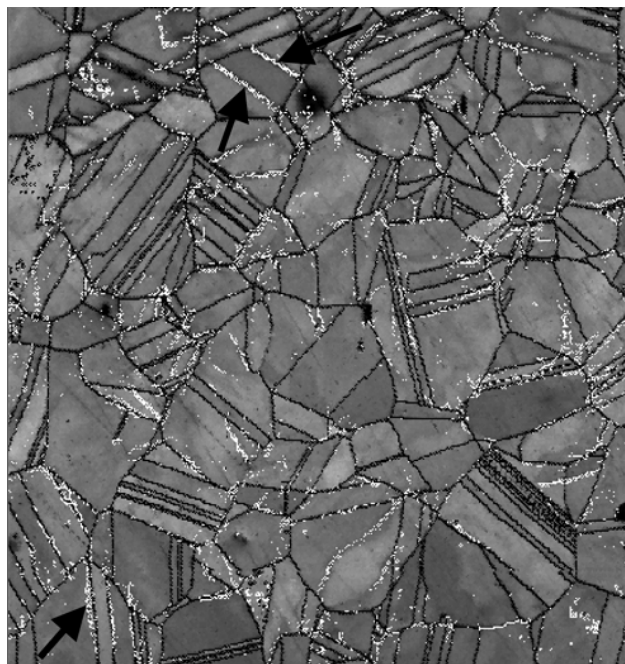


Figure 6. OIM image showing the low-angle grain boundary structure (white lines) in Cu-30% Zn sample annealed at 700°C for 1 hour.

This may provide evidence of twin grain boundaries acting as preferential dislocation sources. Decomposition of twin boundaries at high temperatures leaves behind a low-angle grain boundary and a grain boundary with a misorientation different from the original twin orientation.

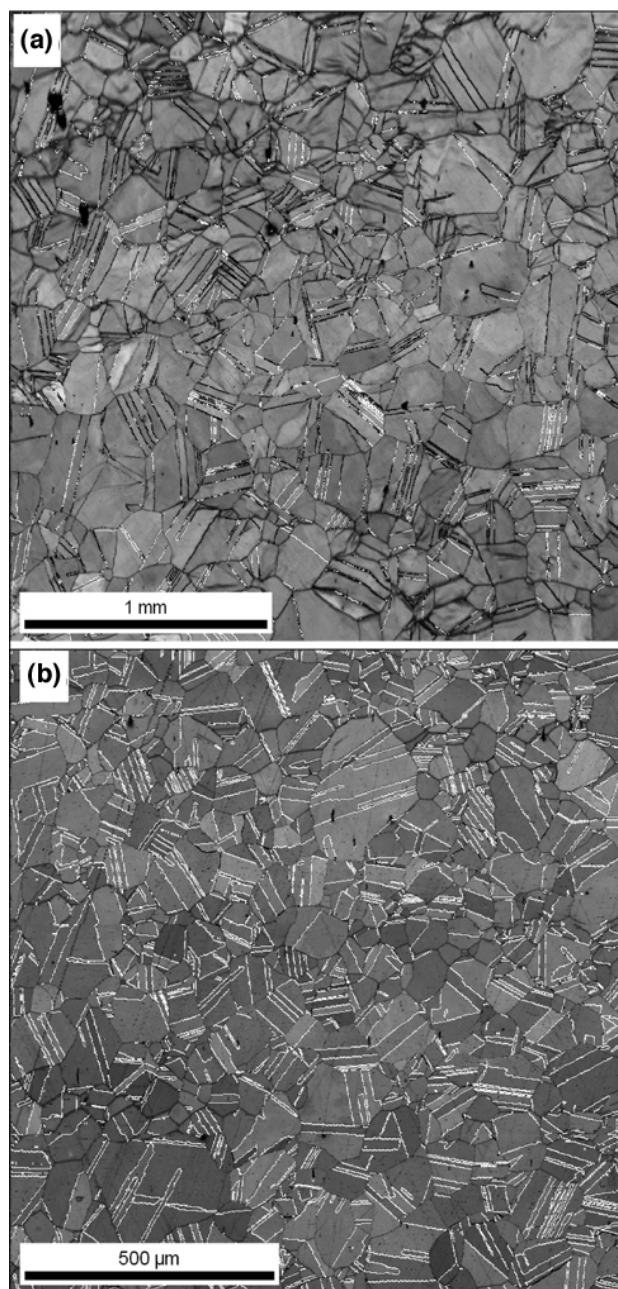


Figure 7. The Cu-30% Zn sample annealed at 700°C (a) exhibits twin boundaries that deviate up to about 9° from the exact twin boundary orientation (black boundaries). Annealing at 600°C (b) results in twin boundaries that deviate by $\leq 3^\circ$ from exact coincidence (white boundaries).

This would support past findings that the flow stress correlates with the twin grain boundary density, implying that twin boundaries act as dislocation sources during deformation. Further analysis of this sample to confirm this finding is under way. The

findings will be published in a peer-reviewed journal.

Conclusions

During FY 2004, work focused on developing ECAE processing schedules to optimize mechanical properties. Billets of a commercial magnesium alloy, ZK60A, have been ECAE processed by five new processing schedules. Preliminary superplastic studies show that the processing schedules may potentially yield a lightweight material capable of high strain rate superplasticity. Such a material will be more economically competitive (high production rate coupled with minimal scrap) with other traditional structural materials such as steel. Considerable weight savings and increased fuel efficiency could be realized by using magnesium alloys in place of iron-based materials.

ECAE processing also appears to be a means of improving the mechanical properties of MMCs. The proper combinations of ECAE processing temperatures, back stress, and the number of passes through the ECAE die result in MMCs with better strength, ductility, and elastic modulus. The elastic modulus is still significantly lower than the theoretical value, and microstructural studies indicate residual porosity, both suggesting that further improvements can be made with optimized ECAE processing schedules. Increased ductility afforded by ECAE process

ing offers the potential for improved fabricability and wider application of MMCs. Lightweight, high-stiffness MMCs may then be employed as structural members in transportation applications, leading to more fuel-efficient vehicles.

Publications and Presentations

S. R. Agnew, J. A. Horton, T. M. Lillo, D. W. Brown, "Enhanced Ductility in Strongly Textured Magnesium Produced by Equal Channel Angular Extrusion," *Scripta Mat.*, **50**, 377–381 (2004).

D. P. Field, M. M. Nowell, P. Trivedi, S. I. Wright, and T. M. Lillo, "Local Orientation Gradient and Recrystallization of Deformed Copper," accepted for publication in *Proceedings of the International Conference on Textures and Anisotropy of Polycrystalline Materials*.

D. P. Field, B. W. True, T. M. Lillo, J. E. Flinn, "Observation of Twin Boundary Migration in Copper During Deformation," accepted for publication in *Materials Science and Engineering A*, 2004.

M. M. Nowell, D. P. Field, S. I. Wright, and T. M. Lillo, "In-Situ EBSD Investigation of Recrystallization in ECAE Processed Copper," *Mater. Sci. Forum*, **467–470**, 1401–1406 (2004).

R. B. Schwarz, T. D. Shen, U. Harms, and T. Lillo, "Soft Ferromagnetism in Amorphous and Nanocrystalline Alloys," *Journal of Magnetism and Magnetic Materials*, **283**, 223–230 (2004).

E. Development of an Advanced Squeeze Casting Process for the Production of High-Integrity Truck Components

Principal Investigator: David C. Weiss

Eck Industries, Incorporated

1602 North 8th Street, Manitowoc, WI 54221-0967

(920) 682-4618; fax: (920) 682-9298; e-mail: dweiss@eckindustries.com

Technology Development Area Specialist: Sidney Diamond

(202) 586-8032; fax: (202) 586-1600; e-mail: sid.diamond@ee.doe.gov

Field Technical Manager: Philip S. Sklad

(865) 574-5069; fax: (865) 576-4963; e-mail: skladps@ornl.gov

Contractor: Eck Industries, Incorporated

Contract No.: 4000022893

Objective

- Develop the equipment and process technology for an advanced squeeze casting (ASC) process to enable production of high-integrity cast metal components.
 - Integrate the advantages of two casting methods—low-pressure permanent mold and direct squeeze casting—to attain non-turbulent fill of the die, high solidification rates to refine microstructural features, and solidification under pressure to minimize microporosity.
 - Design and build a new kind of casting machine and develop process technologies needed to cast high-integrity truck components from nonferrous alloys.

Approach

- Design and construct a casting machine that integrates a low-pressure metal delivery system suitable for either aluminum or magnesium alloys, reliable gate shut-off technology, and direct application of squeeze pressures of up to 103 MPa (15,000 psi). This machine is intended for production.
- Develop a gate shutoff mechanism that will operate reliably in a production environment.
- Select a casting that will be produced in the casting machine built for this project.
- Use fluid-flow and solidification analysis to predict optimum flow conditions for metal entering the mold and differential squeeze pressure requirements.
- Design and build cast tooling.
- Develop process technologies for the low-pressure/squeeze casting of aluminum alloys and evaluate the effect of various process parameters on casting integrity.
- Apply developed technologies to the production of a selected automotive component.

Accomplishments

- Completed design of ASC machine.
- Reached 80% completion of fabrication of ASC machine.
- Designed and fabricated data acquisition system.
- Designed and fabricated gate shutoff mechanism.

- Designed and fabricated squeeze cast tooling.

Future Direction

- Complete fabrication of ASC machine and install data acquisition system.
 - Install ASC machine at Eck Industries.
 - Integrate operation of gate shutoff mechanism with the casting machine control system.
 - Develop and evaluate ASC process technologies.
 - Demonstrate production viability of ASC casting machine and process.
-

Introduction

Squeeze casting is the solidification of liquid metal under pressure in a closed metal die. The resulting casting has improved properties and a more uniform microstructure compared with those produced by traditional molten metal fabrication techniques. The higher properties are achieved through controlled entry of the metal into the die through large gates, which reduces turbulence, and high solidification rates, resulting in refinement of microstructural features.

There are two squeeze casting methods—direct and indirect. The method and efficiency of pressure application distinguish the two processes. Direct squeeze casting applies pressure directly on the casting. Indirect squeeze casting applies pressure via the gating system. The length of the gating system and any partial solidification prior to complete solidification of the part reduces the magnitude of the pressure applied and may result in casting porosity. For the indirect squeeze cast method, the dimensions of the die cavity control the part dimensions. For direct squeeze casting, the part dimensions are controlled by the die cavity dimensions and the finish position of the top die. Thus the direct squeeze cast method requires precise machine control to attain the desired part dimensions. In addition, the direct method requires in-gate shutoff technology to control pressure during cavity pressurization. Both methods suffer from poor metal handling from the furnace into the mold or gating system. Inadequate control of pouring speed generates turbulence and casting defects, such as oxide inclusions, that reduce fatigue properties.

Earlier attempts to improve the squeeze casting process by combining the advantages of low-

pressure die fill with those of squeeze casting demonstrated substantial mechanical property improvement and reduced component porosity. However, continuous production operation of the equipment was not achieved. The machines used were not specifically designed to meet the needs of the process.

Technical Approach

The results of this project will provide (1) a production-viable ASC machine, (2) process technology that will improve the strength and reliability of cast automotive components, and (3) demonstrated production viability of the equipment and process.

Machine Design. Previous efforts have demonstrated that modification of existing cast machine designs does not provide a production-capable ASC machine. An assessment of the capabilities and limitations of existing machine designs demonstrated that

- Low-pressure casting equipment typically does not have the structural rigidity needed to withstand the high pressures required of squeeze casting.
- Die-casting and currently available squeeze casting machines are not designed for proper (nonturbulent) molten metal entry into the die cavity.
- Neither type of equipment is typically available with the hydraulic and electronic controls necessary to attain the die cavity motions required for the direct squeeze casting process.

After much consideration, the project team decided it was easier and more cost-effective to build a machine from the ground up than to modify an existing cast machine design. To facilitate this design and construction, the team partnered with Empire Castings, Inc., an experienced producer of low-pressure casting equipment.

Process Development. Bendix, Inc. is an industrial manufacturer of truck components with an interest in reducing manufacturing cost by the use of high-quality castings. Consultation with Bendix led to the selection of an air compressor connecting rod for prototype production in the ASC machine. This component has a level of complexity that can demonstrate the production capability of the ASC machine and process and the need for mechanical properties higher than those attainable with commercially available castings, and it provides an opportunity for production with the ASC process.

The cast part will be modeled for fluid flow and solidification. This work will be done in parallel with equipment design. Simulation will provide an understanding of optimum metal flow conditions and squeeze requirements, if any, to contend with solidification shrinkage. This is very important to the success of the program and potentially to the details of the machine design. The ASC machine will have two mechanisms to feed the casting—low-pressure, nonturbulent fill of the die cavity and high-pressure, direct squeeze to minimize solidification shrinkage. Modeling experiments will explore the interaction of the two feed mechanisms and select process parameters that lead to process optimization. Modeling results will be used to refine the die design and select initial casting process parameters.

After tooling construction and ASC machine delivery, castings will be made under the range of process conditions anticipated during modeling. A variety of both cast and wrought alloys (Table 1) will be used. Evaluation of those castings will include radiography, die penetrant inspection, tensile testing, and functional component testing at Bendix. It is anticipated that this part of the program will require multiple iterations to produce the desired product quality. Some equipment and tooling modification may be required during this part of the program.

Table 1. Aluminum alloys to be used for casting trials

AA 380	AA 206
AA 356	AA 6061
AA 357	AA 535
AA 319	AA 388

After successful production of development castings, the production viability of the equipment and process will be demonstrated by

- Production of a connecting rod with reduced porosity and improved mechanical properties compared with the current die-cast connecting rod used by Bendix.
- Continuous production with the ASC machine and connecting rod tooling to include at least one 5-h continuous run with the equipment running at least 3 days in a week.

The goal of the project team is to implement part production on an ongoing basis. The production phase of the project will include detailed cost analysis of part production, determination of die-life parameters, and ongoing equipment and tooling development for maximum uptime.

Program Status

ASC machine. The design (Figure 1) for the 600-ton capacity ASC machine has been completed. Positioning of the top die is accomplished independently of the squeeze-cast cylinder. To maximize machine capability, the melting vessel is equipped with a crucible furnace. This facilitates the melting of both cast and wrought aluminum and magnesium alloys as well as aluminum and magnesium metal matrix composite alloys.

To match the dimensional capabilities of the die-cast process, a closely controlled volume of liquid metal must be fed into the die cavity. Conventional low-pressure fill technology does not have the capability to accurately meter a fixed amount of liquid metal into the die. Therefore, we will accurately position (± 0.13 mm) the top die to obtain the desired fill volume and use a fill sensor and an independently controlled gate shutoff to control metal volume. Development of a reliable gate shutoff technology is a key part of the ex-

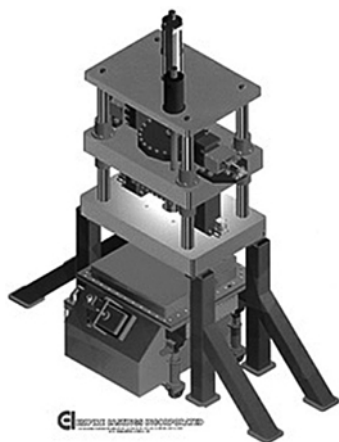


Figure 1. Design for 600-ton ASC machine.

perimental program. Gate shutoff system components are shown in Figure 2.

Data acquisition system. A computerized data acquisition system has been designed to interface with the displacement, pressure, and temperature sensors located on the ASC press and cast tooling. Analysis of these data will be critical in understanding the operation of the ASC process. This system will be installed on the machine in early November.

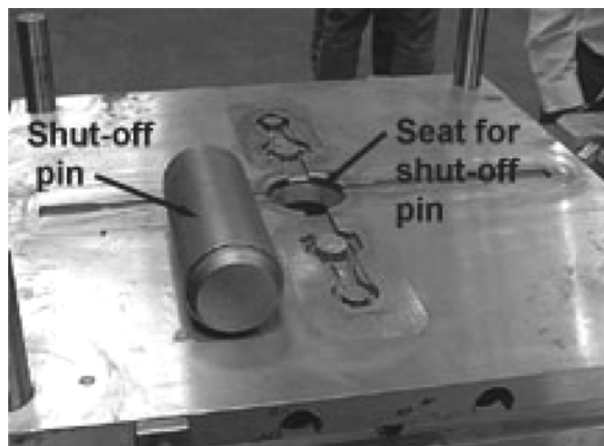


Figure 2. Components of the in-gate shutoff system.

Cast tooling. The die for casting air-compressor connecting rods and tensile test bars has been completed. As shown in Figure 3, the tooling consists of a die holder and individual die inserts for the particular part being cast. This tooling will be used for the machine run-off.



Figure 3. View of cast tooling.

Conclusions

Good progress has been made on the project. The steel shortage and prior commitments of the machine builder delayed press construction by about 6 months. This is reflected in the revised schedule (Table 2). All other tasks of the project are on schedule. The results of casting simulation should decrease the process development time required to the 3 months reflected in the revised schedule.

F. Thermomechanical Processing of Ti and Ti-6Al-4V Sheet and Plate

Principal Investigator: Craig A. Blue

Oak Ridge National Laboratory

Oak Ridge, TN 37831-8063

(865) 574-4351; fax (865) 574-4357; e-mail: blueca@ornl.gov

Field Project Manager: John D. K. Rivard

Oak Ridge National Laboratory

Oak Ridge, TN 37831-8063

(865) 241-8113; fax (865) 574-4357; e-mail: rivardjd@ornl.gov

Technology Development Area Specialist: Sidney Diamond

(202) 586-8032; fax: (202) 586-1600; e-mail: sid.diamond@ee.doe.gov

Field Technical Manager: Philip S. Sklad

(865) 574-5069; fax: (865) 576-4963; e-mail: skladps@ornl.gov

Participants

Evan K. Ohriner, Oak Ridge National Laboratory

David C. Harper, Oak Ridge National Laboratory

Jim O. Kiggins, Oak Ridge National Laboratory

Paul A. Menchhofer, Oak Ridge National Laboratory

Lance Jacobsen, International Titanium Powder, L.L.C.

Dariusz Kogut, International Titanium Powder, L.L.C.

Contractor: Oak Ridge National Laboratory

Contract No.: DE-AC05-00OR22725

Objective

- Investigate and develop vacuum hot pressing (VHP) methods for the production of titanium (Ti) and Ti-6Al-4V plate from Ti and Ti-6Al-4V powder provided by International Titanium Powder, LLC (ITP).
- Simulate a roll compaction method for the manufacturing of Ti and Ti-6Al-4V thin-gage sheet from Ti and Ti-6Al-4V powder provided by ITP.
- Demonstrate the ability to process thin-gage sheet using powder Ti precursor and plasma arc lamp processing.
- Mechanically test Oak Ridge National Laboratory (ORNL)-produced materials
- Optically and chemically analyze ORNL-produced materials.

Approach

- Conduct parametric studies using VHP to consolidate ITP Ti and Ti-6Al-4V powder to demonstrate the feasibility of powder use for further experiments.
- Develop roll compaction techniques for the production of thin-gage Ti and Ti-6Al-4V from ITP powder using infrared (IR) heating from tungsten halogen lamp furnaces and plasma arc lamp.

- Characterize ORNL-produced material properties.
- Develop approach to scaling processing techniques for large-scale production applications.

Accomplishments

- Successfully consolidated ITP Ti and Ti-6Al-4V powder using VHP.
- Developed processing techniques for production of thin-gage sheet using IR heating.
- Evaluated physical, microstructural, and chemical properties of ORNL-produced materials

Future Direction

- Partner with ITP and Ametek to scale process to produce Ti and Ti-6Al-4V sheet and plate at substantially reduced cost using a lab-scale roll compaction process as a basis for commercial processing.
- Partner with Universal Alloy Cooperation to extrude ITP Ti and Ti-6Al-4V rod and plate. Plates up to 40 in. wide can be extruded.

Introduction

The aircraft industry is currently the single largest market for Ti and Ti alloy products primarily because of the exceptional strength-to-weight ratio, elevated temperature performance, and corrosion resistance.

Titanium usage, however, is strongly limited outside the aerospace industry by its higher cost relative to competing materials, primarily aluminum alloys and steels. Although Ti possesses an attractive set of properties, including high specific strength and corrosion resistance, and allows for damage-tolerant design, cost limits applications to selected markets. Many automotive systems would benefit from the use of Ti products. Automotive exhaust systems could save as much as 50% of their current weight by integrating Ti parts. Titanium valves and valve springs, connecting rods, suspension springs, wheels, drive shafts, underbody panels, side impact bars, and half shafts are just some of the automotive applications that could benefit from the use of Ti.

The present market comparison for the use of engineering materials shows that steel is the most widely used material, with 800 million tons used each year. Aluminum, stainless steel, and copper are used at a rate of 22 million tons, 16 million tons, and 12 million tons, respectively. Titanium is much less widely used at 0.05 millions tons per year.

Potential technical problems preventing the integration of Ti, apart from cost of manufacturing, include wear resistance, a lower modulus than steel, and machining difficulties. Wear resistance can be

addressed by coatings/reinforcements; the modulus can be increased by reinforcing the part with a second material; and the machining difficulties can be reduced by the production of near-net-shape parts. The major problem is that Ti costs substantially more than competing materials.

Although the cost of Ti ore is significantly more than that of other competing materials, the difference in the cost of sheet is a result of processing. Processing of Ti from ingot to plate accounts for 47% of the total cost of the material.

Current melting techniques include vacuum arc remelting (VAR), electron beam melting, and plasma arc single-melt processes. VAR is used to clean and refine air-melted ingots and to improve homogeneity and refine grain size. To VAR-cast an ingot, a dc arc is struck between a Ti electrode and a base plate. The intense heat melts the electrode, and the Ti is cast into an ingot. VAR requires 20 hours and large-scale equipment.

Electron beam and plasma arc single-melt processes have the advantage over VAR in that an air-melted ingot is not required. In these two processes, ingots are cast directly from melted feed sponge. But the cast ingot still requires post-processing, which accounts for 47% of the total cost. The plasma arc melt process is similar; plasma arc torches are used in place of electron beams for melting.

Alternative processing methods such as casting, laser forming, and spray forming have also been explored. Casting is best suited for complex shape forming and is not economical for sheet processing. The process requires extensive tooling and frequent

inspections. A post-hot isostatic pressing (HIP) is needed to eliminate porosity. Laser forming uses a raw powder stream injected into a rastered laser beam to melt, form, and build up sheet. Spray forming operates similarly, although a plasma torch melts the powder. Laser forming and spray forming have the advantages of using less material, requiring minimal tooling, and needing short cycle times. But it is difficult to control the thermal history of laser forming, and both methods suffer from residual porosity. In addition, both of these methods require conventionally produced and atomized powder, which is very costly.

Although much time and effort has been invested in the development of these processing techniques, the cost of Ti still remains high because of the cost of raw materials, cost of post-processing, and yield losses. In recent work performed at the Infrared Processing Center at ORNL, new methods of Ti sheet and plate processing have been investigated. VHP, high-density infrared (HDI) processing, and roll compaction processing were explored. All three methods used powder provided by ITP. ITP has developed a new low-cost method of powder production and is currently running a pilot processing facility.

Experimental Procedure

ITP Ti powder was processed into plate and sheet using three methods, VHP, HDI, and roll compaction. ITP Ti-6Al-4V was processed into plate and sheet using VHP and roll compaction. VHP, a batch process, was used to make Ti and Ti-6Al-4V plate. HDI and roll compaction were both used to make Ti sheet. Roll compaction also was used to make Ti-6Al-4V sheet. HDI uses a plasma arc lamp to heat and liquid-phase-sinter vacuum-cold-pressed Armstrong Process Ti powder. Sintered compacts were repeatedly cold-rolled and flash-annealed under the plasma arc lamp in order to make sheet. Similarly, roll compaction uses medium-density tungsten-halogen-based radiant heating to solid-phase-sinter vacuum-cold-pressed Armstrong Process Ti and Ti-6Al-4V powder. Sintered compacts were repeatedly cold-rolled and annealed until thin-gage sheet was produced.

VHP was used to make four samples of Ti plate and one Ti-6Al-4V plate. Each of the four samples was pressed under vacuum in a graphite element radiant furnace. The three Ti samples and the Ti-

6Al-4V sample were pressed in a 63.5-mm-diam graphite die. The fourth sample was pressed in a 178-mm-diam die. For each of the pressing operations, the die was lined with Grafoil and a measured amount of Ti powder was poured into the die. For the 63.5-mm-diam samples, the die was filled with 36 g of Ti or Ti-6Al-4V powder. And for the 178-mm-diam sample, the die was filled with 130 g of Ti powder. To prevent mechanical interaction between air and the powder, no pre-pressing was applied. A special collar was placed under the die to keep it in place while the powder was being pressed. When the rams were jogged into place, the furnace was closed, sealed, and evacuated. The furnace was back-filled with argon gas and evacuated three times in order to ensure a clean processing environment. The 63.5-mm-diam Ti samples were pressed at a pressure of 55.3 MPa. One sample was pressed at 750°C for 15 min, another sample was pressed at 900°C for 15 min, and the final sample was pressed at 900°C for 30 min. The Ti-6Al-4V 63.5-mm-diam sample was pressed at a pressure of 55.3 MPa for 1 hour at 950°C. The 178-mm-diam Ti sample was pressed at a pressure of 11.7 MPa for 1 hour at 900°C. All five samples were allowed to furnace cool after the heating cycle was completed. After the samples were removed from the furnace, the sample surfaces were ground and polished, and the densities were measured by immersion in ethanol (Archimedes method). Tensile specimens were machined from each 63.5-mm-diam sample. The tensile specimens were machined to the SS3 standard. Mechanical testing, chemical analysis, and optical microscopy were performed on the samples.

Roll compaction was developed by Ametek Corporation for the commercial production of nickel and other advanced alloy sheet. With ITP Ti powder costing as little as \$4/lb, and with the greatly reduced effort needed to obtain sheet compared with the ingot processes, roll compaction could eliminate a large portion of total Ti sheet fabrication costs dedicated to forming. Roll compaction begins with raw powder fed into rolls from a hopper. The rolls compact the ductile powder into sheet. The sheet is then fed into a furnace where the sheet is sintered. Subsequent roll and sinter operations are performed continuously until a dense, thin-gage sheet is produced.

To simulate a roll compaction process on a laboratory scale, thin-gage sheet was produced by sinter-

ing powder compacts in an IR furnace followed by cold rolling. First, 18 g of Ti or Ti-6Al-4V powder was vacuum-cold-pressed in a 50.8-mm-diam die at a pressure of 48.3 MPa. Powder compacts were heated in a 33-kW IR furnace that contains a 152-mm-inside-diam quartz tube that allows for vacuum and argon gas flow in the chamber.

The Ti sample was heated to 1200°C, held for 2 hours, and then furnace-cooled and cold-rolled. The initial thickness was 3.25 mm; after rolling, it was 1.29 mm. The sample was again heated at 1200°C for 2 hours in the IR furnace. The sample was then cold-rolled from 1.29 to 0.53 mm. A final anneal of 1200°C for 1 hour was then performed on the sample.

The Ti-6Al-4V sample was heated to 950°C and held for 2 hours and then furnace-cooled and cold-rolled. The initial thickness was 4.06 mm, and thickness after rolling was 1.90 mm. The sample was again heated at 950°C for 30 min in the IR furnace. The sample was then cold-rolled from 1.90 to 0.97 mm. Another intermediate anneal was performed by heating the sample to 950°C for 30 min. A final cold-roll was performed, and the final gage thickness was measured at 0.61 mm. A final 950°C/30-min stress relief was also performed.

From each final sheet, tensile specimens were machined and tested, chemical analysis was performed, and the microstructure was investigated.

HDI processing is similar to roll compaction but uses heating the sample to the liquid phase to achieve bonding. In order to achieve temperatures above the 1650°C melting point of Ti, a plasma arc lamp is used to rapidly heat a vacuum-cold-pressed compact. The plasma arc lamps use a unique technology to produce extremely high power densities with a single lamp. Instead of an electrically heated resistive element, controlled and contained plasma is used.

The lamp is sealed at the ends where the cathode and anode are located. Deionized water mixed with argon gas enters at the cathode side through high-velocity jets impinging at a given angle. Because of the high velocities and pressure, the deionized water is impelled to the wall of the quartz tube and spirals down the length of the tube in a uniform 2- to 3-mm-thick film. This water film serves two purposes: to cool the quartz wall and to remove any tungsten particulates that may be expelled from the electrodes. The gas moves in a spiral fashion through the

center of the tube, and a capacitive circuit initiates the plasma. The lamp operates at 750,000 W and is fitted with a reflector that illuminates a 20×15 cm area with a power density of up to 460 W/cm². The plasma, which has a temperature in excess of 10,000 K, is stable and produces a radiant spectrum from 0.2 to 1.4 μm.

The processing steps for HDI were very similar to those for roll compaction. First, 9 g of raw Ti powder was vacuum-cold-pressed in a 50.8-mm-diam steel die under 48.3 MPa pressure. The cold-pressed compact was then placed in an environmentally controlled processing box. The box was water cooled and vacuum-tight. The box was evacuated and back-filled with argon gas to reduce oxidation during processing.

The sample was moved into position under the lamp and liquid-phase-sintered at 280 W/cm² for 8.5 s. The thickness after sintering was measured at 1.8 mm. After a cold-rolling operation, the sample measured 0.95 mm. The cold-rolled sample was flash-annealed under the lamp at 280 W/cm² for 5 s. The sample was then rolled to 0.62 mm. A second flash anneal was performed at 280 W/cm² for 5 s. A final cold roll was performed, and the final thickness measured 0.40 mm. The sample was flash-annealed at 100 W/cm² for 5 s. The thin-gage, annealed sheet was mechanically tested, chemically analyzed, and observed under a light microscope.

Results and Discussion

After the post-pressing grinding and machining was performed on the VHP Ti and Ti-6Al-4V consolidated powder, the samples were polished. Figure 1 shows the final Ti plates.

The density of each plate was measured by the Archimedes method to be 100%. But metallographic observations performed on a light microscope showed differences in the levels of sintering obtained for the three pressing conditions. Figure 2 shows the microstructure of the VHP samples

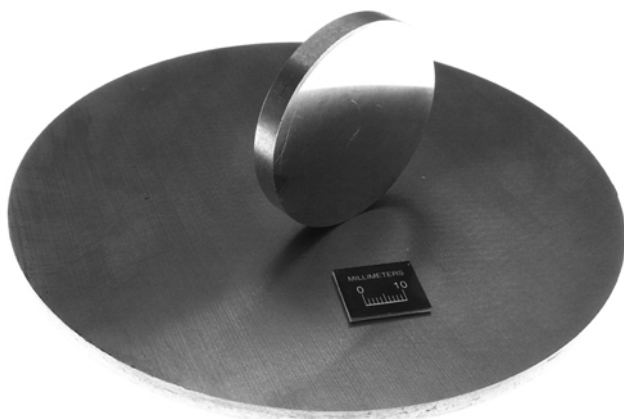


Figure 1. As-VHP and machined Ti plates, 63.5 mm diameter and 178 mm diameter.

at 750°C for 15 min, 900°C for 15 min, and 900°C for 30 min.

Figure 2a shows that sintering in the 750°C/15 min samples was incomplete, and many voids in the microstructure still remained. Figure 2b shows that increasing the pressing temperature to 900°C helps to reduce the amount of void present. But the best results were obtained by pressing at 900°C for 30 min. Figure 2c shows the least amount of void after pressing at 900°C for 30 min and shows that grain growth has occurred, indicating that the particles have fully bonded to each other. Figure 2d shows the microstructure of the VHP Ti-6Al-4V samples.

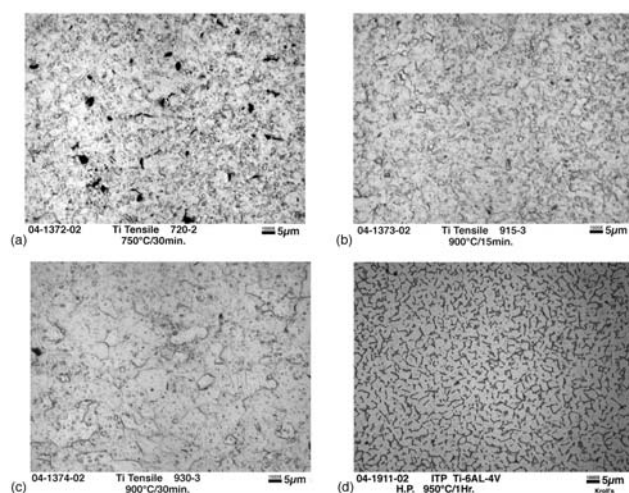


Figure 2. Microstructure for VHP samples (a) Ti 750°C/15 min, (b) Ti 900°C/15 min, (c) Ti 900°C/30 min, and (d) Ti-6Al-4V 950°C/1h.

The lack of sintering at 750°C and 900°C/15 min was also apparent in mechanical testing. Each of

the SS3 tensile specimens machined from the 63.5-mm-diam plates was tested in tension with a cross-head speed of 0.51 mm/min. The mechanical testing results are shown in Table 1.

According to Allegheny Ludlum, Grade 2 Ti has comparable properties to the 930°C/30 min VHP samples. The Ti-6Al-4V VHP samples also exceeded the properties published for this material. Chemical analysis showed that the VHP Ti samples were all below the maximum allowable limits of O₂, N₂, and C for Grade 2 Ti. The O₂ content of the VHP Ti-6Al-4V slightly exceeded the upper limits for Grade 5 Ti-6Al-4V, but the high oxygen level did not adversely affect mechanical testing results. The results of the chemical analysis are shown in Table 2.

Microstructural investigations were performed on the HDI-processed roll-compacted Ti and on roll-compacted Ti-6Al-4V thin-gage sheet materials. Both samples were cut from the as-annealed sheet, mounted, polished, and etched with Kroll's reagent. Optical microscopy revealed that the roll-compacted sample had a standard annealed Ti microstructure. Throughout the entire cross section, the roll-compacted sheet was virtually free of flaws with a very consistent microstructure. The HDI-processed material showed that the intense, short-duration, and directional heating of the plasma arc lamp caused large grains to grow on the top surface during the final anneal. But the structure remained equiaxed alpha with beta spheroids. Also, microscopy showed that many rolling lapses remained in the final HDI-processed sheet. Investigation of the structure of the roll-compacted Ti-6Al-4V sheet showed that a significant amount of retained oxygen-stabilized-α was present. Figure 3 shows the microstructure of the HDI-processed Ti sheet, the roll-compacted Ti sheet, and the roll-compacted Ti-6Al-4V sheet.

Mechanical testing of the HDI-processed and roll-compacted sheet was performed. Tensile testing results are shown in Table 3.

The lack of ductility of the HDI-processed samples was due to the observed rolling lapses. This is similar to the lack of complete sintering in the 750°C/15 min VHP sample. The mechanical properties of roll-compacted Ti sheet showed that the strengths are comparable to Grade 4 Ti. But the oxygen content of the roll-compacted samples exceeded the allowable limit for Grade 4, and the ductility suffered as a result. The chemical analysis

Table 1. Mechanical testing results of VHP Ti and Ti-6Al-4V plates

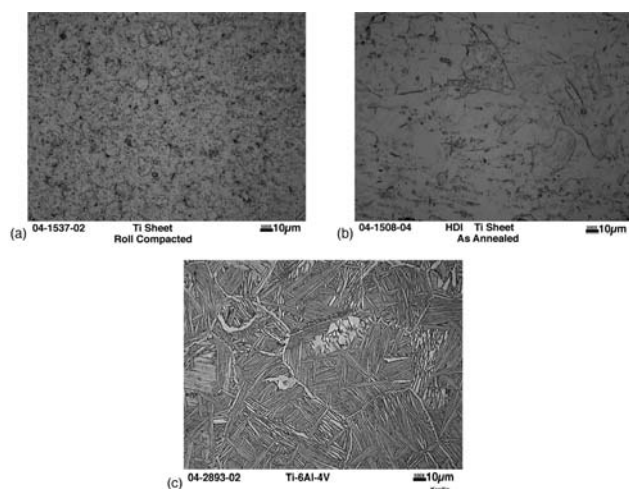
Sample	Yield strength [MPa]	Tensile strength [MPa]	Elongation [%]
Ti 750°C/15min	532	571	1.7
Ti 915°C/15min	544	636	14.9
Ti 930°C/30min	517	617	20.7
Ti grade 2 (min values)	345	448	20.0
Ti-6Al-4V 950°C/1 hour	963	994	13.8
Ti-6Al-4V grade 5 (min values)	828	897	10.0

Table 2. Chemical analysis of VHP Ti and Ti-6Al-4V plate (nominal %)

Sample	O ₂ [%]	N ₂ [%]	C [%]
Ti 750°C/15min	0.23	0.01	0.05
Ti 900°C/15min	0.25	0.01	0.06
Ti 900°C/30min	0.24	0.01	0.03
Ti grade 2 (max limits)	0.25	0.03	0.08
Ti-6Al-4V 950°C/1hour	0.28	0.01	0.04
Ti-6Al-4V grade 5 (max limits)	0.20	0.05	0.08

Table 3. Mechanical testing results of HDI-processed and roll compacted Ti sheet

Sample	Yield strength [MPa]	Tensile strength [MPa]	Elongation [%]
HDI-processed Ti	486	598	8.8
Roll-compacted Ti	529	656	9.6
Ti grade 4	483	552	15.0

**Figure 3.** Microstructure for thin-gage sheet samples (a) roll-compacted Ti, (b) HDI-processed Ti, and (c) roll-compacted Ti-6Al-4V.

of the HDI-processed and roll-compacted material is shown in Table 4.

Summary

These are the highlights of the progress during FY 2004:

1. Production of VHP Ti plate with mechanical properties comparable to those of commercially pure Ti grade 2.
2. Production of VHP Ti-6Al-4V plate.
3. Roll compaction of Ti and Ti-6Al-4V thin-gage sheet.
4. Production of HDI-processed Ti thin-gage sheet.
5. Mechanical, optical, and chemical analysis of ORNL-produced sheet.

Conclusions

Although Ti and Ti-6Al-4V have attractive properties that would benefit a great number of engineering applications, their use is limited by the cost of the raw material and the processing that is necessary to make a usable product. But with the recent advancements in low-cost powder production at ITP, in conjunction with processing techniques

Table 4. Chemical analysis of HDI-processed and roll compacted thin gage Ti sheet

Sample	O ₂	N ₂	C
HDI-processed Ti	0.29	0.01	0.03
Roll-compacted Ti	0.42	0.01	0.03
Ti grade 4 (max limits)	0.40	0.05	0.08

developed at ORNL, the cost of Ti sheet and plate is predicted to decrease. While VHP on a large scale may not be an economical method of plate production, it does demonstrate that ITP powder can produce a viable product. HDI-processing could be developed into a commercial process, but liquid-phase processing may not be desirable. Furthermore, HDI-processed Ti sheet lacks the mechanical properties necessary. Roll compaction is the best alternative to the current VAR and other ingot metallurgy

processes used to process Ti. Processing facilities are in place to produce nickel alloys and could easily be modified to process Ti. Lab-scale roll compaction produced thin-gage Ti sheet with the appropriate microstructure, mechanical properties, and chemical composition. Although the ductility is slightly below acceptable levels, a scaled-up facility will have better control over oxygen contamination, eliminating this problem. Results suggest that the roll compaction of Ti sheet should be further explored.

4. ENABLING TECHNOLOGIES

A. Improved Friction Tests for Engine Materials

Principal Investigator: P. J. Blau

Oak Ridge National Laboratory

P.O. Box 2008, Oak Ridge, TN 37831-6063

(865) 574-5377; fax: (865) 574-6918; e-mail: blaupj@ornl.gov

Technology Development Area Specialist: Sidney Diamond

(202) 586-8032; fax: (202) 586-1600; e-mail: sid.diamond@ee.doe.gov

Field Technical Manager: Philip S. Sklad

(865) 574-5069; fax: (865) 576-4963; e-mail: skladps@ornl.gov

Contractor: Oak Ridge National Laboratory

Contract No.: DE-AC05-00OR22725

Objectives

- Develop a realistic, engine-correlated laboratory-scale test method to be used to evaluate new diesel engine piston ring and liner materials
- Work with ASTM, through an industry-based advisory group, to establish a standard practice for testing the friction of piston ring and liner material combinations.
- Investigate the ability of the new test method to detect small friction and wear differences due to the effects of engine conditioning of the lubricants.

Approach

- Review and critique past attempts to develop laboratory tests for piston ring and liner materials.
- Develop a testing protocol for friction and wear in reciprocating, lubricated contacts that simulate key aspects of the diesel engine environment.
- Study the characteristics of diesel-engine-conditioned oil and determine how to simulate its effects on the friction and wear response of candidate materials.
- Work with ASTM through Committee G-2 on Wear and Erosion to develop and approve a standard practice for conducting laboratory-scale piston ring and liner friction and wear tests.

Accomplishments

- Published a report describing and critiquing past efforts to develop engine-correlated, laboratory-scale tests for materials and lubricants proposed for use in both spark-ignition and diesel engines.
- Established an ASTM task group on Ring and Liner Wear within Committee G02.40 on Non-Abrasive Wear. Populated the task group with representatives from diesel engine companies, automotive companies, testing machine manufacturers, oil companies, government laboratories, and universities.
- Developed a technique for simulating the surface finish of production cast iron cylinder liner bores on simple test coupons.

- Obtained samples of oils run in standardized engine tests and used them to determine the sensitivity of the new test method to delineate lubricant condition.
- Prepared a draft standard practice for ASTM subcommittee review, submitted it for balloting, and revised it based on the results. The revised document is in process of final committee approval.

Future Direction

- Having established the standard, prepare a research report that documents its development, and use the standard to determine the friction of several promising engine ring and liner materials.
-

Introduction

Friction robs engines of useful energy and lowers the vehicle's fuel economy. Depending on engine speed, the piston ring and liner system in an internal combustion engine can account for more than 50% of the total frictional losses in an engine. New materials, lubricants, and coatings offer the potential to reduce such frictional losses; but the development cost can be high, especially when full-scale engine tests are used. Smaller-scale, simulative laboratory tests are an attractive lower-cost alternative, but they are useful only if the results correlate well with the materials' performance in fired engines.

The design of cost-effective, laboratory-scale ring and liner simulations presents a complex challenge. Improperly designed simulations can produce misleading results. Materials and lubricants must be induced to react in tests as they would in actual service. Tests should enable the ranking of alternative materials and lubricants in the same order of merit as they would perform in service. That requires identifying and controlling the major mechanical, thermal, and chemical factors that influence the materials' friction and wear characteristics.

The development of a standard practice through ASTM was thought to be the best way to produce a rigorous friction test for ring and liner materials, one that would meet with industry approval through a consensus voting and approval process. ASTM is an international organization that develops consensus material testing standards. By working through ASTM Committee G-2, Oak Ridge National Laboratory (ORNL) was able to draw on dozens of experienced testing professionals.

In FY 2001, key elements required for effective ring/liner simulation were identified. In FY 2002, the effort was focused on building an industry advisory group and involving ASTM. In FY 2003, fric-

tion and wear tests were conducted in new and used engine oils to refine the test methodology and prepare it for the rigorous ASTM standardization process. In FY 2004, the balloting process was conducted. The following section describes this evolutionary process.

Development of the Standard

This formal development of the standard document began with the establishment of a task group on Ring and Liner Wear, by ASTM Committee G02.40, under the auspices of the Subcommittee on Non-Abrasive Wear. In parallel, ORNL researchers began to evolve new laboratory testing procedures and to acquire samples of well-characterized, standard diesel engine test oils from Southwest Research Institute. These engine-conditioned oil samples were comprehensively characterized by sending them to a company that specializes in motor oil analysis.

During that period, decisions had to be made regarding contact geometry, specimen fixturing, cylinder liner surface roughness, surface finish directionality ('lay'), and the use of special running-in procedures to ensure proper specimen alignment. In fact, a special method to simulate the roughness of honed cylinder liners was developed in the course of this work and subsequently published in the *Proceedings of the American Society of Mechanical Engineers, Internal Combustion Engine Division*. Results of reciprocating friction tests on a Caterpillar diesel engine ring and liner combination revealed that the proposed standard could indeed discriminate between subtle changes in the oil condition. This first work was presented in December 2003 at a joint workshop between ASTM committees D-2 (Lubricants) and G-2 (Wear and Erosion).

After an iterative review by task group members, balloting on the draft standard was conducted first at the subcommittee level and then at the main

committee level. Results of the latter are scheduled for discussion and resolution at the November 2004 ASTM G-2 Committee meeting in Washington, D.C.

Description of the New Standard Practice

The title of the document is *Standard Practice for Conducting Friction Tests of Piston Ring and Cylinder Liner Materials Under Lubricated Conditions*. It begins with a scope statement, followed by references to other applicable ASTM standards. The terminology section introduces a definition for engine-conditioned oil. The use of engine-conditioned lubricating oil is a key aspect of this practice because it provides the means to evaluate materials under conditions that simulate not only the mechanical and thermal aspects of a ring and liner interface, but the chemical aspects as well.

The basic procedure involves the geometry shown in Figure 1. A piston ring segment oscillates with a load, stroke length, and rate appropriate for the engine of interest. Before the tests are conducted, the surfaces of the ring and liner are worn under low load to seat them properly. Early tests showed that failure to run-in the specimens carefully can increase the scatter and decrease repeatability of the test results.

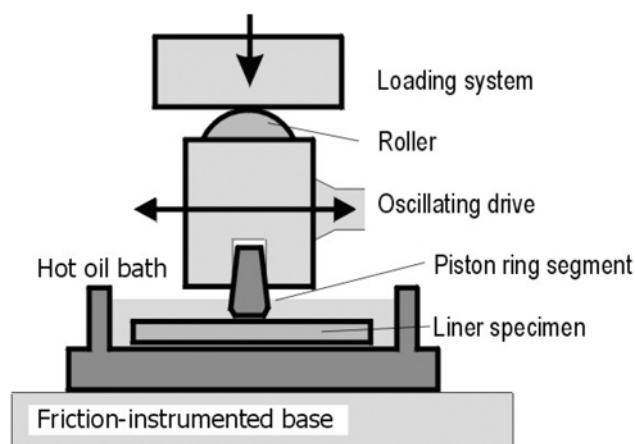


Figure 1. Side view schematic diagram of the ring-on-liner test.

Additional Use for Wear Measurement

The effects of oil condition on wear can also be studied using a variant of this test method. It is known that used engine oil tends to be depleted of its friction-reducing and wear-reducing additives. Such oils also contain soot, a by-product of combus-

tion. The effects of oil condition on wear are illustrated in Figures 2 and 3. Both tests involved the same starting material combination (a chromium-plated diesel engine ring on cast iron). Tests were run for 6 h in oil at 100°C. In the first case, the lubricant was fresh 15W40 grade diesel engine oil (Cummins Blue); and in the second case, the lubricant was a high-soot test oil from Southwest Research Institute (called “M11 HST oil”). Using a surface profiling instrument, the wear volumes and wear rates of the specimens can be determined. In the example shown here, the wear rate of the cast iron in engine-conditioned test oil was four times higher than in the fresh oil. Therefore, as an added benefit, the basic friction test procedures developed in the course of this project can be extended, with minor procedural modifications, to measure the wear of new ring and liner materials as well.

Plans for FY 2005

A workable method for friction testing of ring and liner materials having been established, three remaining tasks are planned for FY 2005:

1. Resolve any negative votes that may arise from the fall 2004 main G-2 committee ballot.
2. Prepare a research report that will be kept on file at ASTM headquarters. This is a society requirement



Figure 2. Wear scar on cast iron produced by 6 h of testing at 240-N load, 10-mm stroke, 10 cycles/s, in fresh 15W40 diesel oil. The normalized volumetric wear factor was $1.9 \times 10^{-7} \text{ mm}^3/\text{N-m}$.

Figure 3. Wear scar on cast iron produced by 6 h of testing at 240-N load, 10-mm stroke, 10 cycles/s, in M11 HST test oil. The normalized volumetric wear factor was $7.7 \times 10^{-7} \text{ mm}^3/\text{N-m}$.

that serves to support the technical basis for each new standard.

3. Use the new practice to evaluate a selection of candidate engine materials and surface treatments, thereby demonstrating the usefulness of the standard in supporting other heavy vehicle materials and surface engineering development efforts.

A portion of the experimental findings on which the ASTM research report is to be based has been accepted for presentation at the 2005 International Conference on Wear of Materials and will be published in a special volume of the journal *Wear*.

Conclusions

Coupling a team of industry experts with laboratory experiments, ORNL has been able to develop a useful method for assessing the friction of piston ring and liner material combinations under mechanical, thermal, and chemical conditions that are similar to those in engines. The new method has been

shown to discriminate between the frictional behavior of five standard test oils. Test oils can now be selected to evaluate new ring and liner materials under different degrees of lubricant deterioration and wear severity. A standard practice for lubricated diesel engine piston ring and liner materials testing is nearing final ASTM approval. Validation of the practice on other material pairs is planned for FY 2005.

Publications

J. J. Truhan, J. Qu, and P. J. Blau, "The Effect of Lubricating Oil Condition on the Friction and Wear of Piston Ring and Cylinder Liner Materials in a Reciprocating Bench Test," accepted for publication in *Wear*.

B. Laser Glazing of Railroad Rails to Reduce Friction

Principal Investigators: George Fenske, Saud Aldajah, Oyelayo Ajayi, and Ron DiMelfi

Argonne National Laboratory

9700 S. Cass Ave.

Argonne, Illinois 60439

(630) 252-5190; fax: (630) 252-4798; e-mail: gfenske@anl.gov

Technology Development Area Specialist: Sidney Diamond

(202) 586-8032; fax: (202) 586-1600; e-mail: sid.diamond@ee.doe.gov

Field Technical Manager: Philip S. Sklad

(865) 574-5069; fax: (865) 576-4963; e-mail: skladps@ornl.gov

Contractor: Argonne National Laboratory]

Contract No.: W-31-109-ENG-38

Objective

- Determine the potential of laser glazing to lower parasitic energy losses between the flange and the rail in rail transport.
- Develop a fundamental understanding of the metallurgy associated with the formation of low-friction surface layers during laser glazing processing and how these layers reduce friction between rail and wheel

Approach

- Develop advanced laser glazing processes to form glazed regions on carbon steels.
- Perform benchtop tests, full-scale rig tests, and field tests of glazed steels and rails to quantify the impact of glazing on parasitic friction losses.
- Characterize glazed and nonglazed steels to elucidate the impact of glazing on the microstructure.

Accomplishments

- Optimized laser processing conditions under which uniform glazed surfaces form on carbon steels.
- Evaluated the friction and wear performance of glazed (and unglazed) rail steel by using benchtop and wheel/rail rig tests.
- Characterized the microstructure and hardness of glazed steels.
- Developed a deformation theory for nanocrystalline materials to model friction in glazed steel.
- Demonstrated the efficacy of laser glazing to reduce friction on a full-scale test rig using prototype wheels, loads, and speeds.

Future Direction

- Perform high-tonnage field tests at the Association of American Railroads (AAR)/Transportation Technology Center, Inc. (TTCI) Facility for Accelerated Serving Testing (FAST) in Pueblo, CO.
- Characterize the microstructure of a glazed rail subjected to AAR/TTCI FAST tests.

- Make go/no-go decision to proceed with development of rail glazing technology.
- If go/no-go decision is to proceed, establish project with a railroad track maintenance equipment and service organization

Introduction

Wheel/rail interaction accounts for a significant fraction of the energy consumed in rail transport. Past studies have indicated that energy savings could be as high as 24% when friction at the wheel/rail interface is properly managed. The key aspect is control of the friction forces. At the locomotive, high friction between the rail (specifically the top of the rail) and the wheel is desired to ensure adequate traction to keep wheels from slipping and sliding when power is applied. Friction is also required under braking conditions to control the speed of downhill-bound trains or to bring a train to a safe stop. The trailing cars, however, require much lower friction levels under normal train operations. At these cars, a low, controllable friction is desirable and can significantly reduce the energy required to pull a train. Two regions account for most of the frictional losses between the wheel and the rail: the region between the top of the rail and the wheel tread, and the region between the wheel flange and the gage face of the rail. Current wheel/rail lubrication (e.g., application of degradable greases and lubricants) is inconsistently applied and often disengaged by train crews. The research described herein focuses on the development of a laser glazing technique that imparts a durable, low-friction surface to the gage face of the rails to reduce parasitic frictional losses between the flange and rail gage.

Approach

The objective of this activity was to develop an advanced laser modification process to form a glaze on the gage face of the rail. Initial results and models predicted the formation of a nanocrystalline surface layer that would impart low-friction properties at the interface. The tasks associated with this project involve

- Process development (laser glazing)
- Microstructural characterization of laser-modified surfaces
- Development of a model (of surface deformation)

- Lab-scale friction and wear testing of laser-modified surfaces (glazed and shot-peened)
- Full-scale friction testing of laser-glazed steel

Results

The development of the laser glazing processes used in these studies^{1,2} was documented in the FY 2003 Annual Report. Several approaches were investigated; two involved laser glazing, and a third investigated a laser shock-peening technique. Parametric studies were performed to optimize the conditions under which a glazed layer forms on 1080 steel. For this purpose, an ElectroX 1.6-kW pulsed Nd:YAG laser with fiber-optic beam delivery and special beam shaping optics was used in Argonne National Laboratory's (ANL's) Laser Applications Laboratory. Two approaches were developed: one involved a single pass of the laser over a given area, and the other involved multiple overlapping passes. The Knoop hardness of the martensitic glazed regions was 2–3 times greater than that of the substrate, depending on whether a single-pass (factor of 3 times harder) or multipass (slightly over 2 times harder) process was employed. A commercial laser glazing process that used high-power diode laser technology was also investigated. In this case, bars of 1080 steel were processed by a commercial vendor (NuVonyx) and subsequently tested at ANL.

Friction and wear studies were performed using a number of lab-scale systems. Block-on-ring tests performed by Falex Corp. showed static friction coefficients of ≈ 0.35 – 0.45 for untreated 1080 steel that dropped to values ranging from 0.2 to 0.4 for differing glazing conditions. Large-scale (using a glazed segment of rail and a full-size wheel) "block-on-ring" tests performed at the AAR/TTCI Pueblo facility showed the static friction coefficient of the untreated 1080 rail varied from 0.2 to 0.5, depending on the applied load, whereas the friction coefficient of the glazed regions varied from 0.1 to 0.25. Dynamic friction coefficients for the glazed regions varied from 0.2 to 0.35, depending on load, compared with 0.2 to 0.55 for unglazed regions.

Benchtop pin-on-disc tests at ANL used flats of 1080 steel, glazed and unglazed, that rubbed against stationary balls or pins (52100 steel, 1080 steel, 440C steel, or alumina). The tests revealed that the composition of the pin/ball had a significant impact on the friction coefficient. The general trend was that the glazing reduced the friction coefficient by 3–35%, depending on the material. The greatest reduction was for the alumina ball sliding against the 1080 steel, suggesting that a strong chemical adhesion mechanism may be active with the metallic counterparts.

Twin roller tests were conducted at ANL with 1045 steel rail and wheel discs that were through-hardened (Rc 40) or glazed. The glazing effectively reduced the friction coefficient from roughly 0.4 for the unglazed condition to 0.3 for the glazed rail rotating against an unglazed 1045 steel counterpart.

The most recent set of tests was performed in a twin-roller test rig at the Canadian National Research Center (CNRC) Wheel, Bearing, and Brake (WBB) facility in Ottawa, Ontario (Figure 1). The WBB Facility uses conventional and instrumented full-scale wheelsets loaded against large 63-in.-diam rims that simulate the track. The system is designed to operate at prototypical speeds and loads (30 mph and 33,000 lb in these tests). The instrumented wheelset allowed continuous monitoring of the lateral, longitudinal, and vertical forces during the tests—a feature that was used to measure differences between glazed and nonglazed regions on rim A in Figure 1.

The WBB tests were performed to confirm the friction reductions observed in the lab-scale tests and to evaluate the durability of the glazed regions before glazed rail segments were installed in the FAST loop at the AAR/TTCI facilities. A 180° segment of rim A was sent to NuVonyx, where two 10–12-mm-wide tracks were glazed along the circumference of the rim—one track along the gage face and the second track on the top of the rail approximately 5 mm from the gage point.

A series of runs was performed over a 5-day period to evaluate the efficacy of the glazing to reduce lateral and longitudinal forces (e.g., reduce friction) and to evaluate the durability of the glazing after

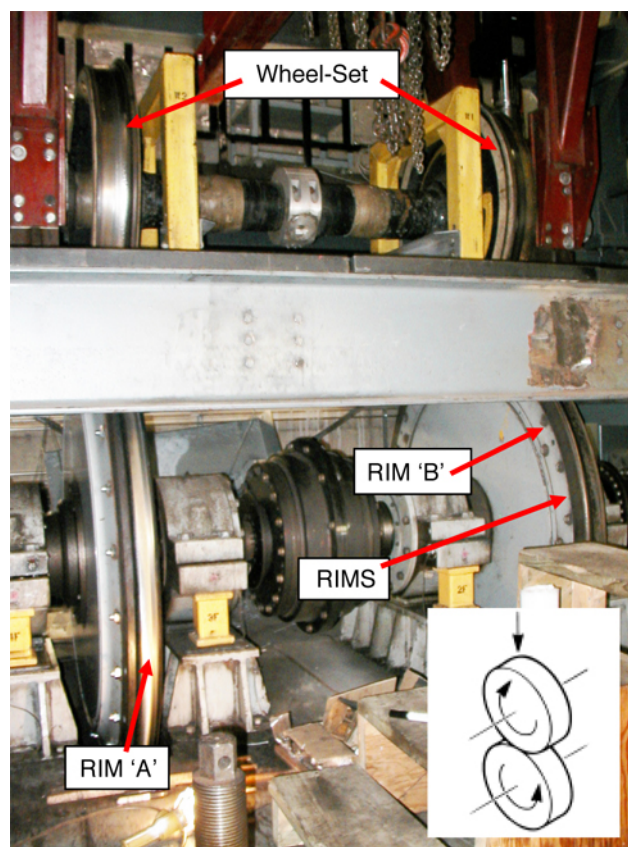


Figure 1. CNRC Wheel, Bearing, and Brake Test Facility.

moderate tonnage. The friction measurements were performed with an instrumented wheelset that permitted direct measurement of the forces using strain gauges applied to the rotating wheels. These provided a continuous measurement of the lateral, longitudinal, and vertical forces. Figure 2 shows an example of the vertical load and friction coefficient measured during a lightly loaded (10,000 lb), low-speed (6 mph) run at the start of the tests.

Because the laser-glazed rim was not re-profiled before the start of the CNRC tests, the vertical loading trace (see Figure 2) provided an easy method to determine when the wheelsets were running against the 180° glazed segment or the non-glazed segment. As seen in Figure 2, the friction shows a cyclic period of approximately 2 seconds, corresponding to one revolution of the bottom rims (at 6 mph). When the wheelset is running on the smooth, nonglazed 180° segment, the friction coefficient is high (approximately 0.18 in Figure 2). When the wheelset runs on the glazed segment, the friction drops to approximately 0.16—a decrease of 10 to 11%.

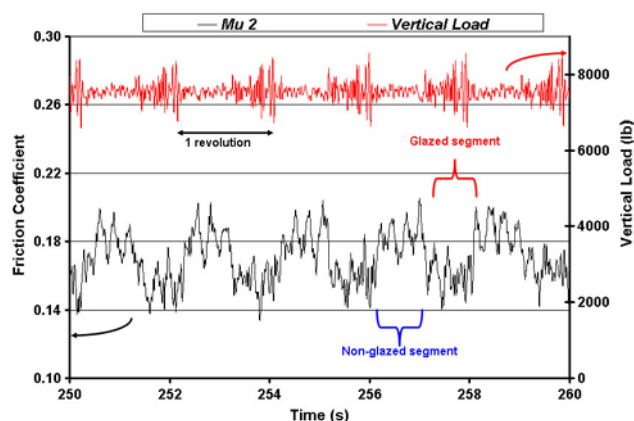


Figure 2. Friction and WBB vertical load between 250 and 260 seconds during run 1b of the ANL/CNRC rail glazing tests.

The data shown in Figure 2 present a snapshot in time during this particular run, during which the top wheelset was gradually yawed with respect to the bottom rims—a process that simulates a train passing through a curve, or the wheels hunting back-and-forth down a straight tangent run. Figure 3 summarizes the impact of the glazing observed during the entire duration of this particular run (run 1b). The magnitude of the friction reduction depends on a number of factors, including the yaw angle. As the yaw increases, the magnitude of the lateral and longitudinal forces increases and thus the friction coefficient increases, from values near 0.1 at low yaw to 0.4 to 0.5 at high yaw. The impact of the glazing on reducing the friction was not as significant at higher yaw, where the lateral forces dominated the friction measurements. Overall, Figure 3 shows that the glazing treatment reduced the friction coefficient by 8 to 50% depending on the yaw—with the greater friction reductions occurring at low yaw.

After the initial series of friction tests, a conventional wheelset was installed and a series of long-duration runs was initiated at high yaw and side loadings to expose the glazed regions to high tonnage to determine if the glazing was durable. Approximately 1 MGT (million gross tons) was applied to the glazed regions. The instrumented wheelset was then reinstalled and another series of friction measurements performed.

The magnitude of the friction reduction decreased from values observed during the initial measurements (run 1b); nevertheless, friction reduce

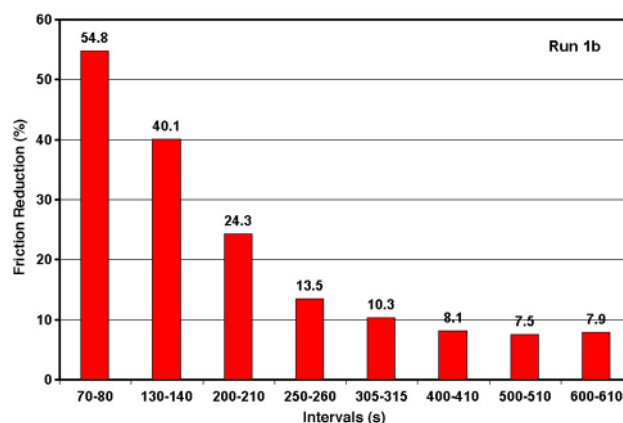


Figure 3. Friction reduction on glazed rim (normalized to the unglazed rim segment) for run 1b.

tions in the range of 8 to 40% were consistently observed.

Figure 4 shows a photograph of the bottom rim after the high-tonnage runs. These runs consisted of 2–3 days of operation at high loads (33,000 lb), high speed (30 mph), and high yaw that accumulated roughly 6 hours of run time. White paint, applied early during the runs to adjust the position of the top wheelset to ensure it was running on the glazed tracks, indicated the glazed track on the top of the rail was in contact with the wheelset. Magnaflux characterization of the rim further indicated the

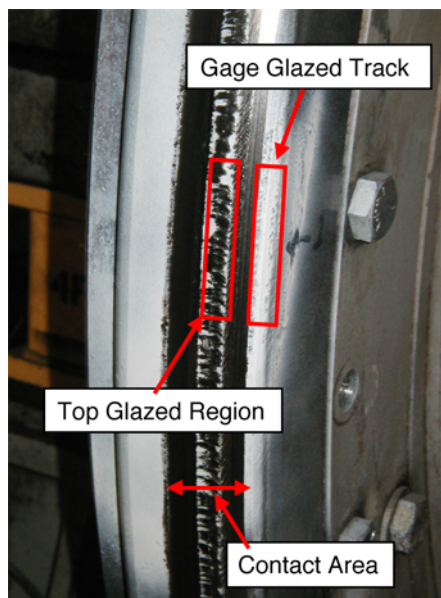


Figure 4. Macrophoto of glazed rim after run 4d.

glazed track remained intact over most of the 180° segment, although a short segment of glazed material (approximately 3 mm wide by 5 cm long) was removed after the severe high-load, high-yaw runs. The loss of the glazed material was aggravated because the glazed tracks were tested in the “as-glazed state” (a condition in which the glazed region was significantly rougher than a conventional rail profile), resulting in high contact stresses. Re-profiling the as-glazed track will reduce the high contact stresses and thus should mitigate fatigue-induced pullout/loss of glazed material.

Conclusions

Testing of laser glazing to improve the friction (and wear) performance of steels continues to progress. Initial lab-scale tests showed significant friction reductions, and the more recent studies at CNRC Ottawa have confirmed the friction reductions using full-scale wheels under high loads and prototypical speeds. Friction reductions in the range of 10 to 40% have been observed—the magnitude of the reduction being dependent on the yaw and side loading.

Efforts are in progress to establish a team to commercialize this technology with a rail maintenance firm. Plans are being developed to glaze a series of 20- to 40-foot-long track segments that will be installed in the FAST loop at the AAR/TTCI facility in Pueblo. The FAST loop tests will involve

track segments in the as-glazed, and as-glazed and re-profiled state. The FAST loop tests are designed to put significant levels of tonnage on the treated track (upward of 100 MGT). If they are successful, arrangements are being made to incorporate a laser-glazing system on a rail maintenance vehicle.

References

1. S. H. Aldajah, O.O. Ajayi, G. R. Fenske, C. Reed, and Z. Xu, “Effect of Laser Surface Modifications on Tribological Performances of 1080 Carbon Steel,” submitted to *ASME Journal of Tribology*, October 2004.
2. Saud Aldajah, George Fenske, Layo Ajayi, Claude Reed, Zach Xu, and Ron DiMelfi, *Laser Glazing of Rails—WBB/IWS Tests (CNRC-Ottawa)*, Argonne National Laboratory.

Publications/Presentations

S. Aldajah, G. R. Fenske, O. O. Ajayi, and S. Kumar, “Investigation of Top of Rail Lubrication and Laser Glazing for Improved Railroad Energy Efficiency,” *Journal of Tribology*, **125**, 643–648, July (2003).

S. H. Aldajah, O. O. Ajayi and G. R. Fenske, “Effect of Laser Glazing and Laser Shock Peening on Tribological Performance of 1080 Carbon Steel,” presented at the 2004 STLE/ASME Intl. Joint Tribology Conference, Long Beach, CA, October 24–27, 2004.

C. Laser Texturing of Materials

Principal Investigators: Ali Erdemir, Oyelayo Ajayi, Andriy Kovalchenko, Kursat Kazmanli, Robert Erck, Osman Eryilmaz, George Fenske

Argonne National Laboratory

Energy Technology Division, Argonne, IL 60439

(630) 252-5190; fax: (630) 252-4798; e-mail: gfenske@anl.gov

Principal Investigator: Izhak Etsion

Technion University

Technology Development Area Specialist: Sidney Diamond

(202) 586-8032; fax: (202) 586-1600; e-mail: sid.diamond@ee.doe.gov

Field Technical Manager: Philip S. Sklad

(865) 574-5069; fax: (865) 576-4963; e-mail: skladps@ornl.gov

Contractor: Argonne National Laboratory

Contract No.: W-31-109-ENG-38

Objectives

- Assess and optimize the tribological performance of laser-textured (or -dimpled) surfaces under sliding and/or rotating contact conditions.
- Determine durability and operational limits of dimpled surfaces with respect to dimple size, depth, and density.
- Elucidate fundamental tribological mechanisms involved with laser-dimpled surfaces.
- Design and produce novel hard coatings over dimpled surfaces and explore any beneficial synergistic effects that such coatings may have on friction and wear.

Approach

- Control and optimize parameters used in the laser-texturing process in order to obtain the most desired dimple size, depth, and density on a series of steel and SiC samples.
- Control and eliminate bulges and other surface irregularities caused by the dimpling process on and around the rims of dimpled spots. Use a post-process grinding/polishing procedure to remove such irregularities.
- Thoroughly examine and characterize dimpled surfaces by optical and electron microscopes and by a 3-dimensional (3D) surface profilometer. Determine dimple size, depth, and density. Take several representative images.
- Develop a test matrix, specify test conditions, and perform well-controlled tests with unidirectional and reciprocating wear test machines.
- In collaboration with Izhak Etsion (who supplies the dimpled surfaces), analyze test results and make judgments on the performance of the dimpled surfaces.
- Specify and apply hard coatings over laser-dimpled surfaces. Characterize and perform standard tests to assess performance improvements.
- Promote/present findings at appropriate forums and generate more industrial interest.

Accomplishments

- Demonstrated lower friction and wear under mixed lubrication regimes using a unidirectional test rig.
- Demonstrated an increase of up to 90% in resistance to scuffing on laser-dimpled surfaces using a reciprocating test rig.
 - Modified a reciprocating test rig that can now simulate the motion between a piston ring (or skirt) and cylinder liner of an internal combustion engine.
 - Initiated series of tests on cut segments of piston rings and cylinder liners using the modified reciprocating test rig.
 - Successfully produced and optimized shallow (5 to 6 micrometers deep) dimples on mechanical face seals and demonstrated superior performance, lower torque (more than 40% lower), and minimal wear for dimpled surfaces (especially under lower face pressures).
 - Performed series of tests on coated and laser-dimpled surfaces and determined operating conditions under which maximum beneficial synergistic effects can be realized.

Future Direction

- Concentrate on laser-dimpled piston rings and cylinder liners; perform friction and wear tests under conditions that represent actual engine applications.
- Analyze friction and wear data; characterize worn surfaces; determine levels of improvements provided by dimpling process.
- Assess friction reduction and energy-saving benefits of laser-dimpled rings and liners.
- Perform more studies on laser-dimpled seal faces.
- Determine effects of depth, size, and density of microdimpling on scuffing performance of surfaces coated with hard and soft films. Specifically, evaluate the effects of an MoN coating on friction and wear of laser surface texturing-treated surfaces.
- Determine effects of oil viscosity and/or ambient temperature on friction and wear behavior of dimpled surfaces.
- Determine microstructural, chemical, and mechanical characteristics of heat-affected zones at or near the dimpled areas and determine their impact on friction and wear.

Introduction

Argonne National Laboratory has entered into an exploratory research program with Technion University to evaluate the potential usefulness of a laser surface texturing or dimpling technology for engine and drivetrain applications. This technology produces shallow dimples (typically 4–10 μm deep) 70 to 100 μm in diameter on metallic or ceramic surfaces (see Figure 1). When such surfaces are used under mixed or hydrodynamic regimes of lubricated contacts, substantial reductions in friction and wear are observed. A major goal of this project is to produce and further optimize such dimples on sliding and rotating contact surfaces of critical engine parts

and components to reduce friction and wear. Furthermore, synergistic effects of hard coatings on friction and wear of laser-dimpled surfaces are being explored.

Laser texturing may be an ideal technology for applications in mechanical face seals, as well as in various engine and drivetrain components such as piston rings and cylinder liners and wrist pins. In such applications, shallow dimples can serve as reservoirs for fluid media (i.e., oil and/or water) and thus increase the hydrodynamic lubrication efficiency of these surfaces. Furthermore, dimples can effectively trap wear debris or third-body particles generating at sliding interfaces as a result of contact

sliding and thus reduce wear. Overall, when such optimized dimples are produced on various engine and drivetrain components, much improved fuel economy due to reduced friction or torque can be expected, and reduced wear translates into longer durability and hence reliability.

Accordingly, during this work period, we have prepared large numbers of SiC face seals, AISI H-13 steel flats, and cut segments of piston rings and cylinder liners for laser texturing at SurTech. Dimpled samples were returned to Argonne for surface characterization and tribological testing. Some of the dimpled seals were subjected to rigorous wear testing, while others were used in a seal tester to measure torque. Some of the dimpled steel substrates were further coated with a superhard nanocomposite MoN film in order to further improve their friction and wear performance, especially under harsh sliding conditions that can lead to scuffing and hence major wear losses.

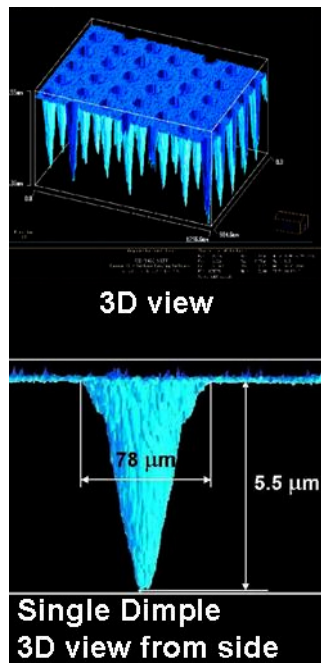


Figure 1. 3D images of dimpled surface and individual dimple.

Results

Effects of Point and Conformal Contacts on Friction and Wear

Figure 2 shows surface conditions of three different samples (polished, ground, and dimpled) that were used in a series of sliding tests in a unidirec-

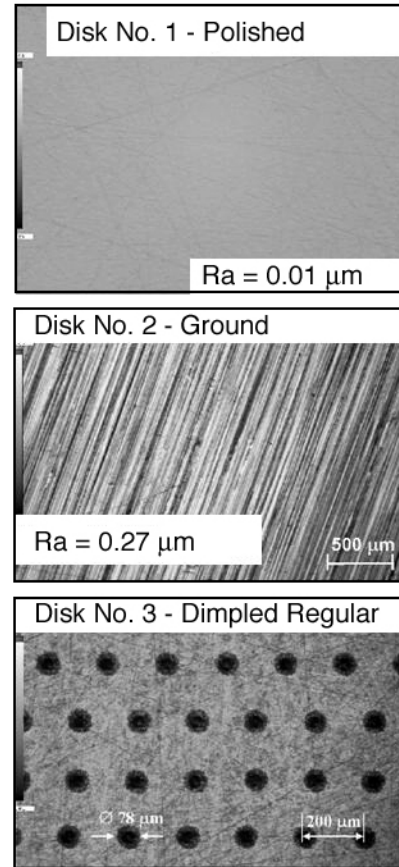


Figure 2. Surface conditions of H13 steel flats used in sliding experiments with point and conformal contacts.

tionally sliding wear test machine. These samples were rubbed against both spherical balls (≈ 10 mm in diameter) and flat-ended pins under lubricated sliding conditions. Figure 3 shows the variation of friction coefficients of balls and flat pins against polished, ground, and dimpled H13 steel surfaces as a function of increasing sliding time and speed. As is clear, under both contact configurations, a dimpled surface (Disk #3) provided the lowest friction (especially against the flat-ended pin). However, the friction coefficient of dimpled surfaces was much higher than when they were rubbed against the spherical ball. This may have been due to the relatively high contact pressures that can be generated under such point contact situations. Formation of a complete or continuous hydrodynamic film (which is key for separation of the sliding surfaces) also becomes very difficult under high-pressure point contact. The higher overall roughness of the dimpled surfaces may also have an adverse effect on friction behavior. Specifically, relatively rough sur-

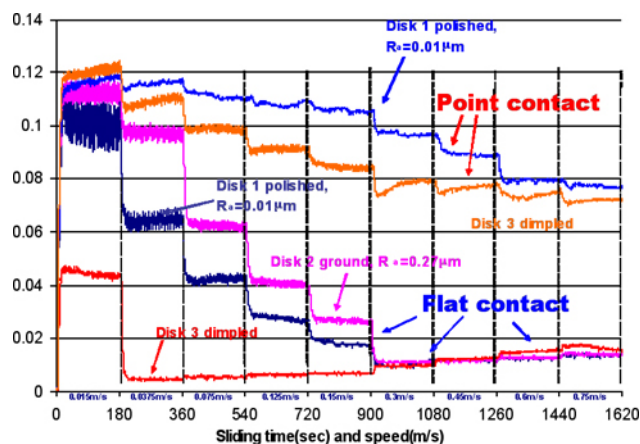


Figure 3. Frictional performance of steel balls (point contact) and flat-ended pins (conformal contact) against polished, ground, and laser-dimpled H13 steel surfaces.

faces of dimpled samples may adversely affect the formation of a continuous hydrodynamic film, leading to increased friction between the sliding surfaces.

Figure 4 summarizes the friction and wear behavior of a polished and laser-dimpled H13 steel surface under boundary-lubricated sliding conditions during a constant-speed sliding test over a long duration. Highly polished surfaces of ball and flat samples become very rough as a result of wear under the severe contact pressures of point contact sliding condition, and the friction remains high (i.e., 0.09). For the laser-dimpled surface, friction is high initially but decreases steadily during successive sliding passes and eventually reaches a value of 0.05. The contact surfaces of steel balls wear out and become highly polished. It is quite possible that substantial reduction in friction during sliding may have resulted from ball wear and hence an increasingly conformal contact between ball and dimpled flat.

Integrating Dimpling with Hard Coatings

Some of the laser-dimpled H13 steel flats were further given a superhard coating. Friction and wear tests were performed in a reciprocating test machine under both point and conformal contact conditions. Figure 5 shows the details of a dimple and the hard coating produced over it.

Figure 6 compares the friction performance of as-received base steel, laser-dimpled steel, and su-

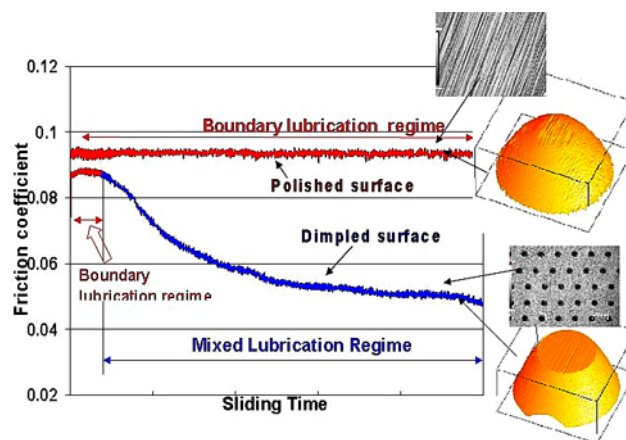


Figure 4. Friction and wear performance of M50 balls during sliding against polished and laser-dimpled H13 steel flats.

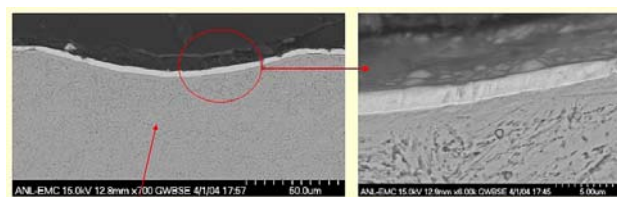


Figure 5. Hard coating applied over a dimple, and magnified details of segment showing coating and steel substrate.

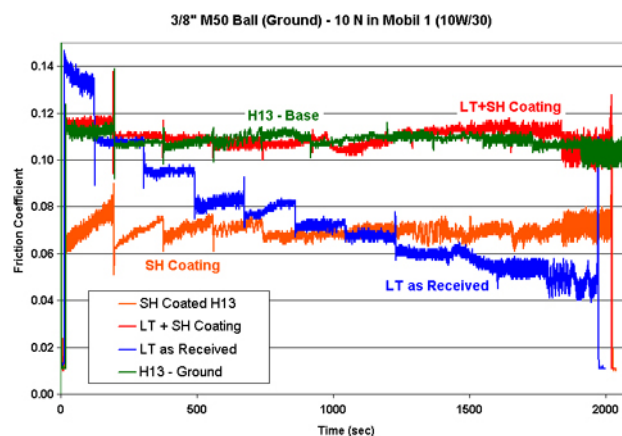


Figure 6. Friction behavior of as-received, laser-dimpled, and laser-dimpled + superhard MoN-coated surfaces under boundary-lubricated sliding conditions.

perhard-coated + laser-dimpled steel surfaces under boundary-lubricated sliding conditions.

Based on the results of Figure 6, it is clear that laser-dimpled and superhard-coated steel surfaces give fairly low friction coefficients, while the base steel and laser-dimpled + superhard-coated surfaces provide the same levels of friction. Surface studies

after the tests indicated that despite their relatively higher friction, laser-dimpled + superhard-coated surfaces suffered the least wear regardless of contact loads (see Figure 7).

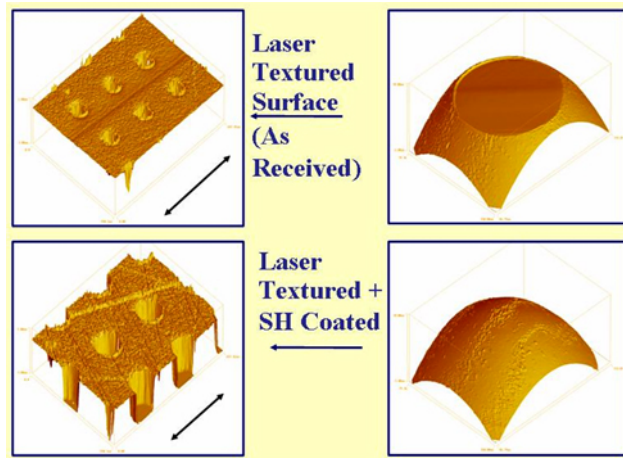


Figure 7. Wear performance of sliding ball surfaces against laser-dimpled and laser-dimpled + superhard MoN-coated (SH) flat steel samples

Laser-Dimpled SiC seals

During this work period, we have performed numerous torque measurements on dimpled and as-received (undimpled) SiC seal faces using an instrumented seal test machine. Figure 8 summarizes the results of these measurements. As is clear, frictional torque on undimpled seal faces increases almost linearly with increasing face pressure. The dimpled SiC seal faces show essentially the same trend, but the magnitude of frictional torque is at least 50% lower across the pressure range evaluated in these studies. Clearly, the dimpled seal faces provide much lower torque and hence may be very beneficial for demanding mechanical face-seal applications, including water pump seals of heavy-duty diesel engines.

Reciprocating Tests with Dimpled Piston Rings and Liner

During this period, we have cut and prepared a number of segments of actual piston rings and cylinder liners for friction and wear studies using a reciprocating test machine. Figure 9 shows the layout of this machine, while Figure 10 shows a 3D image of a cut segment of a ring with dimples produced on

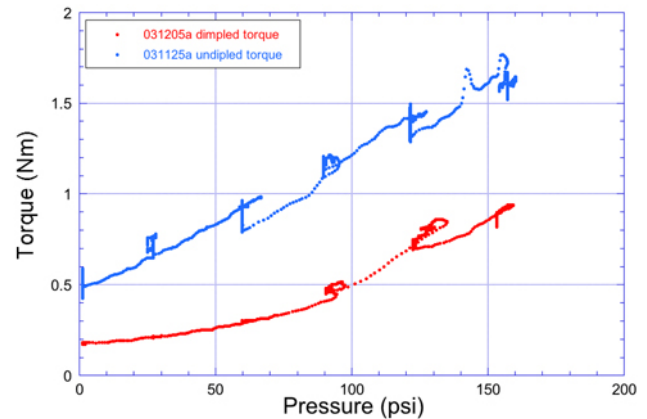


Figure 8. Summary of torque measurements on dimpled and undimpled SiC seal faces.

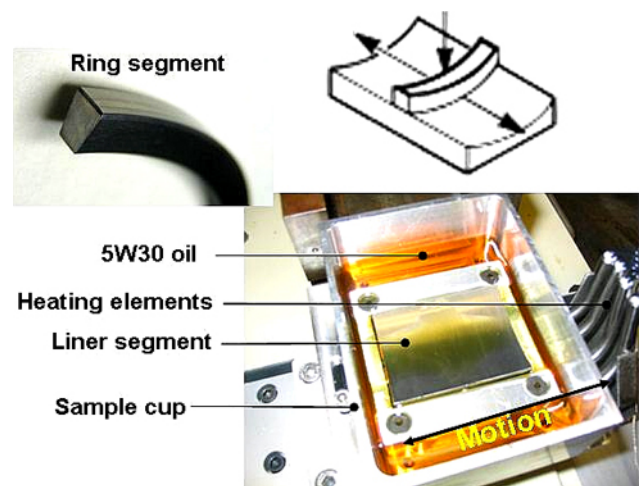


Figure 9. General layout of cut segments of dimpled piston ring and cylinder liner placed in its holder in a reciprocating test machine.

its crown. Work is in progress, and the results of initial studies look very promising.

Conclusions

During FY 2004, we have made great progress in the optimization, testing, and diverse utilization of a laser-texturing process. When used on coated or uncoated surfaces of steel or ceramic (SiC) test pairs, the process results in substantial reductions in friction and/or torque. When combined with a superhard coating technology, it can lead to superior wear performance. Used on SiC seal faces, it can reduce frictional torque by more than 50%. During this fiscal year, we have also produced well-controlled dimples on the surfaces of both piston

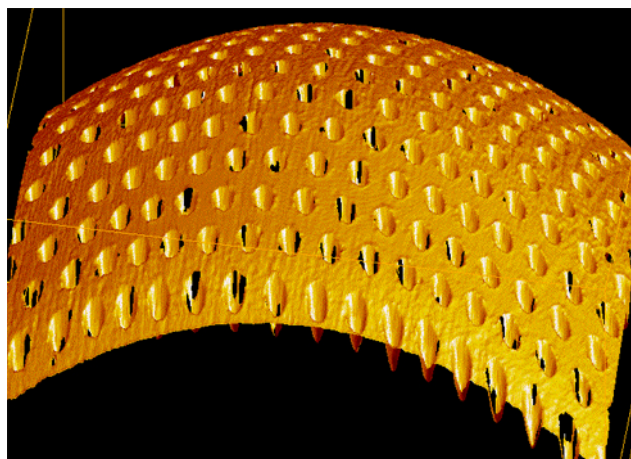


Figure 10. 3D image of laser-dimpled ring sample to be tested in reciprocating test machine.

rings and liners. A series of tests is currently under way and covers a wide range of test conditions.

Patents

An invention disclosure has been filed with Argonne's Intellectual Property Department. This invention covers structural and chemical modulation of tribological surfaces by combined use of laser texturing and low-friction superhard coatings.

Publications

A. Kovalchenko, O. Ajayi, A. Erdemir, G. Fenske, I. Etsion, "The Effect of Laser Texturing on Steel Surfaces and Speed-Load Parameters on the Transition of Lubrication Regime from Boundary to Hydrodynamic," *Tribology Transactions*, **47**(2), 299–307 (2004).

A. Erdemir, "Review of Engineered Tribological Interfaces for Improved Boundary Lubrication," *Tribology International*, in press.

A. Erdemir, "Smart Surface Engineering for Improved Boundary Lubrication," pp. 13–20 in *Proceedings of 14th International Colloquium on Tribology and Lubrication Engineering*, Stuttgart, Germany, January 13–15, 2004 (invited keynote paper).

C. Donnet and A. Erdemir, "Historical Developments and New Trends in Tribological and Solid Lubricant Coatings," *Surface and Coatings Technology*, **180–81**, 76–84 (2004).

K. Kazmanli, O. L. Eryilmaz, O. Ajayi, A. Erdemir, I. Etsion, "Effects of Soft and Hard Coatings on Tribological Behavior of Laser Textured Surfaces," submitted for presentation at the 60th Annual Meeting of the Society of Tribologists and Lubrication Engineers, May 15–19, 2005, Las Vegas.

A. Erdemir, "Engineered Tribological Interfaces for Improved Friction, Wear and Lubrication in Engines," invited panel presentation at Engine and Drivetrain Session of 59th Annual Meeting of the Society of Tribologists and Lubrication Engineers, Toronto, Canada, May 17–20, 2004.

A. Kovalchenko, O. Ajayi, A. Erdemir, G. Fenske, I. Etsion, "The Effect of Laser Surface Texturing on Transitions in Lubrication Regimes during Unidirectional Sliding Contacts," *Tribology International*, in press.

D. Joining of Advanced Materials by Plastic Deformation

Principal Investigator: J. L. Routbort

Argonne National Laboratory

9700 S. Cass Avenue, Argonne, IL 60439-4838

(630) 252-5065; e-mail: routbort@anl.gov

Technology Development Area Specialist: Sidney Diamond

(202) 586-8032; fax: (202) 586-1600; e-mail: sid.diamond@ee.doe.gov

Field Technical Manager: Philip S. Sklad

(865) 574-5069; fax: (865) 576-4963; e-mail: skladps@ornl.gov

Participants:

D. Singh, Argonne National Laboratory

F. Gutierrez-Mora, Argonne National Laboratory

K. C. Goretta, Argonne National Laboratory

Contractor: Argonne National Laboratory

Contract No.: W-31-109-Eng-38

Objectives

- Join advanced materials such as ceramics, cermets, intermetallics, composites, and biomaterials by plastic deformation.
- Collaborate with industry and universities to produce sensors.
- Characterize the interfaces.

Approach

- Apply a modest compressive load to two pieces of similar or dissimilar materials that have had little surface preparation in the temperature region where the materials are known to deform by grain-boundary sliding.
- Examine interfaces by scanning electron microscopy (SEM).
- Measure residual stresses after joining dissimilar materials and compare with finite element analysis.
- Measure strength of the interface by 4-point bend tests.
- Characterize electrical properties of sensors.

Accomplishments

- Made strong, pore-free joints with various ceramics, cermets, intermetallics, composites, and more recently, biomaterials, with and without various interlayers. Fracture occurs away from the interface.
- Achieved joint strength equal to that of the monolithic.
- Filed patent disclosure for producing oxygen sensor.

Future Direction

- Join intermetallics to ceramics.
- Join biomaterials.
- Use functionally graded materials to distribute and reduce interfacial stress concentrations.
- Measure in-situ grain rotation during deformation or joining using the Advanced Photon Source, pending funding.

Introduction

Joining by plastic deformation has been successfully applied in this program to various advanced ceramics: yttria-stabilized zirconia (YSZ)/alumina composites, mullite, silicon carbide and titanium carbide whiskers in a zirconia-toughened alumina (ZTA) matrix, metal-matrix composites and even an electronic ceramic, $\text{La}_{0.85}\text{Sr}_{0.15}\text{MnO}_3$.¹⁻⁵ Techniques have been developed to minimize sample preparation procedures and the temperature at which the joining takes place. Among them, a spray application technique² or use of nanocrystalline powders or dense interlayers stand out.^{2,6} A patent application is pending. More recently, we have formed pore-free joints in Ni_3Al .

Although it is clear that joining by plastic deformation has few, if any, serious deficiencies for joining similar materials, some issues remain to be addressed when dissimilar materials are to be joined. The situation is different because of the residual stresses generated upon cooling after materials with different coefficients of thermal expansion (CTEs) are joined at the high temperatures required. The thermal residual-stress distribution has been characterized in YSZ-alumina composites by finite element analysis (FEA) simulation and later compared with experimental observation from Vickers indentation measurements.¹

During FY 2004, we completed the 4-point bend tests on joined pieces of the same and different compositions of YSZ/alumina ceramics that were discussed in the annual report for FY 2003. Fracture mechanics principles, in conjunction with fractographic analysis, are used to explain strengths of joined ceramics in the presence of residual stresses. We have also characterized the high-temperature mechanical properties of hydroxyapatite and successfully produced pore-free joints. Collaboration with Ohio State University

has resulted in a patent application for an oxygen sensor with a built-in reference.

Summary of 4-Point Bend Tests

Table 1 is a reproduction from the FY 2003 annual report showing the fracture stress of the various monoliths of YSZ/alumina and of the ZT50A/ZT50A joint. The designation is YSZ containing 50% alumina.

Table 1. Flexure data for monolithic ceramics. Al_2O_3 and ZTA from literature

Material	Strength (MPa)
Al_2O_3	300
ZT80A	560 ± 70
ZT60A	580 ± 80
ZT50A	650 ± 100
ZT20A	1020 ± 150
YSZ	1030
ZT50A/ZT50A	620 ± 100

The ZT50A/ZT50A joint fractured, on the average, about 2 ± 1.5 mm from the interface, clearly indicating the strong nature of the joint.

Table 2 presents the results of the flexure test data for dissimilar joined materials.^{7,8}

Table 2. Flexure data for dissimilarly joined ceramics

Joint	Strength (MPa)	Distance—fracture to interface (μm)
ZT50A/ZT50A	620 ± 100	1950 ± 1540
ZT60A/ZT40A	365 ± 135	335 ± 150
AT60A/ZT40A	500 ± 50	690 ± 110
ZT60A/ZT0A	440 ± 80	380 ± 1008

FEA was conducted to determine the effect of residual stresses generated during joining of dissimilar materials on the mechanical behaviour of joined samples. Figure 1 shows the distribution of normal residual stresses generated as ZT60A

joined to ZT20A cools from the joining temperature.¹ A high tensile stress (~250 MPa) perpendicular to the joint interface develops in the material with a lower CTE. In our case, this material corresponds to the composite with a lower YSZ volume fraction (ZT60A), because the CTE of the alumina is considerably lower than that of YSZ.¹ Also, the location of peak residual tensile stress normal to the interface is 150–200 μm away from the physical interface in the ZT60A composite. Moreover, normal stresses parallel to the interface are compressive in the material with lower CTE (ZT60A) and tensile for the material with higher CTE (ZT20A). This high tensile residual stress perpendicular to the interface has an important effect on mechanical performance of the joined dissimilar materials during flexure tests. Similar simulations were also conducted for ZT60A/ZT40A and ZT60A/ZT0A joined samples.

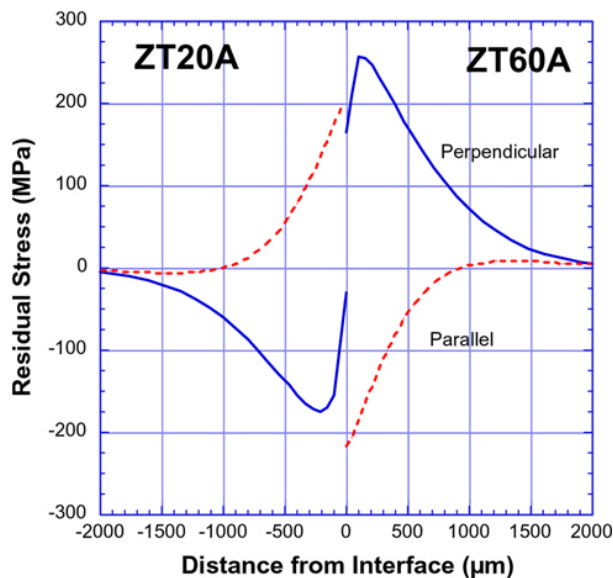


Figure 1. Distribution of residual normal stresses per FEA simulation for a ZT20A/ZT60A joint.

In addition to the normal stresses, shear stresses are also generated, and their variation for ZT60A/ZT0A joined samples determined by FEA is shown in Figure 2. Shear stresses are developed close to the interface; they fall off rapidly within a short distance from the interface. The magnitude of shear stresses is small compared with the normal tensile stresses. Thus it is expected that failure

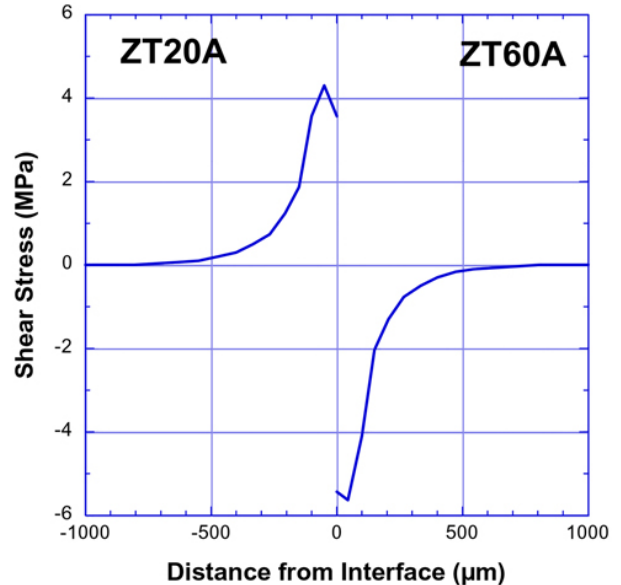


Figure 2. Distribution of residual surface shear stresses per FEA simulation for a ZT20A/ZT60A joint.

will be controlled by the normal tensile stresses of these joined samples.

Several key inferences can be drawn from the results of dissimilar joined samples. First, all samples failed in the ZT60A portion, the lower-strength material with tensile stresses normal to the interface. Second, for ZT60A joined to ZT20A and ZT0A, the strength of joined samples decreased as the difference in composition between the parts joined or the CTE mismatch increased. For the experiment in which there was the largest difference in composition (YSZ joined to ZT60A), flexure strength decreased by 25% compared with the strength of monolithic ZT60A. However, strengths for ZT60A/ZT40A joined samples showed lower mean strength and large scatter compared with joined samples of ZT60A/ZT20A and ZT60A/ZT0A. Reasons for this will be discussed. Third, for all the dissimilar joints, failure was found to be away from the interface, again confirming the strong interface and efficacy of the joining process for materials with dissimilar compositions and CTEs.

The decreased strength of ZT60A when joined to compositions with a lower volume fraction of alumina, compared with the strength of ZT60A, can be attributed to the presence of tensile residual stresses and the location and size of the failure-causing flaw. It is expected that the reduction in strength in the joined sample will depend on the

region of near-maximum tensile residual stresses. In this regard, the distance from the interface at which fracture occurred is especially revealing. For the ZT60A/ZT20A joint sample, the average failure location is about 700 μm away from the interface in the ZT60A section (Table 2). This corresponds to about 100 MPa tensile residual stress as per FEA simulations, as shown in Figure 1. By simple superposition of the residual stress intensities on the applied stress intensity during flexure tests, the failure strength for ZT60A should be reduced by 100 MPa. This is in agreement with the reduction of approximately 80 MPa in flexural strength of ZT60A when joined to ZT20A. Similar correlations between residual tensile stresses and flexural strength for ZT60A/ZT0A have been made.

Strengths of ZT60A/ZT40A were somewhat lower and were 201, 360, and 530 MPa for the three joined samples tested. Close inspections of the fracture sites were made for all samples. The lower strengths of 360 and 201 MPa observed for the two samples is believed to be due to the presence of larger flaws. To confirm this, fractography was conducted on the two low-strength samples. SEM photomicrographs revealed surface damage on the tensile surfaces in the two low-strength samples. It is speculated that this damage was introduced during the sample preparation steps or handling. Typical lengths of this damage were 70–90 μm . Using a nominal crack length of 80 μm , apparent toughness of 3.6 $\text{MPa}\sqrt{\text{m}}$ for ZT60A, and fundamental fracture mechanics,⁹ the fracture strength was calculated to be approximately 350 MPa. This calculated fracture strength is consistent with the measured strength for the low-strength ZT60A/ZT40A sample. Thus, in addition to the residual stresses, the size and distribution of failure-causing flaws in the ceramic materials will control the strength of the joint. This also explains why failure location in the joined samples does not necessarily coincide with the peak tensile residual stresses.

Design and Fabrication of Air- Reference Free Potentiometric Planar

A realistic miniaturization of a high-temperature, potentiometric planar oxygen sensor is possible by replacing the open-air reference column in current sensors with a metal/metal oxide

Rhines pack at high temperatures. Gas-tight sealing of the internal reference oxygen pressure was a problem, but eventually perfect seals were obtained by joining the edges of the ceramic components by plastic deformation. This design, free of external reference, enables position flexibility and mobility of the sensor inside all combustion units. This report will detail the work that was performed in conjunction with a team from Ohio State University after it contacted ANL and detailed the sealing problems they were encountering using more conventional methods.

The main components for the sensor fabrication are made of yttria-doped tetragonal zirconia polycrystalline (YTZP) ceramics, pellets, a ring, and green tapes. One YTZP pellet is partly covered with platinum ink, and a small-gauge platinum (Pt) wire is placed within intimate contact of the Pt ink in order to create a reference electrode. This electrode ink on the pellet (electrolyte) is fired at 1000°C in order to cure the electrode ink. The Pt wire is slipped between two rings of YTZP green tapes, and the pellet is placed wire-down onto the other fabrication components as shown in Figure 3. The components are joined together in a two-step process. The first joining step produces a cylinder, after which Ni/NiO powder is inserted into the cylinder and lightly compacted. Finally, the tapes and electrodes with the Pt wire are joined to the filled cylinder. Joining was readily achieved at 1200°C in an argon atmosphere using a nominal strain rate of $4 \times 10^{-5} \text{ s}^{-1}$.

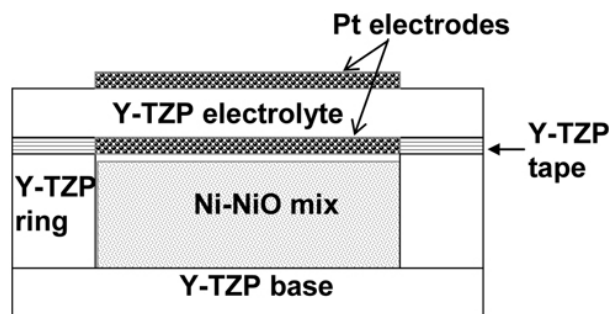


Figure 3. Ceramic components and stacking of the internal reference planar oxygen sensor.

An SEM micrograph of the top joint (with tapes) is shown in Figure 4. The sharply delineated edges of the joint shown in the low-magnification micrograph are the result of a slight offset between

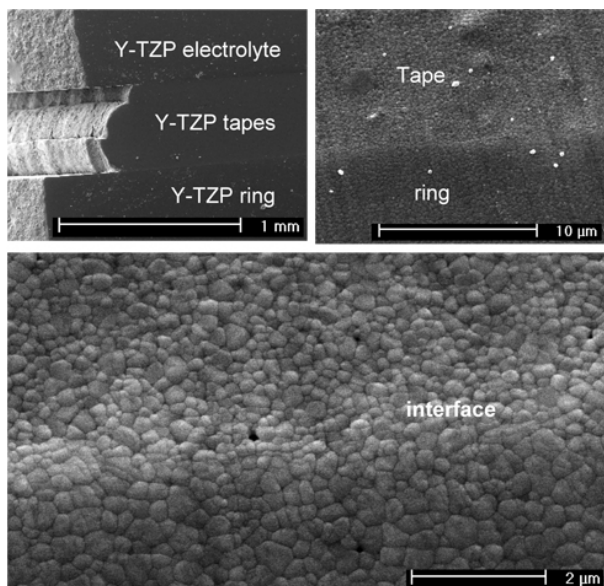


Figure 4. Top joint microstructure (with tapes).

the top disk, the green tapes, and the cylinder. However, it can be seen that the joint contains only a very limited amount of porosity that was present in the initial materials.

The electromotive force (EMF) as a function of oxygen partial pressure at 600°C is shown in Figure 5. These tests, performed as a function of time, indicate that the joints are indeed gas tight.

Summary of Sensor Production

The plastic joining technique works and produces gas-tight seals. The sensor is viable and has the required sensitivity and response time. However, the EMF does not agree with the theoretical calculated EMF. This is most likely because the Ni/NiO was reduced by joining at 1200°C in an argon atmosphere. In the coming fiscal year, experiments will be performed to produce sensors joined in air or even in pure oxygen. Furthermore, several candidate reference materials under consideration may yield higher sensitivities. This work will form part of the Ph.D. thesis of John Spirig.

Joining of Hydroxyapatite

Hydroxyapatite (HA) is a very common biomaterial that is generally used as a coating over a non-biocompatible material for implants such as teeth. Of course, coatings can be inexpensively applied using a number of different techniques.

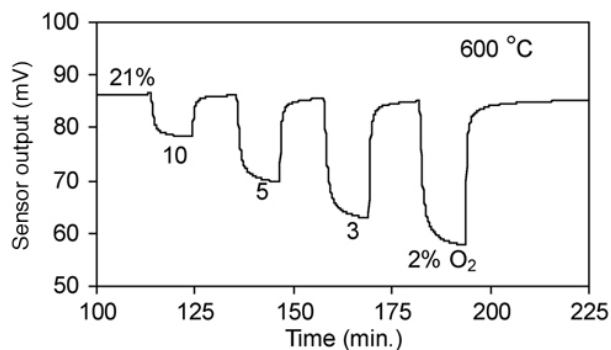


Figure 5. Oxygen sensing response at 600 °C of the fabricated sensor. Sensor has been gas-tight for several months.

However, producing complex shapes by these techniques is difficult. Joining by plastic deformation presents a new possibility for production of complex pieces of HA. Therefore, the first phase of this work was to determine the conditions under which HA exhibits plasticity.

HA was obtained from Professor Eldon Case of Michigan State University. The material was > 98% of theoretical density and had a bimodal grain size distribution with the largest grains being $\approx 5 \mu\text{m}$ and the smallest $\approx 1 \mu\text{m}$. Figure 6 indicates that HA deforms into nearly a steady-state stress between 2.0 and 2.5 MPa at 1275°C at a strain rate of 10^{-5} s^{-1} . Strains of over 0.08 were achieved without fracture.

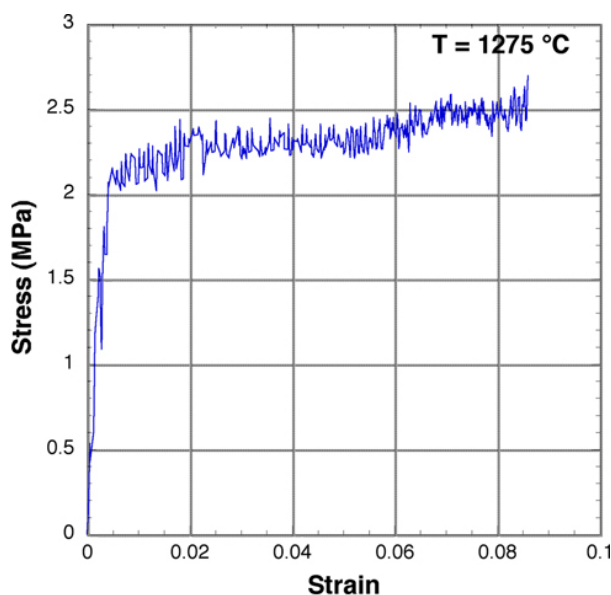


Figure 6. Stress-strain data obtained from hydroxyapatite at 1275°C at a strain rate of 10^{-5} s^{-1} .

Two pieces of HA were placed in the Instron and compressed to about 8% strain at 1275°C using a strain rate of 10^{-5} s^{-1} . The pore-free joint that was produced is shown in Figure 7. The joint is indistinguishable from the matrix. It is also noteworthy that the microstructure was unchanged. The next step will be to determine the temperature, strain, and strain rate region over which joining by plastic deformation is possible.

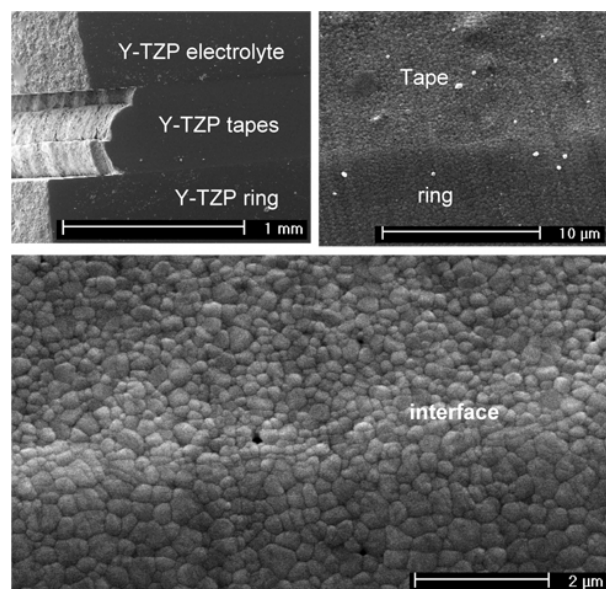


Figure 7. Joint in hydroxapatite produced at 1275°C at a strain rate of 10^{-5} s^{-1} . Arrows indicate the interface between the two joined pieces.

Conclusions

We have shown that we can form pore-free, very strong joints in a wide variety of important materials by plasticity. Previously we have reported on joining structural and electronic ceramics, metal-matrix composites, Ni_3Al , whisker-reinforced ceramics, and cermets. Previous work has shown that experimental determinations of the residual stress agree with calculated values. Little surface preparation and modest temperatures are required for deformation joining. Those factors make the process attractive for commercialization. Using the alumina/zirconia system as a model material, we have shown that the fracture of a joined bar of the same composition has the same strength as the matrix. The fracture of a joined 4-pt bend bar of dissimilar compositions does not fracture at the interface, but at a position near the maximum residual tensile stress.

We have continued to expand the materials that can be joined by plastic deformation. In this fiscal year, we have studied high-temperature deformation and joined a biomaterial, HA. We have applied the technique to a practical problem, producing a gas-tight oxygen sensor.

Future work will concentrate on joining dissimilar materials, such as intermetallics, to ceramics. We also plan to join optical materials and assess the quality of the join using optical transmission. Preliminary feasibility studies to perform an in-situ deformation study of grain rotation are under way. We are investigating the deformation characteristics of several possible candidate materials with a view of choosing one that has suitable X-ray transmission properties, but that deforms into steady state at modest temperatures by grain boundary sliding. Preliminary designs of a furnace and deformation apparatus will be considered in FY 2005, pending funding.

References

1. F. Gutiérrez-Mora, K. C. Goretta, S. Majumdar, J. L. Routbort, M. Grimdich, and A. Domínguez-Rodríguez, "Influence of Internal Stresses in Superplastic Joining of Zirconia Toughened Alumina," *Acta Materialia*, **50**, 3475–3486 (2002).
2. K. C. Goretta, F. Gutiérrez-Mora, J. J. Picciolo, and J. L. Routbort, "Joining Alumina/Zirconia Ceramics," *Mat. Sci. and Eng.*, **A341**, 158–162 (2003).
3. F. Gutierrez-Mora, K. C. Goretta, J. L. Routbort, and A. Dominguez-Rodriguez, "Joining of Ceramics by Superplastic Flow," in *Advances in Ceramic Matrix Composites VII, Ceramic Transaction # 128*, ed. N. P. Bansal, J. P. Singh, and H. T. Lin, p. 251, The American Ceramic Society, Westerville, Ohio (2002).
4. N. Chen, F. Gutierrez-Mora, R. E. Koritala, K. C. Goretta, J. L. Routbort, and J. Pan, "Joining Particulate and Whisker Ceramic Composites by Plastic Flow," *Comp. Struct.*, **57**, 135–139 (2002).
5. F. Gutierrez-Mora and J. L. Routbort, "Electrical Characterization of a Joined Electroceramics $\text{La}_{0.85}\text{Sr}_{0.15}\text{MnO}_3$," *J. Am. Ceram. Soc.*, **85**(9), 2370–2372 (2002).
6. F. Gutiérrez-Mora, A. Domínguez-Rodríguez, J. L. Routbort, R. Chaim and F. Guiberteau, "Joining of Yttria-Tetragonal Stabi-

lized Zirconia Polycrystals using Nanocrystals,” *Scripta Mat.* **41**, 455–460 (1999).

7. F. Gutierrez-Mora, D. Singh, N. Chen, K. C. Goretta, J. L. Routbort, and A. Dominguez-Rodriguez, submitted to *J. European Ceramic Society*.

8. F. Gutierrez-Mora, K. C. Goretta, N. Chen, and J. L. Routbort, “Joining of Advanced Ceramics by Plastic Flow,” *Ceramics Intl.* **30**, 1945–1948 (2005).

9. H. L. Ewalds and R. J. H. Wanhill, *Fracture Mechanics*, p. 37, Edward Arnold, Delftse, The Netherlands (1984).

Publications and Presentations

A. Dominguez-Rodriguez, F. Gutierrez-Mora, M. Jimenez-Melendo, J. L. Routbort, and R. Chaim, “Current Understanding of Deformation of Y-TZP and Superplastic Joining of Ceramics,” *J. Mater. Engr.* **A302**, 154–161 (2001).

A. Dominguez-Rodriguez, F. Gutierrez-Mora, M. Jimenez-Melendo, R. Chaim, and J. L. Routbort, “Superplasticity and Joining of Zirconia-Based Ceramics,” presented at the Materials Research Society Symposium, Proceeding 601 99-104, 2000.

F. Gutierrez-Mora, K. C. Goretta, J. L. Routbort and A. Domínguez-Rodríguez, “Joining Ceramics by Superplastic Flow,” *Ceramic Transactions* **128**, 252–258 (2002).

K. C. Goretta, F. Gutierrez-Mora, J. J. Picciolo, and J. L. Routbort, “Joining Alumina/Zirconia Ceramics,” *J. Mater. Engr.* **A341**, 158–162 (2003).

A. R. De Arellano-Lopez, U. Balachandran, K. C. Goretta, B. Ma, and J. L. Routbort, “High-Temperature Deformation of $\text{Sr}(\text{FeCo})_{1.5}\text{O}_x$ Ceramics,” *Acta Materialia* **49**, 3109–3116 (2001).

F. Gutierrez-Mora, K. C. Goretta, S. Majumdar, J. L. Routbort, M. Grimdisch, and A. Dominguez-Rodriguez, “Influence of Internal Stresses on Superplastic Joining of Zirconia-toughened Alumina,” *Acta Materialia* **50**, 3475–3486 (2002).

E. Wuchina, M. Opeka, F. Gutierrez-Mora, R. Koritala, K. C. Goretta, and J. L. Routbort, “Processing and Mechanical Properties of Solid-solutions of Hf-N,” *J. European Ceramic Soc.* **22**, 2571–2576 (2002).

N. Chen, F. Gutierrez-Mora, R. E. Koritala, K. C. Goretta, J. L. Routbort, and J. Pan, “Joining

Particulate and Whisker Ceramic Composites by Plastic Flow,” *Composite Structures*, **57**, 135–139 (2002).

A. R. de Arellano-Lopez, J. J. Melendez-Martinez, A. Dominguez-Rodriguez, T. A. Cruse, R. Koritala, J. L. Routbort, and K. C. Goretta, “Compressive Creep of Mullite Containing Y_2O_3 ,” *Acta Materialia* **50**, 4325–4338 (2002).

F. Gutierrez-Mora and J. L. Routbort, “Electrical Characterization of a Joined Electroceramic, $\text{La}_{0.85}\text{Sr}_{0.15}\text{MnO}_3$,” *J. American Ceramic Society* **85**, 2370–2372 (2002).

F. Gutierrez-Mora, J. M. Ralph, and J. L. Routbort, “High-temperature Mechanical Properties of Anode-Supported Bilayers,” *Solid State Ionics* **149**, 177–184 (2002).

A. R. de Arellano-Lopez, K. C. Goretta, E. T. Park, S. E. Dorris, U. Balchandran, and J. L. Routbort, “High-temperature Deformation of a $\text{BaCe}_{0.8}\text{Y}_{0.2}\text{O}_{3-y} + \text{Ni}$ Composite,” *J. European Ceramic Society* **22**, 2555–2560 (2002).

J. L. Routbort, J. Ralph, R. E. Cook, C. Clauss, and A. R. de Arellano-López, “Creep of $(\text{La}_{0.55}\text{Sr}_{0.45})_{0.99}\text{Mn}_{1-y}\text{Ga}_y\text{O}_3$,” *Phys. Chem. Chem. Phys.* **5**, 2232–2236 (2003).

K. C. Goretta, F. Gutierrez-Mora, N. Chen, J. L. Routbort, T. A. Orlova, B. I. Smirnov, and A. R. de Arellano-López, “Solid-Particle Erosion and Strength Degradation of $\text{Si}_3\text{N}_4/\text{BN}$ Fibrous Monoliths,” *Wear* **256**, 233–242 (2004).

J. Martinez-Fernandez, A. R. de Arellano-Lopez, F. M. Varela-Feria, T. S. Orlova, K. C. Goretta, F. Gutierrez-Mora, Nan Chen, and J. L. Routbort, “Erosion and Strength Degradation of Biomimetic SiC ,” *J. European Ceramic Society* **24**, 861–870 (2004).

K. C. Goretta, Nan Chen, F. Gutierrez-Mora, J. L. Routbort, G. C. Lukey, and J. S. J. van Deventer, “Solid-Particle Erosion of a Geopolymer Containing Fly Ash and Blast-Furnace Slag,” *Wear* **256**, 714–719 (2004).

F. Gutierrez-Mora, K. C. Goretta, Nan Chen, and J. L. Routbort, “Joining of Advanced Ceramics by Plastic Flow,” *Ceramics International* **30**, 1945–1948 (2004).

F. Gutierrez-Mora, D. Singh, N. Chen, K. C. Goretta, J. L. Routbort, and A. Dominguez-Rodriguez, “Fracture of Composite Alumina/Yttria-stabilized Joints,” *J. European Ceramic Society*, in press

K. C. Goretta, T. A. Cruse, D. Singh, J. L. Routbort, A. R. de Arellano-Lopez, T. S. Orlova, and B. I. Smirnov, "Ceramic Fibrous Monolithic Structures," *Composite Structures* **66**, 547–553 (2004).

D. Singh, F. Guiterrez-Mora, N. Chen, K. C. Goretta, and J. L. Routbort, "Joining of Advanced Structural Materials by Plastic Deformation," *Advances in Ceramics*, in press.

F. Guiterrez-Mora, K. C. Goretta, D. Singh, J. L. Routbort, S. Sambasivan and K. Steiner, "High-Temperature Mechanical Behavior of Alu-

minum-Phosphate Based Glass Ceramics (Cerab-lak)," *J. European Ceramic Society*, in press.

Patent Applications

K. C. Goretta, J. L. Routbort, and F. Gutiérrez-Mora, "Joining of Advanced Materials by Plastic Deformation, invention report, 0003/00950.

J. L. Routbort, et al., "Method Of Fabrication of a High-Temperature Potentiometric Oxygen Sensor," invention report ANL-IN-04-105

E. Friction Stir Joining and Processing of Advanced Materials Including Metal Matrix Composites

Principal Investigator: Glenn J. Grant

Pacific Northwest National Laboratory

P.O. Box 999, 902 Battelle Blvd., Richland, WA 99352

(509) 375-6890; fax: (509) 375-44; e-mail: glenn.grant@pnl.gov

Project Manager: Moe Khaleel

Pacific Northwest National Laboratory

P.O. Box 999, 902 Battelle Blvd., Richland, WA 99352

(509) 375-2438; fax: (509) 375-6631; e-mail: moe.khaleel@pnl.gov

Technology Development Area Specialist: Sidney Diamond

(202) 586-8032; fax: (202) 586-1600; e-mail: sid.diamond@ee.doe.gov

Field Technical Manager: Philip S. Sklad

(865) 574-5069; fax: (865) 576-4963; e-mail: skladps@ornl.gov

Participants

Bill Arbogast, Glen Stone, Stan Howard, Casey Allen

Advanced Materials Processing Center

South Dakota School of Mines and Technology

Rapid City, S.D.

Contractor: Pacific Northwest National Laboratory

Contract No.: DE-AC06-76RLO1830

Objective

- Investigate and develop friction stir joining (FSJ) and friction stir processing (FSP) as viable industrial joining and processing techniques for advanced materials, including aluminum metal matrix composites (MMCs), titanium, and advanced high-strength steel. During FY 2004, this project focused on two main task areas: the development of appropriate tooling and process parameters that will allow friction stir welding (FSW) to be used in abrasive and/or high-temperature materials, and the use of the FSP process to modify the surfaces of materials for advantageous near-surface mechanical and thermal properties.

Approach

- Develop new tooling designs and fabricate tools from advanced tooling materials (Ni-alloy and Fe-matrix TiC MMCs).
- Develop weld process methods, such as induction preheating, to lower process forces and reduce wear or tool breakage issues in hard-to-weld materials.
- Experimentally determine the feasibility of making near-surface graded composites by FSP in aluminum and steel to create functionally graded materials with enhanced surface-engineered properties.
- Investigate the new method of friction surface reaction processing (FSRP) in which a friction stir tool is used to initiate in situ solid-state reactions that can stabilize new phases or ultra-fine grained phases in the near-surface regions of bulk materials for enhanced surface properties.

- Investigate the application of FSJ to ferritic oxygen-dispersion-strengthened (ODS) alloys, including MA957.
- Investigate the use of FSP to create robust thermal barrier coatings on steel.

Accomplishments

- Fabricated tools using new unique designs that will be used in coatings and wear studies.
- Developed, at the South Dakota School of Mines and Technology, induction preheating techniques that facilitate FSJ/P in steels and cast iron.
- Created near-surface regions in aluminum and steel that are enriched in ceramic particulate by physically stirring powders into the surface using a spinning friction stir tool.
- Began experimental studies into FSRP by plasticizing and reacting elemental powders and oxides beneath a spinning tool during FSP.
- Performed preliminary experiments on using FSP to plasticize MA957, a ferritic ODS alloy.
- Used FSP to process pre-existing thermal barrier coatings on steel to create diffuse, interface-free, near-surface zones that have unique thermal properties.

Future Direction

- Further develop tool materials and designs for steel and titanium FSJ/P
- Develop process parameters and conditions necessary for surface modifications of steel and titanium
- Develop friction stir surface processing for thermal barrier applications
- Develop the process of reaction surface processing to create, by solid-state chemical reaction, new phases at the surface.

Introduction

Friction Stir Joining

One of the key strategies for making a vehicle energy-efficient is to manufacture it from lighter materials. Structural and functional requirements, however, lead to a situation where no single lightweight material is appropriate for all applications. A modern, weight-optimized vehicle structure is a hybrid of many materials. A critical problem that has emerged in the development of these hybrid structures is that for many material combinations, traditional joining technologies (e.g., fusion welding or mechanical fastening) are not appropriate. For some highly specialized materials, like aluminum MMCs, titanium, and advanced high-strength steels, a better joining technology can have significant impact on whether these materials have a role in future vehicle structures.

In the last 15 years, the new joining technology FSJ has emerged that has the potential to join many lightweight materials. Invented by TWI, Ltd., FSJ is

a solid state process that employs severe plastic deformation to create joints between a wide variety of different materials. A typical FSJ butt joint is depicted in Figure 1. The weld is created by clamping the materials to be joined and plunging a spinning tool into the surface. The spinning tool is then translated down the joint line, leaving behind a weld zone characterized by a fine-grained, dynamically recrystallized microstructure. Typically, the tool is spun at 400 rpm to 2000 rpm and translated down the joint line at a rate of 4 to 300 in./min, depending on tool design, base material, and thickness. As the tool rotates and translates, complex flow patterns develop in the base material that create an intimate mixing of materials from both sides of the weld. Heat input during plastic deformation generally creates a temperature in the weld between 0.6 and 0.8 of the absolute melting temperature so that no liquid phase is generated.

FSJ is capable of producing aluminum and magnesium alloy welds as good as or better than fusion welds in terms of joint efficiency, mechanical

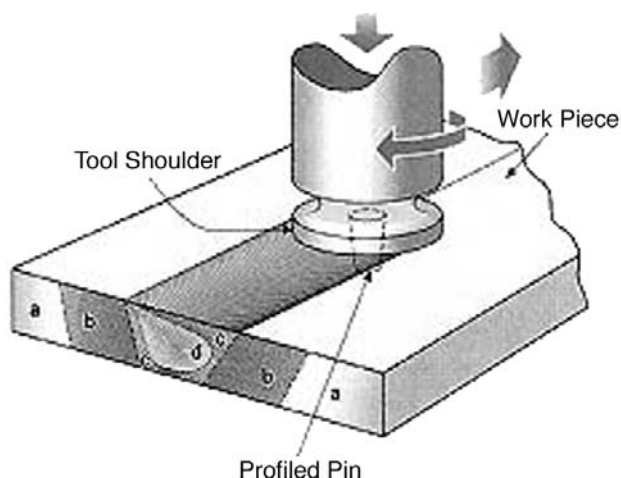


Figure 1. Friction stir joining and processing are accomplished by plunging a spinning tool into a material and translating the tool across the surface to form either a joint or a surface processed region (TWI, Ltd.).

properties, and environmental robustness. A significant advantage of the process, for application to hybrid structures, is that since there is no melting during the process, a large variety of dissimilar material joints are possible, including dissimilar aluminum and magnesium joints that are not possible with conventional fusion welding.

In the last five years, FSJ has been shown to be a commercially important, energy-efficient, and environmentally friendly process for joining aluminum. However, there are many opportunities for other higher-strength lightweight materials to be considered if there existed good joining technologies for these materials as well. The objective of this project is to investigate how FSJ can be applied to advanced materials including AL-MMCs, titanium, and steels. Moving the FSJ process from “soft” materials like aluminum and magnesium into advanced, higher-strength alloys has proved to be challenging because of the mechanical and thermal demands on the tool materials. In steels, for instance, the tools must survive high forge loads as well as tool temperatures of up to 1100°C. A primary challenge is to develop pin tool designs and materials that can survive the high-temperature and/or abrasive-wear conditions under which the tool will be forced to operate.

Friction Stir Processing

Recently, a new research direction has emerged, as an outgrowth of FSJ, that recognizes that the same solid state deformation process can be used to mod-

ify the surface of a monolithic material for enhanced properties. This new research direction is called FSP.

Several applications of FSP have been investigated during the course of this project including surface modification for wear resistance, for creation of bulk superplastic properties, and for improvement to the near-surface defect and porosity distribution in Al-MMC castings. Work during FY 2004 concentrated on creating wear-resistant surfaces by FSP particle incorporation, on creating engineered surfaces by solid state reaction- processing, and on basic experiments in creating thermal barrier coatings by FSP.

This work was designed to test the feasibility of using FSP to create engineered surfaces. During previous years, this work demonstrated that it is possible to create a particle-reinforced zone of 20-micron SiC or Al₂O₃ particles in a 6061 aluminum base alloy (Figure 2). Microscopy has shown that the stirred region is developed as deep as the pin probe (2–3 mm in our tests), which is defect-free and forms a graded metallurgical bond with the underlying surface. No interface is developed between

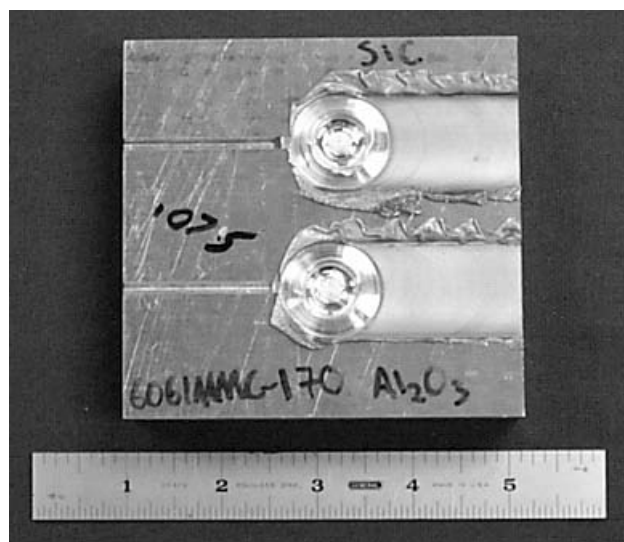


Figure 2. Friction stir processed 6061 plate with ceramic particulate incorporated into the surface.

the composite zone and the base material. The surface zone has the potential to be orders of magnitude thicker than conventional coating technologies; and it has the added benefit of producing a graded structure that does not have a sharp interface with the underlying substrate, thereby avoiding many of the problems seen in conventional coatings (coefficient of thermal expansion mismatch, etc.).

While lightweight wear-resistant materials could benefit from this compositing technique, perhaps the greater application could be in ferrous or hard alloy systems. Hard particle reinforcement of the surfaces of steels, titanium, brasses, or cast iron may have numerous industrial applications in reciprocating assemblies, engines, brake disks, or other situations where both bulk strength and surface wear resistance is needed. Lightweight high-strength steels with surface wear resistance may have numerous applications in both lightweight structures and lightweight vehicle power systems. Work during FY 2004 focused on developing methodologies to successfully surface-process high-temperature materials including steels and cast iron.

Approach

The basic objective of this project is to investigate and develop FSJ and FSP as viable industrial techniques for advanced lightweight materials. The approach used has been to (1) seek to develop new tool materials and designs that will allow successful joins to be made in Al-MMCs, titanium, and steel; and (2) explore the potential to modify the surfaces of both conventional aluminum and magnesium alloys and advanced materials toward the goal of improving wear, corrosion, or mechanical properties.

The FY 2004 program is divided into three main tasks. The first task focused on developing tool designs and fabricating tools in some of the tool materials defined by last year's efforts. The second task area broadly investigated using FSP to create engineered surfaces. Surface modification was investigated in three areas: (1) particle incorporation to create near-surface MMCs in aluminum and steel, (2) surface alloying by reaction processing, and (3) surface modification of pre-existing thermal barrier coatings to possibly create graded structures with unique thermal properties. In addition, to facilitate FSP in steels, we investigated the use of induction preheating to lower process forces in these hard-to-process materials. Finally, the third main task was a

small investigative effort into the feasibility of using FSJ to join or process a ferritic ODS alloy, MA957. This material is a creep-resistant high-temperature steel that has potential application in high-temperature environments such as solid oxide fuel cells.

Results

Tool Materials and Designs

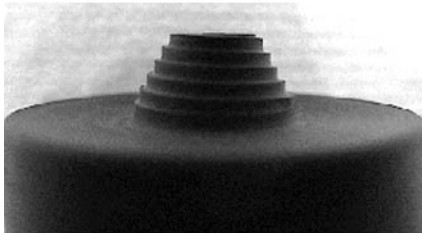
During FY 2003, promising tool materials were identified for each material system. In FY 2004, tools were fabricated from some of these materials, and the tools were used to process aluminum and steel surfaces. Figure 3 shows several tools made from H13 (baseline), MP159 (a cobalt-nickel alloy), and FerroTiC (an iron-based TiC MMC). These tool materials show virtually no wear during FSJ of standard aluminum alloys. However, creating surface-modified regions enriched in ceramic particles requires tool materials to have strong wear resistance. In aluminum MMC systems with either SiC or Al₂O₃ particulate, H13 and nickel alloy materials showed significant wear, while FerroTiC showed



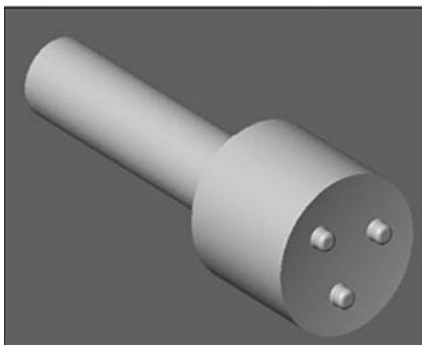
Figure 3. Tool materials clockwise from lower left: MP159 (a cobalt-nickel-chrome-moly alloy), H13 tool steel, and FerroTiC (35% TiC in an impact-resistant, iron-based tool steel)

virtually no wear. This project also investigated stirring ceramic particulate into steel substrates. In these cases, tools were composed of tungsten 25% rhenium.

Particle distribution within a surface-modified layer is dependent (among other things) on tool design. During FY 2004 this project investigated numerous tool designs in an effort to improve particle distribution and placement with a processed layer. Figure 4 shows tools of differing designs, including wide pins, narrow pins, scrolled shoulders, and multi-pin tools. The basic design philosophy is to create a wide stir zone (Figure 5) with a high degree of vertical mixing to drive the particulate from the surface to the deepest part of the processed region



Step Spiral Tool



Three Pin Tool



Three Paddle Tool

Figure 4. Different tool designs produce different particle distributions and flow characteristics.

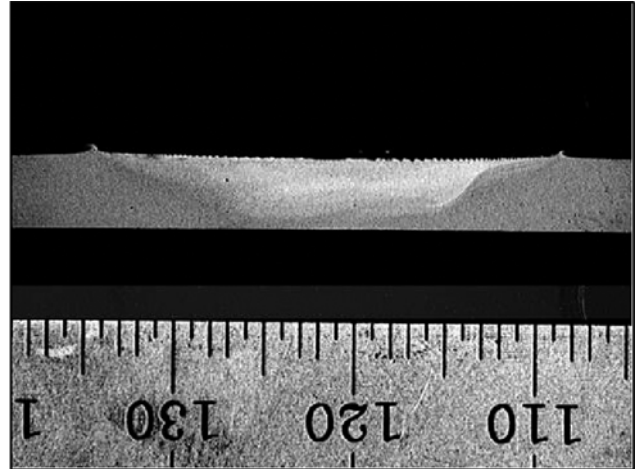


Figure 5. Wide stir zones can be created using three-pin tools. Wide zones are important to minimize passes required to process larger areas.

(Figure 6). Experimental work has shown that both the three-pin designs and the wide stepped spirals can achieve this goal.



Figure 6. Tool design affects material flow during FSP. Features on the tool surface can promote flow from surface to base of processed region and channel surface powders, for instance, to the pin root zone.

Friction Stir Surface Processing

Much of the effort in FY 2004 was directed toward the new field of FSRP. Thermodynamic calculation of numerous potential solid state reactions indicates that energies available during FSJ/P may be high enough to initiate the formation of some compounds like TiB_2 from elemental constituents, especially considering all the new surface being generated by the severe plastic deformation under the pin tool. This process opens the possibility of making very finely divided reaction products in the near-surface region of a bulk material (see Table 1). These reactions can be tailored by the composition of the elemental powders introduced on the surface. In addition, highly exothermic (thermite style) reactions may be possible that can put large amounts of heat into the surface and potentially reduce the flow stress of hard-to-weld alloys, or allow the FSJ process to occur without significant tool wear. Claddings of materials rich in fine oxide dispersions, or other in situ-formed ceramic-rich materials, may be possible on low-cost ferritic base alloys (creep-resistant surfaces for engine applications).

from X-ray diffraction analysis. Despite the highly favorable Gibbs free energies for these reactions, only limited reaction products were formed. The large driving force for reaction with little reaction is a clear indication that the activation energy for the reaction was not satisfied. Higher temperatures decrease the activation energy, making spontaneous reaction more likely. In FY 2005, the project will investigate the FSRP process in higher-temperature processing environments like those found when processing iron- or titanium-based materials. In addition to higher temperatures, catalysts may also be employed as a means of lowering the activation energy. Additional work is planned on this as well as on other reaction systems, as outlined in Figure 9, including systems where the tool pin is a reactant and thermite-type systems.

Work was also initiated on a study of the potential for using FSP to process previously deposited thermal barrier coatings (TBCs). In many applications, TBCs can show reliability problems as a result of cracking and spalling of the coating at the

Table 1. Reaction modes

Mode	Reaction	Examples
I	Base Metal (Al) + Reactant	$3 \text{SiO}_2 + 4\text{Al} \longrightarrow 3\text{Si} + 2\text{Al}_2\text{O}_3$
	\longrightarrow Product	$3 \text{TiO}_2 + 4\text{Al} \longrightarrow 3\text{Ti} + 2\text{Al}_2\text{O}_3$
		$\text{BN} + \text{Al} \longrightarrow \text{AlN} + \text{B}$
II	Pin Tool (Ti) + Reactant	$3 \text{Ti} + 2 \text{BN} \longrightarrow 2 \text{TiN} + \text{TiB}_2$
	\longrightarrow Product	$\text{Ti} + \text{AlN} \longrightarrow \text{TiN} + \text{Al}$
		$\text{Ti} + \text{C} \longrightarrow \text{TiC}$
		$\text{Ti} + 2\text{B} \longrightarrow \text{TiB}_2$
III	$\text{A} + \text{B} \longrightarrow \text{C} + \text{D}$	$4\text{Al}_{(\text{powder})} + 3\text{SiO}_2 \longrightarrow 3\text{Si} + 2\text{Al}_2\text{O}_3$
		$4\text{Al}_{(\text{powder})} + 3\text{TiO}_2 \longrightarrow 3\text{Ti} + \text{Al}_2\text{O}_3$

Work in FY 2004 concentrated on reactions in the aluminum system, as outlined in Table 1.

Reactant powders were placed between plates of 1100 alloy aluminum as shown in Figure 7. The assembly was then friction-stir-processed to produce a microstructure, as shown in Figure 8. The nugget region contains very finely dispersed precursor reactants but only a small amount of reactant product coating/substrate interface. FSP may be able to cre-

ate more robust coatings by disrupting the sharp interface and creating a graded structure. Issues with coefficient of thermal expansion mismatch may be reduced by creating this graded stir zone. Most TBC systems are in materials that are very difficult to FSP because of their hot hardness or lack of plastic properties needed to form good FSP microstructure.

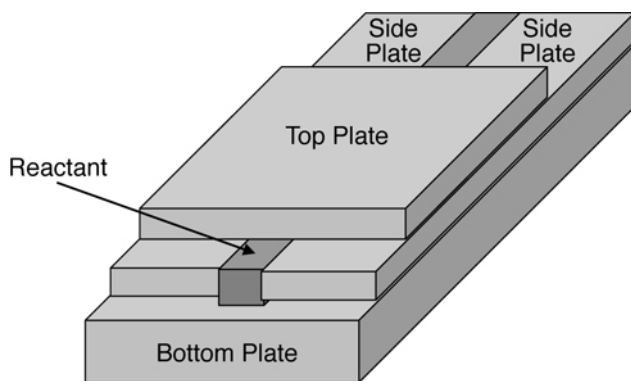


Figure 7. Reactant oxide powders are placed between plates, and the stir tool processes the entire thickness

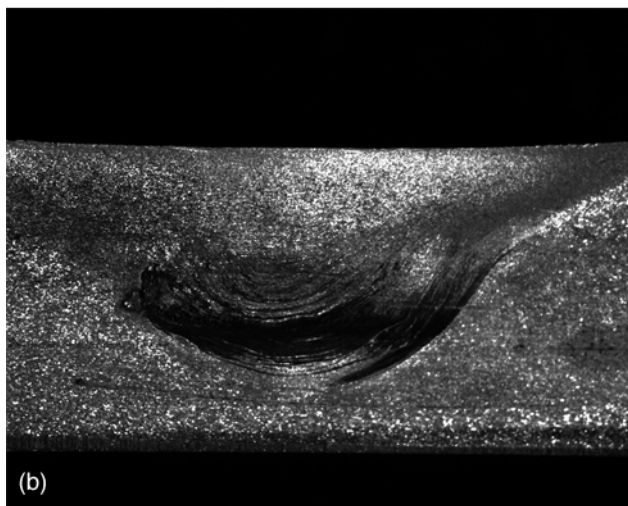
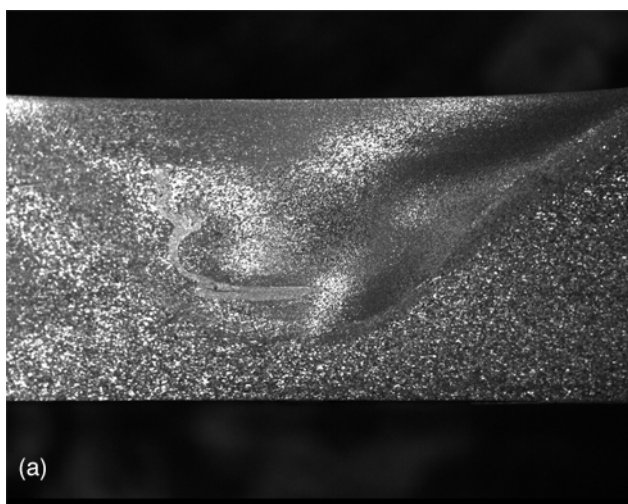
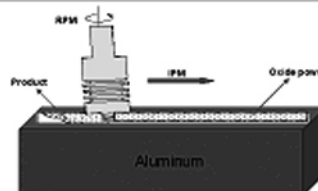


Figure 8. Cross sections showing fully consolidated weld zone. FSRP zone is 3/8-in (9.52 mm) thick: (a) SiO₂ and (b) TiO₂.

Mode I

Base metal reacts with the oxide powder introduced during the friction stir welding process.



Reactions of interest:



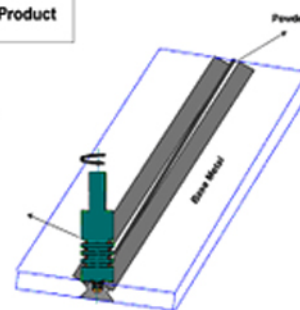
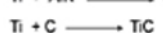
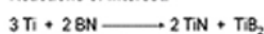
Note: non-oxide powders may also be used

Mode II

The pin tool material reacts with the powder which is placed between two plates during the friction stir welding process.

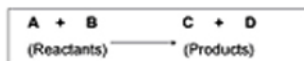


Reactions of interest:



Mode III

Two different materials react to form products. The two materials can be in powder or wire form.



Reactions of interest:

All the reactions that were used for Mode I & II will be considered

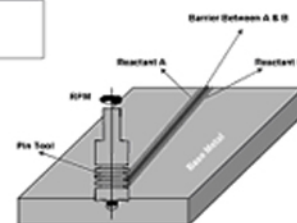


Figure 9. Different modes of reactions and experimental work planned in the current program.

Most of the work in FY 2004 was directed at finding process conditions in which the coating, usually a zirconia-based material, could be successfully mixed into the substrate, usually a steel. Figure 10 shows typical flame spray coatings investigated in this study. These are usually characterized by a top coat of ceramic material underlain by a bond coat of NiCrAlY on a steel substrate. The project investigated various combinations of coating thicknesses

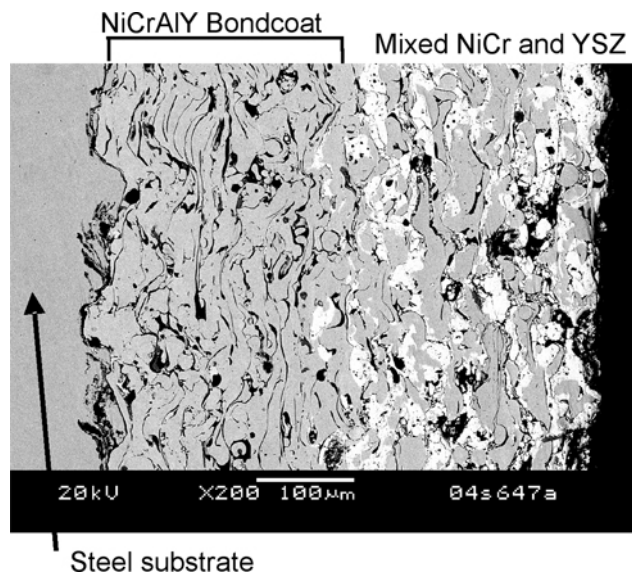


Figure 10. Typical flame spray deposited thermal barrier coating.

and graded metal ceramic coatings for their potential to be plasticized and processed using FSP. Figure 11 shows an example of a processed plate both during and after FSP. In some cases, especially with thick ceramic top coats, a large percentage of the top coat was chipped off during processing; but in other cases of graded or mixed ceramic/bond metal coatings, much of the coating was stirred into the nugget region.

Currently this project is investigating the thermal diffusivity/conductivity of these modified surfaces relative to the original coating; it is also investigating ways to better optimize the process so that less of the coating is lost during FSP.

Research at the South Dakota School of Mines and Technology has shown that induction preheating of the substrate prior to FSP can have an important effect on process forces and perhaps on the quality of the weld in difficult-to-weld materials. Figure 12 shows the induction heater mounted on the spindle head of the friction stir machine. Figure 13 shows that for 1018 steel, induction preheating can reduce process forces throughout the weld or processed region length.¹ Reduced process forces can be correlated with lower tool wear and better material flow in the weld. Additional work is planned in FY 2005 to define the effects of induction preheating better in steel and difficult-to-process materials.

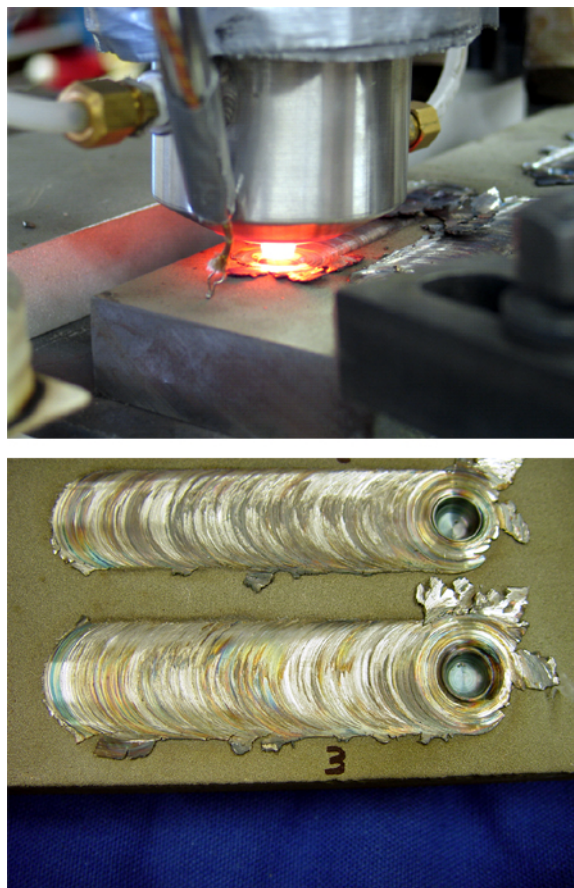


Figure 11. Zirconia-based thermal barrier coatings undergoing friction stir processing to mix coating into base material.

A final area investigated in FY 2004 was the applicability of FSJ/FSP to ferritic ODS alloys. These alloys have very good elevated-temperature creep properties resulting from the presence of fine dispersions of yttria in the steel matrix. One problem in using these materials for high-temperature applications is that they are very difficult to join. Few processes exist that can join these materials to other structures, or to themselves, without destroying the yttria dispersion and losing the high-temperature properties that make these materials attractive. Fusion welding can cause particle segregation, growth, or dissolution. FSP, however, is a solid state process and has the potential to join and process these alloys without destroying the yttria dispersion. Preliminary work during FY 2004 has shown that FSP can plasticize these alloys. Extruded tubes (25 mm in diameter with 3-mm wall thickness) of MA-957 with Inconel 625 inner rods were friction-stir-processed using a less than optimum

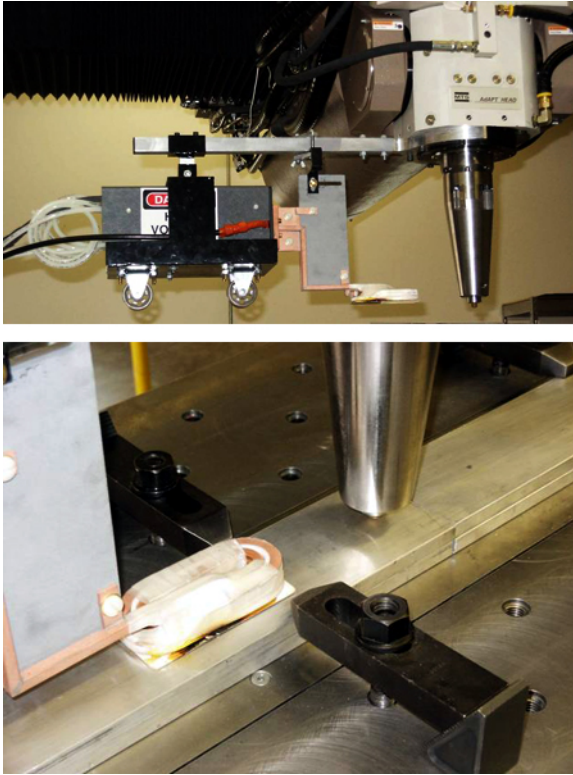


Figure 12. Induction pre-heating head mounted to FSJ machine spindle.

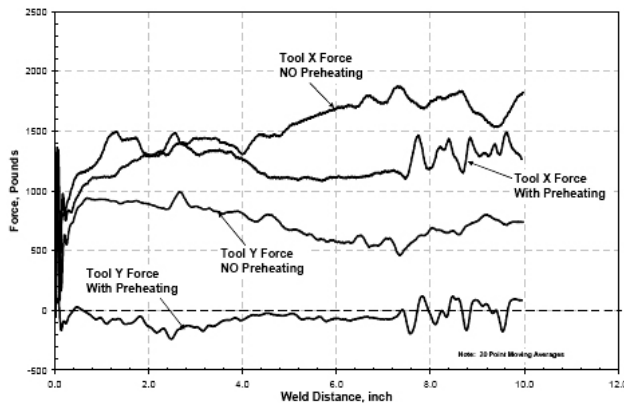


Figure 13. Work at South Dakota School of Mines and Technology has shown that induction preheating can lower process loads in difficult-to-weld materials like 1018 steel. (Figure courtesy of Tweedy, Arbegast, Allen 2004).

tool. Figure 14 shows plasticized material in the processed region. Transmission electron microscopy analysis and mechanical testing are under way to

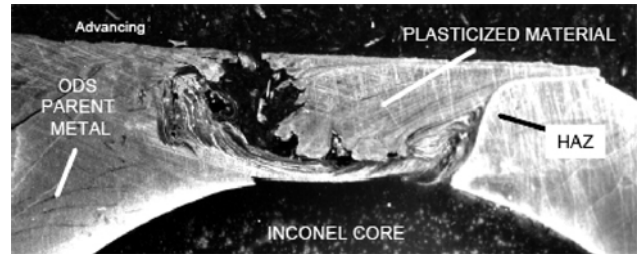


Figure 14. Cross section of ODS alloy tube plasticized by friction stir processing. Processed region is not consolidated due to tool-part mismatch, but plasticized region shows nature of flow and confirms that ODS alloys can be processed using FSP.

determine the effect of FSP on the yttria dispersion and whether creep properties are preserved.

Conclusions

FSJ and FSP are technologies that will enable the application of many lightweight materials in the next generation of transportation systems. Many advanced materials, such as Al-MMCs and certain high-strength steels (including ODS), are in need of effective joining technologies before their widespread use can be considered. Solid state FSJ/P avoids many of the problems with fusion joining and represents a revolutionary change in joining technology. FSP also has numerous opportunities in the growing field of surface engineering and thermal management.

The results of this work will allow designers to anticipate and implement structures that are a hybrid of many different materials, facilitate new applications, and suggest new materials and engineered surfaces that can help deliver lighter and more fuel-efficient vehicles.

References

1. B. M. Tweedy, W. Abergast, and C. Allen, "Friction Stir Welding of Ferrous Alloys using Induction Preheating," in *Friction Stir Welding and Processing III*, ed. K. V. Jata, M. W. Mahoney, and T. J. Lienhart, TMS, 2005.

Presentations/Publications

- G. J. Grant, *FY 2004 Semi-Annual Report: Friction Stir Joining and Processing of Advanced Materials, Including Metal Matrix Composites*, June 2004.

G. J. Grant, *PNNL Milestone Report PNNL 15534: Project:Friction Stir Joining of Advanced Materials including AL-MMCs: Complete Analysis and Characterization of FSP Process Parameters Needed to Fabricate Surface-Modified, Ceramic-Reinforced Metals*, Pacific Northwest National Laboratory, June 30, 2004.

S. M. Howard, W. Arbegast, B. Jasthi, G. J. Grant, D. R. Herling, "Friction Surface Reaction Processing On Aluminum Substrates," abstract submitted for 2005 TMS Annual Meeting, San Francisco.

S. M. Howard, W. Arbegast, B. Jasthi, G. J. Grant, D. R. Herling, "Friction Stir Welding Of MA 957 Oxide Dispersion Strengthened Ferritic Steel,"

abstract submitted for 2005 TMS Annual Meeting, San Francisco.

U. Ramasubramanian, W. Arbegast, G. Stone, G. J. Grant, "Friction Stir Processing Of Ferrous Alloys For Increased Wear Resistance," abstract submitted for 2005 TMS Annual Meeting, San Francisco.

R. L. Veluchamy, W. Arbegast, G. Stone, G. J. Grant, "Incorporating Titanium Powder to Create in-situ Composites on the Surface of Cast Iron via Friction Stir Reaction Processing (FSRP)," abstract submitted for 2005 TMS Annual Meeting, San Francisco.

F. Friction-Stir–Joined Aluminum Sheet Materials for Heavy Vehicle Cab Structures

Principal Investigator: Richard W. Davies

Pacific Northwest National Laboratory

P.O. Box 999, Richland, WA 99352-0999

(509) 375-6474; fax: (509) 375-4448; e-mail: rich.davies@pnl.gov

Technology Development Area Specialist: Sidney Diamond

(202) 586-8032; fax: (202) 586-1600; e-mail: sid.diamond@ee.doe.gov

Field Technical Manager: Philip S. Sklad

(865) 574-5069; fax: (865) 576-4963; e-mail: skladps@ornl.gov

Participants:

Scott Wazny, Leon Kaunitz, and Brian Fulbright, Freightliner LLC

Douglas Waldron and Keith McTernan, Advanced Joining Technologies, Inc.

Tom Sanor, Drive Automotive

Gene Paik, Alcoa, Inc.

Contractor: Pacific Northwest National Laboratory

Contract No.: DE-AC06-76RL01830

Objective

- Develop and deploy friction stir joining (FSJ) as a weight- and cost-saving manufacturing technology for heavy vehicle cab structures.

Approach

- Demonstrate the use of aluminum tailor-welded blanks (TWBs) for heavy vehicle applications.
- Develop and characterize TWBs prepared via FSJ.
- Develop and prototype several cab-in-white structures for Class 8 trucks.

Accomplishments

- Conducted preliminary stamping trials, which indicated that some material combinations and weld geometries can be successfully stamped into parts; this application has the potential for a significant cost and weight savings in heavy vehicle cab structures.
- Investigated new part configurations, using thin-gage heat-treatable alloys and dissimilar alloy combinations (5000 and 6000 series aluminum TWBs).
- Developed welding process parameters to minimize cost and maximize performance of truck components.
- Characterized the formability of welded assemblies through optical strain analysis.
- Characterized the local mechanical properties of the weld metal and surrounding region of AA5052-H32 and AA5182-O TWBs to understand the effect of the welding process on the ductility of the weld metal.
- Assembled successful parts into cabs and conducted full cab durability and crash testing at full truck load.

Future Direction

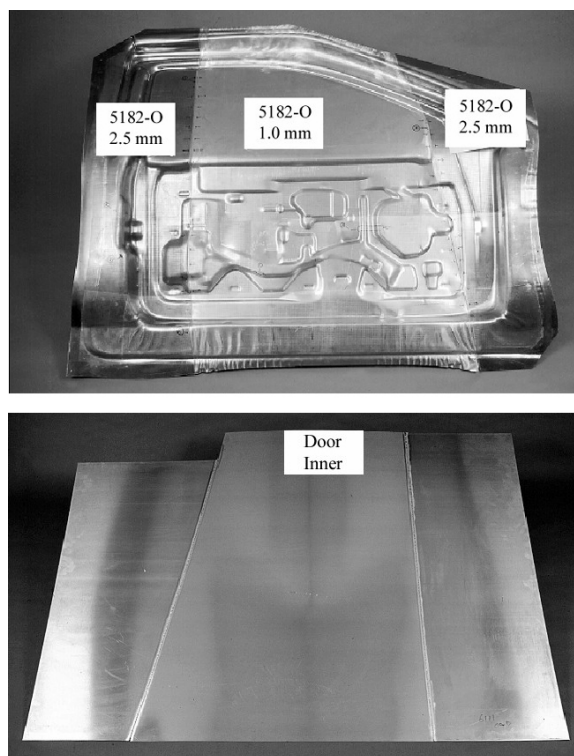
- Continue with the weld process development of 6000 series aluminum to increase the formability.
- Continue with weld process development of aluminum alloy 5052-H32 TWBs and optimize the welding process parameters.
- Investigate the interaction between the weld in the TWB and the joining method used to assemble the blank into the vehicle and determine how this interaction may influence long-term vehicle durability and crashworthiness.
- Develop and optimize the welding process parameters of dissimilar aluminum alloys of different thicknesses (5182-O and 6022 aluminum alloys).
- Conduct a design of experiments on tool development and design to determine the speeds and performances of different tools.
- Focus on FSJ as a low-cost enabler of lightweight, low-cost vehicle assembly (non-TWB).

Introduction

This work is a collaborative effort between Pacific Northwest National Laboratory (PNNL), Freightliner, LLC, Advanced Joining Technologies, Inc., Drive Automotive, and Alcoa. This project aims to develop and deploy FSJ as a cost- and weight-saving manufacturing technology for heavy vehicle cab structures. To date, the project has focused on (1) developing and characterizing TWBs prepared via FSJ and (2) demonstrating their use by prototyping several cab-in-white structures and body panels for Class 8 trucks.

Aluminum TWBs consist of multiple-thickness and multiple-alloy sheet materials welded together into a single, variable-thickness blank. Figure 1 shows a typical fusion-welded TWB before and after a stamping application. A TWB is assembled as a series of flat sheets joined together, which are then submitted to a stamping process. The technology allows production of a weight-optimized, variable-thickness vehicle body component. TWB technology gives automotive and truck designers the ability to selectively vary body panel thickness to optimize the use of material. Successful use of the technology ultimately results in reducing vehicle weight without compromising final strength, stiffness, and durability. The manufacture of TWBs and their application in body panels requires that the weld material deform under biaxial loading during sheet metal stamping. The deformation of weld materials and their limits of formability are important aspects of TWB technology.

The primary challenge of using aluminum TWBs in the past has been the relatively low quality



Photos courtesy of Reynolds Metals Company and Ogihara America Corp.

Figure 1. Left: A TWB viewed in the as-welded condition, ready for submission to the stamping process. The shape shown is typical for a door inner stamping operation. Right: Aluminum TWB after stamping to produce a door inner panel.

of aluminum fusion welds, which often results in premature fracture or lack of reliability of weld materials during stamping. Improving aluminum weld quality, understanding and describing the formability of the weld region, and predicting its formability

are the primary technical challenges in using aluminum TWBs.

FSJ is a revolutionary joining technology that employs severe plastic deformation to create solid state joints between wide varieties of different materials. Invented by TWI, Ltd., about 12 years ago, FSJ is capable of producing aluminum alloy welds as good as (or significantly better than) fusion welds in terms of joint efficiency, mechanical properties, and environmental robustness. The advantage of using this solid state joining technique is the ability to avoid liquid metal during joining, where aluminum has low molten viscosity, high reflectivity, and a relatively high propensity to form internal porosity because of the high solubility of hydrogen in liquid aluminum.

Friction stir welding (FSW) can also eliminate hot cracking and minimize heat-affected-zone (HAZ) issues in 6000-series heat-treatable aluminum alloys. Avoiding the liquid phase of the materials also avoids the formation of various large eutectic constituent particles or other undesirable intermetallic particles that develop in particular alloys or with certain types of weld or materials contamination. The use of FSW also better facilitates welding of heat-treatable materials, since the HAZ is normally smaller or less pronounced compared with fusion welding. The use of solid state joining also enables a variety of types of dissimilar aluminum alloy joining not normally possible using fusion welding methods.

FSJ Process Parameter Development

In a previous feasibility study, some alloy combinations were successfully stamped from TWBs fabricated by FSJ. However, weld line failures occurred in many other alloy combinations. The main thrust of this program is to better understand the weld process, forming parameters, and performance characteristics of TWBs and to apply them to a wider range of cab components. The use of FSJ to produce TWBs may result in dramatically improved weld quality and formability of aluminum TWBs—thereby enabling this weight- and cost-saving technology.

In order to develop and use FSJ to make high-quality aluminum TWBs for intermediate- and high-volume truck applications, the FSJ process must be competitive with laser welding and other fusion welding technologies from a production rate per-

spective. The target weld speeds are 2–5+ meters/minute. The friction stir welds must be of significantly higher formability compared with conventional fusion welds.

This project will develop process parameters to make successful welds in the following weld combinations, as they are representative of typical truck alloys and material thicknesses:

- 5182-O 2 mm to 5182-O 2 mm
- 6022-T4 2 mm to 5182-O 1.6 mm
- 6022-T4 2 mm to 5182-O 2 mm
- 5182-O 2 mm to 6022-T4 1.6 mm
- 5182-O 2 mm to 5182-O 1.6 mm
- 6022-T4 2 mm to 6022-T4 1.6 mm
- 6022-T4 2 mm to 6022-T4 2 mm
- 5052-H111 1.27 mm to 5052-H111 1.27 mm
- 5052-H32 1.6 mm to 5052-H32 1.6 mm

This project will determine, within the “defect-free” process window, where a set of parameters exists that produces a TWB with the best formability (see Figure 2). The process and forming parameters are being developed by FSJ test coupons at a range of weld conditions, which are then subsequently tested for strength and formability to establish optimum weld conditions for each material and thickness combination of interest. The following section details the weld characterization performed to determine the optimum joining process parameters.

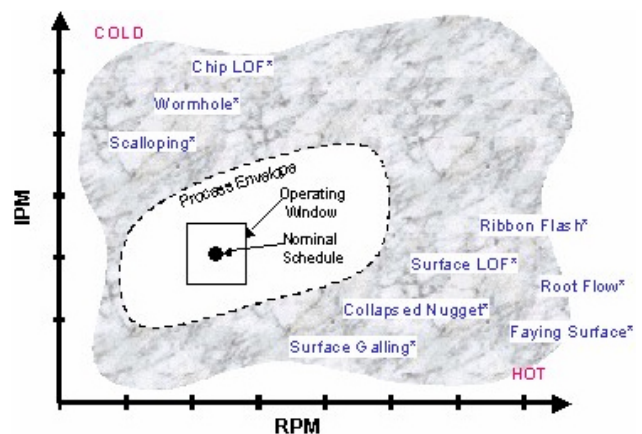


Figure 2. An illustration of the process parameter window to determine the optimum set of parameters that produces a TWB with the best formability.

Weld Characterization

Coupons of the material combinations were friction stir welded by AJT and sent to PNNL for testing and evaluation. These coupons were subjected to limited dome height (LDH) testing, mechanical tensile testing, and microscopic analysis. The results of these studies allow for bracketing of appropriate weld process parameters (i.e., weld speed, heat input, and tool design) that could produce TWBs with the best formability in a stamping process.

LDH testing is used to provide joint metal formability data. Figure 3 shows a typical weld process parameter development matrix. For that particular material combination, the formability increased with weld speed up to 150 ipm, and then the weld quality degraded. Figure 4 shows typical punch-load versus LDH results for ductility and strength of a single

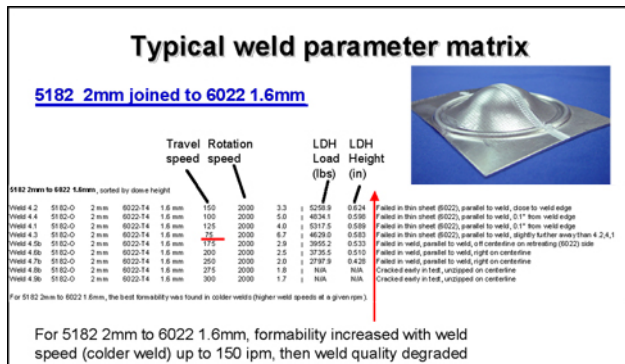


Figure 3. LDH testing conducted to define appropriate weld parameters to produce the highest potential TWB ductility during stamping.

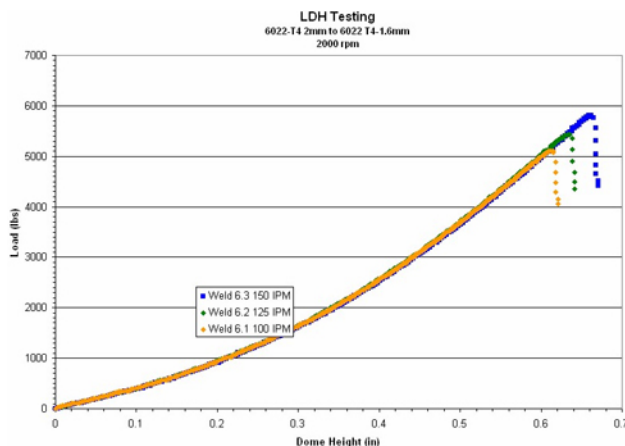


Figure 4. A typical series of LDH tests illustrating ductility and strength trends with changing weld process parameters.

population of welded blanks. LDH data also provide strain limits that guide weld placement in die design and predict the chances for successful stamping. Once the most formable FSW process parameters are established, LDH specimens are characterized for surface strains via strain grid analysis. LDH testing can help characterize the maximum strain that can be achieved in the weld or parent material adjacent to the weld. Figure 5 shows a typical illustration of the surface strains measured after LDH testing.

Miniature tensile tests are conducted to characterize the local mechanical properties of the weld metal and surrounding region, as well as to ultimately understand the effects of the welding process on these mechanical properties. Figure 6 is an illustration of the miniature tensile specimen.

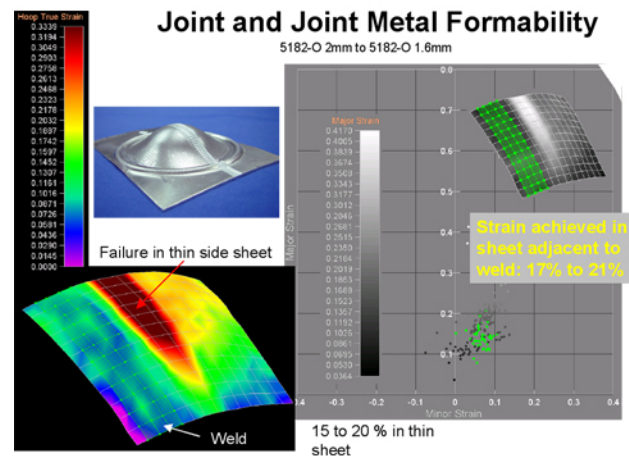


Figure 5. Typical results from LDH strain analysis. Maximum achievable homogeneous true strain in the thin side sheet is 17 to 20% at the point when necking develops.

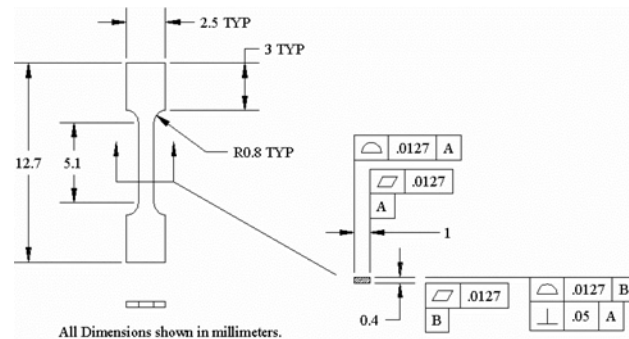


Figure 6. A detailed drawing of the miniature tensile specimen. All dimensions are in millimeters.

Figure 7 shows the location of some specimens extracted from a weld. The miniature tensile results

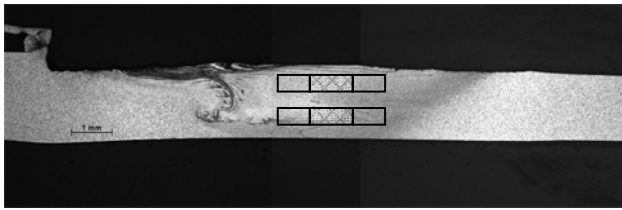


Figure 7. An illustration of miniature tensile specimen locations superimposed in the weld region.

show what mechanical property gradients exist in the weld metal, thermo-mechanically affected zone, HAZ, and parent material. The goal is to match weld metal and parent material flow stresses as well as minimize property gradient across the weld.

For example, miniature tensile specimens were removed from the weld metal and surrounding region of 5052-H32 (1.6 to 1.6 mm) and 5182-O (2 to 1.6 mm) friction-stir-joined TWBs. These experiments showed that significant variations in mechanical properties existed within the weld metal and surrounding regions for 5052-H32 aluminum TWBs, whereas little variation in mechanical properties was observed in 5182-O aluminum TWBs (Figures 8 and 9, respectively).

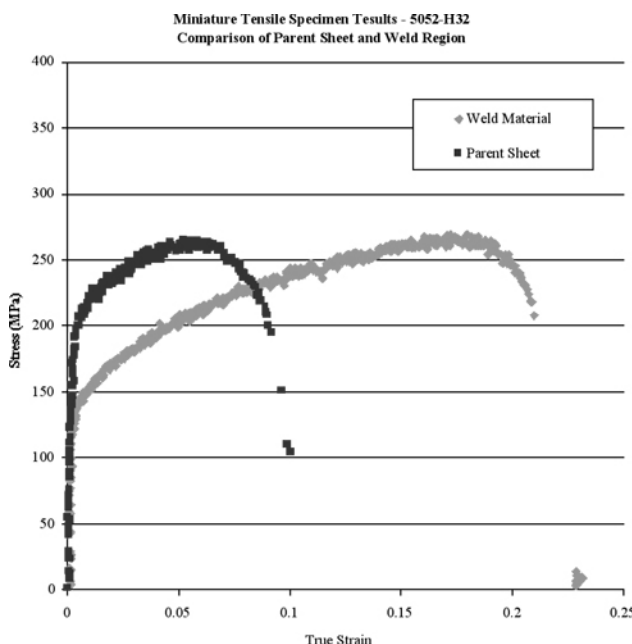


Figure 8. Miniature tensile test results for 5052-H32 aluminum TWB. Specimens shown were extracted from the weld metal and parent sheet material.

Figure 8 shows that the 5052-H32 TWB weld metal is ductile; however, differences in flow stress

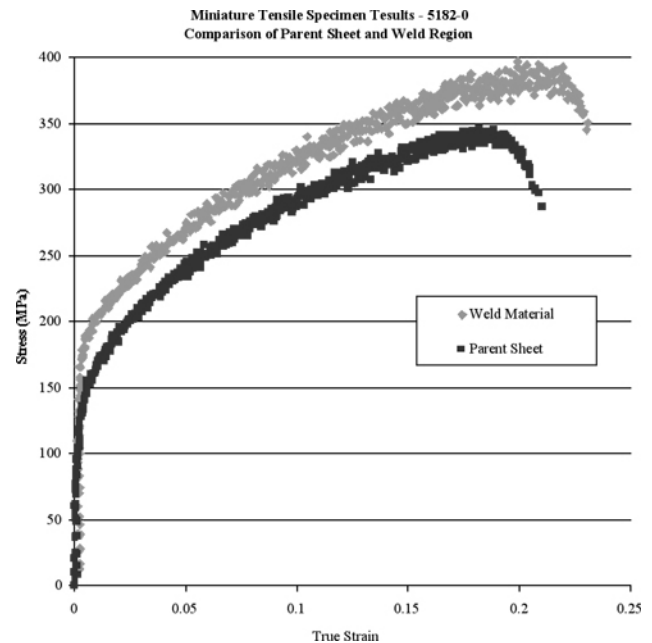


Figure 9. Miniature tensile test results for 5182-O aluminum TWB. Specimens shown were extracted from the weld metal and parent sheet material.

can lead to early localization during forming even though the weld metal shows good ductility. Therefore, one should expect that biaxial stretching (stamping) of the 5052-H32 TWB population will result in greater plastic deformation in the weld than in the parent sheet (and increasing weld failure probability); whereas biaxial stretching of the 5182-O population should result in similar plastic deformation in the weld metal and parent sheet. Further development of the process parameters for 5052-H32 TWBs is needed to determine the optimum joining process for formability.

Conclusions

From this investigation, the following conclusions were derived:

- FSJ appears suitable for fabricating aluminum TWBs.
- The FSJ process is stable, is tolerant, and produces high-quality welds when the weld process parameters are defined.
- The FSJ process is customizable. A wide range of weld heat, plastic work, and weld metal grain-size manipulation is possible with FSW by changing tool design and process parameters. These may be manipulated to achieve the opti-

mum joining process for formability and to create an even property gradient across the weld metal.

- Process parameters can be refined for formability by choosing weld parameters from formability tests (LDH), by adjusting weld heat per unit of weld length to minimize the effect of thermal softening in the HAZ, and by closely matching the weld metal flow stress to that of the parent sheet.

Publications/Presentations

“Evaluation of the Mechanical Performance of Self-Piercing Rivets in Friction Stir Welded Structures,” accepted for publication by *Proceedings of Society of Automotive Engineers 2005 World Congress*.

“The Formability of Friction Stir Welds in Automotive Stamping Environments,” accepted for publication by *Proceedings of Society of Automotive Engineers 2005 World Congress*.

“Friction Stir Welded Tailor Welded Blanks for Automotive Applications,” presented at 2004 TMS Annual Meeting and Exhibition, Charlotte, NC, March 16, 2004.

“Weld Region Mechanical Properties of Friction Stir Welded 5052 and 5182 Aluminum TWBs,” proprietary technical report prepared for Freightliner LLC.

G. Friction Stir Welding and Processing of Advanced Materials

Principal Investigator: Zhili Feng

Oak Ridge National Laboratory

1 Bethel Valley Road, Oak Ridge, TN 37831

(865) 576-3797; fax: (865) 574-4928; e-mail: fengz@ornl.gov

Technology Development Area Specialist: Sidney Diamond

(202) 586-8032; fax: (202) 586-1600; e-mail: sid.diamond@ee.doe.gov

Field Technical Manager: Philip S. Sklad

(865) 574-5069; fax: (865) 576-4963; e-mail: skladps@ornl.gov

Participants:

Michael L. Santella, Oak Ridge National Laboratory

Tsung-Yu Pan, Ford Motor Company

Naiyi Li, Ford Motor Company

Contractor: Oak Ridge National Laboratory

Contract No.: DE-AC05-00OR22725

Objective

- Develop the technological basis for friction stir welding and processing (FSW/P) of advanced high-strength and lightweight materials for the automotive industry.
- Gain fundamental understanding of the relationships between workpiece and tool material properties during FSW/P.
- Characterize the mechanical properties and microstructures of joints.
- Correlate the properties and microstructures produced by FSW/P to the process conditions.

Approach

- Conduct experimental welding and processing tests on advanced materials using the state-of-the-art FSW/P process development system.
- For particular workpiece materials, select the tool material based primarily on high-temperature strength, wear resistance, and chemical compatibility.
- Evaluate mechanical properties and their correlation with microstructures produced by FSW/P.
- Develop predictive modeling capability to study the properties as function of process conditions.

Accomplishments

- Achieved drastic improvements in the fatigue life of FSP cast aluminum alloys.
- Completed a study on FSW of cast magnesium alloy AM60B.
- Conducted FSW tests of high-temperature materials using the tool materials developed at Oak Ridge National Laboratory (ORNL).
- Completed initial development of friction stir spot welding (FSSW) of aluminum alloys.

- Developed an integrated thermal-mechanical-metallurgical model for FSW of aluminum alloy.

Future Direction

- Investigate the effects of heat treatment on the fatigue life of FSP cast aluminum alloys.
 - Carry out FSP of magnesium cast alloy.
 - Explore FSSW of advanced high-strength steels for automotive body structures.
 - Develop new approaches for FSSW without the exit hole for improved structural properties of the joint.
 - Carry out FSSW of other lightweight materials and dissimilar welds.
 - Use transmission electron microscopy to characterize the microstructure improvements to the cast surfaces.
 - Assess the ability of FSP to produce rapidly solidified surface microstructures.
-

Introduction

FSW is a relatively new solid state joining method, invented in 1991. The process characteristics and advantages for joining materials that are difficult to join by conventional fusion welding processes were discussed in the 2003 annual report.

Applications of FSW to aluminum alloys have been a great success. Currently, the technology forefronts are rapidly evolving: there is tremendous interest in and efforts to extend the technology to welding high-performance and high-melting-temperature materials. Other novel applications of the process are emerging. For example, it can be used to thermomechanically process a material for microstructure refinement and property improvement.

This program aims at advancing FSW/P technology to promote the increased use and adoption of high-strength lightweight materials in automotive structures, particularly heavy vehicles, to support the goals of the Office of Heavy Vehicle Technology to increase fuel efficiency and reduce emissions of heavy trucks by weight reduction without sacrificing strength and functionality.

FSP Surface Modification of Aluminum Castings

Last year, we began to investigate the application of FSP to modify the microstructures and properties of aluminum alloy castings. Two types of cast alloys were used: A319 (Al-6Si-3.5Cu wt %, nominal) and A356 (Al-7Si-0.3Mg wt %, nominal). Both alloys can be produced as either sand castings or permanent mold castings that are widely used in en-

gine, driveline, and suspension components in a wide variety of automobiles and light trucks. Most of these applications involve dynamic loading, and the primary interest in FSP is for use as a means of improving the durability and reliability of a casting part by locally refining the cast microstructure at critically stressed locations.

Experiments were conducted in collaboration with Ford Research and Advanced Engineering. Testing plates were machined from casting ingots to dimensions of $16 \times 50 \times 200$ mm. FSP was applied on the face of the testing plate to produce an approximately 3-mm-deep processed surface layer. Optical microstructural examination showed that FSP breaks down the coarse dendrites and closes the solidification shrinkage porosity and voids in the original cast microstructure. The resulting refined uniform distribution of eutectic particles increases substantially the static strength and ductility of the FSP region. These results were reported in last year's annual progress report.

This year, the R&D efforts focused on the fatigue life of the FSP material. The procedure to obtain the fatigue life test specimen was the same as in last year's static mechanical property test. A sub-sized tensile fatigue specimen with gage dimensions of $2 \times 2 \times 15$ mm was then cut from the processed material. The testing gage length is entirely within the processed region and transverse to the FSP bead, as shown in Figure 1.

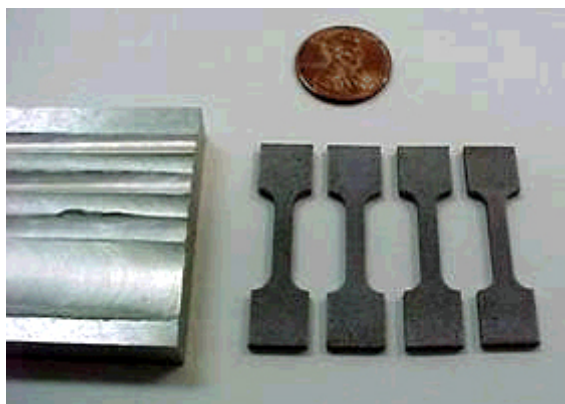


Figure 1. Tensile specimens used for fatigue life testing of FSP aluminum castings.

Tables 1 and 2 show fatigue life testing results for A356 and A319 cast alloys, respectively. It is evident that the FSP material showed drastic improvement in fatigue life, compared with the as-cast material, for both cast alloys. The increase in fatigue life can be attributed to the substantial strength and ductility improvements and the elimination of solidification shrinkage porosity (crack initiation sites) associated with the thermo-mechanical processing of cast microstructures during FSP.

Table 1. Fatigue testing results for A356 cast aluminum alloy

Condition	Applied strain	Stress amplitude, ksi @ ½ life	Neuber stress range ksi @ ½ life	Life, # of reversals
As-cast	2.0×10^{-3}	15.5	39.0	7,700
FS processed	2.0×10^{-3}	19.4	43.9	93,848

Table 2. Fatigue testing results for A319 cast aluminum alloy

Condition	Applied strain	Stress amplitude, ksi @ ½ life	Neuber stress range ksi @ ½ life	Life, # of reversals
As-cast	1.4×10^{-3}	13.4	29.0	100,980
FS processed	1.5×10^{-3}	18.0	39.0	281,442

The findings from this program show that FSP has potential as a very effective process to locally modify cast microstructures at critical locations to improve the overall durability of the component. This would open new opportunities to support wider use of aluminum castings in vehicles, which could directly impact weight reduction. We plan to conduct more comprehensive study on this subject in the future phases of this program.

FSW of Cast Magnesium Alloy

The use of magnesium has grown considerably in the past 10 years and continues to rise in the automotive industry. This increase is mainly attributed to the lightness of magnesium—it is one-third lighter than aluminum and four-fifths lighter than steel. Magnesium also has the highest strength-to-weight ratio among the commonly used metals. Moreover, it has many other advantages, e.g., good

castability, high die casting rates, electromagnetic interference shielding properties, parts consolidation, dimensional accuracy, and excellent machinability. With these characteristics, magnesium provides opportunities for the automotive industry, in which weight reduction, fuel economy, and environmental friendliness of vehicles are increasingly demanded.

Despite its good castability, it is not always possible or economically viable to cast complex magnesium parts. Joining of the same or different types of magnesium alloys, as well as joining magnesium to other materials, is essential to enable the economical manufacturing of complex parts and structures.

An increasing number of magnesium components for automotive applications are fabricated by high-pressure die-cast process. This type of magnesium casting has limited ductility, contains gas occlusions, and is generally difficult to weld satisfactorily by fusion welding techniques.

In this part of the program, we conducted a study on FSW of AM60B, an Mg-Al-Mn cast alloy under development for automotive applications. The experiments were conducted in collaboration with the Research and Advanced Engineering Lab of Ford Motor Company.

The AM60B cast plates were produced by the high-pressure die casting process. The nominal dimensions of the casting plate were $127 \times 25.4 \times 6$ mm. Two die-cast plates were FSW butt-welded along their long dimensions, as shown in Figure 2. In consideration of the typical automotive production environment, all welds were made without any special cleaning of the as-cast surface. In other words, the welds were made under the as-cast surface condition. In addition, no shielding gas was used during welding.

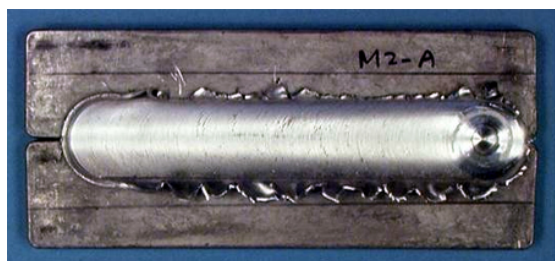


Figure 2. A friction-stir butt weld between two casting plates (450 rpm).

FSW was conducted using the FSW process development system acquired by ORNL with funding support from the HSWR Materials Program and other DOE programs. The machine is capable of simultaneous force-controlled or displacement-controlled operation of three independent axes with adjustable, adaptable pin tools for on-the-fly mode switching between fixed, adjustable, and self-reacting welding modes. It also handles computer-controlled operation and key process parameter monitoring and is capable of making non-linear, variable-thickness, and double-curvature welds.

The FSW tool was made of H13 tool steel. The shoulder diameter was 0.75 in. (19 mm), and the threaded pin was 0.25 in. (6.35 mm) in diameter. The length of the pin was 0.185 in. (4.7 mm), slightly shorter than the thickness of the plates. Two rotating speeds were used in this study, 375 and 450 rpm. The linear welding speed was kept at 152.4 mm/min. No elaborate attempt was conducted

to optimize the process conditions in this phase of the study.

The optical macroscopic photo in Figure 3 shows the cross-section of the weld joint. The gas pores were clearly visible in the base metal as a result of the high gas content in the high-pressure die casting process. In the stir zone, the pores were significantly reduced on one side of the weld but still visible in the other side, which is characteristic of all the welds examined in this study.

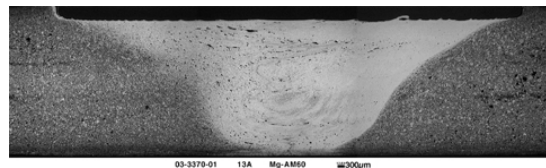


Figure 3. Transverse section of a friction stir weld of AM60B.

To determine the strength of the welded joint, tensile testing samples were machined out from the middle of the specimen, as shown in Figure 4, and prepared in accordance with ASTM B557 specifications. Tensile properties of the base metal were also determined for comparison.

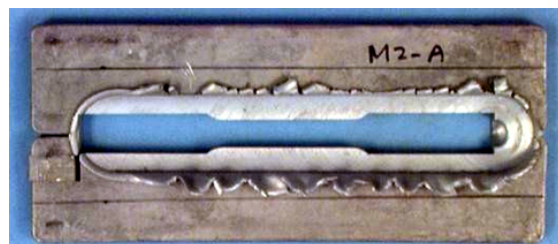


Figure 4. Longitudinal tensile sample per ASTM B557 sub-size specimen.

The tensile testing results are presented in Figure 5 and 6. The weld made under the low-rpm condition (M1) maintains the ultimate strength of the base metal but doubles the ductility. The high-rpm condition (M2) slightly lowers the weld tensile strength but still offers significant improvement in ductility.

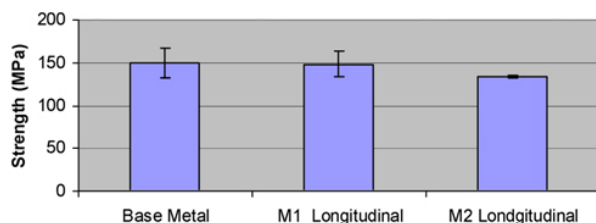


Figure 5. Longitudinal tensile strength of FSW alloy AM60B.

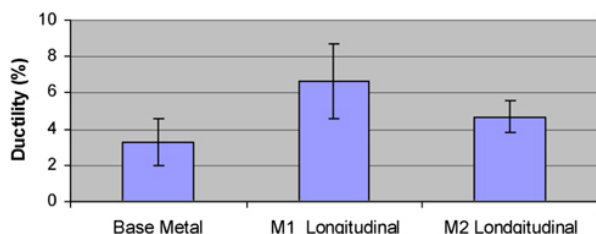


Figure 6. Longitudinal ductility of FSW alloy AM60B.

FSW of High-Temperature Materials

In 2003, tool material design activities at ORNL led to the development of two new alloys for use as tool materials for FSW/P of high-temperature materials. In 2004, we conducted initial welding trials using the new tool materials developed by ORNL. Welds were successfully made for the following alloys: mild steel, stainless steel 304, CP Ti, and Ti-6Al-4V.

Initial testing showed that the ORNL tool materials exhibit minimal tool wear and deformation. The tungsten-based tool material has excellent toughness over the temperature range from the ambient to at least 1500°C. The tool material was very forgiving of unexpected sudden temperature and load changes during the welding trials, which would have led to premature failure of other tool materials under similar situations. Additional evaluations of the performance of the tool material, as well as the microstructure and properties of the friction stir welds of high-temperature materials, are currently under way.

Figure 7 shows the tungsten-based and irridium-based tool materials developed at ORNL. Figure 8 shows the process in action in welding stainless steel 304. Figure 9 shows two examples of high-temperature friction stir welds made with ORNL's tungsten-based tool material.

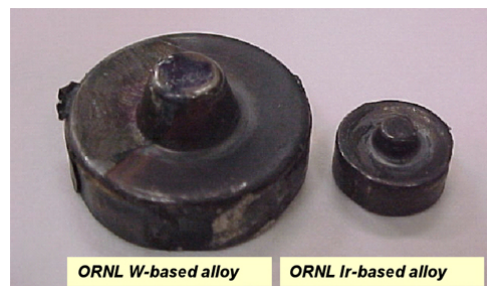


Figure 7. Two development-grade FSW tool materials developed at ORNL.

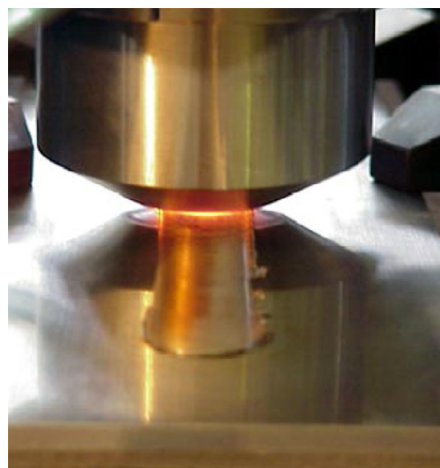


Figure 8. FSW of stainless steel.

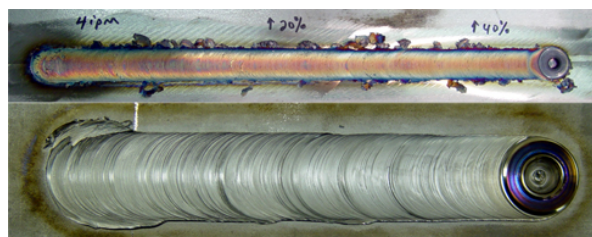


Figure 9. Sample welds made with ORNL tool material. Above: stainless steel 304, below: Ti-6Al-4V. Plate thickness: 0.25 in. (6.35 mm).

FSW of Aluminum Alloys

FSSW, or spot friction welding, is a new welding process invented by Mazda in 1993. It has been a subject of great interest for the U.S. automotive industry because of its process simplicity, low capital investment cost, and significant energy savings (up to 99% in the case of aluminum welding), compared with conventional resistance spot welding.

We are collaborating with Ford to further advance the technology for the U.S. automotive industry.

FSSW creates a spot lap-weld without bulk melting. The principles of the process are schematically illustrated in Figure 10. Similar to linear FSW, FSSW uses a cylindrical tool with a co-axial protruded pin. The welding cycle begins when the pin plunges into the upper sheet of the lap joint. The plunge load is supported from the bottom side with a backing plate or anvil to sustain the plunging load. The heat generated by the rotating pin softens the material and facilitates the penetration of the pin. Much more heat is generated to further soften a large region of the material underneath the tool shoulder after the tool shoulder contacts the top surface of the upper sheet. The softened material is pushed and stirred to form the metallurgical bond around the rotating pin. The forge pressure from the tool shoulder also keeps the interface between the two workpieces in intimate contact to facilitate the bonding. The tool is retracted at the end, leaving the characteristic hole in the middle of the weld.

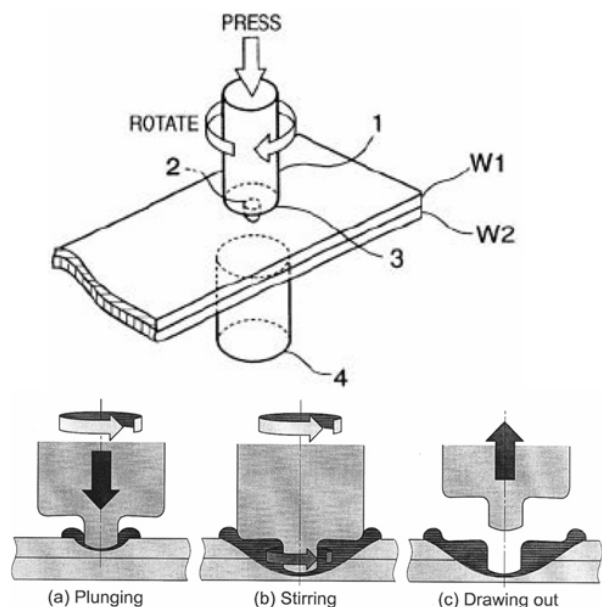


Figure 10. Principles of FSSW with fixed pin.

Currently, FSSW is load controlled. This study was to develop a displacement-controlled operation mode that is more suitable for a high-volume production environment.

Figure 11 illustrates schematically the basic operation of a displacement-controlled FSSW process. After the tool starts rotating, it is driven into the sample at a controlled plunging rate to reach a predetermined depth. The process then stops and the tool retracts. The normal force, recorded as an output, increases to a relatively low plateau when the pin initially plunges into the material. It then increases to a higher value when the shoulder of the tool touches the sample.

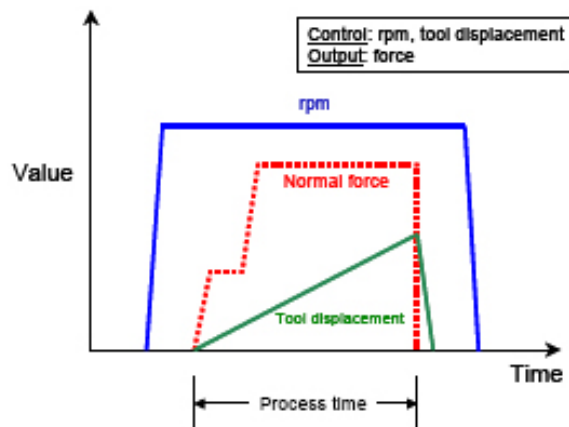


Figure 11. Schematic diagram of a displacement controlled FSSW operation.

The experiments were carried out on ORNL's FSW process development system. Specimens of aluminum alloy 6111-T4, 25.4 mm in width, 101.6 mm in length, and 0.94 mm in thickness were used. The standard overlapping distance of 25.4 mm was adopted. The weld was made at the center of the overlapping region. The spot weld was made at 2000 rpm. The tool plunging displacement was set at between 1.6 and 1.9 mm.

Figure 12 shows the lap shear tensile results of samples made between 1.6 and 1.9 mm in depth. Each data point represents an average of at least three samples. Initially the joint strength increased with the plunge depth. It reached a maximum value and then dropped off as plunge depths were further increased. The maximum lap-shear strength exceeded 3 kN at about 1.8 mm plunge depth. It is important to note that the tensile strength obtained in our study generally exceeded these reported with the load controlled operation.

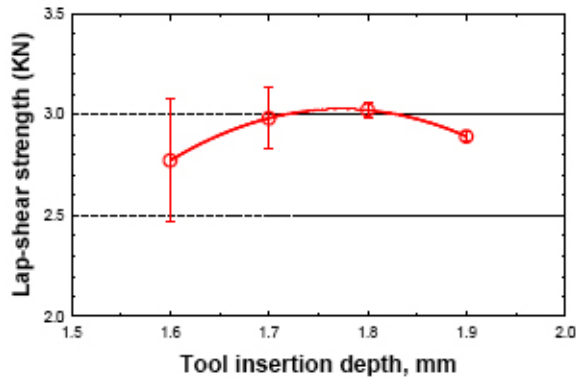


Figure 12. Lap-shear strength of spot friction welded 6111-T4 samples at different insertion depths by displacement control welding.

Figure 13 shows a micrograph of the cross-section of a sample with a plunge depth of 1.7 mm. Figure 14 (a) and (b) show the microstructures in the parent material region and stirred zone, respectively. The refinement of grain size in the stirred zone is obvious: it is about 3–5 times smaller compared with the grains in the parent material.

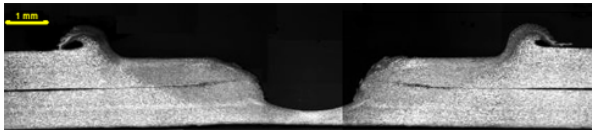


Figure 13. Macro cross-section of a spot friction stir weld of Al611-T6.

Modeling of FSW

As with many other welding processes, residual stresses are expected in a friction stir weld. The welding thermal cycle also introduces microstructural changes in the weld region of many high-performance engineering materials. The resultant property and residual stress fields in a friction stir weld joint often govern the mechanical strength of the welded structures. For automobile structures, this affects both the durability of the vehicle in service and the formability of the welded part during post-welding forming and stamping operations.

An integrated thermal-mechanical-metallurgical model was used to study the residual stress field and the spatial property gradient in an Al6061-T6 friction stir weld. The simulations were conducted using a 3-dimensional model, accounting for the frictional heating, aging, and dissolution processes

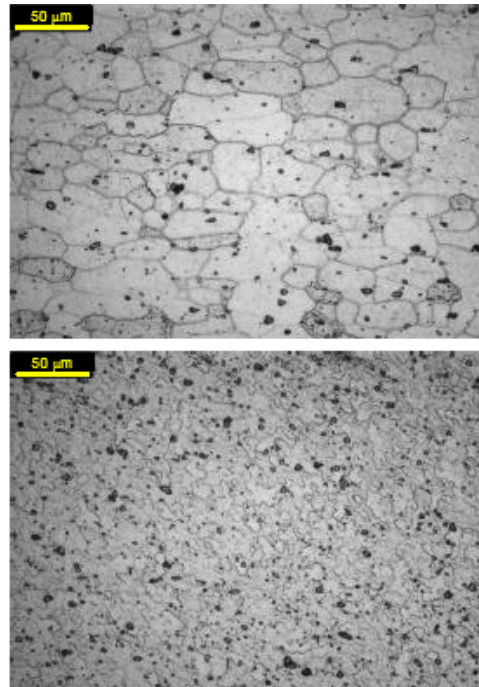


Figure 14. Micrograph of the base metal (top) and stir zone (bottom) of SFW 6111-T4.

of the precipitates and the mechanical contact of the moving tool.

Temperature-dependent material properties were used in the simulation. In addition, the residual stress fields were measured using the neutron diffraction mapping technique to validate the model predictions.

The integrated model enables high-fidelity simulations of the thermal, mechanical, and metallurgical changes during the FSW process and the resulting microstructure, property, and residual stress inhomogeneity in the weld region. This type of model would make it possible to effectively interrogate the influence of various aspects of the process (process parameters, material, and geometry) on the performance of a friction stir weld under different post-welding fabrication conditions (such as stamping and forming) and in-service loading conditions. As an example, Figure 15 shows simulation results for temperature, hardness, and residual stress fields in the weld, and their combined effects on the deformation and failure behavior of an aluminum alloy Al6061-T6 friction stir weld in the tensile test.

For the friction stir welds investigated, it was found that the residual stress distribution is strongly

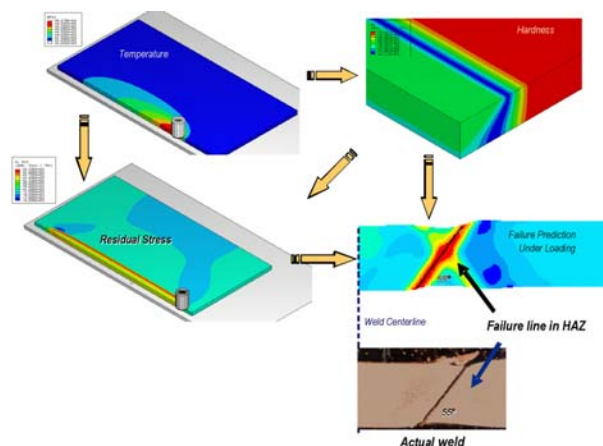


Figure 15. Integrated thermal-mechanical-metallurgical friction stir welding simulations provide insights into the performance of welded structures.

dependent on the welding process parameters and the degree of material softening during welding. The failure of a friction stir weld under tensile load is controlled by a combination of material softening and the high residual stresses in the heat-affected zone.

Conclusions

This program has made considerable progress in FY 2004 in advancing the FSW/P technology: FSP of cast aluminum alloys resulted in drastic micro-

structure and property improvement. A cast magnesium alloy was friction stir welded. FSW of high-temperature materials was explored, as well as FSSW of aluminum alloy. Integrated modeling was used to study the property and residual stresses and their effects on the performance of aluminum weld structures.

Publications

N. Li, T-Y Pan, R. P. Cooper, D. Q. Houston, Z. Feng, and M. L. Santella, "Friction Stir Welding of Magnesium Am60 Alloy," pp. 19–23 in *Magnesium Technology 2004, 2004 TMS Annual Meeting*, TMS, Charlotte, NC, 2004.

Z. Feng, X-L Wang, S. A. David, and P. Sklad, "Modeling of Residual Stresses and Property Distributions in Friction Stir Welds of Aluminum Alloy 6061-T6," in *5th International Symposium on Friction Stir Welding*, Metz, France, 2004.

T-Y Pan, A. Joaquin, D. E. Wilkosz, L. Reatherford, J. M. Nicholson, Z. Feng, and M. L. Santella, "Spot Friction Welding for Sheet Aluminum Joining," in *5th International Symposium on Friction Stir Welding*, Metz, France, 2004.

H. Basic Studies of Ultrasonic Welding for Advanced Transportation Systems

Principal Investigator: Zhili Feng

Oak Ridge National Laboratory

1 Bethel Valley Road, Oak Ridge, TN 37831

(865) 576-3797; fax: (865) 574-4928; e-mail: fengz@ornl.gov

Technology Development Area Specialist: Sidney Diamond

(202) 586-8032; fax: (202) 586-1600; e-mail: sid.diamond@ee.doe.gov

Field Technical Manager: Philip S. Sklad

(865) 574-5069; fax: (865) 576-4963; e-mail: skladps@ornl.gov

Participants:

Michael L. Santella, Oak Ridge National Laboratory

Edward A. Kenik, Oak Ridge National Laboratory

Xiaoguang Zhang, Oak Ridge National Laboratory

Hsin Wang, Oak Ridge National Laboratory

Keyu Li, Oakland University

Contractor: Oak Ridge National Laboratory

Contract No.: DE-AC05-00OR22725

Objective

- Develop a fundamental understanding of the ultrasonic welding (UW) process.
- Establish process conditions to optimize joint properties of aluminum alloys for auto body applications.
- Explore opportunities for joining dissimilar materials.
- Explore the feasibility of ultrasonic processing in other novel and unique situations in materials processing, such as making powders more dense, producing functionally graded components, modifying surface properties, and producing dissimilar material joints.

Approach

- Perform UW experiments to develop correlations of process parameters with joint properties.
- Characterize details of joint microstructures.
- Model the fundamental interactions of ultrasonic waves with solids.

Accomplishments

- Related the microscopic features at the interface region to process conditions.
- Initiated a study toward the geometric effects on ultrasonic energy generation and dissipation during the welding process.
- Completed a preliminary study of acoustic energy distribution by means of infrared thermography.
- Initiated an experimental study of residual stress distribution in the bonding region.

Future Direction

- Continue welding process development for dissimilar materials, including joining of amorphous metals.
- Study the structure-property relationship of joints.
- Model the acoustic energy distribution in the weld joint.
- Study the residual stress distribution in the bonding region.
- Assess the ability of ultrasonic processing to enhance the densification of powder metal compacts.

Introduction

UW uses high frequency mechanical vibrations to produce a solid-state metallurgical bond (weld) between metals. The basic process setup is illustrated in Figure 1 for a typical spot weld configuration. An electro-mechanical converter converts high-frequency electric current to mechanical vibrations. The mechanical vibration is then modulated and amplified by the booster/horn before it is applied to the overlapping workpiece through the sonotrode. A moderate clamping force is applied to ensure the mechanical vibration is transferred to the sheet-to-sheet interface (the faying surface) where the weld is created. Typically, the mechanical vibration is at 20–40 kHz with an amplitude range of 5–50 μm . The power delivered to the workpiece is in the range of several hundred to several thousand watts.

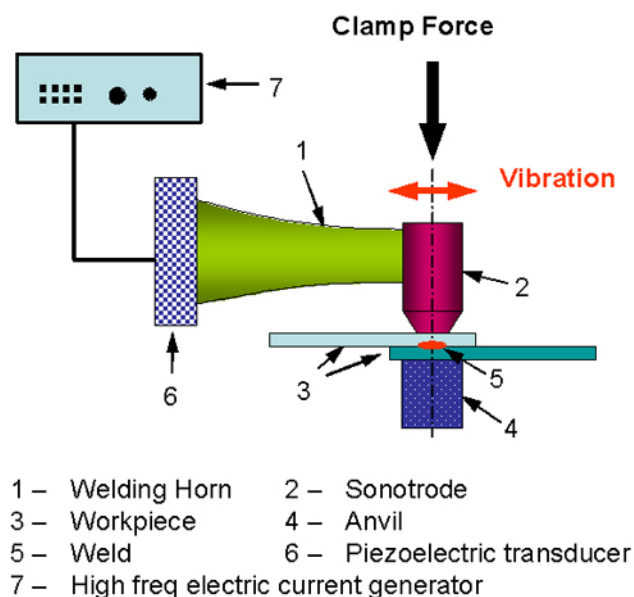


Figure 1. Schematic setup of ultrasonic welding process.

The principles for the formation of the metallurgical bond are illustrated in Figure 2. The combination of clamp pressure and mechanical vibration produces several important effects in the formation of the metallurgical bond at the workpiece interface. The lateral mechanical vibration of the sonotrode causes a small amount of relative motion at the interface between the two workpieces. The frictional action at the interface due to the relative motion and the pressure breaks the surface oxides and other contaminants. As a result, clean metal surfaces are brought into contact under pressure. Frictional heating also occurs at the bond interface. The heating promotes both localized deformation and diffusion in the region where the pressure is applied. When the process conditions are right, metallurgical bonds can be obtained without melting at the bonding interface. The self-cleaning nature of UW and its ability to form metallurgical bonds without melting are both important advantages of the process.

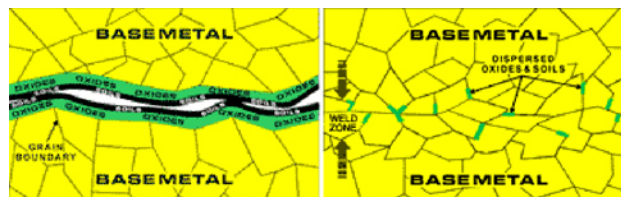


Figure 2. Schematic representation of bond interface before (left) and after (right) UW.

UW creates a joint without bulk melting. Thus the ultrasonic weld is inherently immune to welding defects associated with the solidification process in fusion welding. These include solidification cracking and porosity due to absorption of gaseous impurities (N, H, O) by the liquid metal that are common in electrical resistance spot welding (RSW) (the most widely used joining process in auto body assembly) of many classes of materials used in auto-

motive body structures. Also, unlike the copper-based electrode used in RSW, the sonotrode in UW can be made of high-strength materials that are inert to chemical attack from the material to be welded. Therefore, UW offers several significant potential advantages in joining aluminum alloys and other high-performance lightweight materials for auto body structures.

This program started in FY 2003. The FY 2003 study demonstrated the feasibility of UW of aluminum alloys, magnesium alloys, and steel to themselves, and the feasibility of joining dissimilar metals (aluminum alloy to steel). The FY 2004 efforts included microstructural characterization at the bonding interface, study of ultrasonic energy distribution in the weldment, and exploratory investigation of welding residual stresses. We also initiated the development of theoretical models that would eventually allow for interrogation of geometry effects on the distribution of acoustic energy, an important issue for application of the UW process. The variation of weld strength as a function of time was also observed.

Welding

All welding trials were conducted on a Sonobond ultrasonic welder. The machine operated at 20 kHz and had a maximum rated power output of 2500 W.

All welds were made using 25-mm-wide and 100-mm-long specimens. This is a standard coupon dimension commonly used by the auto industry for weldability testing of resistance spot welds. All specimens had a nominal thickness of 1 mm. For bonding interface microstructural characterization, a standard 1-in overlapping configuration shown in Figure 3 was used. The weld was made at the center

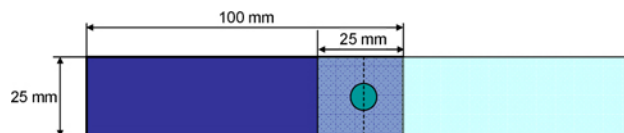


Figure 3. Weld coupon dimensions used in the study.

of the overlapping region. For study of the geometry effects, the amount of overlap and the location of the weld were systematically varied.

Microstructure Characterization

Because of the solid-state nature and minimal thermomechanical excursion of the ultrasonic bonding process, the bonding interface between the same metal (for example, Al6061 to Al6061) was difficult to observe experimentally. To aid the bonding interface study, a series of dissimilar welds between two different aluminum alloys (Al6061-T4 and Al2024-T3) were used. These two aluminum alloys have very different etching responses to Keller's reagent. This allowed for selective etching to reveal the interface region of the weld.

The nominal mechanical properties of the two aluminum alloys are summarized in Table 1. As shown in the table, Al6061 is always softer and has better ductility than Al2024 over the entire temperature range. The differences in the mechanical properties of the two alloys are considerable at the ambient temperature, but they diminish as the temperature increases. At 370°C, the tensile strength and ductility of the two alloys are very close to each other. The differences in mechanical properties are considered to be an important factor affecting the interfacial deformation and bonding behavior during welding.

Table 1. Mechanical properties of Al6061-T4 and Al2024-T3 at selected temperatures
(Source: *Properties of Aluminum Alloys*, AMS International, 1999)

	25°C			260°C			370°C		
	Yield (MPa)	Tensile (MPa)	Elong g (%)	Yield (MPa)	Tensile (MPa)	Elong g (%)	Yield (MPa)	Tensile (MPa)	Elong (%)
6061-T4	145	241	25	165	172	17	55	59	35
2024-T3	345	483	17	241	269	17	69	76	35

We have discussed some of the general microstructural characteristics in the bonding interface region as a function of welding process parameters in the FY 2003 annual report. Additional observations are reported here. All the cross-sectional photos were taken along the plane cut through weld center, as depicted by the dashed line in Figure 3.

Figure 4 shows the bonding interface at two different energy levels. The pictures were taken near the center of the weld (labeled A in Figure 5). At low energy levels, the bonding interface is quite flat microscopically. The interface becomes wavy, and considerable microscopic swirling deformation is evident at high energy levels. The microscopic swirling deformation is confined primarily on the softer Al6061 material side.

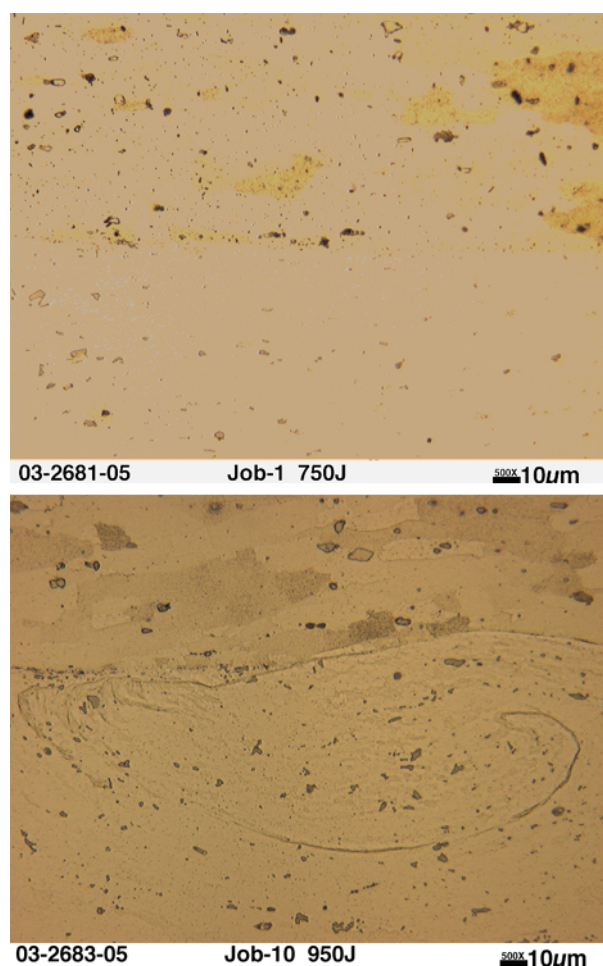


Figure 4. Changes in bonding interface flatness as a function of UW energy level. Top: 750J; bottom: 950J. Other process conditions: 2400 W and 70 psi. Al2024 is the upper sheet.

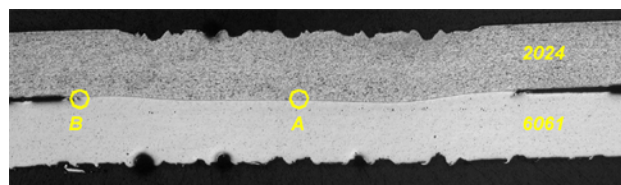


Figure 5. Macro view of the weld cross-section. The observation positions in Figure 4 and Figure 6 are labeled A and B, respectively. Point A is near the center of the weld; Point B is at the edge of the bonded region.

Figure 6 shows the deformation near the periphery (region B in Figure 5) of the bonded interface in the low-energy-level case (750J). It was taken from the same 750J weld as the top photo of Figure 4. It suggested that, even though the interface was relatively flat when the energy level was low, the microscopic deformation was still extremely large and mainly confined on the softer Al6061 side.

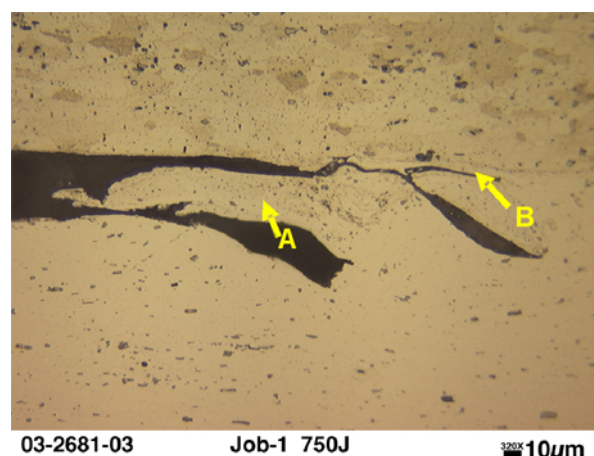


Figure 6. Local deformation of Al6061 at the periphery of the bonding interface. The photo was taken at position B of Figure 5. Arrow B points to the region where “coating” is formed. Energy level: 750 J.

These observations suggest that there is considerable shearing deformation at the interface, under the lateral rubbing motion of the sonotrode, under all energy levels studied in this program. On the other hand, the material deformation or motion vertical to the interface is secondary to the bonding process and only becomes noticeable when the ultrasonic energy level is high.

Another intriguing observation is the “coating” phenomenon at the interface. As pointed to by arrow B in Figure 6, a thin layer of Al6061 is “coated” and bonded onto the Al2024 side, while this thin layer is

still disconnected with the bulk of the Al6061 material. This phenomenon is more evident in Figure 7, where only intermittent, partial bonding is achieved at the interface at a very low energy level (550J).

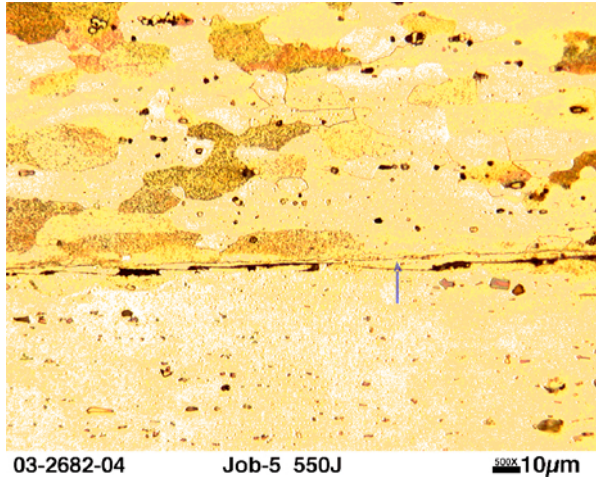


Figure 7. Coating of Al6061 to Al2024 at a low energy level (550 J) that could form only partial bonding.

Although the causes for formation of the coating layer are not clear at this time, the fact that it forms in the early stage of the bonding process would be an important aspect of the bonding process during UW.

At higher energy levels, the bonding interface becomes wavy and is generally considered to be beneficial to the joint strength of the ultrasonic welds. However, excessive energy could cause cracking of the material, as shown in Figure 8. For the Al6061-to-Al2024 welds, the cracking always occurs on the Al2024 side, more or less parallel to the bonding interface at a distance about 50 to 100 µm from the interface. One possible cause would be related to the lower ductility of Al2024 between the room-to-intermediate-temperature range as shown in Table 1.

Geometric Effects on the Ultrasonic Bonding Process

We observed strong geometric dependence of the process: the weld quality, energy input, and energy distribution are all strongly dependent on the geometric arrangements of the test. Such dependency needs to be thoroughly understood because of

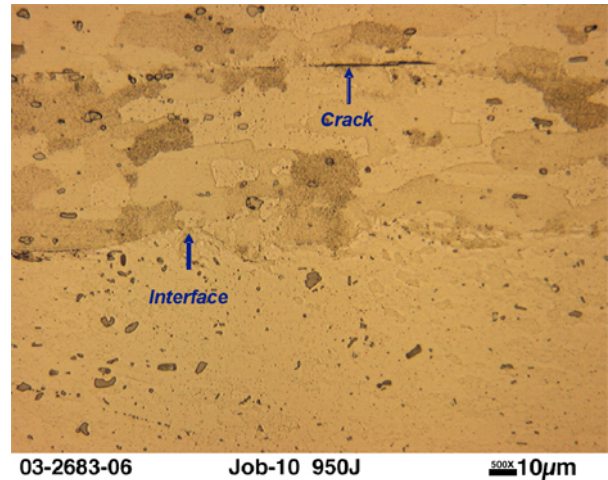


Figure 8. Cracking at Al2024 side of bonding interface due to excessive energy input.

its important implications in the industrial applications of the process.

Effects of vibration direction relative to weld coupon orientation. Figure 9 compares two welds made when the direction of the applied lateral mechanical vibration from the sonotrode was changed relative to the specimen orientation. The direction of vibration is depicted by the arrow next to the weld in the figure. All other welding conditions were identical when these two welds were made. When the vibration was in the width direction of the specimen, two cracks formed at the edge of the specimen, as shown in the lower part of Figure 9. Such cracking was absent when the vibration was applied along the length direction of the specimen. This suggests that the acoustic energy distribution in the weld coupon (or welded structure) is strongly dependent on the vibration direction relative to the geometric orientation of the part.

It is also important to note that, although the two cracks are relatively symmetric to the weld, they are not connected to the weld. This indicates that the cracks are not originated by the directly applied vibration of the sonotrode. Rather, there must be high energy concentration points (hot spots) near the edge of the plate, caused by the complex interaction of the propagating acoustic wave from the excitation source and the reflected wave from the free boundaries of the specimen.

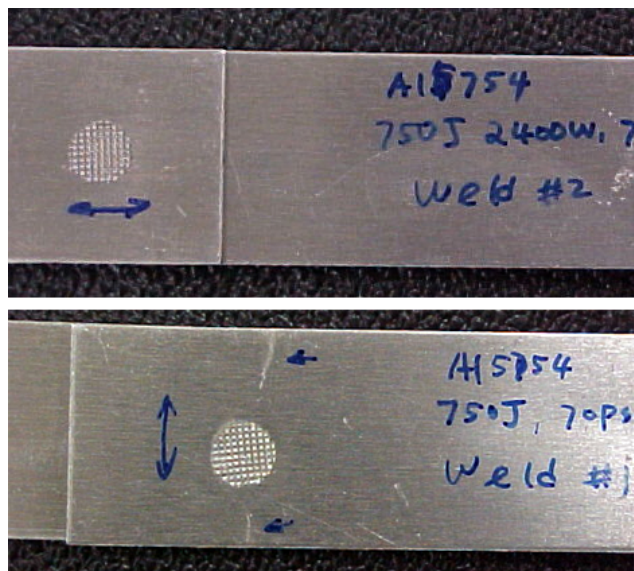


Figure 9. Effect of vibration direction for Al5754. 750 J, 2400 W, 70 psi. Top: vibration parallel to specimen length. Bottom: vibration parallel to specimen width.

Clearly, proper control and elimination of undesired hot spots would be a critical issue for the application of UW.

Interactions of multiple welds. Auto body structures generally require multiple spot welds to connect two structural members. On average, about 3000 to 5000 spot welds are used in assembling a passenger vehicle. In this study, the three-weld test arrangement commonly used in RSW was used to investigate the interactions between the adjacent ultrasonic welds, and the results are intriguing.

Figure 10 shows the three-weld arrangement used in the study. The two 25 × 100 mm Al5754 coupons were overlapped by approximately 75 mm in the length direction. The three welds were made one after another, following the sequence labeled in the figure. The first weld was placed at the center of the 75-mm overlap (i.e., 37.5 mm from the edge of the plate). The second and third weld were made respectively to the left and the right of the first weld, at a nominal distance of 20 mm from the first weld. The welds were produced with identical settings: 2400 W, 70 psi, and 0.35 s. The vibration from the sonotrode was along the width direction of the specimen as illustrated in the figure.

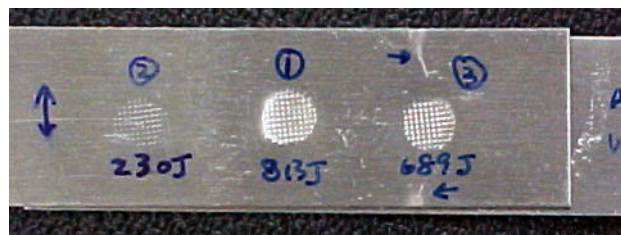


Figure 10. Interactions of multiple welds on the energy input level. All three welds were made with the same welding parameters: 2400 W, 70 psi, and a welding time set at 0.35 s. Weld ID = 4. Material: Al5754.

The energy output as recorded by the ultrasonic machine was drastically different. The system delivered 813 J of energy when making the first weld, quite close to the theoretical value of 840 J (100% energy efficiency) under perfect acoustic impedance matching. However, because of the constraint changes induced by the first weld (as well as the location effect of the second weld), the energy output when making the second weld was only 230 J, less than 1/3 of the energy output in making the first weld. In this particular case, metallurgical bonding was not achieved in the second weld because of the inadequate energy input. The energy output in making third weld was 689 J. Note again the cracks near the third weld that were produced in making the third weld.

The multiple-weld study clearly shows that the acoustic impedance of the UW system can be greatly affected by prior welds made during the assembly process. This would have profound influence on the energy output level and could cause considerable weld-to-weld quality variations.

Infrared Thermography Study of the UW Process

The welding trials clearly show that the distribution of the acoustic energy in a UW workpiece is very complicated and has a profound influence on the weld quality. To further understand this matter, a study was initiated in FY 2004 in which real-time infrared (IR) thermography was used to capture the temperature changes during the UW process. Both the spatial distribution and the temporal variation of the temperature field were used to infer how the heat (the dissipative part of the acoustic energy) is generated and distributed during UW.

The real-time IR measurements were conducted using a high-speed, high-sensitivity (0.015 K) and high-spatial-resolution (5 $\mu\text{m}/\text{pixel}$) IR camera. In the first test, the energy distribution across the workpiece thickness was captured with a special experimental set-up, as shown in Figure 11. The welds were made at the edge of the two workpieces, and the sonotrode vibration was parallel to the long side of the specimen. This special experimental setup preserved the process symmetry in an actual welding situation, while allowing the weld cross-section to be exposed to the IR camera during welding.

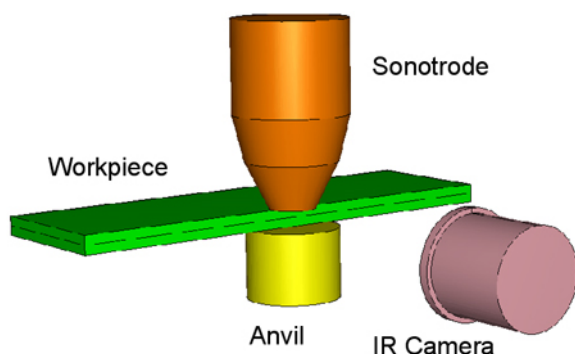


Figure 11. Experimental setup for observing the heat distribution across the weld cross-section.

Figure 12 shows the progression of the heat generation and distribution during welding. The three snap thermal image shots were taken, respectively, at the beginning, middle, and end of the welding cycle. The interfaces and the sonotrode are highlighted to provide the spatial reference frame. It is clear from these images that the heating is predominately generated at the interface and diffused into the workpiece and the sonotrode.

IR thermography was also used to study the formation of cracks caused by the complex acoustic wave distribution in the workpiece. The results are presented in Figure 13. There are two hot spots at the edge of the specimen that were not connected to the main hot spot underneath the sonotrode. This suggests that high level of acoustic energy is concentrated at these locations and causes noticeable heating and cracking at these hot spots.

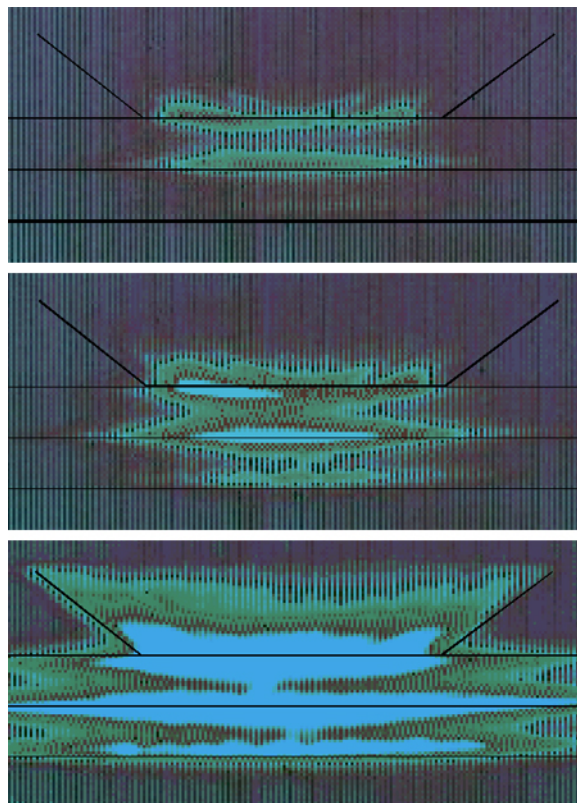


Figure 12. Snapshots of thermal images captured by IR camera at three progressive time instances.

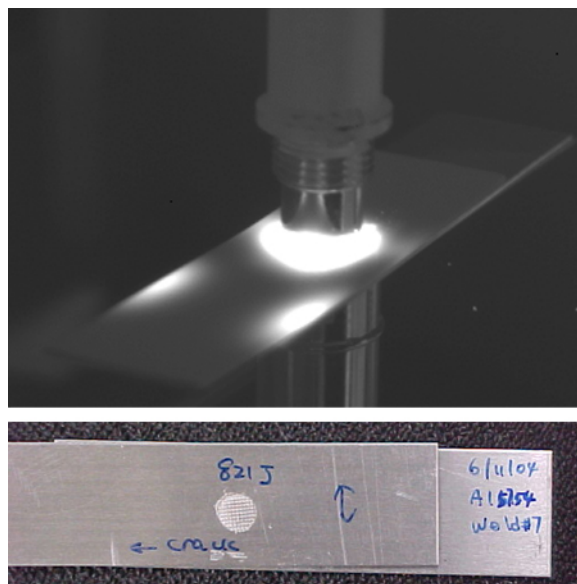


Figure 13. Top: IR thermal image of the "hot" spot. Bottom: the corresponding cracked weld sample.

Figure 14 presents a thermal image of a three-weld sample when the third weld was being made. The weld arrangement and the welding sequence are the same as for the weld sample shown in Figure 10. The concentration of the acoustic energy at the second weld is clearly observed. On the other hand, there is no noticeable heat generation at the first weld, although the first weld is closer to the source of vibration. Also, edge hot spots are evident near the third weld where cracking had been observed.

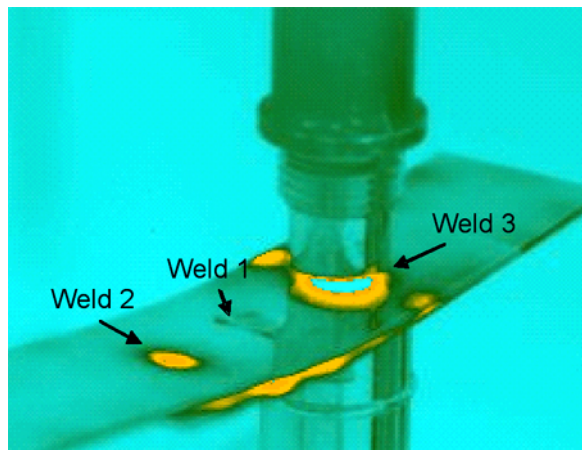


Figure 14. IR Thermal image of multiple spot welds. The third weld is being made.

The initial IR experiment conducted in FY 2004 clearly showed the potential of IR thermography as a tool to study the fundamentals of the UW process. More detailed IR experiments are planned in FY 2005.

Residual Stress Measurement

As in the case of many other welding processes, residual stresses are expected in an ultrasonic weld. High residual stress levels in the bonded region could affect the long-term stability of weld properties in aluminum welds.

Because the bonded region in a spot weld is located between two thin workpieces, measurement of the residual stress in the bonded region is difficult for many measurement techniques such as X-ray diffraction and neutron diffraction.

In this study, the interferometric strain/slope rosette (ISSR) measurement technique, developed by Li and colleagues of Oakland University, was used as an exploratory attempt to investigate the residual stress in a UW weld. The unique features of the

ISSR technique include relatively small gauge size, high precision, and the ability to determine the stress gradient through the workpiece thickness.

The measurement was taken at the center region of the spot weld of Al6061-T6 alloy. The residual stress distributions as a function of the depth from the back side of the weld sample are plotted in Figure 15. σ_{xx} and σ_{yy} are the two normal stress

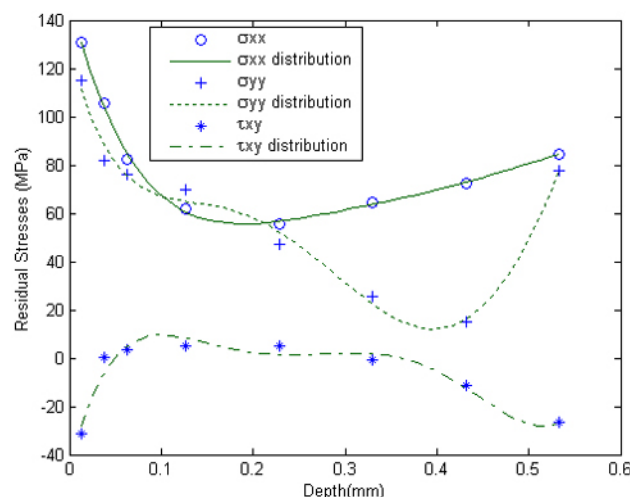


Figure 15. Residual stress as a function of the depth from the back side of an Al6061-T6 weld sample.

components along the length and width of the specimen, respectively, and τ_{xy} is the shear stress component.

The ISSR measurement shows that there are considerable tensile residual stresses in the center region of the ultrasonic weld. The maximum is at the surface of the specimen and reached the yield strength of the material (Table 1). Additional residual stress measurements are planned in FY 2005 to study the effect of welding process conditions on the residual stress.

Conclusions

The research efforts during FY 2004 have resulted in considerable progress toward the understanding of UW process fundamentals. The bonding interface study on dissimilar aluminum alloy welds revealed several important aspects of the interface deformation and bonding process. The profound geometric effects on the acoustic energy propagation and dissipation and the resultant weld properties were identified and characterized.

Publications

W. Ren, K. Li, and Z. Feng, "Ultrasonic Welding Stress Distribution Measured with Optical Rosette/Ring-Core Method," *SAE 2005 Congress*, SAE-International, Technical Paper No 2005-01-1035, 2005.

I. Attachment Techniques for Heavy Truck Composite Chassis Members

Principal Investigator: Lynn B. Klett

Oak Ridge National Laboratory

P.O. Box 2008, Oak Ridge, TN 37831-6053

(865) 241-8112; fax: (865) 574-8257; e-mail: klettlb@ornl.gov

Principal Investigator: Darrell R. Herling

Pacific Northwest National Laboratory

P.O. Box 999, Richland, WA 99352-0999

(509) 375-6905; fax: (509) 375-4448; e-mail: darrell.herling@pnl.gov

Technology Development Manager: Sidney Diamond

(202) 586-8032; fax: (202) 586-1600; e-mail: sid.diamond@ee.doe.gov

Field Technical Manager: Philip S. Sklad

(865) 574-5069; fax: (865) 576-4963; e-mail: skladps@ornl.gov

Contractors: Oak Ridge National Laboratory, Pacific Northwest National Laboratory
Contract Nos.: DE-AC05-00OR22725, DE-AC06-76RL01830

Objectives

- Overcome the technical issues associated with joining composite materials in heavy vehicles by developing technically robust and economically attractive joining techniques.
- Develop and validate one or more joint designs for a composite structural member attached to a metal member that satisfy the truck chassis structural requirements both economically and reliably.
- Solicit input from truck original equipment manufacturers (OEMs) and suppliers on the technical hurdles and needs associated with joining structural composite members in heavy vehicles. Use this information to guide the joint design and development activities.
- Publish information on the design, modeling, and testing methodologies that are developed to support the incorporation of composite materials into other chassis components.

Approach

- Collaborate with Delphi and its OEM partners to identify and address technical needs related to the manufacturing, joining, and implementation of a composite chassis component.
- Design attachment components and configurations in close coordination with the composite structural component development.
- Use modeling techniques to predict the performance of various joint designs, taking into account damage mechanisms and fatigue/life requirements.
- Characterize various composite materials and mechanical joint configurations through mechanical testing, considering variables such as hole size, hole fabrication method, bolt pre-load, inserts, combined loading, vibration, fatigue, and durability.
- Validate joint design for the composite structural member through track testing.

Accomplishments

- Conducted static and fatigue tests on a commercially available, component-independent, pultruded fiberglass composite material.
- Investigated several hole fabrication techniques, including water jet cutting, laser cutting, punching, drilling with a standard drill bit and Forstner bit, and drilling undersized holes and then reaming.
- Ran static and fatigue tests of composite specimens with holes fabricated by various methods to identify the method preferred for the least damage in the composite at an acceptable cost and complexity.
- Identified thermography as a reliable nondestructive technique for evaluating damage due to hole fabrication.
- Ran static and fatigue tests on Extren®/steel joints and baseline steel/steel joints (lap shear and cross tension).
- Conducted finite element analysis (FEA) modeling to optimize the geometry of a metallic insert for an all-carbon-composite component to address the bolt loosening due to creep in the composite member.
- Presented two papers at the 2004 SPE Automotive Composites Conference and Exposition in Detroit.

Future Direction

- Conduct bolt bearing and fatigue tests to investigate design modifications, such as inserts, molded-in holes, and 3-dimensional (3D) reinforcement to minimize the damage in the composite and improve the fatigue life of a composite-to-steel joint.
- Evaluate the impact of using adhesive bonding in place of and in combination with bolting, as well as the effects of environmental exposure and testing rate for the composite/steel Mode I and Mode II fatigue specimens.
- Use FEA modeling with input from the composite and joint tests to optimize and predict the performance of the composite/steel joint.
- Continue to work closely with the industrial team to develop the composite component and composite-to-steel joint design solutions to meet the demanding requirements of the heavy vehicle chassis environment.

Introduction

In May 2003, researchers at Oak Ridge National Laboratory (ORNL) and Pacific Northwest National Laboratory (PNNL) began collaboration on a 4-year research effort focused on developing technically robust and economically attractive joining techniques to overcome the technical issues associated with joining lightweight materials in heavy vehicles. This work is being performed concurrently with an industry program led by Delphi to develop and commercialize composite chassis components, which will require resolution of the joining challenges. The industry project serves as a “focal project” that provides real load and service data to this project and will potentially field-test and implement the technology developed in this project. The initial focus of research is development and validation of one or more joint designs for a composite structural member attached to a metal member that satisfy truck chassis structural requirements both economi-

cally and reliably. Broadening the effort to include other structural joints, including composite-to-composite joints, is anticipated. Durability track testing of the first prototype composite component and joint is planned for the last half of 2005.

Component-Independent Material Evaluation

To gain an understanding of the performance of composite materials in a heavy vehicle structural chassis application, a commercially available pultruded fiberglass composite—Extren®, manufactured by Strongwell—was chosen for initial component-independent study. The pultruded composite consists of a continuous-strand mat with unidirectional rovings in the axial direction and a surface veil for corrosion and ultraviolet protection. The results will serve as a baseline for further testing of composites with 3D reinforcement and with low-cost, lightweight design modifications—such as

modified washers, inserts, or adhesive bonding—to improve performance at the joint.

Hole Fabrication Techniques

The initial joint design for a composite component-to-steel member will likely include mechanical fasteners requiring holes in the composite member. The use of bolts through holes in the composite is a concern, especially because of the severe loading conditions and the long service life resulting in high cycle fatigue. Several hole fabrication techniques have been evaluated, including drilling with a Forstner bit, drilling with a standard tapered bit, laser cutting, water jet cutting, and punching. For each method, 12.7-mm-diam holes were machined in the center of $76.2 \times 254 \times 3.2$ mm Extren® coupons.

Many of the water jet cut specimens had visible delaminations and cracks around the hole diameter. In some cases, the damage produced at the edge of the hole spread through the laminate thickness, puckering the coupon's surface layers around the hole at the back of the laminate during machining. Additionally, the cut was jagged instead of smooth and circular. This amount of damage was quite unexpected because of the prior success with the fiber-glass composite for straight cuts. Two water jet cutting facilities, including one with significant experience with composite materials, attempted to machine the holes. In both cases, some of the specimens looked fairly good, but many had large areas of damage.

Although the laser-machined holes (conventional laser with 127–152 cm/min linear feed rate) had no visible damage, there was some residual carbon dust on the cut surfaces, as is normal in laser-machined polymers.

Open-hole tensile, static, and fatigue tests have been conducted on the specimens with holes fabricated with different methods. The results shown in Figure 1 indicate that the specimens drilled with the carbide-tipped Forstner bit have the highest average tensile strength with the least scatter in the data. As anticipated, the water-jet-cut specimens did not perform well because of the large amount of damage in many of the specimens. The results of the fatigue tests with $R = 0.1$ and a frequency of 5 Hz (Figure 2) at 70%, 50%, and 30% of ultimate stress do

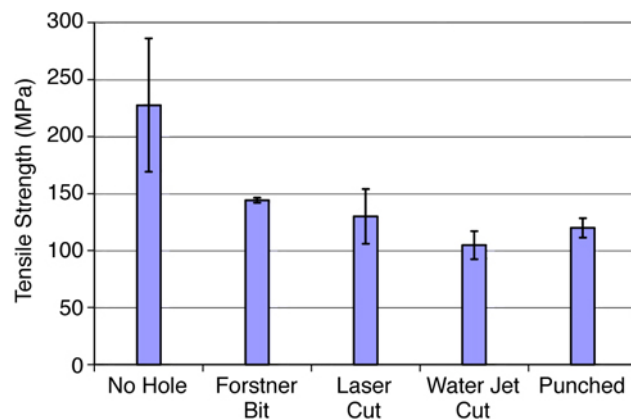


Figure 1. Comparison of ultimate tensile strengths for specimens with holes fabricated with different methods and the material with no hole.

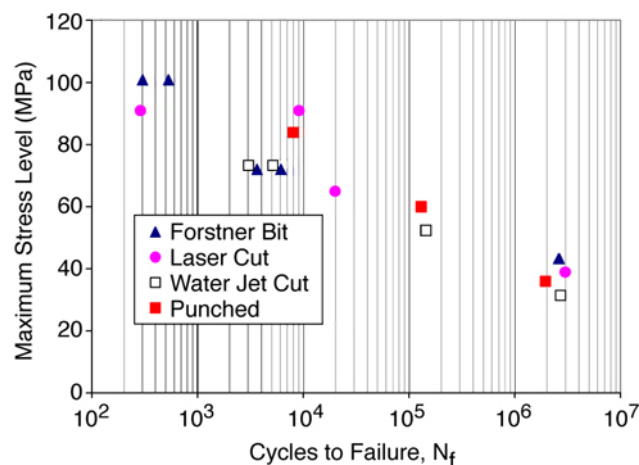


Figure 2. Fatigue testing results for specimens with holes fabricated with different methods.

not show a dramatic difference in fatigue performance between the specimens with different hole fabrication techniques. However, a difference will likely be detected at higher stress levels because of the variations in the static failure stresses. Additional tests are under way.

Specimens with a preferred hole fabrication method will be tested in bolt bearing and fatigue to evaluate design modifications, such as bolt pre-load, inserts, molded-in holes, and 3D reinforcement of the composite. The goal will be to minimize the damage in the composite and improve the fatigue performance of the resulting composite/metal joint.

Methods for Damage Detection

Several methods have been investigated for evaluating the damage associated with hole fabrica-

tion in the Extren® composite material, including dye penetrant analysis and flash thermography. The flash thermography method has good correlation with the X-ray dye-penetrant results.

Although the results from dye penetrant can be very good, the drawbacks include the time required for soaking, the contamination of the composite with the solution, and the requirement for an X-ray source. Additionally, for each material density and thickness, the time of exposure and power level must be optimized to get the desired results.

The flash thermography method was used to evaluate several of the water-jet-cut coupons. Thermography is a nondestructive technique that involves applying a heating (or cooling) stimulus to the surface of a test piece and imaging its thermal response with an infrared (IR) camera. In flash thermography, the thermal stimulus is in the form of a short-duration flash uniformly applied to one side of the part. The IR camera records the surface temperature of the opposite side of the part as a function of time. If sufficient temperature contrast can be obtained, changes in through-the-thickness diffusivity of the material can be measured.

Thermal diffusivity is the property governing the rate at which heat flows within a material; and any delaminations or cracks will affect the heat diffusion rate, thereby changing the surface thermal response. Therefore, by studying the time evolution of the surface temperature distribution, it is possible to obtain information on the depth, spatial extent, and thermal character of subsurface structures and defects.

The IR camera used in this study was a Raytheon Radiance-HS IR camera with a 50-mm lens, which operates in the 3–5 μm spectral range. With this camera, data are recorded as full field-of-view at a rate of 142 images/second and with a time resolution of 0.007 s. The flash system used was an Acute2 (2400 W·s) xenon flash lamp. The thermal images after flash were recorded for both sides of the coupons.

One advantage of flash thermography is that it can provide an indication of depth below surface that X-ray and visual examination cannot. The depth limit of flash thermography with this particular setup appeared to be about one-half of coupon thickness (1.5 mm). Possibilities to further enhance the thermal images and depth resolution of the flash ther-

mography technique include the step-heat and lock-in techniques.

Additionally, because this is a nondestructive and noninvasive technique, flash thermography can be used during fatigue testing to monitor damage development and propagation in the composite material.

Extren® Static and Fatigue Testing

Baseline static and fatigue tensile testing was conducted for the pultruded fiberglass material. The fatigue tests were run with $R = 0.1$ at 70%, 50%, and 30% of ultimate stress at a frequency of 5 Hz (Figure 3). Although there was a fairly high level of scatter among the tensile specimens, the fatigue behavior was fairly consistent. Several of the specimens at 30% of ultimate stress reached runout with more than 1,000,000 cycles. As expected, the ultimate stress levels are significantly higher for the specimens with the loading axis in line with the axial reinforcing fibers.

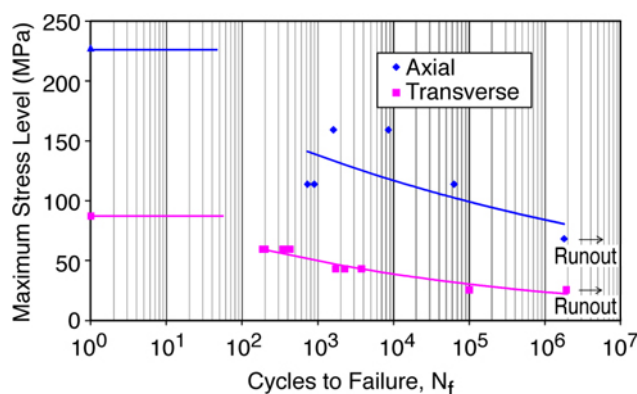


Figure 3. Tensile fatigue behavior of Extren® fiberglass composite.

To determine the feasibility of testing at a higher rate, the surface temperature of the composite specimens was monitored at both 5 and 20 Hz. Room temperature was approximately 23°C. At 70% of ultimate (between 300 and 1250 cycles to failure), the maximum temperature of the samples at 5 Hz was 27.5°, compared with 34.5°C for 20 Hz. This is the most severe loading case; but it has the shortest life, so the temperature does not reach equilibrium. For tests at 40% ultimate (40,000–45,000 cycles), the specimens at 5 Hz reached 27.6°, while the 20-Hz specimens reached 34.1°C. These temperature measurements are for the surface; the material is

probably reaching a higher heat internally. In order to keep within the ASTM-recommended 10° temperature rise for these tests, the tests should be run slower than 20 Hz. However, the results indicate that a frequency greater than 5 Hz could possibly be used.

Bolt Torque and Pre-Load Investigation

A test methodology has been developed to study the effects of bolt torque levels on composite materials. Information derived from this work will ultimately be used to support the characterization of bolted composite assemblies tested as part of this program, as well as provide insight into the design and manufacture of a composite truck chassis.

When a composite assembly is bolted together, the tightened bolts and other hardware (e.g., washers, nuts) apply an external compressive stress to the composite through the thickness. This bolt pre-load may be beneficial or detrimental to the composite, depending on the amount of applied pressure. Snug bolts can minimize slippage or movement of the bolt shank in the composite hole, thereby reducing the possibility of wear and abrasion at the edge of the hole. The additional compressive force may also help “clamp” the individual composite layers together, resisting delamination propagation when other external forces are applied to the assembly. Alternatively, too high a pre-load could cause the clamping force to exceed the transverse compressive strength of the composite, essentially crushing the material or forcing penetration of the bolt hardware into the composite surface.

Figure 4 is a schematic of the basic test setup used to characterize the effects of bolt pre-load on test specimens. An Interface washer load cell, model LW2050, was positioned between the composite laminate backed by a hardened flat steel backing plate, and a second backing plate. Applying a torque to the bolt applies a compressive force to the assembly, which is in turn measured by the washer load cell.

For a given material and thickness, the washer load cell setup has proved useful to study the effects of a number of factors on joint design, including (1) composite pre-load as a function of bolt torque, (2) the effects of multiple bolt tightening/loosening cycles, (3) specimen-to-specimen variability, (4) the

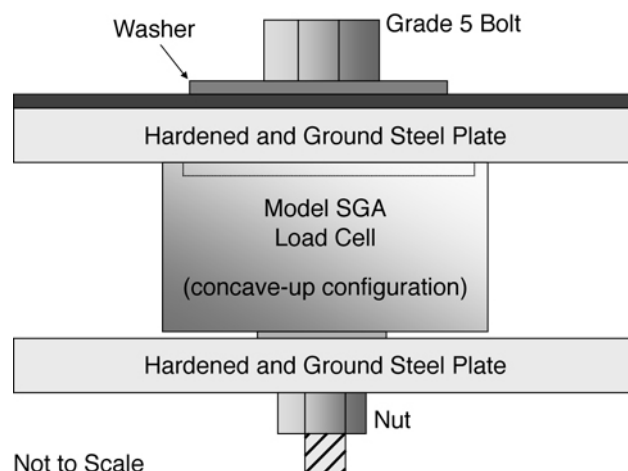


Figure 4. Bolt pre-load test schematic.

effects of re-tightening bolts, and (5) the loss of bolt pre-load with time.

Hardened flat steel plates are required on both sides of the washer load cell to ensure that the load is aligned correctly on the load cell. The use of this stack-up in bolted assemblies for static and fatigue testing may be impractical. Strain-gaged bolt load cells are under evaluation for use as an alternative to the washer load cells to monitor the bolt load during mechanical testing.

Figure 5 shows the loss of pre-load as a function of time for various test materials that have been bolted together with a 67.8 N-m (50 ft-lb) applied torque. The loss of pre-load with time is relatively low for a steel-to-steel bolted assembly and increases for the composite assemblies. The greatest loss of pre-load occurs with the thick composite substrate (6.35 mm). This likely results from the increase in the thickness of the glass fiber mat in the thicker composite.

A significant part of the loss of pre-load for these samples occurs during the first 5 minutes after the bolt has been tightened. A very rapid decrease in pre-load occurs within the first 30 seconds after application of the torque. Initial test results suggest that retightening the bolts within a few minutes of the initial assembly may help reduce the bolt's pre-load loss rate with time, and the overall loss of pre-load.

To determine the effects of the level of bolt pre-loading on the mechanical properties of the composite materials, bearing tensile and fatigue tests will be

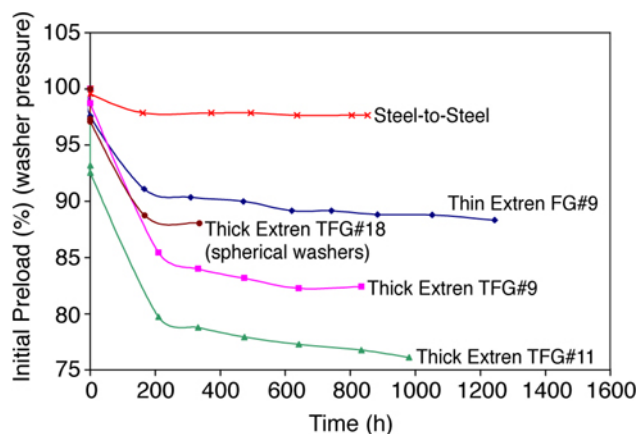


Figure 5. Loss of pre-load for various bolted assemblies.

conducted on the pultruded fiberglass composites. Varying levels of torque on the bolts, as well as Huck bolts, will be evaluated. It is anticipated that the Huck bolts will yield a more consistent pre-load level.

Evaluation of 3D Reinforced Composite

Static tensile and fatigue tests have been conducted on 3D glass-reinforced composites to determine the effects of the 3D reinforcement and to evaluate their feasibility for use in the structural chassis component. The initial composites tested had both high levels of voids and a clay filler material that contributed to a decrease in static strength and poor fatigue performance. Once the processing was improved to eliminate the clay filler and reduce the void content, the static tension and fatigue properties improved significantly. Several material systems are under evaluation, and the fatigue curve for one of the 3D glass-reinforced polymers is shown in Figure 6.

Additionally, hole fabrication techniques were compared for the 3D reinforced material to ensure that the results seen in the pultruded polymer composite (with significant chopped glass mat) would translate for a highly oriented composite. For the Extren® material, the water jet cut specimens showed the most damage. However, the delamination occurring in the 3D reinforced material was limited to the midplane of the composite and did not appear at the surface. Again, the specimens cut with the carbide-tipped Forstner bit had the least visible damage.

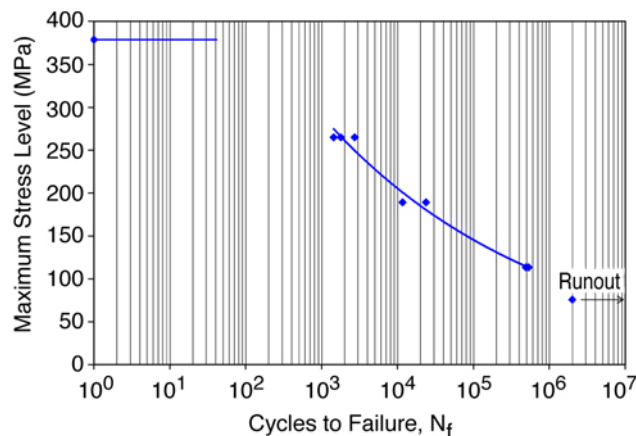


Figure 6. Tensile fatigue behavior of 3D reinforced glass/polymer composite.

Steel-to-Steel Joint Evaluation

To establish design targets of an existing chassis joint, 6.35-mm-thick grade 6 steel plates were joined by a Huck bolt to achieve two testing configurations commonly used in joint performance evaluations, lap shear and cross tension. This baseline will be used to design and optimize the composite/steel joint. Static and fatigue tests were conducted to characterize the performance of the joints. In the static tests, a bearing failure mode (composite material shear-out) was observed for the lap shear specimens, whereas bolt failure (stripping of the nut collar) occurred in the cross tension specimens. The failure load for the lap shear specimens were approximately 128 kN, while the cross tension specimens failed at approximately 175 kN.

Cyclic fatigue tests were also performed on the joints under a tension–tension ratio of $R = 0.1$ for both lap shear and cross tension configurations. Figure 7 illustrates the fatigue strength of the lap shear and cross tension specimens for all completed tests. Unlike for the static tests, the fatigue failure for the cross tension fatigue tests initiated from the steel/steel contact periphery on the faying interface where the structural stress is maximum. Additional tests are ongoing.

Extren®/Steel Joint Evaluation

Preliminary composite/steel joints (both lap shear and cross tension coupons) were assembled and tested to understand the fatigue behavior and failure mechanisms associated with joining the fi-

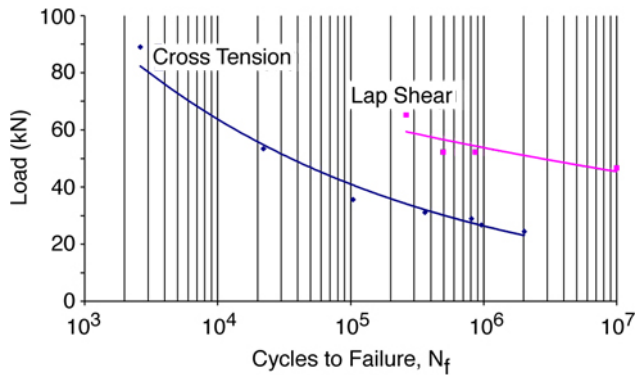


Figure 7. Fatigue test results of the lap shear and cross tension steel assemblies joined by a Huck bolt.

berglass composite to steel with a bolt. Joints were assembled using 3.2-mm-thick composite with 1.4-mm-thick 1008 steel. All composite/steel joints were joined with 6.35-mm grade 5 bolts, torqued to 13.6 N-m (10 ft-lb).

The following joining and testing parameters for joint strength are under investigation:

- Effect of washer size
- Effect of fatigue test frequency and temperature rise
- Effect of structural adhesive
- Effect of environmental exposure

Washer Size Effects

Figure 8 illustrates the static strength comparison among lap shear samples with a nominal size washer (15.9 mm diam), an oversize washer (25.4 mm diam), and a steel plate washer (50 × 35 × 6 mm). Under lap shear loading, the static strength increases approximately 10% with an oversize washer and approximately 20% with a plate, compared with the nominal washer. The samples with nominal and large washers show the typical characteristics of a bearing type of failure, but the samples with the constraining plate do not show a clear load drop prior to the peak strength. A similar cleavage tension failure mode was observed in all three washer types, and the damage initiated from the periphery of the bolt hole.

Figure 9 illustrates the fatigue strength comparison of lap shear and cross tension samples with the

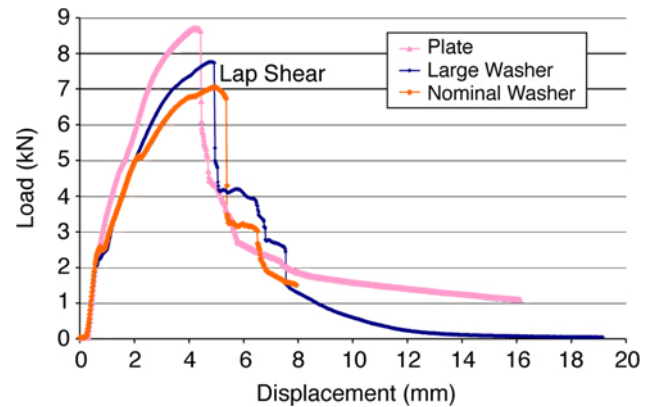


Figure 8. Static strength comparison of washer size effect.

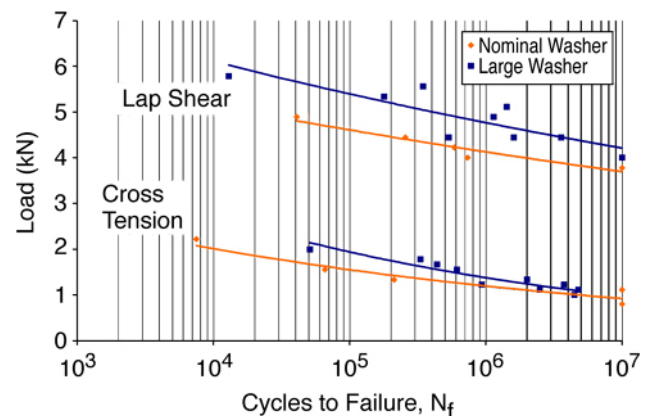


Figure 9. Fatigue strength comparison of washer size effect.

nominal and oversize washer. On average, joints with larger washers yield higher fatigue strength than joints with nominal washers. This effect is more prominent under lap shear loading than under cross tension loading conditions. Under fatigue loading, damage on the composite plates initiated right underneath the periphery of the washer for both loading cases.

Frequency Effects

Fatigue tests are normally carried out at the highest frequency possible in order to minimize test duration. Typically, the maximum temperature rise allowed in the test material should be less than 10°C during fatigue testing. To study the effects of frequency on the composite/steel joint, lap shear fatigue tests were conducted at 5, 15, and 20 Hz with $R = 0.1$. The coupon temperature was monitored with thermocouples, and the maximum temperature rise for each frequency was recorded. At a frequency

of 15 Hz, the maximum temperature rise was 5°C; at 20 Hz it was 9°C, which is just below the threshold value. Because of the degree of scatter in the material properties of this material, no significant change in the fatigue life at each fatigue level was apparent. Based on these results, a maximum test frequency of 15 Hz was chosen for the composite/steel joints to avoid inducing significant temperature changes in the sample during fatigue testing.

2D vs 3D Polymer Composites

Lap shear coupons were assembled with a 3D reinforced glass composite to investigate the fatigue behavior and failure mechanisms associated with joining the composite to steel with a bolt. The joint static and fatigue performance was then compared with the performance of the pultruded composite/steel joints.

The 2.54-mm-thick composites were joined to steel in the same manner as the Extren®/steel bolted joints with a 25.4-mm washer. The static strength of the 3D composite is approximately 3 times greater than that of the 2D Extren® composite. However, hybrid joints assembled from each composite substrate with steel yielded comparable static strengths (Figure 10). A cleavage tension failure was observed in joints assembled with Extren®, and a shear-out failure mode was observed in joints assembled with the 3D composite.

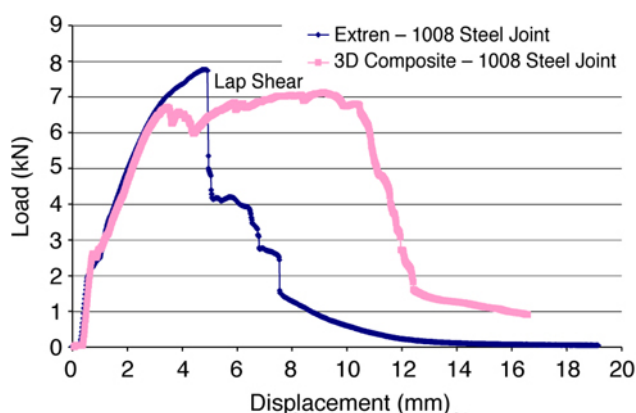


Figure 10. Static joint strength comparisons of composite/steel joints.

The fatigue strength of the hybrid joints assembled with the 3D composite was also comparable to that of the 2D composite. Figure 11 is an illustration of the fatigue strength comparison in terms of percentage of peak load. These testing results indicate

that the fatigue strength of this type of hybrid joint is more sensitive to the geometry of the joint design than to the material substrate.

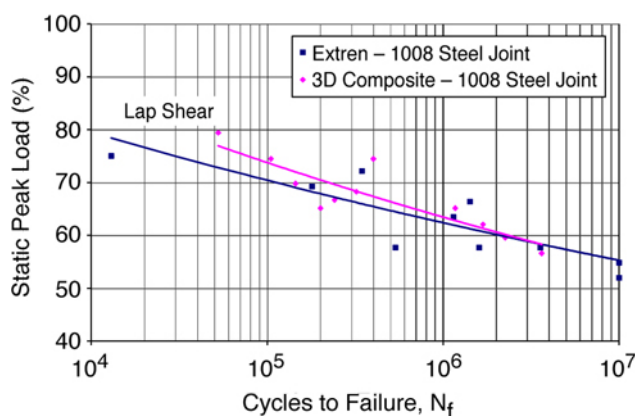


Figure 11. Fatigue joint strength comparisons of composite/steel joints.

Modeling

Genoa Evaluation

The joining team has investigated the commercial software GENOA to evaluate the feasibility of using it to predict the static and fatigue strength of composite/steel joints. Three staff members from ORNL and PNNL attended the GEONA training classes.

GENOA is an integrated structural analysis and design software that originated in the aerospace composite community. Its progressive failure analysis module predicts crack initiation, growth, and final failure for monolithic and 2D/3D braided, laminated, stitched, and woven composite materials based on the unit cell formulation originated by the National Aeronautics and Space Administration. The initiation and damage growth can be due to static, fatigue, thermal, and impact loading; and it is identified by the industrial team as the candidate software to be used in their project.

The feedback on the software from the staff members that attended the training classes was mostly positive. GENOA couples analyses on different scales and provides progressive failure analysis capabilities that are specifically tailored for composites. However, the current version has the following limitations that may hamper its use for the joint analysis:

- GENOA does not support more than one element type. Therefore, modeling of the joint area

would have to be performed using solid elements.

- GENOA does not have contact modeling capability. Therefore, the interaction between the fastener and the plate materials, critical for predicting the fatigue life of the joint, cannot be modeled with this contact included.
- GENOA has demonstrated its ability to predict failures of composite samples with continuous fibers. Its capability to predict progressive damage for composites with randomly distributed chopped fibers needs to be further evaluated and established.

Joint Modeling

ABAQUS was used to analyze the effect of washer size in a bolted joint consisting of pultruded fiberglass composite and steel. The solid models were linear elastic, and the pre-load was produced by turning the nut by 90°, simulating a torque of 13.6 N-m (10 ft-lb). A small washer resulted in 20% more compressive strain in the composite than in the large washer. This prediction was validated through the joint mechanical testing results showing an improved static strength and fatigue resistance for a larger washer.

For an all-carbon reinforced composite component bolted to a steel component (design provided by the industrial team), three insert geometries were evaluated under two loading conditions. The metal inserts were selected so that the compressive load caused by the bolt tightening is fully carried by the metal insert, and the load is transferred to the composite through the bond between the insert and the composite. This will mitigate the issues associated with bolt loosening due to creep and/or damage in the composite during bolt installation.

The three insert designs include a cylindrical steel insert, a tapered insert with the large diameter at the bolt head side of the composite, and a tapered insert with the large diameter on the steel side of the composite. One assembly is shown in Figure 12. The model was evaluated under two loading conditions: a bending force and a lap shear force. The measure of performance to compare the different insert geometries was a component of traction nor-

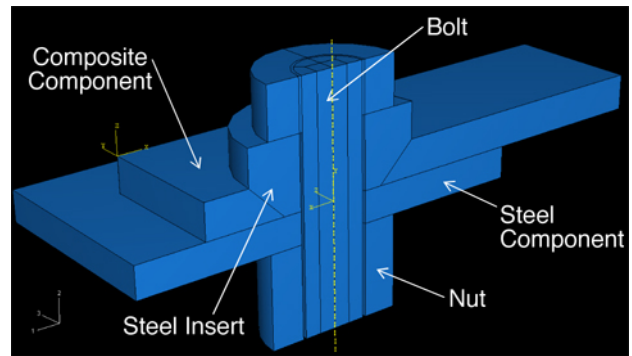


Figure 12. Finite element model of composite/steel bolted joint with tapered insert.

mal to the composite/insert interface that would produce a peeling stress in the adhesive. Because actual loads are not yet available for the actual chassis component, failure stresses from the steel/steel joint testing for lap shear and cross tension (bending) were used with the model. This is a worst-case load application and is unrealistic because the pre-load in the bolt is overcome, and contact between the steel and the composite are lost.

Qualitatively, the results match the results obtained for lower load levels: the tapered insert with the large diameter at the bolt head side of the composite exhibits the best performance. The model of the joint and insert will be added to the system model for additional investigation. As design and material changes are made and the loading cases are refined, further optimization of the joint, including inserts, will be possible.

Fatigue

Components in a truck chassis undergo complex random variable fatigue loading during their lifetime. The loading spectrum can be estimated from measurement results acquired in field tests or test-track runs, where a component is instrumented with accelerometers, strain-gages, and linear variable differential transformers. A majority of the cycles reach low load levels and are generally of concern only if their frequency approaches a resonant frequency of the structure. Resonance issues can be eliminated by adequate design of a component. Higher loads commonly take place at lower frequencies. Repetitive loads below the static limit can initiate damage, especially in the vicinity of stress raisers such as bolt holes and contacts. Therefore, the prediction of low-

frequency fatigue life is of prime interest for chassis structural application.

Cumulative damage caused by low-frequency cycles is estimated using certain damage laws in conjunction with the results of constant amplitude fatigue tests. One of the most common damage laws is the Palmgren-Miner linear relationship. This law assumes that fatigue cycles at a specific load level always result in the same damage regardless of the loading history. The Palmgren-Miner model yields acceptable results for metals and is almost exclusively used for life predictions in practical applications. A literature review has revealed that this relationship may grossly overestimate or underestimate the fatigue life of composites. Because of this, empirical and semi-empirical non-linear damage laws have been developed for a variety of composites. In addition, Goodman diagrams can be used to account for varying R ratios of constant amplitude fatigue tests that are used as a basis for fatigue life predictions. All these methods require significant testing.

It will be necessary to evaluate the applicability of Palmgren-Miner's law for selected materials as part of this project in order to predict long-term fatigue performance. If this law does not reasonably represent actual material behavior, then an appropri-

ate nonlinear relationship must be determined through additional testing, or the uncertainty must be taken into account by using appropriate safety coefficients during design. Although GENOA has shown promise for predicting the fatigue performance of the 3D reinforced composite material at constant stress levels, the software uses Miner's rule for variable stress levels.

Presentations

L. Klett, B. Frame, and V. Kunc, "Damage at Holes in Bolted Composite/Steel Joints for Heavy Vehicle Chassis Components," presented at the 2004 SPE Automotive Composites Conference and Exposition, Detroit, September 14–15, 2004.

X. Sun, D. Herling, and E. Stephens, "Static and Fatigue Strength Evaluations for Bolted Composite/Steel Joints for Heavy Vehicle Chassis Components," presented at the 2004 SPE Automotive Composites Conference and Exposition, Detroit, September 14–15, 2004 .

Acknowledgements

The principal investigators would like to acknowledge the valuable contributions of other members of the research team, including Barbara Frame and Vlasta Kunc at ORNL and Xin Sun and Elizabeth Stephens at PNNL.

J. Rapid, Low-Cost Tooling Development

Principal Investigators:

Cliff Eberle

*Oak Ridge National Laboratory, Oak Ridge, TN 37831-8048
(865) 574-0302; fax: (865) 574-8257; e-mail: eberlecc@ornl.gov*

Curt Lavender

*Pacific Northwest National Laboratory, 902 Battelle Blvd, PO Box 999, Richland, WA 99352
(509) 372-6770; fax: (509) 375-4448; e-mail: curt.lavender@pnl.gov*

Technology Development Area Specialist: Sidney Diamond

(202) 586-8032; fax (202) 586-2476; e-mail: sid.diamond@hq.doe.gov

Field Technical Manager: Philip S. Sklad

(865) 574-5069; fax: (865) 576-4963; e-mail: skladps@ornl.gov

Contractor: Oak Ridge National Laboratory

Contract No.: DE-AC05-00OR22725

Objectives

- Assess status and need for low-cost tooling technologies for lightweighting materials.
- Evaluate state-of-the-art capabilities for rapid, low-cost tooling approaches.
- Determine the socioeconomic factors that are likely to significantly impact the development and implementation of advanced tooling technology.

Approach

- Conduct a workshop to solicit industry input. Follow the workshop by privately interviewing key participants throughout the value chain.
- Conduct energy analysis to estimate potential energy savings from improved tooling technology.
- Review tooling industry socioeconomics and potential impacts of technological change in the industry.
- Report key findings and plan the path forward.

Accomplishments

- Conducted two industry workshop sessions.
- Recorded preliminary findings from workshop sessions and published summaries on the web
- Performed energy analysis.
- Conducted follow-up interviews with key industry workshop contacts.
- Reviewed socioeconomic indicators of tooling industry health and potential impacts of technological change or lack thereof.
- Developed a plan to engage industry in roadmapping and collaborative technology development.
- Issued draft report to DOE.

Future Direction

- Work with industry to foster communication and collaboration, and to develop an “industry-owned” roadmap.
 - Engage other interested government parties to co-sponsor research and development (R&D).
 - Commence performing selected R&D.
-

Introduction

The introduction of advanced polymer-based composites and lightweight material manufacturing processes to commercial vehicle manufacturers and their supplier base is thought to be severely impacted by the high cost of tooling and long tooling development time. Often the use of lower-cost materials and less efficient structural designs is dictated by the fact that tooling for the manufacture of advanced composites and other lightweight materials cannot be justified from a cost-per-part basis, and from the long development times or procurement lead times that are required. In addition, the unique production volumes associated with commercial vehicles—which are significantly lower than automotive production volumes, yet well above aerospace production numbers—make current tooling design and development methods unsuitable.

An example of the cost and schedule challenges faced by commercial vehicle manufacturers is that a fully tooled door system for a Class 8 tractor can cost upward of \$20 million and require over 24 months to fabricate and qualify the tooling. When advanced materials such as carbon fiber composites or lightweight metals such as aluminum or magnesium are considered, tooling design, material forming characteristics, and surface finish requirements make today’s manufacturing approaches very high-risk. The result is often that manufacturers fall back on less efficient structures that use conventional steel and fabricated structural designs.

The purpose of this project is to assess current tooling technologies to identify key deficiencies in cost, prototype and fabrication methods, and design and modeling tools that prevent the increased use of lightweight metals and composites structures in low- and medium-volume commercial vehicles. Data have been gathered from government–industry workshops, published data sources, and numerous follow-up interviews with workshop participants and other key industry experts. The team intends to work with industry to develop a roadmap that will guide the development and implementation of advanced

tooling technology that reduces the risk of using advanced lightweight materials in commercial vehicle applications.

Project Deliverables

In late FY 2004, the project team delivered to DOE a draft report containing findings from the industry workshop, follow-up interviews, energy analysis, and socioeconomics review. The primary future deliverables are a roadmap for tooling technology development and implementation, and a list of co-sponsors that will share the R&D costs with DOE.

Technical Approach

The technical approach for this project is largely based on gathering and analyzing information to enable informed decision-making regarding future R&D investments. A key part of the project has been to plan and conduct a workshop that served as a forum for soliciting information from industry experts and for networking among industry peers. The workshop was followed by interviews with selected key industry contacts, most of whom were attendees at one or more workshop sessions, to validate the workshop findings. Additionally, potential energy and socioeconomic impacts were analyzed. In the future, a roadmap and program plan will be developed.

Industry Workshop

Oak Ridge National Laboratory (ORNL) and Pacific Northwest National Laboratory (PNNL) co-hosted a two-session industry workshop entitled “Tooling Technology for Low-Volume Vehicle Production.” The workshop scope principally addressed tooling needs for large, lightweight components or parts, manufactured in production volumes from 1,000 to 30,000 parts per year, using closed or two-

sided forming or molding processes. Topics covered at the workshop included

- Large class-A components
- Large structural components
- Computer-aided design/computer-aided engineering/computer-aided manufacturing/CIM (CAD/CAE/CAM/CIM) efficiencies
- Rapid prototyping
- Predictive modeling

The target audience included truck, bus, automotive, recreational vehicle, and marine original equipment manufacturers (OEMs) and suppliers; tooling suppliers and designers; tooling material suppliers; rapid prototyping suppliers; CAD/CAE/CAM/CIM suppliers and developers; and machine tool suppliers.

Session one, hosted by PNNL in Seattle on October 28, 2003, focused on identifying needs and goals. It was attended by approximately 30 industry experts with a high representation from truck OEMs and upper-tier suppliers. Session two, hosted by ORNL in Detroit on November 18, 2003, focused on roadmapping solutions and strategies. It was attended by approximately 50 industry experts, with a high representation from companies that were offering new technology that they consider applicable to the tooling industry.

Preliminary workshop observations included these:

- Tooling technology development does not have a home or champion.
 - OEMs and upper tier suppliers push it down the supply chain.
 - Tool suppliers are too small to accept the risk (see socioeconomics discussion).
 - The value chain is very fragmented, and there is poor up-down communication.
 - This workshop appeared to be the first forum that had fostered communication throughout the tooling value chain.
- Tool manufacturing is moving offshore.
- High tooling cost kills development projects.
- Improved tooling technology may lead to reductions in vehicle mass and aerodynamic drag.
- There are some novel technologies and ideas that merit further development.

- The business case can favor composites (and perhaps other lightweighting materials) at low vehicle production volumes.

To date, follow-up analysis has confirmed some of these observations and found others to be suspect. Workshop session summaries and invited presentations are posted on the worldwide web at <http://www.pnl.gov/energy/tooling/default.htm>.

Energy Analysis

An energy savings analysis was conducted by ORNL, using survey data from the workshop sessions. The results suggest that, at full market penetration, probable energy savings attributable to improved tooling are about 4% for heavy trucks and 6% for passenger cars. Details of the analysis, such as assumptions and sensitivity estimates, are available in the full report.¹

Socioeconomics

A socioeconomics review was conducted to assess the tooling industry's health and impacts on U.S. economic prosperity. Key findings are discussed below.

The U.S. tool, die, and mold (TDM) industry consists exclusively of small businesses and is a deeply distressed industry. In 1997, more than 75% of the companies employed fewer than 20 people, and 92% employed fewer than 50 people. In 2001, there were only 16 companies with revenues of \$20 million or more. The largest company had \$80 million in revenues. In 1997, the industry had about 7200 companies and was losing about 200 companies per year—before the most recent recession. Though Commerce Department data are not yet available for 2002 and 2003, our industry interviews suggest that the shake-out of independent TDMs accelerated in those years as a result of the recession.

Apparent U.S. consumption of TDMs remained essentially flat during the 1997–2000 period at \$15 billion before declining in 2001 to \$13.8 billion. Imports and exports showed the same general trend, essentially flat during the 1997–2000 period, followed by a significant decline in 2001. In 2001, the latest year for which data are available, domestic TDM manufacture was \$13.2 billion, imports totaled \$1.7 billion, and exports accounted for \$1.1 billion. In follow-up interviews, we found that those who were importing tools usually were importing from high-cost-of-labor countries that gained their advan-

tage through technology. Although we do not doubt the workshop participants' concerns over imports, it is difficult to ascribe the industry problems to this source.

We discovered that during the 1997–2001 period, the TDM share of total U.S. manufactured goods value declined by 13%. It appears that U.S. manufacturers are reducing the value of TDMs in their finished manufactured products through TDM price reductions, longer use of existing tools, reduced prototyping, and fewer product changes. We believe that these reductions in TDM purchases are also related to increased stamping die production by the major automobile OEMs. Hence we conclude that the major source of the industry's distress is a fundamental shift in its market drivers.

Payment terms, which are driven by the OEMs, are a significant factor in the TDM industry's distress. The OEM often does not pay the first-tier supplier until production begins, which is usually 18 months or more after the TDM buys the tool material. The supplier frequently exacts the same terms from the tool maker. Hence the TDM is essentially compelled to make an interest-free loan to the OEM for several months. Being small companies, the TDMs will generally require bank financing, and banks discount the value of receivables over 30 days. The strain put on banking relations by the recession was certainly a factor in the high rate of TDM company failures during the recession. The truck OEMs and those transplant automobile makers that were interviewed generally have payment policies that are more beneficial to the TDMs than do the U.S. "Big Three" OEMs. However, the domestic automakers comprise the lion's share of independent TDM business in the United States; therefore, their procurement policies are a major factor in TDM industry health.

New technology can significantly reduce the unit cost of tooling. However, the equipment embodying the technology is expensive, especially for small businesses in "cash flow distress," and the resultant improvement in productivity increases the over-capacity in the industry. The reverse of this argument is that the survivors of the shake-out appear to have remained current with technology. This view was strongly reinforced in an interview with a small, but apparently successful, tool maker who suggested that if new technology could reduce tooling costs enough, that could change the paradigm and lead to more vehicle changes and more business

for TDM builders. More vehicle changes translate into more rapid infusion of technology into the vehicles.

Given all of the above, and only minimal government support from the Department of Defense and Department of Commerce, the technology development firms are struggling to survive. The technology developers would like direct government support. However, lacking financial support, they would like to see some mechanism by which the risk of new technology is shared among the TDM builder, the supplier, and the OEM. They feel that the OEM discourages new technology by not being willing to share the risk. Clearly, the TDM builder is the least able to afford the risk of new technology but is one of its biggest beneficiaries. Further, given the lack of real communication in the supply chain, the OEM is essentially oblivious to the problem faced by the TDM builder in adopting new technology.

Conclusions

Tooling is a major expense in manufacturing vehicles, especially at low production volumes. The industry workshop sessions were well-attended, fostered a unique networking opportunity for industry, and provided important information. The energy savings analysis suggests that improved tooling technology should lead to appreciable reduction in petroleum demand. The socioeconomics review found a disconnected value chain, with the TDM manufacturing industry consisting entirely of small businesses and being in severe distress. The good news is that almost everyone with whom we have talked, including prospective co-sponsors such as other government agencies, wants to "do something." It appears that there are opportunities to make a difference with properly planned and targeted technology development and implementation. In FY 2005, we plan to engage the stakeholders to develop a roadmap and begin its implementation.

Acknowledgements

The principal investigators gratefully acknowledge key contributions from many sources. Special thanks is due Jeanne Phillips and Phil Sklad from ORNL, Suzanne Niemeyer and the web hosting group from PNNL, Allan Murray, a consultant to both laboratories, and David Stewart, President of Stewart Automotive Research, for their significant

contributions to workshop planning and execution. Ed Ungar and other Taratec Corporation staff have led the workshop follow-up and socioeconomics review, and ORNL's Rick Schmoyer conducted the energy savings analysis.

References

1. R. L. Schmoyer and C. C. Eberle, "An Analysis of Energy Savings Possible Through Advances in

Automotive Tooling Technology," ORNL/TM-2004/115, Oak Ridge National Laboratory, 2004.

Publication

R. L. Schmoyer and C. C. Eberle, "An Analysis of Energy Savings Possible Through Advances in Automotive Tooling Technology," ORNL/TM-2004/115, Oak Ridge National Laboratory, 2004.

K. Inventory of Heavy-duty Truck Lightweighting Candidates

Principal Investigator: Edwin H. Kraft

EHKTechnologies

10917 SE Burlington Dr.

Vancouver, WA 98664-5383

(360) 896-0031; fax: (360) 896-0032; e-mail: ekraft@EHKTechnologies.com

Technology Development Area Specialist: Sidney Diamond

(202) 586-8032; fax: (202) 586-1600; e-mail: sid.diamond@ee.doe.gov

Field Technical Manager: Philip S. Sklad

(865) 574-5069; fax: (865) 576-4963; e-mail: skladps@ornl.gov

Contractor: EHKTechnologies

Subcontract No.: 4000031071 / 03/22/2004

Objective

- Identify components and systems of heavy-duty trucks that have the greatest total fleet weight savings potential for the purpose of increased fuel efficiency and productivity.
 - Inventory the systems and components of Class 8 tractor-trailers.
 - Model the miles traveled and weight factor for the major component-system-vehicle combinations.
 - Rank and estimate the fuel consumption contribution of the most significant components.
 - Provide a model usable by potential component lightweighting developers to estimate the relative weight-miles contribution of candidate components.

Approach

- Define the industry segments: types of vehicle bodies and vehicle configurations; define the numbers and annual miles of vehicles by type and configuration.
- Compile data on component and system configurations, weights, and materials of construction for the apparent major contributors to vehicle weight.
- Aggregate data on specific component weights and materials to prevent disclosure of individual manufacturers' proprietary information. Select representative values for component weights where a range of designs and weights are common.
- Determine the fuel economy distribution of weight ranges of heavy-duty trucks and calculate a representative fuel consumption of components per pound-mile.
- Design a model of the weight-miles traveled (pound-miles) and fuel consumption for any component or set of components to be considered for fleet weight savings and improved fuel economy.

Accomplishments

- Successfully used the various databases to calculate numbers and total annual miles of vehicles by body type, vehicle configuration (truck and truck-tractor, number of trailers pulled, number of axles and tires), weight sub-classification, and type of cargo hauled.
- Determined that buses and four types of trucks account for >90% of vehicle numbers and miles, and the four truck types account for the most trailer and haul unit miles.
- Determined that weight regulations normally impact the operation of platform, dump, and tank body vehicles, causing them to be weight-limited ("gross out").

- Obtained representative weights of major components common to all vehicle types and those specific to the four primary body types.
- Constructed an Excel-based model of component pound-miles and added a calculation of component fuel consumption.
- Identified the most significant contributors to pound-miles.
- Determined that extensive use of aluminum, high-strength steel, and new designs have already contributed to weight reduction and that further use of these materials plus magnesium, titanium, and composites promises significant additional weight savings.

Future Direction

- Incorporate final manufacturer data in summaries and model.
- Publish final report.
- Present findings to selected industry, government, and professional associations.
- Investigate opportunities and potential impact of materials such as aluminum, magnesium, and titanium.
- Discuss findings with vehicle and component manufacturers for consideration of focused developments.
- Discuss findings with military agencies for applicability to military ground vehicles.

Introduction

The purpose of this project is to assist Oak Ridge National Laboratory (ORNL) and DOE in prioritizing lightweighting technologies for heavy-duty trucks via an inventory of components that may aid in weight reduction. Identifying the components that contribute the most weight in the entire fleet of heavy trucks will enable ORNL/DOE to select projects with the greatest payoff in weight savings and reduced fuel consumption. The inventory must consider not only the weight of typical components but also the number of vehicle miles traveled by heavy trucks using that component over a typical year (pound-miles) and the fuel consumed carrying those components. A model will be provided that allows calculation of the pound-mile and fuel consumption figures for any component under consideration. It will incorporate the effect of applying the component to various truck body types and the miles traveled by trucks that use it. The model may be used to provide a quantitative estimate for comparing the weight and fuel consumption reduction potential of any proposed component.

Project Deliverables

- A presentation has been made to DOE and ORNL personnel.

- A final report will provide details of the methodology and findings.
- A computer disk containing the model will be provided for use by DOE, ORNL, and potential component developers for calculating and identifying the weight and fuel savings potential of any proposed component.

Heavy Vehicle Segments

Some components of heavy duty trucks and tractor trailers are used on every such vehicle; others may only be used on one vehicle type or configuration. In considering the development of a reduced-weight component, it is therefore necessary to understand its potential contribution to weight reduction over the entire vehicle fleet. To do so, it is necessary to have data on the number of vehicles of various types, and the miles traveled by each type, over a representative year. The weight or weight reduction potential of a component is multiplied by the number used on each vehicle type and the miles traveled by that type to obtain the pound-miles for the component. Adding the pound-miles for all vehicle types where a component would be used gives the total pound-miles for that component. If an average fuel economy figure is available for heavy trucks, it may be used to calculate the fuel consumed by each pound of weight of an average vehicle. The

product of the pound-miles and the fuel consumed is an estimate of the fuel savings if that component were implemented across all applicable vehicles.

Several databases were used to construct a master database of numbers and miles traveled for all types of trucks in each weight range of Class 7 and 8 vehicles. It lists 29 body styles, including dry van truck and trailer containers, refrigerated van truck and trailer containers, tank trucks and trailers, flat bed trucks and trailers, dump bodies, and cement mixers. Another truck-trailer classification includes the type of truck (truck or truck tractor), number of trailers pulled, number of axles, and number of wheels. Thus, for example, all tank trucks with 4 axles and 14 wheels pulling a full tank trailer with 3 axles and 12 wheels will have one estimated number with that configuration and total miles traveled. Three-axle, 10-wheel truck tractors pulling one 4-axle, 16-wheel flatbed trailer will have a different estimated number and miles traveled. These differences have been found to be very significant. Analysis of these vehicle types was also expected to assist in focusing effort on the vehicle body types and components with the most contribution to pound-miles and fuel consumption.

This last benefit of the analysis is best accomplished by charting the number and miles traveled for the various truck types, and the number of trailers and “haul units” traveled by those types. A haul unit is defined as one container or support structure for cargo carried by a truck or trailer (e.g., a tank truck pulling a tank trailer constitutes two haul units.)

Figure 1 shows the number of vehicles by type with similar types combined. This result shows that relatively few body types account for the great majority of vehicles. This finding is even more pronounced when the results for body type by miles traveled are shown (Figure 2). We then find that just four body types account for 90% of the miles driven by heavy trucks/tractor trailers: the various forms of vans (dry, refer, insulated, and drop body), platforms (with and without added devices, and drop frame), dump bodies, and liquid haul tanks. Other body types travel far fewer miles and therefore contribute little to the overall miles driven by the total heavy-duty fleet.

Buses, including school, inter-urban, and city transit, have been included in this analysis thus far. It is apparent that they contribute significantly to the total miles driven by heavy vehicles. This analysis

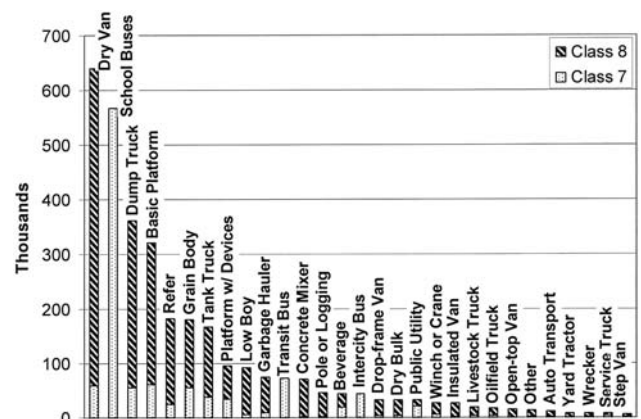


Figure 1. Number of vehicles by type.

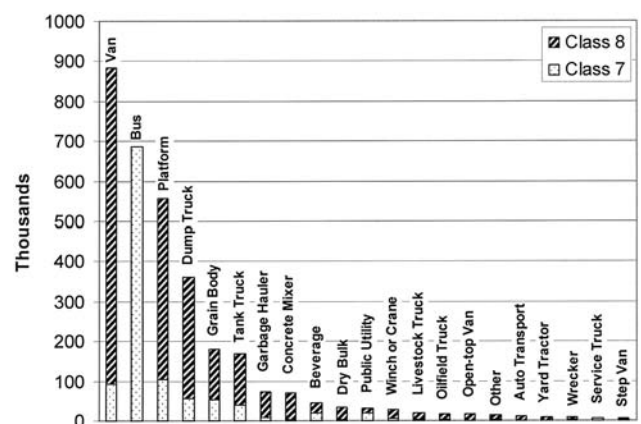


Figure 2. Number of vehicles by type; similar body types combined.

was conducted even though the original project scope included only trucks. During the investigation, it was found that, while bus weight and miles may be significant, the operation of buses is limited by passenger capacity and not by weight in most cases. Fuel savings by reduced weight is a secondary consideration for this industry. Therefore, owners and operators are not generally willing to pay any premium for weight savings. Methods to reduce bus weight may have significant fuel economy payoff but are likely to be adopted only if they carry no cost penalty. Since this topic was not in the original project scope, and buses are not generally weight limited, no further analysis was performed.

The number of trailer miles and of haul unit miles of the various types were analyzed to further confirm the overriding importance of the four types of vehicle bodies. Figure 3 shows the results for haul unit miles.

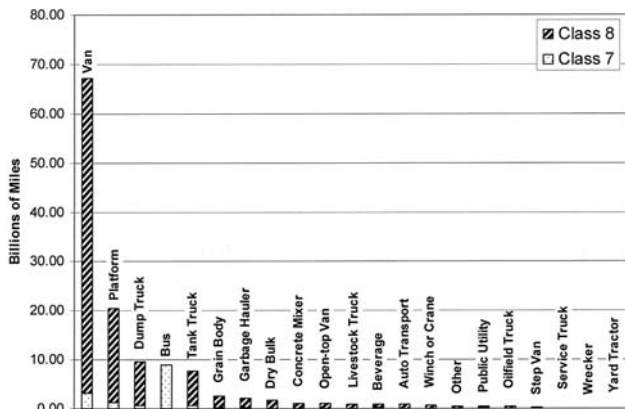


Figure 3. Miles traveled by vehicles of each type; similar body types combined.

We can definitively conclude that vehicles with body types including types of vans, flat beds, dump bodies, and tanks make the most significant contribution to miles traveled by heavy duty vehicles. It is also apparent that Class 8 vehicles other than buses travel far more miles than Class 7 vehicles, which may then be ignored in analysis of potential weight and fuel savings. Analysis of components used either on multiple-body type trucks or on these four primary types will provide the greatest potential for weight and fuel savings.

Major Truck and Trailer Components

Some components of heavy vehicles are used on all body types and vehicle configurations, and others are specific to certain body types. Obviously, a relatively heavy component common to all types of vehicles will contribute much more to total pound-miles than a lighter component specific to only one body type.

Data were collected on the weights of components of all the major systems of trucks, tractors, and trailers. Much of this specific data, however, is proprietary and may not be disclosed. Attempts were therefore made to collect data from multiple manufacturers so that aggregate weights could be used in the analysis. In some cases, particularly where a wide variety of designs and weights are available for a type of component, representative weights were selected to facilitate the comparative analysis. Individual component weights discussed in this report therefore do not represent those of components from any one manufacturer.

Common Components. All truck and truck-tractor components are used in all body types. En-

gines, transmissions, truck frames, exhaust systems, axles, suspensions, cab features, drivelines, wheels, and tires, among others, are common components. Since 70% of haul units are trailers, several other components, such as fifth wheels, couplers, landing gear, “bogie” sliders, bumpers, and underrides, are used by nearly all vehicles. Some components are used on several major body types, such as van and flatbed floors, lower and upper side rails, main and cross beams. It is also important to consider in our analysis that some components are used multiple times per vehicle, including tires, wheels, axles, brakes and suspensions; such multiple use may make a component of moderate weight significant.

The engine is one of the heaviest components and is used on all vehicles. While there are numerous engine designs and engine sizes, many components are common to all or most designs. Figure 4 shows the relative weights of many of the major components. It is apparent that the block and cylinder head are by far the heaviest components and most likely to be significant contributors to pound-miles and fuel consumption. Wheels and tires, used multiple times on all vehicles, have already been the subject of weight reduction efforts. Traditional steel wheels have been partially replaced by light steel and aluminum wheels, with the latter being used on 40–50% of trucks but only about 10% of trailers. Super single aluminum wheel and tire combinations at ~240 lb per set are beginning to replace dual wheel/tires (~390 lb per set for conventional steel). Titanium provides weight and performance improvements for springs.

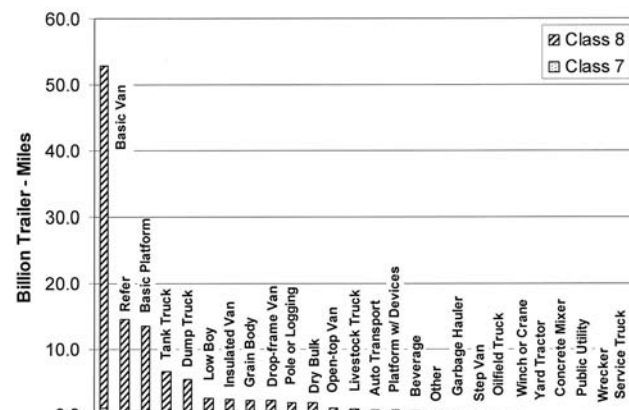


Figure 4. Miles traveled by trailers of each type.

Body-Type-Specific Components. Since four types of bodies predominate in numbers and miles

traveled, we expect that some of their components will be among the largest contributors to pound-miles and fuel consumption. Among those components are the sides of van body trucks and trailers, with typical trailer side weights of 2000–3000 lb per set; the floors of van body vehicles and flatbed vehicles, which also weigh about 2000 lb; and parts such as base/side rails, top rails, floor crossmembers, rear frames, main beams, dump bodies, and liquid haul tanks. Data were collected on more than 100 such component types.

Truck Fuel Economy

Various estimates of the fuel economy of heavy vehicles were encountered. To provide a supportable estimate for use in the comparison model, the VIUS database was exercised to provide the reported fuel economy of each 10,000 lb range in Classes 7 and 8. Class 8 fuel economy averages, weighted on miles reported, were calculated at 5.46 mpg, and the average vehicle weight at 64,400 lb. These points were used to calculate indicative fuel consumption by vehicle components of 2.84×10^{-6} gallons per pound-mile.

Pound-Mile Comparison Model

For the purposes of this study, a computational model is needed that includes the effect of component weight plus the number of times a component may be used in the entire fleet of trucks, and the fuel consumption per pound of vehicle. An MS Excel spreadsheet model was constructed including all of these factors. The full model includes consideration of the nine most common body types and all 49 vehicle configurations. To operate the model, the user enters a component name and weight and then decides the applicability of that component to each of the nine body types.

Applicability may be due to fundamental suitability or to an estimate of the portion of the entire fleet that is likely to adopt the component. The user will next enter the quantity of that component that would be used for each of the 49 configurations of truck and tractor trailer. The spreadsheet model then calculates the pound-miles of that component in the entire fleet, plus an estimate of the fuel that would be consumed by weight-limited vehicles over the entire fleet.

Results

This procedure was followed for 74 of the heaviest components investigated. The results are shown in Figure 5 for the components with the greatest pound-mile and fuel consumption estimates. The values for the other 18 components are very small compared with these 56.

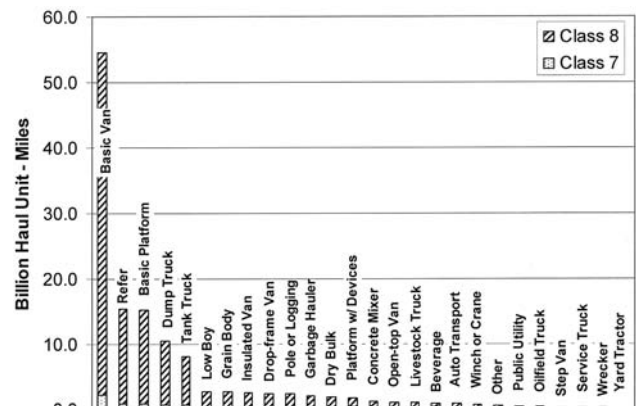


Figure 5. Miles traveled by haul units of each type.

Conclusions

Based on the results of the analysis of heavy vehicle fleet segments, component weights, and the Pound-Mile and Fuel Consumption model, we can provide the following conclusions:

1. Class 8 trucks and tractor-trailers with four body types predominate in number of vehicles, miles traveled, number of trailers, and number of haul units. Weight reduction efforts will have the greatest payoff for vehicles with components common to all types, or to one or more of these four types. The four types are
 - Van bodies (basic enclosed vans, refrigerated vans, insulated vans and drop-frame vans)
 - Platform bodies (basic platforms, platforms with added devices, low boys)
 - Tank bodies (liquid or gas haul tank trucks and trailers)
 - Dump bodies (dump trucks, bottom and rear dump trailers)
2. Several factors act to make some components more likely to be major contributors to total fleet

weight and fuel consumption. They include these:

- All truck and truck-tractor components, and many trailer components, are used by all body types. These include engine, transmission, truck frame, exhaust, axles, suspensions, cabs, drive-lines, wheels, and tires.
 - Since 70% of haul units are trailers, several other components are used by nearly all vehicles, including fifth wheels, couplers, landing gear, suspension sliders, and bumpers.
 - Some components, such as floors, side rails, and main and cross beams, are used by several of the predominant body types.
 - Some components, such as tires, wheels, axles, brakes, support cross members, and suspensions, are used multiple times per vehicle.
3. The pound-miles and fuel consumption contributions of a wide variety of components were determined so that they might be ranked in order of priority for lightweighting effort. The most significant contributors to pound-miles and fuel consumption include engines, tires and wheels, van sides, van and flatbed floors, suspensions, axles, brake drums, all frame members, cabs, couplers and fifth wheels, transmissions, and tanks. Some other component types are also significant contributors.
 4. Efforts to reduce the weight of engine blocks and heads, for example, the use of aluminum or titanium, would likely produce the greatest pay-off. Application of aluminum to additional components and titanium, magnesium, and composites to many components would result in of many trillions of pound-miles of lightweighting and millions of gallons of fuel savings.

L. Truck-to-Auto Technology Transfer for Lightweight Materials

Principal Investigator: Edward Ungar

Taratec Corporation

1251 Dublin Road, Columbus, OH 43215

614-291-2229; fax 614-291-2867; e-mail: eungar@tarateccorp.com

Technology Development Area Specialist: Sidney Diamond

(202) 586-8032; fax: (202) 586-1600; e-mail: sid.diamond@ee.doe.gov

Field Technical Manager: Philip S. Sklad

(865) 574-5069; fax: (865) 576-4963; e-mail: skladps@ornl.gov

Participants

Paula Dunnigan, Taratec Corporation

Mike Carter, Taratec Corporation

Subcontractor: Taratec Corporation

Subcontract No.: 4000033939 under Contract No. DE-AC05-OR22725

Objectives

- Determine the degree to which DOE technology development for heavy trucks is transferred through the supplier base to the automotive industry.
- Determine if this process is applicable to the lightweight materials programs being funded by DOE.

Approach

- Identify suppliers in the DOE lightweight materials program who serve both truck and auto industries.
- Identify individuals at the decision-making level.
- Develop an interview script.
- Conduct five supplier interviews.
- Conduct five interviews with truck and auto original equipment manufacturers (OEMs) and industry groups.
- Summarize findings.

Accomplishments

- Conducted interviews with materials decision-makers in the truck and auto industries to solicit their opinions on the potential for transfer of lightweight materials technologies between trucks and automobiles.

Introduction

Interviews were conducted with key materials decision-makers from the auto and truck industries. The purpose of these interviews was to better understand the potential for the transfer of lightweight

materials technology from the truck to the auto industry.

Comments from the interviewees indicated that some technology transfer between the truck and auto industries will occur spontaneously, but it will be limited. Regarding lightweight materials, there is the potential for significant truck-to-auto technology

transfer with external stimulation of the process. Technologies that require significant change in legacy materials, processing, or auto assembly will require considerably longer for transfer than drop-in materials substitutions.

The following findings represent the input provided by the interviewees.

Key Findings

The technology transfer process is controlled by the advanced engineering groups at the truck and auto OEMs and by the first tier suppliers who serve both industries.

Incentives for technology transfer for both the truck and auto industries stem from improvements in buyer economics or manufacturer's costs. Transfer is hindered by the fact that the truck and auto industries have different production volumes, part sizes, buyer payback calculations, and long-term materials data requirements.

Interviewees cited examples of technology transfer that has occurred previously in both directions. They feel that future technology transfer between the truck and auto industry is possible. Truck-to-automotive technology transfer is likely to involve advanced materials for weight reduction, non-reinforced dicyclopentadiene for body panels and bumpers, adaptive cruise control, and electromagnetic retarder brake systems.

For drop-in materials substitutions, it may take 2–4 years for a product to be commercialized on the second vehicle platform. If the technology requires a change to current forming, joining, or finishing processes, commercialization may require up to 10 years.

The interviewees thought that DOE could catalyze technology transfer between the truck and auto industries by providing leadership, networking opportunities for gatekeepers, and project funding to support data collection for both industries.

Interviewees thought DOE could play a key role in stimulating technology transfer to the auto industry. It would be important to involve the automotive gatekeepers in DOE's lightweight materials truck projects. Projects should be structured to develop economic justification for both truck and auto applications. Long-term performance data should be generated to meet the concerns of both industries. A venue that provides neutral ground where auto and truck gatekeepers can routinely exchange information about new technologies would provide additional stimulus for the technology transfer process.

Conclusions

DOE actions that were seen as particularly helpful in catalyzing technology transfer include these:

- Support of dual-use (truck and auto) programs and forums on neutral ground
- Development of economic justifications for both truck and auto applications
- Investment in the demonstration of technologies at first tier suppliers serving both industries
- Involvement of both truck and auto OEMs in those programs
- Generation of long-term performance data under conditions appropriate for both trucks and autos
- Involvement of industry crossover organizations, such as the U.S. Council for Automotive Research

DOE staff have been briefed on these results and are considering how DOE might best facilitate technology transfer of lightweight materials between the truck and auto industries.

5. LIGHTWEIGHT VEHICLE STRUCTURES

A. Lightweight Stainless Steel Bus Frame—Phase III

Principal Investigator: J. Bruce Emmons

Autokinetics Inc.

1711 West Hamlin Road, Rochester Hills, MI 48309

(248) 852-4450; fax: (248) 852-7182; e-mail: jbemmons@autokinetics.com

Technology Development Area Specialist: Sidney Diamond

(202) 586-8032; fax: (202) 586-1600; e-mail: sid.diamond@ee.doe.gov

Field Technical Manager: Phillip S. Sklad

(865) 574-5069; fax: (865) 576-4963; e-mail: skladps@ornl.gov

Contractor: Autokinetics Inc.

Contract No.: 4000010114

Objectives

- Investigate and demonstrate the mass savings potential of ultra-high-strength stainless steel as applied to the structure and chassis of a full-size urban transit bus.
- Finalize design and analysis and build a full-scale prototype of the body structure and chassis.
- Investigate all of the fundamental feasibility issues related to the structure and chassis:
 1. Fabricate and test large lightweight stainless steel sandwich panels
 2. Fabricate roll-formed, high-strength stainless steel sections
 3. Test the feasibility of lightweight stainless steel cantilever seats
 4. Design and fabricate lightweight stainless steel independent suspension
 5. Integrate the traction motors into the suspension design

Approach

- Execute the basic body structure, including the floor and roof sandwich panels, pillar assemblies, longitudinal rails, and suspension subframes.
- Choose prototyping techniques that emulate the intended production process as closely as possible to aid in developing robust but cost-effective manufacturing techniques essential to meeting the objectives of the project.
- As computer-based design and analysis details of the bus develop, conduct hands-on physical experimentation in parallel to support the concepts and methods.

Accomplishments

- Completed building a specialized resistance welder for joining sandwich panel segments.
- Assembled the floor structure, including all floor sandwich panel segments and subframe subassemblies.
- Assembled the roof structure, including all roof sandwich panel segments.
- Produced a report documenting design enhancements for manufacturability.
- Produced and documented fixture strategy for main assembly.

- Completed assembly of primary structure.
- Fabricated and assembled window and doorframe components.
- Fabricated and assembled front and rear body end sheet metal components.
- Created computer-aided design (CAD) model for seat design.
- Conducted finite element analysis (FEA) for seat design.
- Produced a report documenting side impact analysis results.
- Performed a physical test of crash energy absorber tubes.
- Received delivery of traction motors, inverters, and inverter software (propulsion components)
- Modified design of suspension geometry for compatibility with new motor.
- Modified design of suspension components for compatibility with new motor.
- Provided support for independent cost analysis.

Future Direction

- Assemble closeout panels.
- Complete the fabrication and installation of suspension, steering, and spring components.
- Fabricate driver controls.
- Prototype two seats.
- Assemble propulsion components.
- Testing of structure.

Introduction

Advanced-technology transit bus concepts have made significant advancements in terms of low weight and fuel economy. However, these gains have come at the expense of higher manufacturing costs. In spite of attempts to use life-cycle costs to justify their purchase, initial cost remains a major obstacle to the introduction of fuel-efficient buses.

Autokinetics was approached by DOE for help with solving this problem. Specifically, Autokinetics was asked to develop concepts for a lightweight urban transit bus based on the use of high-strength stainless steel. In the passenger car field, Autokinetics had developed structural and manufacturing techniques for the cost-effective use of stainless steel in spaceframes and suspensions. DOE wanted to determine whether this approach could be applied to transit buses as well.

The program was structured in three phases:

- Phase I—Initial Concept Development
- Phase II—Concept Verification and Initial Design
- Phase III—Final Design and Prototyping of Body and Chassis

Phase I and Phase II have been successfully completed. Phase III will result in a full-size body structure and suspension that will be tested statically and dynamically. The development of an optimized hybrid powertrain and other vehicle systems will be addressed in a separate project.

This project was unusual in that no formal mass or cost targets were given. The object was to save as much mass and cost as possible.

Specialized Segment Welder

Preliminary welding tests indicate that the panel segments can be successfully joined together using

resistance welding. This approach utilizes a joint configuration that reduces complexity and the need for extremely tight tolerances. To create a prototype, spot welds need to be placed along the nearly 8-ft seam between panel segments.

To accomplish this, a special spot-weld gun was required that could reach at least halfway across the floor and roof. The design of this welder was reported on previously. A special support and backup structure were fabricated and fitted with conventional transformer gun components. This arrangement is shown in Figure 1.

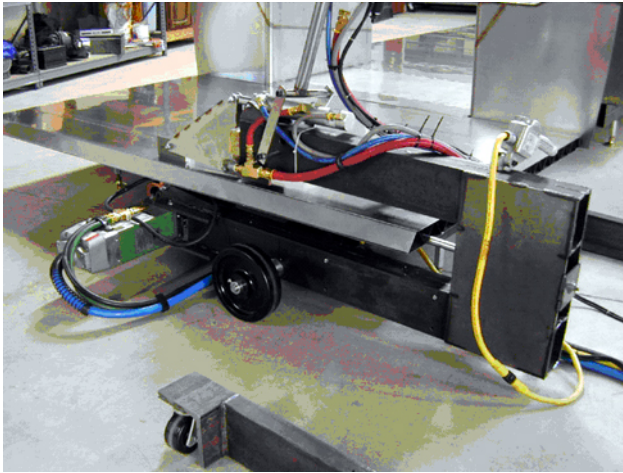


Figure 1. Specialized segment welder.

Special contact tips were also designed and fabricated to accommodate the slightly different configuration of the joint between the subframe and floor panel. As the joining of the panel segments progressed, the contact tips and the welding techniques were refined.

Floor, Roof and Primary Assembly

A major milestone was achieved as the primary body structure was assembled during this reporting period.

The primary structure framing sequence shown in Figure 2 consists of three main elements. First, the floor panel components, including subframes, are located on the framing platform and joined together forming a completed floor assembly.

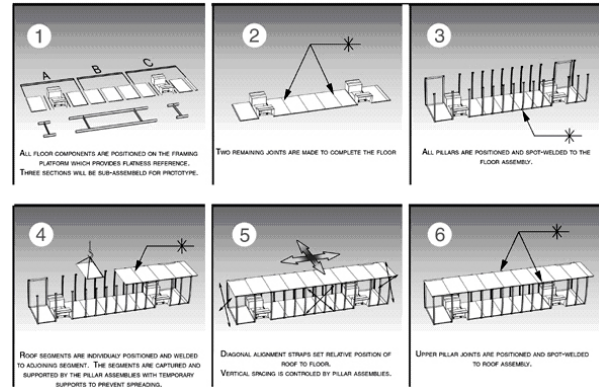


Figure 2. Primary structure framing sequence.

Next all side pillars and door frames are positioned and attached to the floor assembly. Positioning is controlled vertically by the floor, laterally by a taut wire running along the side, and longitudinally by a measured distance. The use of a simple temporary support aid maintains the pillar in a plumb orientation.

Finally, the roof segments are hoisted into position and brought to rest on the pillar brackets. At this point, all roof segments are joined, forming a completed roof assembly. The pillars are then attached to the roof in a similar manner as with the floor.

It was determined that a number of variations on this theme were possible. One such variation, to pre-assemble roof segments into three sub-assemblies, was used for the purposes of this prototype build. This reduced the amount of hoisting and overhead welding. Another was installing the door frames after the roof assembly was complete.

Relative position between roof and floor assemblies was monitored throughout this sequence and found to be virtually self-locating. Figure 3 is a photograph of the completed primary structure.



Figure 3. Primary structure.

Front and Rear End Sheet Metal

During this reporting, the sheet metal components, which close out the front and rear ends of the body, were fabricated and installed onto the primary structure. These components were fabricated to incorporate some design refinements for improved NVH (noise, vibration, and harshness) characteristics. For example, the lower edge of the rear window and front windshield apertures were reinforced, and the sheet gage of the seat pan, compartment bulkheads, and fascia was increased from .030 to .050 in. In Autokinetics' judgment, improved NVH qualities gained by these refinements more than offset the slight weight increase.

For prototype purposes, the large sheet components were fabricated in halves and joined along the vehicle centerline. This would not be necessary in series production.

Figures 4 and 5 are photographs of the completed body end sheet metal.



Figure 4. Rear end sheet metal.



Figure 5. Front end sheet metal.

Seat Design

Beginning with the initial passenger seat concept, a detailed design sufficient for prototyping was created. As shown in Figure 6, the design is a cantilevered type, which attaches by special brackets to two adjacent body pillars. On the seat side, each bracket is attached to a lateral beam. The arrangement is such that the brackets are rigid, movement-carrying connections. Therefore, vertical seat loads are transmitted into the pillar as bending loads.

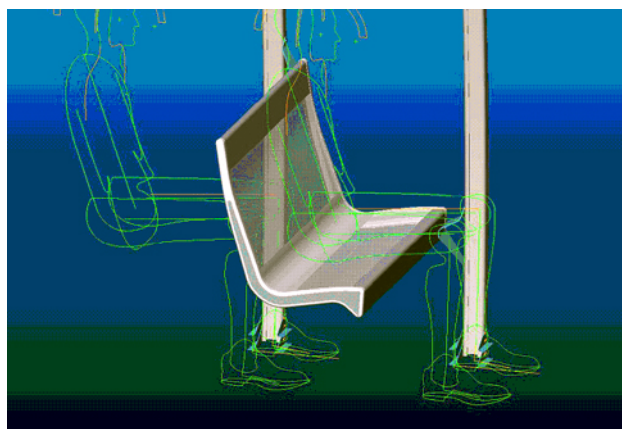


Figure 6. Front end sheet metal.

Completing the design are two L-shaped end caps connecting the lateral beams, and perforated sheet forming the seating surface. A reinforcement pan is attached between the end caps to control local flexing of the seating surface. The entire seat structure will be fabricated in stainless steel and is expected to be lightweight and durable and exhibit very little deflection under normal load.

An FEA model was constructed to verify load capacity and predict deflections. A proof load of 1500 lb was applied to represent a 3-g loading condition with two 250-lb passengers on the seat. The plot shown in Figure 7 indicates the material will remain below yield, while deflection (including pillar deflection) will be on the order of 1.75 in., measured vertically at the most inboard edge of the seat.

Crash Energy Management System

The crash energy management system, based on the principle of inverting stainless steel tubes to absorb crash energy, was described previously. During this reporting period, physical energy-absorbing (EA) tubes were produced and tested.

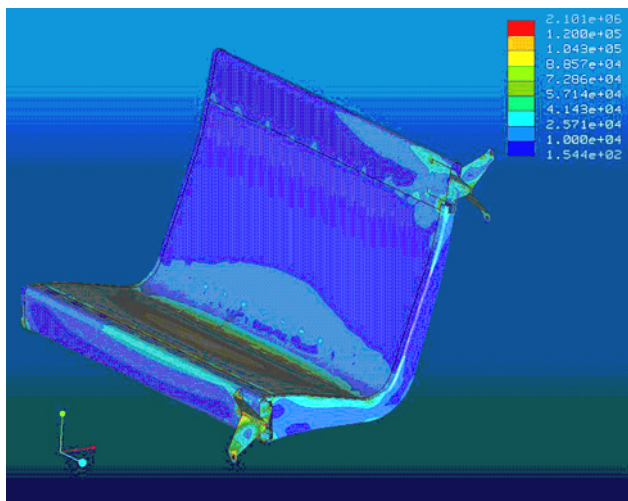


Figure 7. FEA model of passenger seat design.

Autokinetics has specially constructed a machine that applies a force axially to a given tube and measures that force in real time as the tube is worked into an inverted state. Several such EA tube tests were performed on the physical specimens and data were collected.

The tube inversion process inherently results in a very uniform, constant force. The level of this force can be set during design by adjusting certain parameters such as the diameter and wall thickness of the tube. A force level of about 12,000 lb per tube (there are 12 tubes in the front-end system) was chosen as the most appropriate for protecting the occupants of both the bus and the impacted vehicle.

The crash energy management system is well suited for a front-end and rear-end crash event. However, of particular concern for a “low-floor” bus is the side impact crash event. The cause for concern is the fact that bumper of the impacting vehicle will strike the bus several inches above the floor. As a result, the pillars must engage the impacting vehicle and carry the load into the floor without excessive intrusion (3 in. is allowed).

To address this concern, a linear FEA model (shown in Figure 8) was constructed to roughly predict load capacity and deflection. It was determined that reinforcement of the lower inside portion of the pillar would be required to manage the load satisfactorily. In addition, a bumper engagement rail was added along the exterior to ensure a distribution of the load application. With these modifications, model data were prepared and sent to Oak Ridge National Laboratory (ORNL) for a more refined nonlinear analysis capable of predicting deflection

beyond the elastic range of the structure. The ORNL analysis, while promising, indicates that more spot welds will be required to prevent detachment of the pillar reinforcement. Other detail design changes may also be required to fully meet the requirement. Additional funding will be required for ORNL to complete this additional analysis.

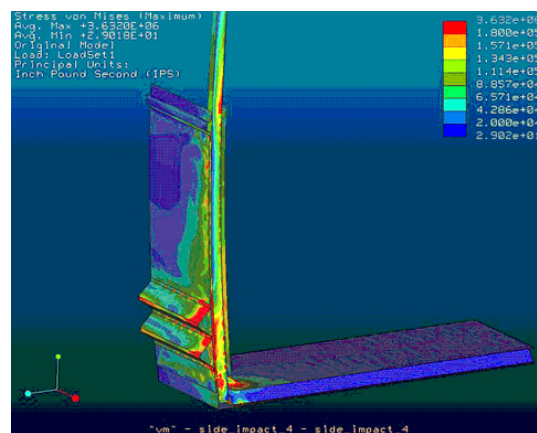


Figure 8. FEA model for side impact study.

Suspension /Driveline (New Motor)

With the vehicle body structure nearing completion, a greater emphasis has shifted to the suspension and driveline.

As reported previously, traction motors and controllers were ordered from PreMag; however, Pre-Mag experienced difficulty in molding the stators and was unable to deliver the motors in a timely manner. Therefore, the decision was made to implement a contingency plan to pursue an alternate motor supplier.

Discussions were initiated with UQM. A motor currently being produced by UQM, the PowerPhase75, was identified as an appropriate selection. Recently developed technology allowing the power of the motor to be upgraded contributed to this decision. The first prototype bus will use the current PowerPhase75, with the intent to use the upgraded version in future buses.

Because the PowerPhase75 is physically different in size and shape from the PreMag motor, a study was conducted to identify any packaging issues. A number of “short-coupled” and hub-mounted concepts were explored. It was found that with some modification to the suspension design, the motors could be hub-mounted. This avoids consid-

erable complexity associated with the short-coupled or right angle drive approach.

Given this information, Autokinetics selected the UQM PowerPhase75 and the hub-mounted configuration as the mainstream approach. Motors and controllers were ordered from UQM and delivered during this reporting period.

The rear suspension design was adjusted to accommodate the increased length of the UQM motor. This required modifications to the upper and lower control arm as well as the knuckle designs. The modified rear suspension corner is shown with the new motor in Figure 9.

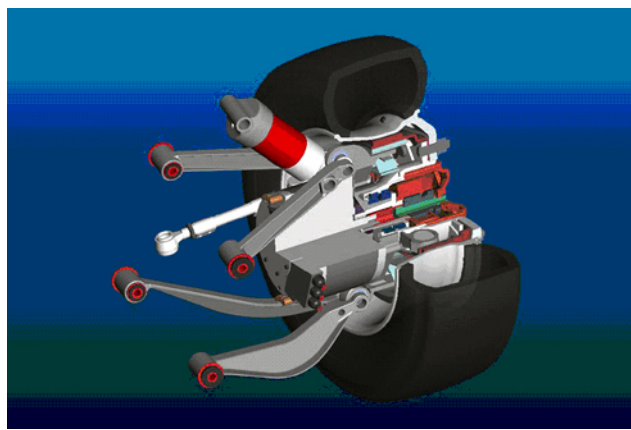


Figure 9. Rear suspension with UQM motor.

Dissemination and Commercialization

10/21/03—Meeting with Advanced Transportation Technology Institute (ATTI). Attended by Phil Sklad, Dick Ziegler, Richard Smith, (ORNL) and John Powell (ATTI).

11/18/03—Emmons attended DOE workshop “Tooling Technology – Low Volume Vehicle Production.”

12/05/03—Presentation to DOE: Entrepreneur John Friedl’s business plan to manufacture commercial vehicles using Autokinetics’ structure technology.

3/10/04—Meeting with Transportation Design and Manufacturing Co. A discussion of hybrid systems integration was attended by Doug Mann and Greg Vanover.

3/04/04—Meeting with Ricardo, Inc. Louis Infante (V.P., vehicle engineering) attended an introduction to the technology. Infante reviewed structural issues with a current project and expressed interest in the technology.

3/19/04—Meeting with Ricardo. Follow-up meeting attended by Mick Winship and Abhay Bhivare.

4/13/04—UQM press release announced UQM’s participation in the project. This statement was subsequently posted on the FreedomCAR website at http://www.eere.energy.gov/vehiclesandfuels/news/fcvt_news_042004.shtml

5/06/04—Meeting with IBIS Associates to initiate information gathering for its cost analysis. Attended by Tony Mascrin (IBIS) and Phil Sklad (ORNL).

6/10/04—Commercialization discussion (under non-disclosure agreement).

6/15/04—Commercialization discussion (under non-disclosure agreement).

6/18/04—Emmons presented a project review at ORNL for Dr. Sidney Diamond (DOE).

9/28/04—Commercialization discussion (under non-disclosure agreement).

Conclusions

Autokinetics remains confident that high-strength stainless steel has the potential to achieve significant mass reductions of bus structures. The bus body structure is now nearly complete; most of the identified technical risk issues have been resolved, and only moderate mass gain has occurred compared with early predictions. Ongoing fabrication of the physical prototype has provided concrete mass numbers, and we now expect the actual mass reduction for the complete vehicle to be close to 50%.

It is also hoped that practical commercialization can be achieved in the not-too-distant future. Low capital investment and an ample knowledge base are key enablers for commercialization. Much has been learned thus far about processing and assembling the body structure, and many useful techniques have been developed. Given the relative ease of constructing this prototype within our own facility, it is quite apparent that capital requirements for commercializing this technology will be relatively small. It is anticipated this will be illustrated by the independent cost analysis commissioned by DOE.

B. Stainless Steel Bus Structure—Manufacturing Cost Analysis

Principal Investigator: Anthony E. Mascarin

IBIS Associates, Inc.

1601 Trapelo Road, Suite 164

Waltham, MA 01720

(781) 290-040; fax: (781) 290-0454; e-mail: tony@ibisassociates.com

Technology Development Area Specialist: Sidney Diamond

(202) 586-8032; fax: (202) 586-1600; e-mail: sid.diamond@ee.doe.gov

Field Technical Manager: Philip S. Sklad

(865) 574-5069; fax: (865) 576-4963; e-mail: skladps@ornl.gov

Contractor: IBIS Associates, Inc.

Contract No.: 4000030946

Objectives

- Provide the bus development program with manufacturing cost analysis and economic understanding to plan a technology and application development strategy.
- Assess the cost of conventional bus structure fabrication.
- Assess the cost of the proposed stainless steel structure.
- Explore the impact of key design and process assumptions.
- Characterize the potential commercial value of the concept.

Approach

- Collect data for scenario and process definition.
- Assemble defining part and process data
- Develop simulation model structure
- Conduct baseline and scenario analyses and comparisons

Accomplishments

- Collected data on conventional bus manufacturing and visited production facilities.
- Completed model development and scenario designs.
- Presented side-by-side cost comparison of stainless steel concept to incumbent practice.
- Analyzed sensitivities to annual production volume, throughput, assembly time, etc.
- Assessed capital requirements, purchase facility investment, and scale-up schedule.

Future Direction

- Modify analyses to account for floor, skin, and roof. These are integral to the stainless steel bus concept but not part of the conventional bus structure. Including them will further improve the side-by-side economics

- Assess the impact of powertrain and interior systems.
 - Analyze life-cycle and usage costs in terms of fuel, operation, and maintenance costs.
-

Introduction

DOE, in conjunction with Autokinetics, is pursuing a design and process technology development program for alternative metropolitan bus structure manufacturing. Central to the effort is the stainless steel roll-formed design concepts developed by Autokinetics. Key to the success of this program is a demonstration of commercial viability: reduced piece cost, lower capital investment, or improved lifecycle economics relative to incumbent practices. Based on process and design scenario information provided to IBIS from the DOE/Autokinetics team, IBIS has evaluated the alternative design concepts for these structures and provided an analysis of manufacturing economics. This analysis seeks to quantify the commercial production economics of the design and production techniques developed by Autokinetics relative to incumbent practices for conventional bus manufacturing.

Bus Structure Scenarios

The basis for comparison of the conventional bus structure to the stainless steel concept is a 40-ft, low-floor metropolitan transit bus.

In summary, the stainless steel concept involves a floor and roof composed of three-layer panels made from welded outer skins and a corrugated, roll-formed core. Roll-formed pillars, rails, and sills complete the skeletal structure. Wheel wells and front and rear cap assemblies are welded from brake or press formings. The structure is assembled using spot welding.

Conventional manufacturing involves labor-intensive arc welding of tube stock. Sides, floors, roofs, and front and rear end units are made separately in subassembly cells on semi-dedicated fixtures (which can be modified for bus length). After final structure assembly, the frame is subjected to grit blasting and a zinc phosphate coating.

Model Development

Existing models of automotive body-in-white manufacturing were used as the starting point for the bus structure technical cost model. This format has the capability to efficiently track the high piece count of individual components involved. IBIS collected additional roll-forming process data and specific stainless steel alloy material properties to update earlier information already in possession. The assembly operations, specifically the custom-designed panel fabrication, were defined in terms of commercial production-rate equipment.

Separate model structures were constructed for conventional and roll-formed designs. Conventional manufacturing, relying principally on purchased tube stock, is modeled as a series of assembly cells. It accounts for material cost as the total of purchased components for each subassembly. A roll-formed structure, on the other hand, is modeled on the basis of each roll forming, with a major assembly operation into a unitized structure.

Data Collection

Data used in the technical cost models were collected through interviews and site visits with many sources, principally existing transit bus and motor coach manufacturers. These include New Flyer, Advanced Bus Industries, North American Bus Industries, Gillis, Orion, and Motor Coach Industries. Equipment manufacturers and municipal transit authorities also provided useful information. Autokinetics provided design information for the stainless steel concept.

Analyses

For comparison and simulation manageability, operations for each scenario were grouped as shown in Figures 1 and 2. The resulting cost comparison and sensitivities are shown in Figures 3 and 4.

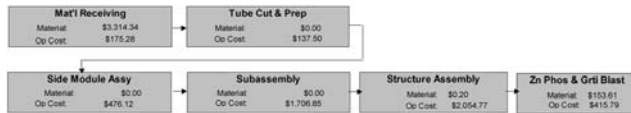


Figure 1. Conventional process flow.

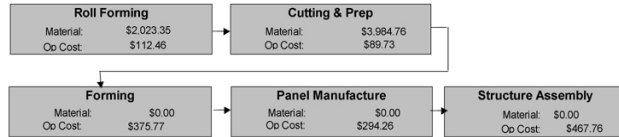


Figure 2. Stainless steel concept flow.

COST SUMMARY BY OPERATION			
	\$/part	\$/part	
	Conventional	Stainless	
Total Material	\$3,468.15	\$6,008.11	Total Material
Mat'l Receiving	\$175.28	\$112.46	Roll Forming
Tube Cut & Prep	\$137.50	\$89.73	Cutting & Prep
Side Module Assy	\$476.12	\$375.77	Forming
Subassembly	\$1,706.85	\$294.26	Panel Manufacture
Structure Assembly	\$2,054.77	\$467.76	Structure Assembly
Zn Phos & Grit Blast	\$415.79		
TOTAL MFG COST	\$8,434.47	\$7,348.08	

Figure 3. Cost comparison table.

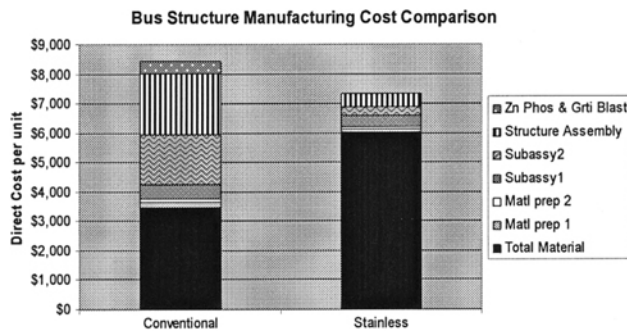


Figure 4. Cost comparison chart.

Conclusions

In addition to the weight savings gained from the stainless steel design (current numbers show approximately 1000 lb, not including additional savings of hundreds of pounds of flooring, skins, and roof already integral to the structure), the manufacturing economics of the stainless steel design are compelling. The combination of the novel design approach, using roll forming and high-rate spot welding (instead of arc welding), allows for a reduction in assembly labor and fixturing to offset the much greater material price of stainless steel relative to the steel tube stock.

As the program moves into the next phase of demonstrating a working powertrain, the extended benefits of the lightweight structure on reduced power requirements and secondary mass savings can be explored. The economic analysis can also be employed to demonstrate to potential manufacturers the specific capital requirements needed for commercializing the proposed concept.

C. Side Impact Analysis of a Lightweight Stainless Steel Bus Structure

Principal Investigator: Srdjan Simunovic

Oak Ridge National Laboratory

P.O. Box 2008, MS-6164

(865) 241-3863; fax: (865) 574-7463; e-mail: simunovics@ornl.gov

Technology Development Area Specialist: Sidney Diamond

(202) 586-8032; fax: (202) 586-1600; e-mail: sid.diamond@ee.doe.gov

Field Technical Manager: Philip S. Sklad

(865) 574-5069; fax: (865) 576-4963; e-mail: skladps@ornl.gov

Contractor: Oak Ridge National Laboratory

Contract No.: DE-AC05-00OR22725

Objective

- Model and assess the structural performance of a lightweight stainless steel bus structure (LSSBS) during a side impact by a sport utility vehicle (SUV).

Approach

- Conduct the impact analysis simulation using finite element method (FEM) computer analysis.
- Develop a detailed model of a central five-column-long section of the LSSBS to model the area of collision, with two semi-rigid components on each end of the deformable section representing the remainder of the bus.
- Simulate a side impact collision scenario using LS-DYNA on supercomputers at the Oak Ridge National Laboratory Center for Computational Sciences.

Accomplishments

- Developed the detailed model of the center section of the LSSBS, including key structural features of the bus relevant to the side impact. The simulations showed overall satisfactory structural response.

Future Direction

- Use the results of the study to modify the bus design to reduce the damage and intrusion resulting from the collision and analyze the design modifications using the same approach.

Introduction

The ultralight stainless steel urban bus concept was developed by Autokinetics, Inc.¹ with the objective of demonstrating the feasibility of a stainless steel structural design for weight reduction in mass-transit vehicles. The resulting bus employs high-strength stainless steels and monocoque design to simultaneously achieve the weight reduction and maintain or surpass the performance of conventional

bus designs. The bus body structure is shown in Figure 1.

Bus performance with respect to torsional and flexural rigidities and axial impact has been investigated using computational models. However, side-impact response has not been fully addressed yet; it is the subject of this research. A collision scenario that is considered to be a good measure of the side-impact performance of the bus is an impact of a mid-size SUV-class vehicle into the half span of

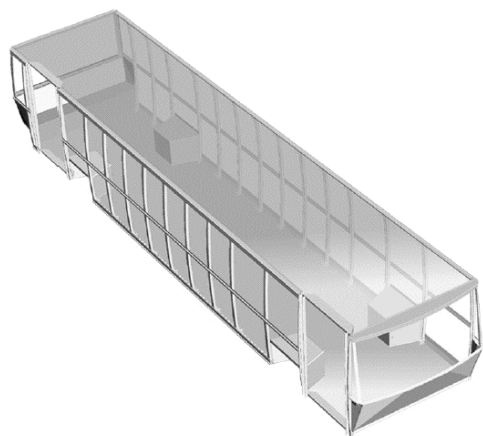


Figure 1. Ultralight stainless steel bus structure.

the bus. SUVs usually have a high ground clearance, and an SUV chassis may not coincide in height with the bus floor. In the case of the current design, it would obviously be desirable to transfer the impact loads into the rigid floor as efficiently as possible without allowing for a significant intrusion into the bus passenger space. The other essential structural component that comes directly into contact with the impacting vehicle is the lower reinforcement rail. This rail is supposed to distribute the impact force between the neighboring pillars. The bus floor and, to a lesser extent, the roof are the final destinations of the SUV impact load. In order to achieve a controlled load transfer into the floor and roof, it is necessary to maintain reasonable stability of the pillars and the reinforcement rail. Joints connecting pillars into the floor/roof must distribute the load very quickly without creating local instabilities or joint failure. Figure 2 shows the pillar joint with the roof.

Location, geometry, and bonding of the joint brackets are important for local load transfer; therefore, it is necessary to model them in sufficient detail to determine the local stability of the connection. Detailed computational models have been developed to adequately address these issues and provide a basis for further performance investigations that require high-resolution, nonlinear FEM analysis.

Development of the FEM Model

The finite element model of the bus structure involves several steps. The basic geometry of the

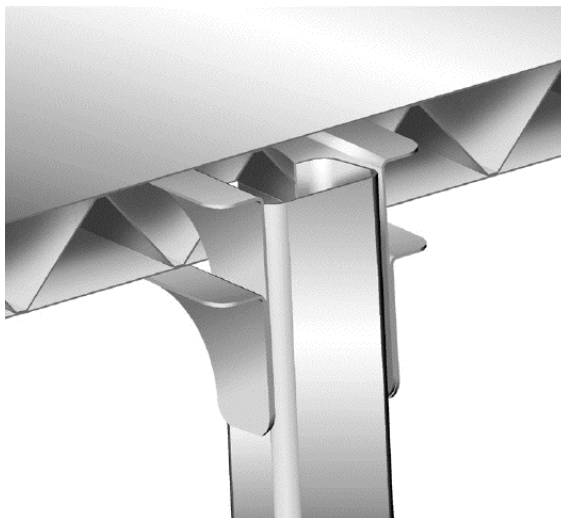


Figure 2. Pillar joint detail.

bus was provided by Autokinetics in the IGES format. The geometry data are used to generate surfaces that are used as projection targets for the FEM mesh generation. The data were provided for a single typical section ('segment') of the structure; Figure 3 shows the segment model. Repeated reflections and translations are used for the generation of the model used in the analysis.

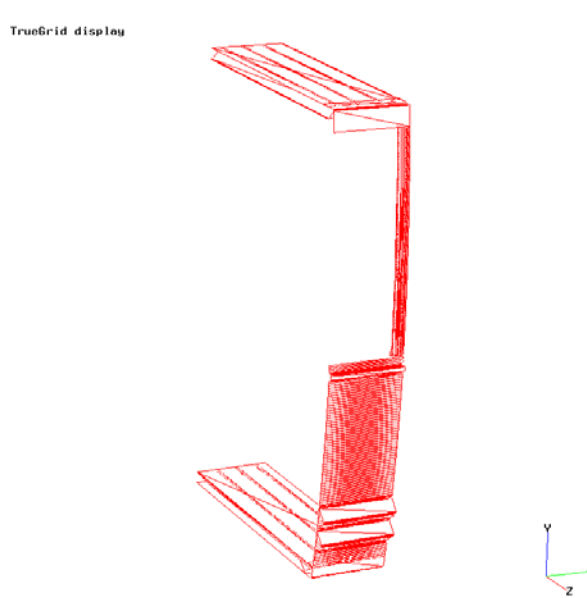


Figure 3. ViewPoint surfaces of bus 'segment' model.

The integrity of the body structure is provided almost exclusively by spot welds. Therefore, in order to create a realistic model for side impact it was essential to include them in the model. The

location of the spot welds was provided in IGES format. A graphical representation of this data is shown in Figure 4.

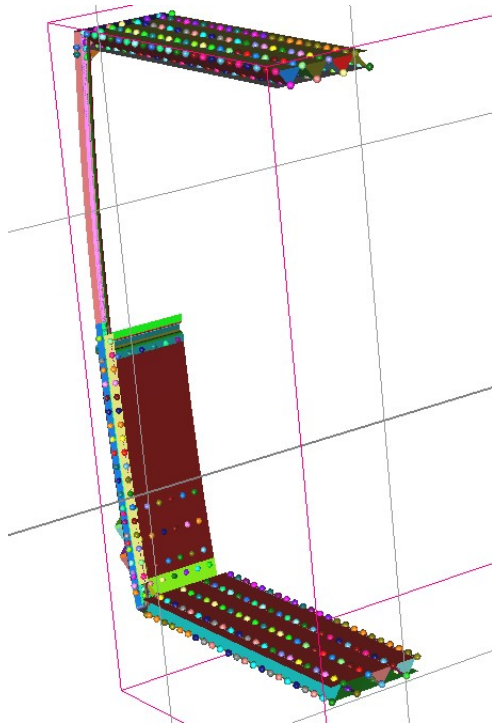


Figure 4. Spot welds in the bus segment.

The FEM model was developed using the spot weld locations as key locations for the mesh generation so that the locations of the spot welds exactly match the locations specified in the IGES geometry. The developed FEM model for the ten base segments, where spot weld locations are denoted by black dots, is shown in Figure 5.

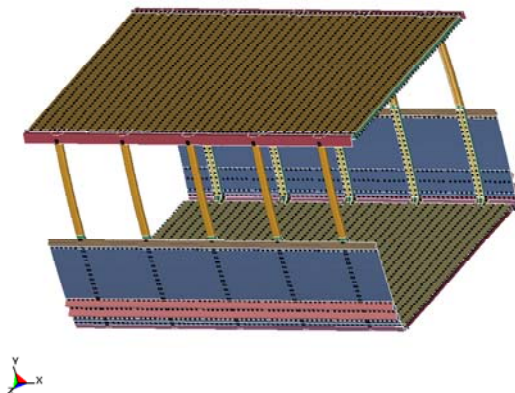


Figure 5. FEM model; black dots denote locations of spot welds.

FEM Simulations of Side Impact

The FEM model of the bus consists of a representative section and approximations of the front and rear of the bus. The approximate parts are modeled as stiff, elastic materials that approximate the areas of the bus that are not going to deform in the impact and provide vertical support relative to the ground of the bus assembly. Ideally, the actual bus geometry could have been modeled, but it was not available at the time of model creation.

Figure 6 shows the entire analysis model of the bus used in the analysis. This model has 287680 nodal points, 280148 shell elements, and 34567 beam elements.

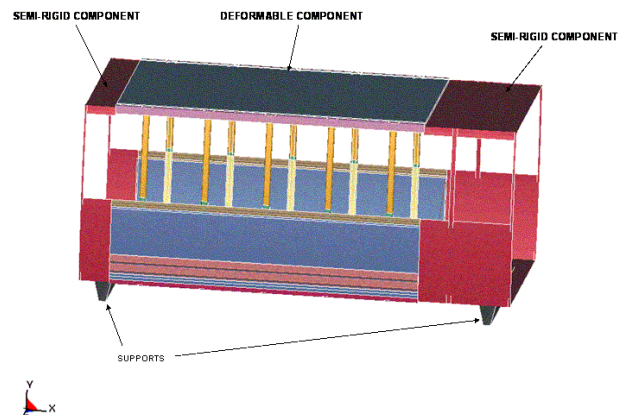


Figure 6. Finite element model of the LSSBS concept.

The FEM model used in the study of the side impact analysis includes a 'bullet' vehicle. For this analysis, the bullet vehicle is an 1998 Explorer SUV.² The representation of the merged bus-Explorer model is shown in Figure 7. Two cases have been considered for the impact analysis: the first one considers the case when the center (across the width) of the SUV engages the bus at a pillar location, and the second case considers the case when the center of the SUV engages the bus at the midpoint between pillars. Figure 7 shows the model of the first case.

The combined model has 427675 nodal points, 281102 hexahedral elements, 414942 shell elements, 280677 beam elements, and 8653 spot welds.

The analysis considers the impact of the SUV traveling at 25 mph at the time of engagement with

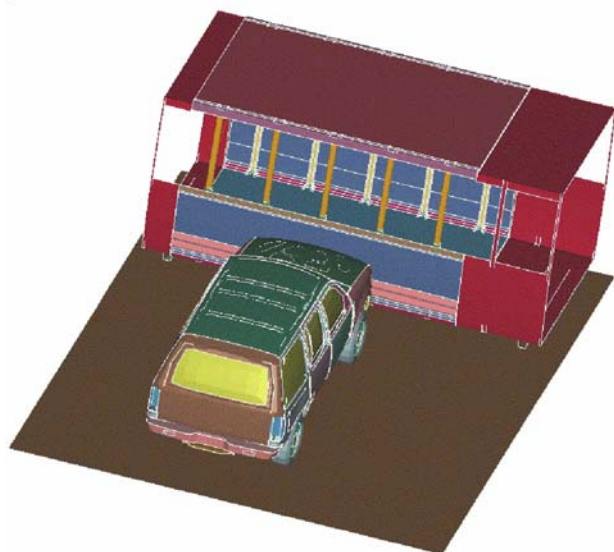


Figure 7. Finite element model for the SUV-LSSBS impact at column.

the stationary bus. The analysis has been performed using the computer program LS-DYNA.³

The following paragraphs discuss the results of the analysis performed to assess the bus integrity when the SUV traveling at 25 mph impacts the bus so that the center of the SUV is between the two bus pillars.

The configuration of the model at a time when the elastic deformation of the bus reaches a condition of quasi-steady state is shown in Figure 8. At this point in the analysis, the SUV-LSSBS assembly moves as a rigid body, and very little relative deformation is imposed upon the bus structure beyond the end time of the analysis.

The intrusion into the bus body, defined as the reduction in width between the outward pillar and the corresponding pillar near the point of impact, was calculated. Two locations along the height of the pillar were chosen for the determination of this parameter: at the vertical level that corresponds to the bumper height of the bullet vehicle, and at the sill level of the bus window opening. Figure 9 shows the time history of these intrusion measurements. The top curve corresponds to the bumper height location; the lower curve corresponds to the sill location. Final intrusion values are 195 mm and 145 mm at the bumper height and sill level locations, respectively.

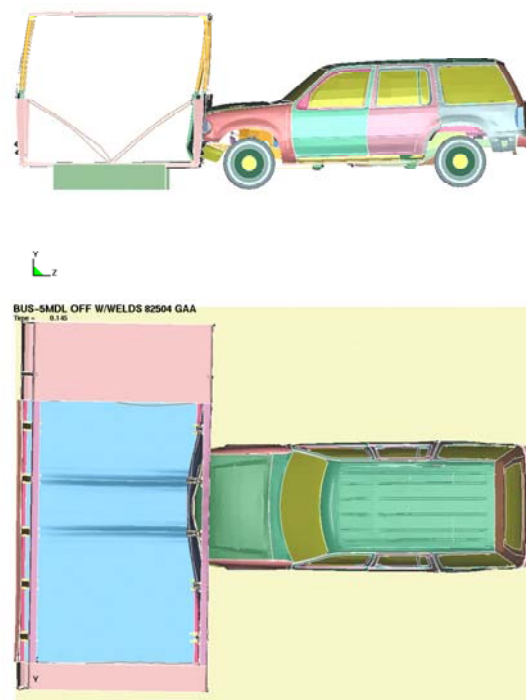


Figure 8. Side view (top) and top view with roof panels removed (bottom) of model configuration at end of simulation.

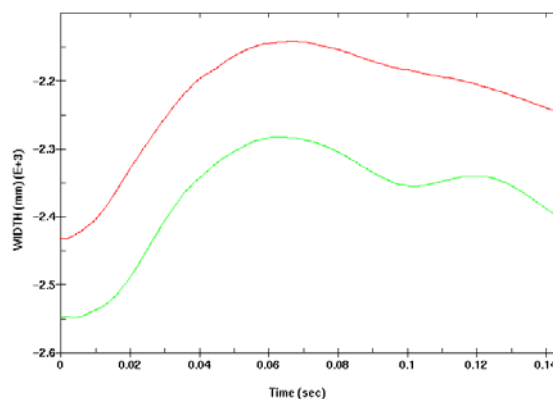


Figure 9. Width measured between columns at center column line.

The integrity of the bus structure can be evaluated in terms of the ability of the brackets to maintain the connection between the floor assembly and the lower pillar sections. Failure of the spot welds at the bracket interface between the floor plates and the lower section of the pillar compromises the integrity of the structure, as most of the stiffness of the assembly depends on the

integrity of the side components. The analysis shows that the lower row of spot welds can fail in the vertical leg of the top brackets that connect to the pillar. The analysis also shows that the connection between the horizontal legs of the bracket that connects to the top floor plate undergoes relatively large deformation. This is attributed to the topology of the spot welds at this interface; only the inner part of the horizontal part of the bracket is attached to the floor plate. The result is a cantilever mode of deformation for the bracket. Potential improvement in the performance of the structure could be achieved if additional reinforcement were provided between the horizontal section of the lower bracket and the floor rail and between the horizontal section of the top bracket and the roof rail. Another possible design modification is reinforcement of the pillar. The corresponding design modifications will be addressed in the continuation of the study.

Conclusions

We have developed an FEM model for the structural analysis of a side impact against a LSSBS.

Results of the study point to areas that may warrant some design modifications in order to reduce the damage and the intrusion of the SUV into the LSSBS. The model can be further refined to allow for more accurate simulation and flexibility for modeling of different loading situations.

References

1. J. B. Emmons, and L. J. Blessing, "Ultralight Stainless Steel Urban Bus Concept," SAE Technical Paper 2001-01-2073, Government/Industry Meeting, Washington, D.C., 2001.
2. G. Aramayo, "Parametric Finite Element Model of a Sport Utility Vehicle: Development and Validation, in *Proceedings of the 7th International LS-DYNA Users Conference*, Dearborn, MI, 2002.
3. J. O. Hallquist, *DYNA-Keyword User's Manual*, Version 970, LSTC, April 2003.

D. New-Generation Frame for Pickup/Sport Utility Vehicle Application

Principal Investigator: Curt A. Lavender

Pacific Northwest National Laboratory

P.O. Box 999, M/S K2-03, Richland, WA 99352

(509) 372-6770; fax: (509) 375-4448; e-mail: curt.lavender@pnl.gov

Kurt M. Knop

DaimlerChrysler Corporation

14250 Plymouth Road

Detroit, MI 48227

(313) 659-6076; fax: (313) 635-5221; e-mail: kmk4@daimlerchrysler.com

Technology Development Area Specialist: Sidney Diamond

(202) 586-8032; fax: (202) 586-1600; e-mail: sid.diamond@ee.doe.gov

Field Technical Manager: Philip S. Sklad

(865) 574-5069; fax: (865) 576-4963; e-mail: skladps@ornl.gov

Contractor: Pacific Northwest National Laboratory

Contract No. DE-AC06-76RLO 1830

Objective

- Evaluate the design of an optimized hybrid materials frame that represents a new generation of pickup/sport utility vehicle (PU/SUV) frame applications and vehicle architecture.

Approach

- Apply high-risk manufacturing and design methods to the PU/SUV frame to reduce mass while meeting cost goals consistent with a high-production vehicle.

Accomplishments

- Established performance, packaging, and weight targets for the second iteration of the new-generation frame, “the next-generation frame” (NGF).
- Created a design for the NGF that projects a greater weight reduction and a decrease in the number of parts compared with the current steel baseline frame.
- Created a computer-aided engineering (CAE) model of the NGF to evaluate impact; noise, vibration, and harshness (NVH); and durability.
- Completed CAE and design iterations to meet impact, NVH, and durability requirements.
- Successfully demonstrated the “5-star” crash rating.
- Established a preliminary cost estimate for frame production and prototyping.
- Established initial cost estimates for the frame that are 12% higher than the current frame with a 200-lb weight savings. The initial cost projections are favorable and are being evaluated in more detail.

Future Direction

- Construct the full NGF frame and perform vehicle testing to validate the CAE-designed NGF.
 - Complete prototype frame component design and procure parts for DCX assembly.
 - Validate the CAE analysis by DCX in a full-frame test to be determined by identifying needs from CAE testing.
-

Introduction

Increased consumer demand for PUs/SUVs has resulted in increased fleet fuel consumption, and the trend toward consumer demand for PUs/SUVs has been predicted to increase. By 2005 the fuel demand for this class of vehicle will exceed that for passenger automobiles.^{1,2} The objective of this project is to explore manufacturing methods and materials to reduce the mass of the SUV/PU frame, thereby reducing fuel consumption for this class of vehicle.

During the second quarter of FY 2003, DaimlerChrysler completed vehicle testing at the DCX Proving Grounds using an SUV/PU platform equipped with a hybrid frame. Results of the accelerated testing have proved that (1) the hybrid frame design had sufficient strength and durability to meet the vehicle performance requirements, and (2) the frame was probably somewhat overbuilt and heavier than required, even with a substantial weight savings over the current baseline steel frame.

The next phase of the project will evaluate the use of a lighter frame, the NGF (Figure 1). The NGF uses a CAE approach and higher-risk manufacturing technologies. The projected weight for the NGF is less than that for the previously tested new-generation frame, and it requires 35% fewer components.

Approach

A CAE model of the NGF was created and design iterations were performed to meet the NVH, impact, and durability requirements for a DCX 5-star rating. A prototype of the frame will be fabricated and evaluated by frame flexure and road tests.

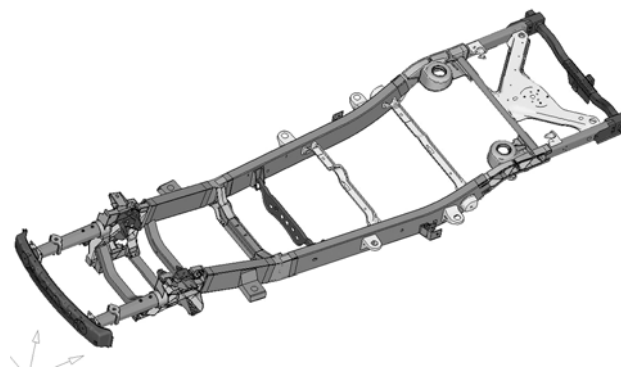


Figure 1. Next-generation frame design.

Progress

CAE analyses of the frame are completed and have satisfied all requirements for impact, NVH, and durability analyses. Owing to the large section height of the aluminum extrusions, intrusion into the passenger compartment during impact analysis proved to be the most challenging problem.

Complete CAE impact analyses (like those shown in Figure 2) have been reiterated upon and reduced the intrusion into an acceptable range. A full 5-star rating has been attained with only minor frame modifications. Intrusion into the vehicle is measured in terms of the maximum displacement of the vehicle into the passenger compartment. The 5-star rating is achieved when all intrusion values are below a “good” rating as determined by DCX safety review. Reiteration on the original NGF design has resulted in all values below the “good” rating, as shown in Figure 3.

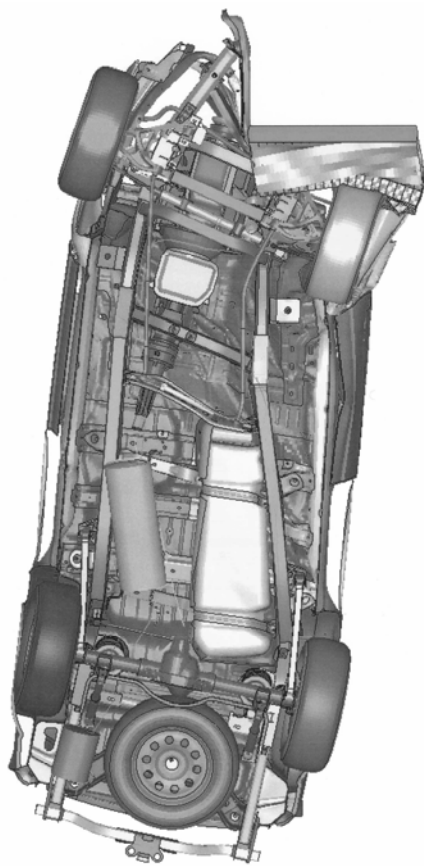


Figure 2. Frontal impact analysis of the NGF.

The aluminum frame complicates the design for intrusion because of the increased section size. The aluminum extrusions are 5 cm taller than the steel frame sections. In order to have an equivalent intrusion, the NGF must be designed not to deflect as much as the steel version. The actual magnitude of deflection at each passenger compartment location, shown in Figure 3, indicates that the additional 5 cm of frame height reduces the allowable deflection of the frame by approximately 30% in locations where a total intrusion of 15 cm is allowed.

The design of the frame has been completed, and a bill of materials (BOM) has been created and used for prototype and future production cost quota

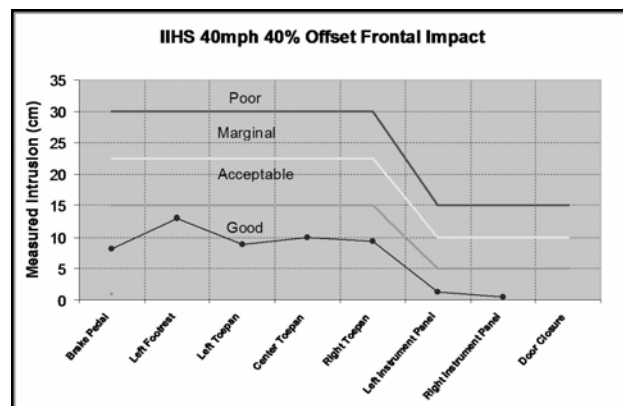


Figure 3. Intrusion measurements for 40% offset frontal impact for the NGF.

tions. Initial cost analysis shows that a 200-lb savings can be achieved with a 12% cost penalty. Additional analyses of cost and re-design for production will be performed.

Future Direction

The CAE/design for the NGF is complete, a BOM has been created, and a suitable frame that shows a weight savings of 200 lb has been proposed. The next step in the frame project will be validation of the CAE results through full-scale vehicle testing and frame flexure tests. A prototype frame will be fabricated, and flexure will be tested by twisting. After flexure testing, the full-scale frame will be assembled into a DCX vehicle platform and evaluated on the test track for durability and driver-felt comfort and performance.

References

1. *EIA Annual Energy Outlook 2002*, DOE/EIA-0383 (2000), Energy Information Administration, December 2001.
2. *Transportation Energy Data Book: Edition 21*, ORNL-6970, Oak Ridge National Laboratory, September 2001.

E. Lightweight Trailer—Liburndas Project

Principal Investigator/Team Leader: Travis McCloud

Heil Trailer International

1125 Congress Parkway, Athens, TN 37303-0160

(423) 745-5830; fax:(423) 745-1943; e-mail:tmcloud@heiltrailer.com

Co-Team Leader/Marketing Liaison: Bill Harris

Heil Trailer International

5741 Cornelison Rd, 6400 Bldg A, Chattanooga, TN 37411

(423) 855-3492; fax:(423) 855-3459 ; e-mail:bharris@heiltrailer.com

Technology Development Manager: Sidney Diamond

(202) 586-8032; fax: (202) 586-1600; e-mail: sid.diamond@ee.doe.gov

Field Technical Manager: Philip S. Sklad

(865) 574-5069; fax: (865) 576-4963; e-mail: skladps@ornl.gov

Contractor: Heil Trailer International

Contract No.: 4000027094

Objective

- Reduce the net weight of an aluminum tank semi-trailer by 20% by using a cylindrical design and assimilating available composite technology for functional components.

Approach

- Develop a new frameless vessel design incorporating a new cross-section, flangeless heads, and internal rings.
- Optimize design through finite element analysis (FEA) and testing.
- Explore existing composite accessories.
- Conduct a focus group and a marketing study, including a campaign for the new design.
- Complete a manufacturing study, including a labor rate analysis.
- Manufacture and test prototype.

Accomplishments

- Completed vessel and bogie (run gear suspension frame) design.
- Completed FEA of vessel and bogie.
- Completed evaluation of friction stir welding samples.
- Completed initial testing of flangeless, dishless head design.
- Defined and approved loading head parameters.
- Completed focus group.
- Started marketing and manufacturing study.

Future Direction

- Complete fifth-wheel design and FEA.
- Complete accessory design and FEA.
- Validate possible composite accessories.
- Complete manufacturing study and marketing report.
- Manufacture prototype and conduct track test.
- Conduct marketing and sales campaign.

Introduction

The Liburndas Project is Heil Trailer International's effort to design and build an aluminum semi-trailer for petroleum products that is lighter, stronger, and safer than any before it. By using a cylindrical cross section and assimilating composites into select trailer components, Heil's Research and Development (R&D) Group proposes to reduce the aluminum tank semi-trailer's net weight by 20 %.

Just changing the geometry of the vessel by re-designing it to a cylindrical shape will allow a reduction in shell thickness and elimination of historical strengthening structures that have plagued equipment with parasitic mass. This new design will also lower the center of gravity (CG) by 25–30%, which enhances the safety of the trailer with respect to roll-over potential (see Figure 1).

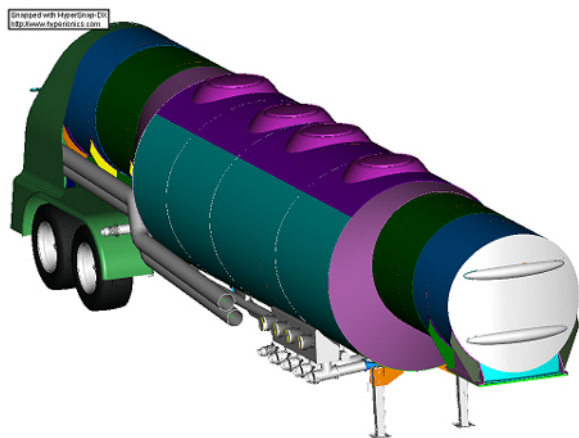


Figure 1. New concept petroleum trailer.

Investigating a new aluminum alloy for weight reduction in areas not regulated by the U.S. Department of Transportation (DOT) is an objective of the project as well. Areas such as the frame rails for the

suspension and fifth-wheel plate are valid candidates. Although some weight savings is possible, this is secondary to the contributions the new cylindrical design and composite accessories will make to Heil's overall weight reduction goals.

Accessories made from composites are critical to meeting weight reduction goals and will ultimately reduce the mass of the trailer and improve corrosion resistance. This project's purpose is not to create or test a new composite for these areas. Existing composites will be explored that have proved successful in the market. Areas that are likely candidates for composites are fenders, cabinets, hose holders, ladders, and suspension support structures.

Although a successful vessel design and notable composite integration will result in reaching weight reduction goals, it is paramount to the project's success that the market accept the new design. Because of the competitive nature of the market, data will be collected covertly, without divulging the new trailer's design or benefit. Therefore, the marketing study initially will determine acceptable envelopes for piping and discharge outlets, as well as conduct a preliminary commercial viability study based on the design's limits and/or restraints. A marketing campaign to bolster product acceptance will take place near the end of the project. The initial marketing study began during Phase 1 of the project and should be completed before the first prototype is built. The marketing campaign will take place during Phase 3 (after the successful field testing of the second prototype) and should result in orders for production models.

A successful product resulting from this project would allow carriers to safely deliver 2000–2500 lb more payload per trip, ultimately reducing the daily average number of miles required to deliver product

by about 1%. On a national level (the current population of petroleum tank trailers is approximately 50,000 units), this could equate to over 200,000 miles per year saved, or 30,000 gallons of fuel per year.

Vessel Design

Cross Section

An important part of Heil's new design concept for its petroleum trailer is the cross section of the vessel. In today's petroleum trailers, the most common cross section used is an elliptical shape, used to lower the overall height and center of gravity of the trailer. Since petroleum trailers are not unloaded or loaded with pressure, the elliptical shape works well.

When the structure of a petroleum trailer's vessel is studied, it is simply analyzed as a supported beam with reactions at the suspension and kingpin plate. This condition places the bottom of the trailer vessel in tension and the top in compression. The advantage of a round cross section under these loads is that the radius of the top is tighter or smaller and therefore more resistant to buckling under the compression loads. This allows the shell thickness of the vessel to be thinned, compared with an elliptical cross section, and thus saves weight and material.

Even though petroleum trailers are not pressurized, they do occasionally see some low vacuum or pressure differentials during loading and unloading. Today's trailers are equipped with vents to prevent damage to the vessel if this condition becomes excessive. In the event of a vent failure, a round vessel is more likely to survive a pressure or vacuum overload, whereas an elliptical vessel will tend to fail.

A round vessel is therefore stronger, lighter, safer, and more stable than an elliptical vessel for an equivalent cross sectional area. The only advantage of an elliptical trailer is its overall lower height and center of gravity. Designing a round vessel with a drop center can offset this advantage (Figure 2).

Drop Center Design

Dropping the center of the vessel in relation to the front and rear not only lowers the center of gravity but also causes the lateral center of mass to stay near the longitudinal center of the trailer, as shown in Figure 3.

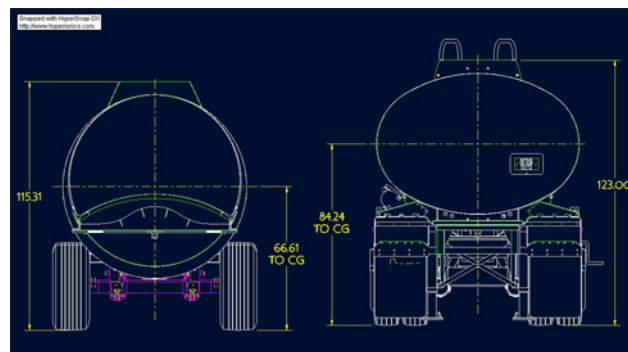


Figure 2. Height and center of gravity comparison.

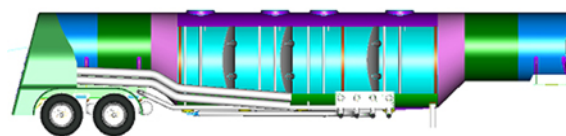


Figure 3. Drop center design.

Federal weight laws call for manufacturers to design trailers with equal loads on the tractor's drive axles and the trailer's suspension. By designing a lower front *and* rear end section of the vessel, we can engineer the trailer so that the mass is equally distributed over the rear of the trailer (bogie) and the tractor's rear axles.

Elimination of Surge Heads

Petroleum tank trailers are designed to DOT 406 specifications as found in the Code of Federal Regulations Title 49. Section 178.345-7 of this code discusses circumferential reinforcements in trailers and mandates that the maximum unreinforced portion of the vessel's shell not exceed 60 in. Traditionally, this has been accomplished in petroleum trailers through the use of surge heads or baffles. These surge baffles are the same heads that separate the trailer's compartments, but they have holes formed in them to allow product to flow through them. These surge baffles help with the surge of the product during acceleration and deceleration and serve as the circumferential reinforcements.

Replacing these surge baffles with an adequately designed internal ring can achieve a considerable weight savings. However, rings will not help with product surge, and drivers will have to be trained to handle the "feel" of the tank in certain road condi-

tions. The market's opinion (business owners and drivers) on internal rings and their advantages and disadvantages will be one of the topics for the focus group and marketing study.

Liquid trailers without surge baffles are not uncommon in the chemical and food industry, where the cleanability of the inside of the trailer is important. Drivers in these industries have learned to drive safely without baffles; therefore, it is anticipated that the weight benefits will outweigh the surge issue. It should also be noted that there is no product surge when a trailer is completely full or empty.

Flangeless, Dishless Heads

A new concept with regard to the vessel design is being applied to the Liburndas Project. This is a redesign of the compartment heads that separate different commodities in a petroleum trailer. These heads are typically dished and flanged bulkheads that are connected to the shell via a single fillet weld. The Liburndas vessel will use a flangeless, dishless head, which will be connected to the shell via two fillet welds. A Pro-E model of the head is depicted in Figure 4.



Figure 4. Flangeless head concept.

The Liburndas vessel is a perfect application for the flangeless head—it is lighter, the welds are stronger, the strength is comparable, and the manufacturability is more precise than for the current style head. The flangeless head is much easier to manufacture and should offset part of the cost of the composites. One of the goals of marketing goals is to ensure that the R&D group's new design—lighter, stronger, and more stable—does not cost more than the market will bear for those benefits. This offset strategy should keep the price of the new design within acceptable limits for the market.

Heil has been working on forming techniques for this new head with the Alcoa Technical Center and has already conducted preliminary testing of a “simulated” prototype head at its Athens, Tennessee, R&D facility. The prototype head can be seen in Figure 5. Initial testing was promising, and advanced prototypes are planned for continued testing.



Figure 5. Flangeless head test vessel.

Framing

The final design and FEA of the bogie frame has been successfully completed. It eliminated some framing requirements (and weight) for both bogie and vessel structure mounting compared with current framing designs. The Liburndas bogie design can be seen in Figure 6 below.

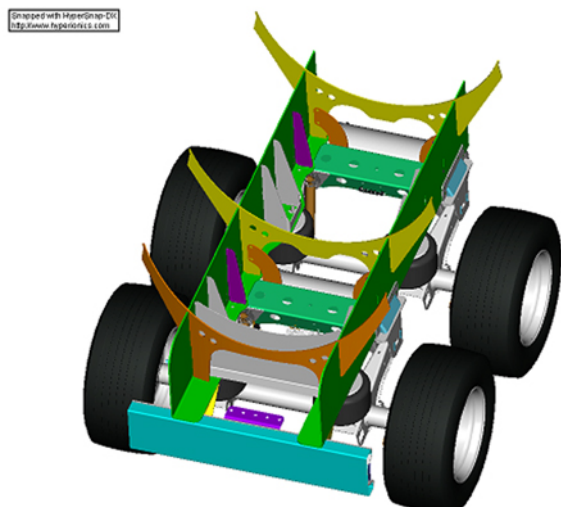


Figure 6. Liburndas bogie frame.

The bogie frame is one of the most critical design areas for a petroleum trailer. The vessel experiences not only loads from the force of gravity acting on the payload but also loads due to articulation or twisting as it maneuvers over the road around corners. Consequently, a leak due to weld fatigue would most likely occur in this area. To simulate road conditions, FEA on the frame was completed for four load cases: (1) 2-G downward, vertical inertial; (2) 2-G forward, horizontal inertial; (3) 1-G lateral, horizontal inertial (10-ton axle load traveling around curves); and (4) 1-G lateral horizontal inertial load (turning on the spot).

The initial analysis indicated that the mild steel crossmember structure gave cause for concern with unacceptable stress levels under the load cases specified. However, the initial FEA model did not take into account the link of the top crossmember to the frame or the correct welding techniques. After further review and FEA remodeling, the bogie frame design actually experienced acceptable stress levels. To confirm our results, the bogie frame design was also tested by Hendrickson, the air ride suspension manufacturer. Hendrickson conducted similar FEA modeling and confirmed our final test results.

Overturn Rails/Vapor Manifold

Finally, the vessel design will eliminate the need for overturn rails on the top of the trailer. The overturn rails act as guards to prevent a manhole from opening during a rollover situation. The flashing rails also act as a manifold for vapor collection and

recovery during the loading and unloading of a trailer. A significant amount of weight can be saved by the successful elimination of the rails. It can be done with the installation of recessed manholes, which are widely used in Europe (see Figure 7).

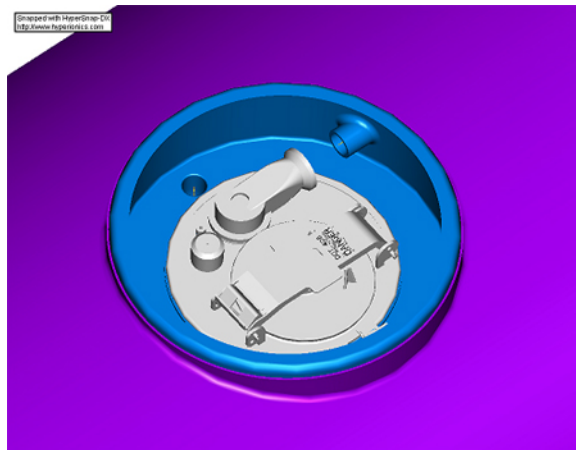


Figure 7. Recessed manhole.

Vapor collection and recovery will be completed using internal vapor lines that drop down through each compartment from the manholes. Lines will be manifolded outside and under the vessel. This configuration has been successfully designed and tested by Heil in Europe. Its application to the Liburndas vessel will save approximately 400 lb, the weight of both flashing rails.

Vessel Weight Reduction

To date, the total weight reduction goals are as follows: from the shell, 15%; from the heads, 20%; by eliminating the overturn/flashing rails, 20%. The remaining 45% will come from the framing and accessories design.

Friction Stir Welding

During the project, Heil is also working closely with Oak Ridge National Laboratory to determine the feasibility of applying friction stir welding (FSW) to the manufacturing process for the Liburndas vessel. The most likely area will be the large, flat aluminum sheets that make up the barrel proper (currently done on a plasma table). FSW samples have been collected, along with both gas tungsten arc and gas metal arc samples, and bend and tensile testing will begin this phase.

Marketing

Focus Group

Heil invited five customers representing a cross section of the industry (major oil companies, jobbers and common carriers) to participate in a focus group this past October. The customers in attendance were positive and encouraged by the information presented. They ranked their needs and wants as follows: first, the capability to haul more payload; second, better operational efficiency; finally, a design as safe as, if not safer than, than current trailers.

As anticipated, an increase in payload capability was the customer's number one requirement for the new design. If afforded the capability to haul more product, they can increase revenue on a per-load basis and reduce maintenance and operational expenses over the life of the trailer.

Although recessed manholes were not seen as an advantage to the customer, they would be "tolerated" if they created the weight savings advertised. Concerns exist over weather caps, internal drains, and internal vapor piping that would exist with the manholes.

The customer's operational and safety requirements may drive a redesign of the accessory location and possibly the vessel diameter. Currently, the Liburndas cabinet and accessories are located at the rear of the trailer, which would be unacceptable to the operators. It was determined during the focus group that the operators' perceptions of the new design will have an important bearing on the success of the Liburndas trailer in the market.

The low belly height was actually a concern because of the potential for side collisions, which was perceived to outweigh the advantages of a lower center of gravity. The trailer may perform better in a rollover situation, but it may be more susceptible to loss of load in a side impact collision. The customers in the focus group recommended we limit the

amount of drop to 50% of the planned design and move the accessories to the side of the vessel. This would make the trailer operationally acceptable and still improve on the safety of the existing trailer in the market.

The project leader is considering reducing the major diameter and increasing the minor end tube diameters to maintain capacity and provide more room for accessories on the side of the trailer, the typical location for accessories in today's trailers.

Conclusions

Excellent progress has been made on the vessel and bogie design and FEA during the first year of the project. Design and FEA of the fifth-wheel plate are now on schedule and should be completed by the end of the month. All Phase 1 deliverables should be completed by the end of the year, according to the project schedule.

Continued study and testing will take place on the flangeless head design. Once a die is acquired and actual test heads are constructed, mock-up prototype testing will be completed. It is anticipated that the flangeless head design will be very successful, which will accelerate the project into Phase 3—field testing of a prototype.

The marketing research completed to date reflects initial acceptance of the new design, with the exception of the existing accessory locations. Redesign of the accessories will take place quickly over the next month. Market acceptance of the cylindrical design, flangeless heads, and internal rings will make the Liburndas trailer a viable alternative to and inevitable replacement for the elliptical trailer. Once it is in the market, the popularity of the trailer is expected to increase exponentially because of its improved fuel delivery capabilities and roll stability.

6. APPLICATION OF INNOVATIVE MATERIALS

A. Advanced Materials for Friction Brakes

Principal Investigator: P. J. Blau

Oak Ridge National Laboratory

P.O. Box 2008, Oak Ridge, TN 37831-6063

(865) 574-5377; fax: (865) 574-6918; e-mail: blaupj@ornl.gov

Technology Development Area Specialist: Sidney Diamond

(202) 586-8032; fax: (202) 586-1600; e-mail: sid.diamond@ee.doe.gov

Field Technical Manager: Philip S. Sklad

(865) 574-5069; fax: (865) 576-4963; e-mail: skladps@ornl.gov

Contractor: Oak Ridge National Laboratory

Contract No.: DE-AC05-00OR22725

Objectives

- Identify, test, and analyze the friction and wear characteristics of advanced materials and surface treatments that enable weight reduction in truck brake components while equaling or bettering their performance. Materials of interest include intermetallic alloys, ceramic composites, titanium alloys, and novel surface treatments.

Approach

- Design and build a subscale brake material testing apparatus to investigate the friction and frictional heating characteristics of advanced materials at speeds and contact pressures similar to those in full-sized brakes.
- Investigate the nature of changes to the surfaces of materials that occur as a result of frictional contact under high energy input conditions—especially the formation of friction-induced films.
- Evaluate friction and thermal characteristics of candidate lightweight materials for heavy vehicle brakes. These include titanium alloys and ceramic matrix composites.
- Examine the characteristics of brake material wear particles, an environmental consequence of braking.
- Understand and model frictional energy dissipation and apply that knowledge to the evaluation of advanced brake materials.

Accomplishments

- Selected and tested a variety of metals, ceramics, and composite materials with the potential to serve as lightweight brake components. Down-selected two material systems, titanium-based materials and ceramic composite materials, for further study during the coming year.
- Worked with a visiting university faculty member to understand and model frictional heat partition.
- Evaluated the effects of wear testing methodology on the relative wear rankings of a series of commercial brake lining materials. Identified the role of entrapped wear particles in affecting these rankings.
- Compared the frictional characteristics of two titanium-based disc materials with those of two ceramic composite disc materials using several candidate lining materials. Compared results with traditional cast iron combinations.

Future Direction

- Evaluate currently available commercial coatings and explore new coating technologies for use on titanium alloys for lightweight brake rotor materials.
- Understand the role of particle loading on friction performance and thermal transport in candidate titanium-based composites.
- Identify lining materials that are frictionally compatible with advanced disc materials.

Introduction

Advanced aerodynamic designs and tires with lower rolling resistance can improve fuel efficiency of trucks. However, as these approaches decrease the drag forces on trucks, the demands on truck braking systems increase. Brake engineering involves design, instrumentation and controls, and materials development. This project specifically addresses the latter. Brake materials must exhibit a balance of properties, including frictional stability over a wide temperature range, appropriate thermal properties, dimensional stability, corrosion resistance to road deicers, and wear resistance. From a practical standpoint, they must also be cost-competitive. Opportunities exist to employ advanced materials to create lighter-weight braking systems that will enable new technologies to raise the fuel efficiency of a vehicle without compromising its safety and reliability.

This project addresses the science and engineering of advanced structural materials and surface treatments that show potential as truck brake friction materials. Testing of such new materials is made more cost-effective by using small specimens to screen the most promising candidates. To this end, a subscale brake tester (SSBT) was designed and built. It was instrumented to measure normal force, friction force, surface temperature, and vibrations during braking. An attachable water spray system enables study of the effects of wet and dry braking. The SSBT has been a workhorse in recent studies involving a variety of both traditional and nontraditional brake materials. Analysis of SSBT results is supplemented by optical microscopy, electron microscopy, and transmission electron microscopy of friction-induced films.

eliminated those with low softening points, brittle behavior, corrosion sensitivity, and environmentally unacceptable wear byproducts. A list of the materials evaluated, along with comments on their advantages and disadvantages, was presented in the FY 2003 Annual Progress Report. Table 1 provides a summary of the materials tested to date. Most of the disc materials, particularly the composites, are not mass produced; therefore, special samples were

Table 1. Candidate friction material combinations

Disc specimen material	Mating material(s)
Traditional gray cast iron	Jurid 539 disc brake lining Performance friction carbon-metallic pad (type 10) Armada AR2, AR4, AR5 drum brake lining materials
SiC particle-reinforced aluminum alloy (Al-MMC)	Specially formulated lining for Al-MMC (Plymouth Prowler)
Fe ₃ Al intermetallic alloy	Jurid 539 disc brake lining
Ceramic composite (C/SiC)—GE Power Systems, LLC	Jurid 539 disc brake lining Same material as the disc
Ceramic composite (SiC/Si)—Redundant Materials	Same material as the disc
Ceramic composite (C/SiC)—Starfire Systems	Carbon felt composite Copper-carbon composite
Titanium alloys (Ti-6Al-4V, and Ti-6Al-2Sn-4Zr-2Mo)—TIMET	Jurid 539 disc brake lining
Titanium matrix composite (TiC)—CermeTi C-10, Dynamet Tech	Performance friction carbon-metallic pad (type 10)
Thermally-sprayed titanium—Red Devil Brakes	Metallic and semimetallic pads materials supplied by Red Devil Brakes

Selection of Candidate Materials

Studies of the structure, composition, and physical properties of candidate materials have

purchased specifically for our tests. The sliding partners (linings) for the disc materials were selected based on factors such as comparison with similar linings tested against cast iron, recommendations from suppliers, and materials having thermo-physical properties that made them likely partners for given disc materials.

After evaluating the materials in Table 1 from an overall performance and cost standpoint, we decided to limit our studies to (1) titanium-based alloys, including composites and coated alloys, and (2) ceramic composites that had shown encouraging results both in our work and in limited vehicle braking tests.

During FY 2004, dozens of experiments were conducted to characterize the effects of speed and contact pressure on the friction coefficient and frictional temperature rise for both titanium-based and ceramic composite disc materials. Results are summarized in the following sections. Polished cross sections of the materials were examined to document their structure, and thermal property measurements were made for use in modeling.

Titanium-Based Disc Materials

Titanium-based materials offer higher temperature resistance and better corrosion resistance than aluminum-based composites, but they are not widely used in brakes. In fact, the current applications for titanium lie mainly in automotive racing (Red Devil Brakes Co., Mt. Pleasant, Pennsylvania). Disc friction surfaces of the titanium alloys are thermal-spray-coated. Such materials were included in our investigation using fully metallic pad materials supplied by Red Devil Brakes.

It was also of interest to determine whether noncoated titanium alloys could be used for brake discs. Therefore, we purchased titanium-based composite material discs from Dynamet (Burlington, Massachusetts) whose CermeTi materials contain hard particles in a titanium alloy matrix.

Figures 1 and 2 summarize friction data on the effects of sliding speed and contact pressure on the friction of titanium-based disc materials against several pad materials. Figures 1 and 2, respectively, show data for 150 N and 300 N applied force. Data for Jurid 539 against gray cast iron (GCI) are also plotted for comparison.

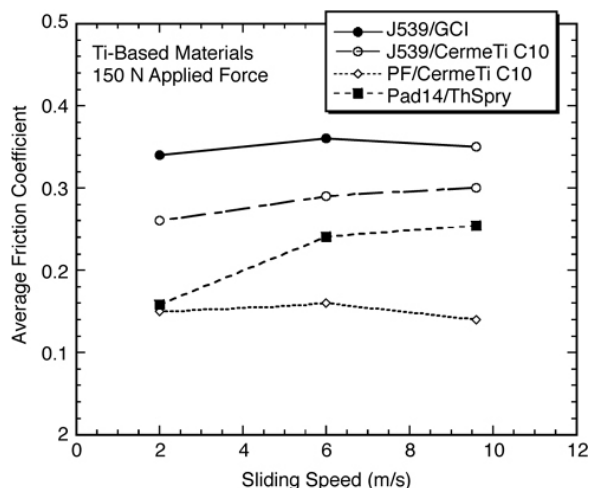


Figure 1. Effect of sliding speed on the friction of several titanium-based disc materials (low applied force).

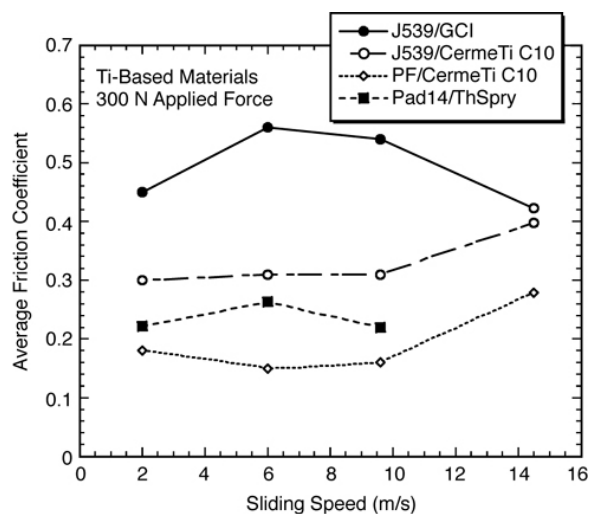


Figure 2. Effect of sliding speed on the friction of several titanium-based disc materials (high applied force).

Friction coefficients for the various combinations spanned a relatively wide range, depending on applied conditions. Other things being equal, the lower the friction coefficient, the more applied force is required to produce the same stopping distance.

At both levels of applied force, the highest friction coefficients were obtained from Jurid 539 sliding on GCI; those for the other material combinations, involving titanium-based discs, tended to be about $\frac{1}{2}$ to $\frac{3}{4}$ as high. However, these results must be viewed with the understanding that our tests do not simulate every aspect of actual truck

braking characteristics. Transfer films seemed to be more difficult to create on the nonferrous materials and took place over a period of time. To precondition the surfaces before taking data, we began with coarsely abraded surfaces and ran a series of conditioning stops. Surface engineering may be required to facilitate transfer film formation, and that subject remains for further investigation.

In general, to obtain the higher levels of friction typical of commercial materials sliding on cast iron, it was necessary that the disc materials be frictionally heated until they became very hot. This temperature characteristic is both an advantage and a disadvantage. The advantage is that titanium-based materials seem less prone to 'fade' (loss of braking at high temperature) and in fact probably behave better at high temperature. The disadvantage is that the titanium brakes tend to run hotter than cast iron brakes, and thermal management would need to be applied in order to use them effectively. Use of vented rotors or other designs to induce forced cooling in the wheel well are other options for addressing that issue.

Ceramic Composite Disc Materials

Ceramic composite materials (CCMs) have been of interest for high-energy braking applications such as high-speed trains, race cars, and high-performance sports cars. Their low density offers the potential for significant weight savings; their high hardness suggests wear resistance; and their high-temperature resistance is attractive. However, the costs and special procedures associated with processing, handling, and finishing CCMs have been significant impediments to their widespread use. CCMs were included in this project to assess any relative performance benefits over titanium materials or conventional materials. Furthermore, there have been limited field trials of lightweight CCM brakes that showed up to 8% fuel economy savings on a GM sports utility vehicle.

Carbon/SiC ceramics were previously tested under a joint project with GE Power Systems. Now we are working with two other CCM suppliers: Starfire Systems (Malta, New York) and Redundant Materials, Inc. (Clarence Center, New York). Test discs were purchased from both of these companies. Previous experience from the GE carbon composites program indicated that good results could be obtained from self-mated sliding

combinations. In addition, two candidate lining materials were provided by Starfire Systems (a carbon-felt composite and a carbon-copper composite). Using the same testing protocols as for the titanium-based materials, a series of friction tests were performed on CCM combinations. Results are summarized in Figures 3 and 4.

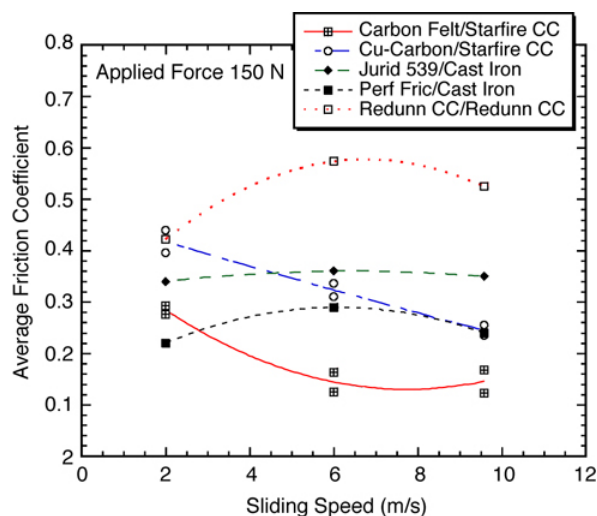


Figure 3. Effect of sliding speed on the friction of various CCM disc/lining material combinations at 150 N force.

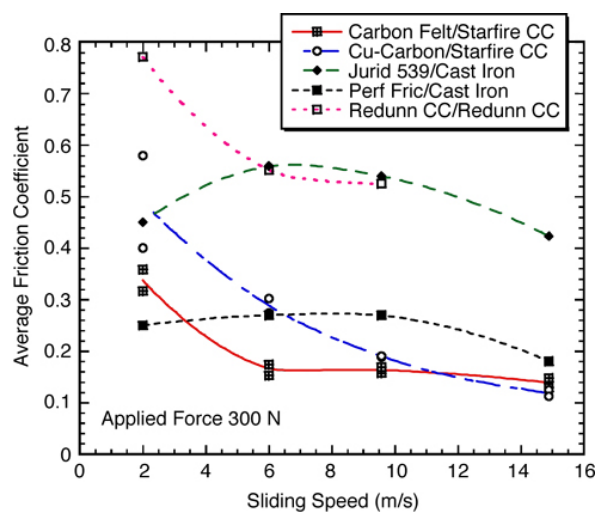


Figure 4. Effect of sliding speed on the friction of various CCM disc/lining material combinations at 300 N force.

Several trends are evident from the data in Figures 3 and 4. The friction coefficients of the CCMs tend to decrease as the sliding speed increases. This is somewhat unexpected, because for

carbon-based brakes, like those used in racing and aircraft brakes, friction tends to increase with severity of use (repeated braking or high-pressure application that increases the brake temperature). Second, the copper-carbon lining material against the Starfire Systems materials produced better results than the carbon felt. Recent discussions with Starfire engineers suggest that further improvements are possible using a new pad formulation against their CCM, and ORNL is in the process of obtaining this material for further testing.

The SiC/silicon material prepared by Redundant Materials had the highest friction coefficients at both low and high pressure, but it suffered from brittleness resulting from the layers of silicon within the composite.

Temperature Modeling

While this report has primarily addressed results from friction measurements, considerable data on temperature rises were also obtained for analysis. One measure of the efficiency by which the energy of braking is converted into heat is the thermal conversion parameter (Q_f) defined here as follows:

$$Q_f = c(\Delta T/Fx)$$

where ΔT is the temperature rise of the disc specimen surface during a constant speed drag, F is the average measured friction force, and x is the distance slid during the drag. The constant c is a function of the testing geometry and the fact that only the heating of the disc is considered, not the heating of the pad as well. Q_f can be thought of as the efficiency of a given rotor material to convert frictional work (Fx) into a certain surface temperature rise (ΔT). The higher Q_f , the more readily the frictional work of braking translates into the heating of the disc surface. Table 2 lists experimentally obtained values for several of the material combinations. For example, for our particular testing configuration, Jurid 539 against CermeTi discs results in $(5.9/1.1 =) 5.36$ times more temperature rise per unit of frictional work than Jurid against GCI.

Table 2. Thermal conversion parameter (Q_f) for various material combinations (300 N test results)

Disc material	Sliding partner	Q_f (°C/N-m)
GCI	Jurid 539	1.1×10^{-3}
GCI	Perf. friction	1.5×10^{-3}
CermeTi C10	Jurid 539	5.9×10^{-3}
CermeTi C10	Perf. friction	6.7×10^{-3}
Red Devil Ti	Pad type 14	15.4×10^{-3}
Starfire CCM	Carbon felt	17.6×10^{-3}
Starfire CCM	Copper carbon	12.4×10^{-3}
Redundant CCM	Redundant CCM	2.70×10^{-3}

During the summer of 2004, ORNL was joined by Timothy Ovaert, University of Notre Dame. He analyzed several current models for heat partition in braking and developed a new model that allows estimation of the partitioning of heat between the slider (pad) and rotor. His model will be used during FY 2005 to help understand the implications of relative heat transfer characteristics when optimizing material combinations for brakes.

Conclusions

Studies have been conducted of a variety of candidate lightweight truck brake materials. Of these, titanium alloys offer a number of attractive characteristics, but their low thermal conductivity and wear behavior must be considered as well. The use of surface coatings or treatments is expected to enable the materials to perform quite well as brakes. Further work in FY 2004 is planned to better understand the friction and wear behavior of titanium alloys and to evaluate several alternative coating methods for rotor surfaces.

Publications

M. Mosleh, P. J. Blau, and D. Dumitrescu, "Characteristics and Morphology of Wear Particles from Laboratory Testing of Disk Brake Materials," *Wear* **256**, 1128–34 (2004).

J. Qu, P. J. Blau, T. R. Watkins, O. B. Cavin, and N. S. Kulkarni, "Friction and Wear of Titanium Alloys Sliding against Metal, Ceramic, and Polymer Counterfaces," *Tribology International*, accepted for publication (2004).

B. Advanced Composite Structural Cab Components

Principal Investigator: Michael A. Wieck

Delphi Automotive Systems

Delphi Steering Division

3900 Holland Road, MDC-2

Saginaw, MI 48601-9494

(989) 757- 4283; fax:(989) 757-4295; e-mail: michael.a.wieck@delphi.com

Technology Development Area Specialist: Sidney Diamond

(202) 586-8032; fax: (202) 586-1600; e-mail: sid.diamond@ee.doe.gov

Field Technical Manager: Philip S. Sklad

(865) 574-5069; fax:(865) 576-4963; e-mail: skladps@ornl.gov

Contractor: Delphi Corporation

Contract No.: 4000009401

Objectives

- Develop an advanced composite cab structural component for a Class 8 tractor:
 - Develop the design, materials, and manufacturing process for using continuous-oriented, fiber-reinforced composites for affordable commercialization within 5 years of beginning the project.
 - Reduce the existing mass by at least 30% from 22.8 to 15.96 kg.
 - Meet or exceed the performance of existing materials.
 - Meet customer target cost.

Approach

- Organize a value analysis/value engineering (VAVE) workshop to generate different options for design and manufacturing.
- Develop finite element analysis (FEA) to develop and optimize design options.
- Perform a process cycle study, make necessary panels, and study Class B surfaces.
- Conduct design failure modes effects and analysis (DFMEA).
- Construct prototype parts and verify the proposed design using a design validation (DV) test.
- Release final designs, construct production tools, perform process failure mode and effects analysis (PFMEA), and undergo process validation (PV) of the production phase.
- Commercialize and start production.

Accomplishments

- During the first half of the fiscal year, completed a proof-of-process study with generic block mold, which demonstrates the feasibility of infusing thin-walled laminates. Then completed a pre-PV study with production foam core and prototype composite mold for areas 3 and 4 of the lower B-pillar.
- Completed DV testing of prototype components in full cab build. (Door slam test had gone through three life cycles and sustained no structural issues) Completed fastener torque studies in molded sample blocks.

- Updated the system DFMEA with suppliers and customer.
- Refined FEA models to include material properties from actual material test data, developed local composite reinforcements to improve stiffness, and studied the effect of processing tolerances for an affordable product.
- Simplified construction in the air duct area by making the air duct a separate, post-mold fastened part.
- Reduced metal usage by eliminating large steel plate and using more localized attachments with composite reinforcements.
- Produced assembly drawings, CAD models, some design details, and specifications for quote packages.
- Selected a production source for final assembly.
- Reduced flange areas to 3 mm in thickness.
- Performed cure-cycle study, made composite panels, conducted Class B surface activities.
- Made plaques and part skins using a conductive gel coat to demonstrate elimination of post-mold spray conductive primer. Validated conductive gel coat to replace post-mold spray primer system (cost savings).
- Finalized metal hardware material specifications.
- Determined optimal machining process parameters (tool shapes, feeds, and speeds for drill/tap of composite laminate over metal hardware).
- Created 2-dimensional (2D) lay-flat fabric patterns from 3D part geometry with slits and darts to minimize fabric shear and to optimize the overall fabric blank size.
- Completed environmental testing.
- Finished final design math model and process.

Future Direction

- Conduct PFMEA with sourced supplier and customer.
- Finalize specifications, assembly, and detail drawings.
- Release final design, release remaining production tools, and validate the production phase.
- Begin production.

Introduction

Significant strides forward were made in FY 2004 on the Advanced Composite Cab Structures project. Within Delphi, the project moved from a development activity to an implementation team; and with the progress outlined in this report, both cost and mass targets were achieved.

To accomplish the project objectives, the Delphi-led team replaced the present production liquid-compression-molded two-component post-bonded assembly made of non-oriented chopped fiberglass with a single resin-transfer-molding (RTM) processed foam core structure enclosed with a thin laminate of oriented and continuous-length fiberglass.

Design and Process Failure Modes and Effects Analysis

A system-based DFMEA was initiated at the Delphi facility in early 2003 and was periodically updated as the production intent design was refined. It included a review at Delphi's original equipment manufacturer (OEM) partner's assembly plant with representation from engineering, quality, and purchasing. Another DFMEA was held in June 2004 with the OEM engineers after the DV tests were completed. The suppliers of individual components and final molder have responsibility for performing PFMEA and creating process control plans after final sourcing. Delphi participates in each FMEA.

Pre-PV Development: Resin Cure Times and Thin-Walled Infused Laminates

To determine the proper tooling and cure cycle, Delphi and Reichhold, a leading resin supplier, conducted multiple cure-cycle studies at Delphi's Composite Lab in Salt Lake City. The goal was to make a resin recipe that would meet a requirement for a 22-min full-cure cycle at 120°F. Initial studies completed in February 2004 indicated that a processing temperature of 120°F for the cure cycle was possible.

One of the major design obstacles of this project was the processing of thin (1.0–1.5 mm) laminates with RTM. Some of the concerns originated around tolerances and geometric stack-ups of all the components within the molded assembly. Secondary concerns included the response of the foam core, tooling, and hardware during infusion. Multiple layers of fabric and reinforcement were located between various foam cores.

To expedite pre-PV development, we selected a small section of the molded assembly, rather than work with the complete assembly. Pre-PV development used results from early proof-of-concept development.

Proof-of-concept development used a rectangular box (4×6×16 in.), a cross section of which is shown in Figure 1. This shape closely represents one of the longest infusion sections of the actual component. The tool was designed to infuse the 16-in. length, with an injection and a vacuum port on opposite ends. The cover of the tool was made of clear glass to allow visual inspection and videotaping of the resin flow front.

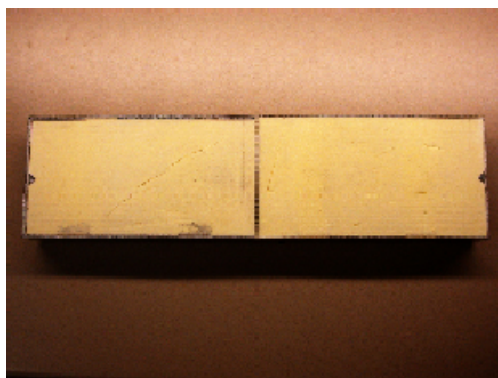


Figure 1. Proof-of-process mold block.

Almost 50 individual infusion runs were conducted with very positive end results. In the course of the proof-of-concept study, it was determined that laminate thicknesses of less than 1.5 mm were achievable. The limiting factors in achieving thin laminates were the tolerances of the tooling and the foam cores; but even on areas where the fabric was pinched because of irregularities or multiple plies, it was still possible to infuse. To maintain regular laminate thicknesses between the top and bottom surfaces, because of pressure gradients, special geometries were added to the foam cores. With respect to internal supports and multiple plies, the development showed a process that was able to fully infuse any of the combinations we were able to create. A close-up view of a proof-of-process through-part reinforcement is shown in Figure 2.



Figure 2. Close-up view of proof-of-process composite block with reinforcement.

Other findings from process development were that pressure/vacuum values as well as the foam density were optimized. With a low-density foam core, vacuum assist, and low resin pressure, consistent processing results were obtained with few air voids and an infusion time of 1 minute. High pressure resulted in foam compression, allowing more resin into the part, and did not shorten the injection time. Finally, a modified resin with less inhibitor was used to allow the cure cycle (from mixing to cured part) to meet an acceptable cycle time (<22 minutes) at a heated tool temperature of <120°F.

The next step in developing the pre-PV molding process was to build a larger tool with the actual part geometry (foam core areas 3 and 4) to ensure pre-PV process capability. Two production-level foam core tools were made to allow refinement of the process

on an actual production geometry tool. Figure 3 shows a view of an open aluminum-based RTM pre-PV tool. Figure 4 shows the first part made out of an aluminum-based pre-PV tool, and Figure 5 shows a cutout portion of a molded part section view from the aluminum pre-PV tool. The part was made using production-intent resin with a low inhibitor level and production-intent foam. The resulting composite part was very close to the targeted weight.



Figure 3. Open view of aluminum-based RTM pre-PV tool for sections 3 and 4.



Figure 4. First pre-PV part made out of aluminum-based RTM tool.

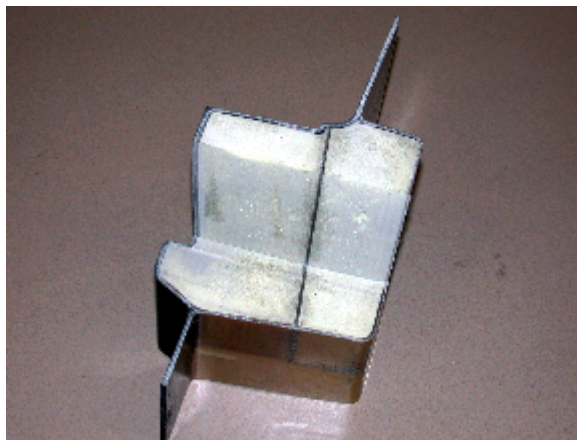


Figure 5. A cutout portion of molded pre-PV part from aluminum tool.

Hardware: Secondary Machining Operations

A key design element to minimize cost was insert molding of the metal fasteners into the foam cores. Another cost-saving method was to ensure that drilling and tapping time were optimized. To ensure optimal drill and tap cycle time after parts were made, a study was conducted. Figure 6 shows a robotic machine cell that was used to optimize the drilling method. Various drill bits and speeds were determined to help remove chips, and countersink methods were developed to avoid composite damage during tapping.

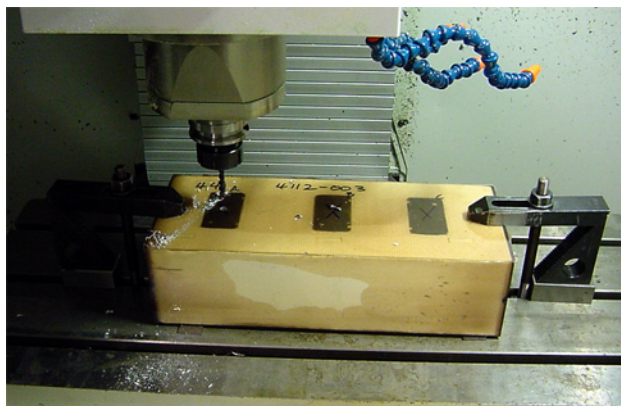


Figure 6. Drill and tap time study fixture for hardware molded test block.

Analytical Work—FEA and Fabric Pattern Development

The production design direction has been finalized, and FEA and CAD data files are undergoing final updates before production release. FEA indicates that all performance requirements will meet or exceed requirements.

Fifteen individual fabric pieces are required in the molding operation. The initial lay-flat patterns developed did not drape well over the foam cores or into the molding tool. Alternative lay-flat software is being investigated.

Cost Reduction: Conductive Gel Coat

A systematic review of the final assembly cost indicated that masking, conductive spray primer, and finish were areas with great cost reduction potential. By implementing a conductive gel coating in the composite molding, preliminary estimates showed that finished assembly cost could be reduced by up to 10%. Delphi identified a conductive gel coat system that had already been approved by the OEM partner in other applications and fabricated flat panels representative of exterior part surfaces (see Figure 7) with this conductive gel coat. These samples were forwarded to the OEM partner for oven and environmental conditioning. Following this conditioning, surface finish and resistivity will be evaluated.

Testing Activities

Fastener testing. Tests for torque and pullout load had been conducted on several M5 and M6 threaded fastener designs in composite panels with steel plates. Other sizes were also tested according to their application category [e.g., Federal Motor Vehicle Safety Standard (FMVSS), heavy load bearing, interior to the door seal, exterior to the door seal].

The foam block with hardware after drilling and tapping can be seen in Figure 8. To ensure that new hardware will work, a study of hardware bonding and corrosion resistance were conducted.

Torque and pullout load between composite and metal hardware embedded in foam was determined using various surface preparations for metal hardware. The torque fixture used for the study is shown in Figure 9. The purpose was to determine



Figure 7. Exterior surface showing conductive gel-coat.



Figure 8. Hardware molded block after drilling and tapping.

that threaded fasteners meet FMVSS requirements. The results showed that all various surface preparations were acceptable for bonding with the proposed composite materials.

Expansion testing. Blocks of the same composition of composite and foam design have been heated to process temperatures of 225°F for

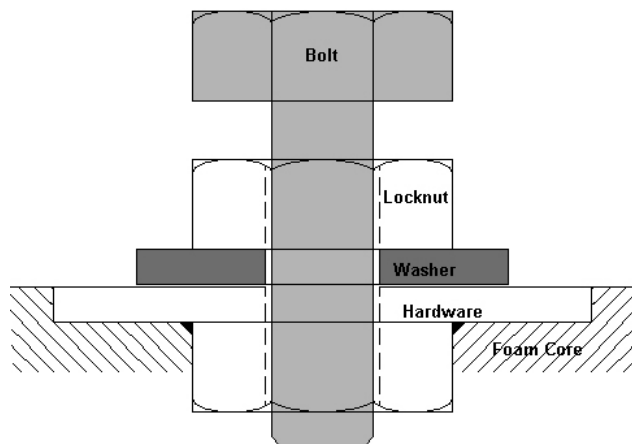


Figure 9. Torque test fixture for hardware molded test block.

one hour with no effects on the part due to variations in expansion rate among the differing materials.

Environmental testing. Environmental testing was conducted on both composite test blocks and cut-away sections of prototype parts (Figure 10). The effect on the foam, the hardware, and the laminate was determined. The results, as expected, verified that the foam and composite laminate construction protect the hardware from the environment and resist moisture penetration into the structure.



Figure 10. Hardware molded block after corrosion.

To meet the corrosion requirement, it was decided, with customer approval, to use stainless steel for machined and tapped holes outside the seal and carbon steel material in areas inside the seal. The corrosion resistance test was performed according to the OEM's standard practice on drilled metal fasteners. The results showed that Dupont's E-coated steel exhibited similar result as current production parts. Since the cost difference was minimal, the team decided to use E-coat to keep with the customer specifications.

Summary

These are the highlights for the progress during FY 2004.

1. Reduced laminate thickness from 3.0 to 1.5 mm using 30% fiber volume with production-intent resin and process. The visual inspection looked good. Performed mechanical testing of the panels and used the test properties to refine the FEA model of the cab structure.
2. Reduced component mass by 32% over current composite technology.
3. In-molded hardware to meet process requirements.
4. Proved 1.5-mm-thick molding process with area 3 and 4 pre-PV tools using foams from production-intent 3 and 4 foam tools.
5. Used in-mold conductive gel coating to reduce process steps and material cost of conductive spray primer.
6. Successfully completed cab shake testing of the cab structure using VARTM thin-walled laminates over foam cores with embedded metal hardware. This same cab structure completed the final stages of DV testing, again with no failures. Torsion and pullout testing also have met specifications.
7. Met all mass, performance, and cost objectives.

C. Advanced Composite Structural Chassis Components

Principal Investigator: David E. Witucki, PE

Delphi Corporation—Saginaw Steering Systems Division

3900 Holland Ave., Saginaw, MI, 48601

(989) 757-4984; fax: (989) 757-4295; e-mail: david.witucki@delphi.com

Technology Development Area Specialist: Sidney Diamond

(202) 586-8032; fax: (202) 586-1600; e-mail: sid.diamond@ee.doe.gov

Field Technical Manager: Philip S. Sklad

(865) 574-5069; fax: (865) 576-4963; e-mail: skladps@ornl.gov

Contractor: Oak Ridge National Laboratory

Contract No.: DE-AC05-00OR22725

Objectives

- Develop an economical, long-fiber-reinforced manufacturing procedure using continuous and/or oriented chopped fibers for structural chassis components for Class 7&8 trucks.
- Reduce the mass of these components by 60%.
- Commercialize and annually produce these components, reducing vehicle mass by about 50 kg/vehicle and significantly increasing North American carbon fiber demand annually, within 5 years of project commencement.

Approach

- Conduct value analysis/value engineering workshop(s) to conduct function analysis and brainstorm composite solutions to each component function.
- Develop finite element analysis (FEA) models on both the component and system level. Conduct structural optimization (topology and shape/sizing) of components for “material-efficient” designs.
- Build and test prototypes.
- Secure production orders for the components developed within the scope of the project.

Accomplishments

- Received production purchase orders from two customers for four different models of composite tie rod tubes to be supplied by Delphi. Current total volume is approximately 6000 units per year. Samples have been supplied to three additional customers.
- Presented the paper “Composite Tie Rods for HD Truck Applications” at the Society of Plastics Engineers (SPE), Automotive Composite Conference. In addition, this product was nominated for SPE’s Plastics Innovation award and has been named a finalist in the run for the award in the Chassis category.
- Completed initial durability and stiffness testing on a “proof-of-concept” composite-reinforced, thin-wall steel tube main support.
- Used composites research/design concepts to develop and commercialize an aluminum z-beam that resulted in over 27 kg mass savings per system.
- Achieved 32 kg of the 50 kg target for system mass reduction with the combined mass savings of the composite tie rod tube and aluminum z-beam.

Future Direction

- Continue investigation into lower-cost tie rod tube designs and processes.
- Validate composite tie rod tube for higher-volume, front steer applications.
- Investigate follow-up project for main support development with second tier-one chassis system supplier.

Introduction

In response to a request for proposals from UT-Battelle/Oak Ridge National Laboratory (ORNL) in February 2001, a submission from Delphi Corporation led to the award of a subcontract for the development of advanced composite structural chassis components with the objectives listed earlier.

Sponsored by DOE, the duration of the subcontract is 3 years with an estimated cost of \$2.5 million. This project is a 50/50 cost share between ORNL and industry. In this project, Delphi Corporation, the world's largest automotive Tier 1 supplier, partnered with an industry leading Tier 1 supplier to the truck and trailer industry and focused on three components in a chassis/suspension system: lateral links, main supports, and z-beams.

Composite Tie Rod Tube Status

Through the third quarter of 2004, more than 6000 carbon-fiber-reinforced tie rod tubes have been installed on passive-steer, auxiliary lift axle systems. Delphi has secured production orders for tubes of four lengths for two customers. Samples have been supplied to three additional customers.

This tube was nominated for the SPE Automotive Division Innovation Award in the Chassis Category and was selected by SPE's board of directors as a finalist. A formal presentation will be made to a blue ribbon panel composed of technical trade publication and industry experts for final evaluation. For more information on the SPE and the award program, visit <http://www.speautomotive.com/inno.html>.

Production tooling has been released for a lower-cost tube assembly, and production-intent samples are currently undergoing validation testing for both auxiliary lift axles and front steer applications. Test results have been mixed so far; durability testing has been favorable, but buckling capacity has degraded with the new design. Additional samples are being fabricated with alternative lay-up and materials, and preliminary

results have been encouraging. Unfortunately, these design changes are beginning to erode the original forecast of 20% cost savings for this design.

Z-Beam Status

Delphi's Tier 1 partner has introduced a cast aluminum z-beam based on FEA topology optimization completed for a composite design. Figure 1 illustrates both a preliminary composite concept and the similar final production aluminum design. The cast aluminum solution reduced the mass by approximately 7 kg and was at cost parity or below current welded steel designs. Since four z-beams are used in each system, 28 kg of total system mass was eliminated.

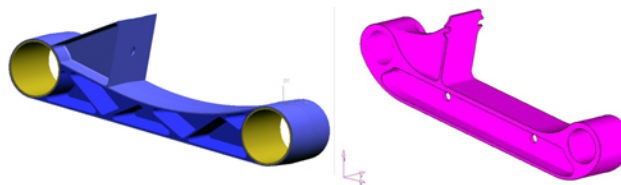


Figure 1. Composite z-beam concept (left) and current production cast aluminum beam.

Main Support Status

Testing has been completed on the first proof-of-concept main support. This assembly consisted of a relatively thin-wall steel tube, welded-in end fittings, and epoxy/carbon fiber composite reinforcement. The test sample completed the side load test schedule but failed approximately two-thirds of the way through the brake load schedule. The failure occurred in the welded joint between the inner steel tube and the end fitting (see Figure 2). It is anticipated that this can be overcome with a slight redesign to the interface of the metal parts and the addition of composite reinforcement around the end fitting.



Figure 2. Proof-of-concept main support after side and brake load testing.

Vertical stiffness measurements were taken of the baseline, current production steel main support, thin-walled steel tube, and final composite-reinforced tube. Stiffness data are shown in Figure 3. The composite-reinforced axle beam very closely matched the stiffness of the baseline steel beam, validating the previous FEA and structural optimization efforts.

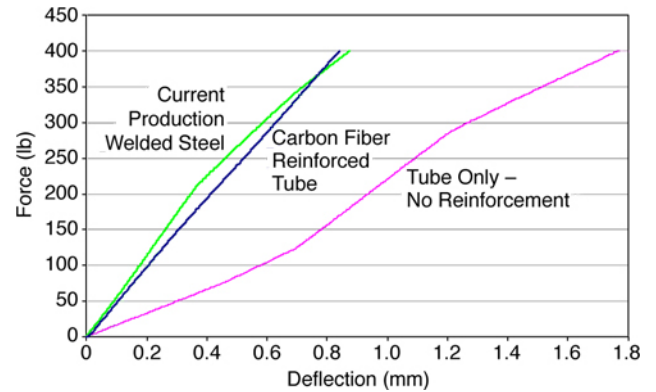


Figure 3. Main support stiffness testing.

The prototype proof-of-concept samples were 26.3% lighter (20.9k kg or 46 lb) than the baseline and employed 5.9 kg (13 lb) of dry carbon fiber fabric. Further mass reduction is anticipated because the tubing selection for fabrication of the prototype was based on availability. The fully optimized design calls for thinner steel tubing.

D. Carbon Fiber SMC for Class 8 Vehicle Hoods

Principal Investigator: Nicholas A. Rini

Volvo Trucks North America, Inc.

P.O. Box 26115, Greensboro, NC 27402-6115

(366) 393-2771; fax: (336) 393-2773; e-mail: nicholas.rini@consultant.volvo.com

Cliff Eberle, Project Manager

(865) 574-0302; fax: (865) 574-8257; e-mail: eberlecc@ornl.gov

Technology Development Area Specialist: Sidney Diamond

(202) 586-8032; fax: (202) 586-1600; e-mail: sid.diamond@ee.doe.gov

Field Technical Manager: Philip S. Sklad

(865) 574-5069; fax: (865) 576-4963; e-mail: skladps@ornl.gov

Contractor: Volvo Trucks North America

Contract No.: 4000010928

Objective

- Develop carbon-fiber (CF) sheet molding compounds (SMCs) and processing techniques that will enable serial production of Class 8 truck hoods with structural integrity, class A surface quality, significantly reduced mass and will be competitive in cost with existing glass-fiber SMC molded components.

Approach

- Accumulate material property data to establish reliable design properties that can be utilized for engineering design analysis.
- Perform finite-element analysis of a CF SMC-based Class 8 hood design.
- Evaluate consistency and repeatability of CF SMC material properties, processing techniques, and surface quality.
- Evaluate mass savings and costs.
- Confirm predicted results by constructing prototype hoods and performing accelerated endurance tests.

Accomplishments

- Designed, built, and used a development tool in CF SMC molding trials.
- Successfully molded CF SMC materials in thicknesses ranging from 1.0 to 3.0 mm.
- Attained CF SMC material for structural applications in near final form, exhibiting good molding characteristics and using manufacturing processes very similar to those for glass-fiber SMC. Costs are reduced by approximately 50% compared with currently available commercial CF bulk molding compound materials.
- Performed initial work on CF SMC with Class A surface quality that has eliminated several proposed surface enhancement materials and processes.
- Conducted adhesive bonding prescreening trials of the CF SMC structural material that have produced data indicating lap-shear values generally two times that of comparative glass-fiber SMC.
- Completed preliminary cost and weight evaluations for the CF SMC hood.

- Completed the design, procurement, building, and installation of a CF SMC compounding line to supply materials supporting this research and development project.
- Built eight prototype hoods using existing production tools to evaluate processing characteristics of various combinations of lightweight SMC materials.

Future Direction

- Continue evaluation of CF materials and surface treatments from various suppliers.
 - Pursue cost reduction and supply stabilization of CF SMC materials.
 - Pursue low-density glass-fiber-reinforced materials and process developments to provide lightweight Class A surface quality exterior panels.
 - Use the CF SMC compounding line to produce CF materials to support ongoing development.
 - Follow up Class 8 truck hood costs and weights based on CF SMC material and process developments.
 - Evaluate CF SMC hood development status and determine if a business case can be made to pursue serial production of CF-reinforced heavy truck hoods.
-

Introduction

The mass of light automotive and commercial heavy-duty vehicles can be reduced using modern lightweight, high-performance composite materials. The reduction in vehicle mass translates into an increase in fuel efficiency. Currently, polymeric CF composites are used in low-volume, high-performance applications such as spacecraft, aircraft, and racecars. The CF-reinforced composites can reduce vehicle body mass by 40% to 60%. However, market conditions and technical barriers inhibit their use in high-volume automotive applications.

Class 7 and 8 trucks offer a lower production volume, lower technical barriers, and financial incentives that can justify a modest price premium for competent lightweight materials. The aim of this project is to accelerate the commercial implementation of high-performance, lower-cost CF SMC material body components for Class 7 and 8 trucks. As utilization of CF SMC develops and the technology matures, it is foreseeable that CF SMC will migrate into the high-volume automotive market.

The project was initiated by performing a comparative finite-element analysis of a hood configuration made of glass-fiber SMC material that had been validated through modeling, accelerated endurance tests, and field test. Based on expected CF physical and mechanical properties, hood structural and surface component material thicknesses were reduced through several iterations

to determine the effect on hood system stress states and displacements. Modal analyses were performed to determine mode shapes, and complete vehicle models were used to obtain dynamic responses in the frequency domain. Fatigue life comparisons were made based on the complete vehicle model transient analyses.

Based on the initial investigation, it was concluded that a competent hood could be produced with a 40% to 60% reduction in hood mass if a CF SMC material could be produced that would consistently provide the physical and mechanical properties targeted.

CF SMC Material Search and Comparative Testing

A search was initiated to find suppliers of polymers and CFs combined in a useable SMC. Materials from Zoltek, SGL, Toray, Grafil, and others were evaluated. Early on, two significant obstacles became evident: completely wetting out the CF and defilamentizing the fiber bundles. Work with suppliers is ongoing to optimize chemistry and processes to consistently provide CF SMC material with the targeted material properties. Short beam shear tests based on ASTM D2344/D 2344M were used to screen material samples with various combinations of resins and additives. More than 150 samples were evaluated. Materials that performed well in the short beam shear screening were used to make plaques to measure material

properties. Good progress has been made in obtaining the targeted mechanical properties, as shown in Table 1.

Table 1. Percentage of target values achieved (updated April 2004)

Percent (%) of Target Value				
Property	Tensile strength	Tensile modulus	Flexural strength	Flexural modulus
Percent achieved	86%	97%	118%	107%
Coefficient of variation	0.05	0.09	0.09	0.10

Class A Surface Quality Development

The development tool was used for Class A surface quality development trials. Parts were molded using combinations of two CF loadings, three resins, two surfacing veils, and in-mold coating. Processing parameters were set similar to those of the glass-fiber SMC components. Although some progress was made, several of the materials and processes were eliminated from further consideration. It appears that a substantial effort will be required in materials and process development to achieve CF SMC panels with Class A surface quality. Because of the anticipated higher cycle times and additional processing steps, the projected cost of CF SMC for Class A surface components was estimated to be too high for commercial truck applications. Therefore, development of CF SMC for exterior Class A surface quality components was held in abeyance in order to pursue lower-cost, lightweight, low-density, glass-fiber-reinforced SMC for Class A surface components.

Assembly Process Evaluation

Preliminary evaluations of bond strength were made for CF SMC plaques at adhesive bond gaps ranging from 0.5 to 3.0 mm. Lap shear tests run at ambient and elevated temperature show CF SMC bond strengths generally twice those of glass-fiber SMC. The evaluation confirmed that the bond strength decreases as the bond gap increases. Ongoing investigations to provide bond performance data for alternative constructions will be required. The data developed will be used in hood finite-element analysis calculations.

To evaluate the processing characteristics of various combinations of lightweight SMC materials, prototype hoods are being built using the production tooling for an existing hood. The prototype hoods are being fabricated using low-density glass-fiber SMC Class A outer panels and inner reinforcements constructed of glass- or CF-reinforced SMC. The prototype hoods will be used to assess manufacturing process variability, dimensional stability, and adhesive bonding characteristics. To evaluate the viability of the lightweight materials in the production environment, the hoods will be run through the normal assembly plant production processes and evaluated for surface quality, paint quality, and bond read-through.

Cost and Weight Evaluation

Initial concept work has concluded that a 40% to 60% weight reduction is within range, as samples in the required reduced material thickness have been successfully molded. Preliminary cost estimates of the CF SMC hood indicated a higher-than-expected cost premium based on the current best estimate of CF SMC material costs. Because CF costs have risen recently as a result of increased world demand and insufficient supply capacity, alternative constructions are under review to reduce CF-reinforced truck hood costs. At this time, it is anticipated that CF production capacity will increase. However, it is difficult to predict whether world demand will also increase and thereby keep CF material costs high. To build a business case for a lightweight CF SMC truck hood, CF material costs must come down and a stable supply must be ensured.

Conclusions

The project has made good progress in finding promising materials and developing processes. The early work is very encouraging because material properties for structural applications are generally on target. Molding processes similar to those for current glass-fiber SMC can be used for structural applications. Assembly bonding processes appear to follow those of glass-fiber SMCs, with significantly increased bond strength. Most of the potential weight reduction has been achieved. CF SMC material costs for components requiring Class A surface quality are projected to be too high for

commercial vehicle applications. Alternative constructions appear to present a more reasonable cost/weight value.

E. Advanced Composite Support Structures

Principal Investigator: Brian Knouff, PhD

National Composite Center.

2000 Composite Drive

Kettering, OH 45420

(937) 297-9458; fax (937) 297-9440; e-mail: bknouff@compositecenter.org

Project Manager: Jay Batten

Delphi Corp.

3900 Holland Rd

Saginaw, MI 48601-9494

(989) 757-3895; fax (989) 757-42950; e-mail: jay.batten@delphi.com

ORNL Project Manager: Cliff Eberle

(865) 574-0302; fax: (865) 574-8257; e-mail: eberlecc@ornl.gov

DOE Technology Development Area Specialist: Sidney Diamond

(202) 586-8032; fax: (202) 586-1600; e-mail: sid.diamond@ee.doe.gov

ORNL Field Technical Manager: Philip S. Sklad

(865) 574-5069; fax: (865) 576-4963; e-mail: skladps@ornl.gov

Contractor: Oak Ridge National Laboratory

Delphi/ORNL Contract No.: 4000021806

Objective

- Lead the rapid implementation of lightweight composite materials in Class 7/Class 8 vehicles via the development of advanced composite support structures, specifically chassis lateral braces, which can number up to six per vehicle. Mass reductions are targeted for 50%.

Approach

- Model composite support structures using progressive failure analysis (PFA) software and finite element analysis (FEA).
- Fabricate prototypes of designed structures.
- Mold composite test plaques to be used in the task on "Attachment Techniques for Heavy Truck Composite Chassis Members." The data from those tests will be integrated into our design models.
- Analyze materials characteristics of the test plaques such as fracture toughness and fatigue life.

Accomplishments

Modeling

- Used PFA software to provide a means of modeling damage and failure in composites, accurately predict the number of cycles to failure as a function of void fraction, and predict the elastic constants.
- Designed all carbon and all glass composite lateral braces using six load cases.
- Optimized the geometry by transforming the current U-channel into a box beam and integrating the end brackets into the center piece.

- Demonstrated weight savings of 70%.
- Fed results in the design iterations back to the Joining Team, which then requested that plaques be molded for various tests.
- Displayed the second all-composite prototype model at the ACSS Program Review and 2nd value analysis/value engineering meeting (VAVE) on August 10, 2004.
- Fabricated several different composite test panels to support both the joining and modeling database programs.
- Discovered that the void content had a dramatic effect on fatigue life and that the plaques were not reaching their ultimate T_g (glass transition temperature) without a postcure.
- Conducted Mode I fracture toughness studies and fabricated Mode II fracture toughness fixtures.

Future Direction

- Complete design validation for this application and then pursue a new application. Associated with this program will be a higher-level effort in composite-to-composite joint design with the added variable of hole placement.

Introduction

The purpose of this effort is to lead the rapid implementation of lightweight composite materials in Class 7/Class 8 vehicles via the development of advanced composite support structures. This task specifically addresses lateral braces; primary beams are being targeted for future work. The mass reduction target is 50%. The benefits of mass reduction in commercial vehicle applications are well known. They include increased fuel economy and a larger payload, which translate into fewer total trips and thus fewer vehicles on the road. This leads to less traffic, which aids highway safety, and decreased emissions. Support structures offer an opportunity for significant weight savings. However, this area of the vehicle also represents a large hurdle in terms of composite applications and market acceptance.

The application of focus is a Class 8 tractor lateral brace (Figure 1). The estimated total annual usage of Class 8 lateral braces could exceed 1 million by 2007. At a current typical weight of 9 kg for Class 8 tractors, weight savings would be 4.5 kg per part. With up to six braces per vehicle, the resulting total weight savings would be 27 kg per Class 8 tractor.

To facilitate this work and future endeavors, advanced FEA and PFA software is being employed and developed. The FEA software contains a unique

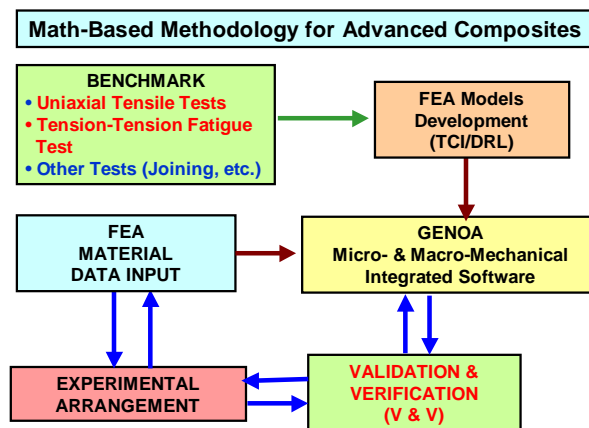


Figure 1. Schematic showing logical synergism between PFA, FEA, and experimental data.

optimization algorithm that allows for the rapid optimization of such design variables as part thickness, fiber angle, fiber type, and even part shape while minimizing mass, strain, or even cost.

PFA, although in development for composites, will provide the ability to model composite behavior in durability and fatigue situations—unlike any other software our team has examined or is aware of.

Modeling

The modeling effort was separated into two parts:

1. PFA
2. Prototype design with FEA

PFA was used to satisfy the following requirements:

- Generate required material database for micro- and macro-mechanical simulation of fracture and fatigue of composite joining systems.
- Develop predictive models of composite joint failure based upon failure mechanics theories.

Figure 1 shows the relationship between physical testing, FEA, and PFA used to develop the math-based methodology for advanced composites. The physical testing of the composites in both static and fatigue supplied the database to model these conditions. In this case, the material was a 3-dimensional (3D) fabric reinforcing a vinyl ester thermoset. An S/N curve of the neat resin matrix was produced (Figure 2). It was required to model the resin behavior for complex geometries, such as the 3D composite material employed.

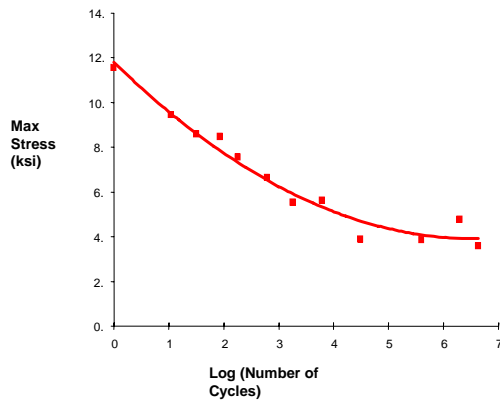


Figure 2. S/N curve for neat resin polyurethane modified vinyl ester system.

Initial results have been promising. PFA has been able to accurately represent the Poisson ratios as well as longitudinal and transverse elastic moduli. An attempt was also made to determine a “Miner’s Rule” for composites, but that has been determined to be somewhat complex and requires further investigation.

The main accomplishment to date is the ability to model the effect of void content on fatigue behavior in the test plaques. Figure 3 shows experimental data with symbols and predictions with

lines. For 13% and 10% void content, the prediction line fell within the scatter from the data. For 2% void content, it actually coincided with the data. This is a major breakthrough, as a void content of 10 to 13% has been shown to decrease fatigue life by a factor of 40 compared with a void content of 2%. This phenomenon has now been not only documented but also modeled and predicted. Without this capability, predictive modeling would have to be generated from empirical correlations.

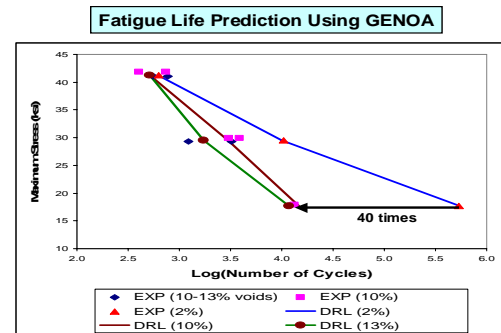


Figure 3. Good correlation between PFA (lines) and data (symbols) for S/N curves at different void concentrations.

Prototype Design with FEA

Actual design requirements of the application lateral brace were not available from the customer. However, the current steel design was in IGES format. This file was imported and meshed for FEA.

No design requirements were associated with this application. In other words, the customer did not know what load levels the part would experience in its life nor how stiff it had to be to perform properly. This is not unusual in the Class 8 truck market. Steel with a thickness of 0.25 in. is an industry standard, and it has been shown to perform well in chassis applications. The customer supplied IGES files of both the center steel brace (stamped) and the cast end brackets.

Each part will experience six basic load cases:

- **Axial extension:** a tensile or compressive load along the length of the brace, perpendicular to the primary beams. This load case will occur during lane changes and cornering, for example.
- **Racking:** an applied load on the brace flanges parallel to the primary beams. It can also occur during cornering and braking, as one side of the chassis lags briefly behind the other.

- **Rolling:** a result of one wheel being elevated above the other on the same axle. Potholes or road debris will cause rolling, which is a force perpendicular to the road surface.
- **Torsion:** a twisting motion that can also occur during a pothole or debris hit. One side of the chassis lifts and pivots to accompany the terrain, resulting in a twisting of the lateral brace.
- **In-plane bending:** a movement applied on one side of the flange around the primary beam. It can occur when one side lifts or when the chassis experiences a jarring motion from rough terrain.
- **Out-of-plane bending:** one primary beam trying to circle the other. Sharp turns can cause this load case to be applied.

The center steel section was first meshed and modeled in FEA. The constraints and loads were applied evenly along the ends. Using the exact same mesh, composite properties were applied to the model and FEA optimized the design variables to satisfy the stiffness requirement. Specifically, the design variables were the thickness and fiber angles of each of eight plies, the single point constraints were all nodes at one end constrained in all six degrees of freedom, the load case was 2000 N-mm at the other end, the design constraint was a maximum deflection of 1.2 mm, and the design objective was the minimization of mass.

The optimization resulted in a lay-up of three stacks of $[0_2/90/23_6/-23_6]_s$ of prepreg with each ply 0.15 mm thick. The total thickness of the part was 13.5 mm and the part weighed 5.3 kg, resulting in a mass savings of 58%.

After this design, a meeting with the customer was held to determine what other options were available. It was determined that the holes were not needed in the center section. Additionally, it was discovered that torsional rigidity was further improved by adding a fourth wall to the bottom, thereby making the brace a box beam.

To minimize assembly time, the design was further optimized by combining the end brackets with the centerpiece. The material was changed from carbon prepreg to 3D carbon fabric to reduce the material cost. A topology was then performed to

determine the areas of most required mass, or stiffness. Figure 4 represents the thick areas with the darker gray areas that make an 'X' shape on both sides of the part. Also, notice the darker areas calling for reinforcement of ends on top and bottom. Using the topology results, the part was then divided into finite elements parts with each part optimized for thickness. The result was an end thicknesses of 5 mm with 1-mm thicknesses for the rest of the part.

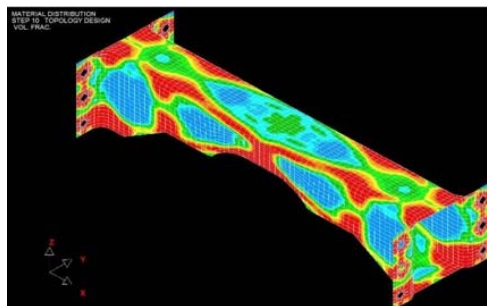


Figure 4. Topology shows areas of high profile (thickness) to accommodate higher-stress regions.

Up to this point, only the torsional load case was considered because of our impression that it was the worst-case scenario. However, with the optimization to a box beam, that was shown to no longer be the case.

Therefore, the additional five load cases were also used for design optimization. All six load cases are shown in Table 1. In the general coordinate system, the X-axis runs longitudinally through the lateral brace itself, the Y-axis is parallel to the primary beams, and the Z-axis is perpendicular to the ground.

For the design of the composite part, the steel lateral brace was loaded until 90% of yield stress failure in each load case. This load then was applied to the composite, which was designed with a safety factor of 2 using Tsai-Wu failure criteria. Table 1 shows the resulting loads used for each case and the corresponding reaction (deflection) of the steel brace.

Table 1. Loads calculated in FEA analysis on steel section to achieve 90% von Mises yield stress. The deflection is also shown.

Load case	Load (kN) (kN-mm)	Max VM (MPa)	DOF	Deflection (mm)
1. Axial	28.08	527.40	F_x	6.32
2. Racking	8.00	527.34	F_y	52.7
3. Roll	8.86	526.90	F_z	12.6
4. Torsion	1003.42	527.11	M_x	40.8
5. In-plane bending	3882.45	525.00	M_y	2.76
6. Out-of-plane bending	1045.29	527.39	M_z	17.7

It was also determined that the brace could be processed much more easily (with less cost and increased yield) by removing the scallop on the underside and making the box beam straighter. In this design, a 7-mm backing plate was also added to represent the attachment to the primary beam. Topology and part optimization was used again to design this iteration. This iteration was used for the prototyping. Figure 5 shows the model after it was optimized for manufacturability.



Figure 5. Optimized geometry smoothed and drafted for manufacturability.

Further investigation took place to optimize the design. Two hybrid designs of steel and glass were investigated first. Both of these hybrid concepts use traditional joining methods because of the steel endplates and offer a potential low-cost alternative.

Five different all-glass composite designs were also considered. The flanges of the endplates are reinforced by geometric hollow ribs in the first concept, whereas these ribs are replaced with an expanding tube at the end in the second. The third concept attempts to decrease the middle section geometry from the previous design. A more radical conceptual design is offered in the fourth: Ribs are

placed longitudinally along the tube, thereby also serving as the attachment flanges. This can be accomplished process-wise by employing foam inserts that remain in the part or using metal inserts that disassemble. The fifth concept uses flat attachment plates instead of the rib design in all four corners of the tube. The novelty of this analysis is that the lateral braces were attached to sections of the primary beams, to which the loads were applied.

Each of the designs has been compared in all six load cases in terms of displacements. These six load cases are

1. Axial extension in the X direction (11-X)
2. Racking in the Y direction (12-Y)
3. Rolling in the Z direction (13-Z)
4. Torsion around the tube (14-MXX)
5. In-plane bending (15-MYY)
6. Out-of-plane bending (16-MZZ)

Table 2 lists the load cases as well as the normalized deflection of each design, with the steel base case having a deflection of 100%. A percentage less than 100% means the composite design was stiffer. Alternatively, a value higher than 100% means it is less stiff, or deflects more as a result of similar applied loads.

In the extensional load case, the hybrid designs were slightly stiffer than the base case. However, each one of the glass designs showed stiffness decreases. The hybrid designs also showed stiffness increases in the racking loadcase, with only concept 2, of the all glass designs, showing a significant increase in stiffness.

None of the designs fared better in rolling than the base design. However, the hybrids performed the best. Contrary to this fact, all of the concepts were torsionally stiffer than the baseline case. However, the in-plane and out-plane-bending cases showed

Table 2. Comparison of seven designs to baseline in the six load cases

Load case	Baseline	Hybrid-1	Hybrid-2	Concept-1	Concept-2	Concept-3	Concept-4	Concept-5
11-X	0.080	0.072	0.079	0.135	0.101	0.113	0.126	0.180
%	100%	91%	99%	169%	126%	142%	158%	226%
12-Y	2.859	1.132	1.212	3.445	1.882	2.631	3.243	4.255
%	100%	40%	42%	120%	66%	92%	113%	149%
13-Z	1.972	2.113	2.320	4.271	2.697	3.182	5.556	6.353
%	100%	107%	118%	217%	137%	161%	282%	322%
14-MXX	3.243E-02	7.168E-04	6.251E-04	4.392E-03	3.442E-03	5.293E-03	4.579E-03	4.159E-03
%	100%	2%	2%	14%	11%	16%	14%	13%
15-MYY	1.981E-05	3.076E-05	5.834E-05	7.315E-05	2.936E-04	3.902E-05	7.241E-05	1.097E-04
%	100%	155%	295%	369%	1482%	197%	366%	554%
16-MZZ	1.279E-03	1.327E-03	1.402E-03	4.603E-03	2.684E-03	4.052E-03	3.862E-03	5.025E-03
%	100%	104%	110%	360%	210%	317%	302%	393%

there to be a considerable need for redesign in each of the seven concepts.

Prototyping

Figure 5 was used as the design for the prototype model. The resin transfer molding (RTM) process with fiber architecture achieved via a bi-axial braided fabric was chosen to fabricate the prototypes. Table 3 lists this architecture. The braided fabric took the form of several layers of a braided sock that could be threaded over a two-piece mandrel and the assembly loaded into a multi-piece aluminum mold.

The aluminum mold (Figures 6 and 7) consisted of six pieces that encapsulated and located the two-piece mandrel covered with the fiber assembly. The mold was cored to allow temperature control via ancillary thermolators to aid in the curing of the injected matrix. The matrix chosen was a two-component epoxy system with good thermal and environmental properties. The resin was injected at an elevated temperature to lower its viscosity and reduce the infusion time. The mold design incorporated a bleeder system that created minimal flash even though the resin injection pressures exceeded 100 psi. The infusion time was less than 5 minutes; however, the cure-demold time took several hours because of the ramp-up and cool-down thermal requirements for the several hundred pounds of aluminum mold. In addition, the multi-piece mold was assembled and disassembled by hand. Production tools will incorporate much easier

assembly/disassembly and will be water-cooled to allow for rapid cycle times.

The parts weighed 7.7 lb with a targeted fiber volume of 55%. Constant fiber content was maintained in the varying cross-section by placing additional layers of braided sock as needed. Bi-axial braided preforms conform much more easily to the variations in the mandrel geometry as opposed to tri-axial braids. Computer-aided part design and tool manufacturing contributed significantly to a time frame of less than 4 weeks from concept to the part shown in Figure 8.

Molding

The fabrics used for this project were

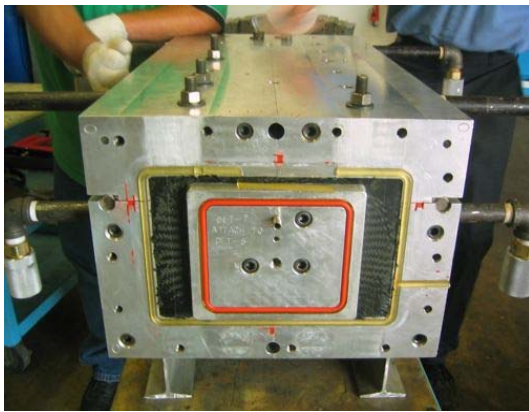
- 3D glass 96 oz/yd²
- 3D carbon 32 oz/yd²
- Stitched glass 0–90° 17.8 oz/yd²
- Plain-weave glass 10.5 oz/yd²
- Unidirectional glass 10 oz/yd²

All panels were molded to a nominal thickness of 0.100 in. To achieve this, the following lay-ups were used:

- 3D glass 96 oz/yd²—1 layer
- 3D carbon 32 oz/yd²—5 layers
- Stitched glass 0–90° 17.8 oz/yd²—5 layers
- Plain-weave glass 10.5 oz/yd²—9 layers
- Unidirectional glass 10 oz/yd²—10 layers

Table 3. Braided fiber architecture used for the prototypes

Braid laminate design for National Composite Center demonstration structure									
	Full-length sleeves			Full-length sleeves			Patch plies		
Product code	Y56L800R			MM26L700R			AP5574		
Box width		4.897	4.897		4.897	4.897	Braid width = 59.2		
Box height		5.358	7.022		5.358	7.022			
Box perimeter		19.179	24.047		19.179	24.047			
Braid condition	Nominal	Use diameter		Nominal	Use diameter		Bias	Warp	Total
Diameter	8.000	6.015	7.65	7.000	6.105	7.65	18.844	18.84	
Angle	45.0	32.7	42.6	45.0	38.1	50.6	60.0	0.0	
Raw Yd/Lb	620	620	620	1800	1800	1800	620	620	
Carrier	272	272	272	500	500	500	336	168	
Ends per carrier	1	1	1	1	1	1	1	2	
Fiber density lb/in. ³	0.065	0.065	0.065	0.092	0.092	0.092	0.065	0.065	
Part fiber volume (%)	51.8%	51.8	51.8	51.8	51.8	51.8	51.8	51.8	
Outputs									
One layer thickness	0.0204	0.0224	0.0204	0.0104	0.0107	0.0106	0.0151	0.0076	0.0227
Number of layers	3			1					??
Local laminate thickness		0.0780	0.0719						0.2039
Overall fiber volume in patch area for an overall laminate thickness of 0.275 in.							52.0%		
Percent coverage (%)	58.5	63.0					45.9		
Oz per yd ²	14.2	15.6	14.3	10.3	10.6	10.5	10.5	5.3	15.8
Ft/lb	4.84	5.76	5.04	7.64	8.50	6.85	2.77	5.54	1.85
ppi	5.4	4.5	5.2	11.4	10.2	12.7	4.9	0.0	
Mtl. reqd. for 3 performs (lb)	6.1			1.4			17.1		

**Figure 6.** Four corners plus two mandrels (ends have been removed).

Two resins were used for the matrix, a polyurethane/vinyl ester blend and a polyurethane modified vinyl ester.

The process chosen to consolidate the constituents was vacuum infusion. Some of the fabric/resin combinations were not infusible. Although the blend of polyurethane and vinyl ester allowed for some gel time extension by changing the chemistry (catalyst, accelerator, and promoter

**Figure 7.** Both top corners removed.

concentrations), the ceiling was found to be between 24 and 30 minutes.

The other resin used in this project was a vinyl ester resin base. This resin showed better infusion properties. The gel time for this resin was extended from 8 minutes (first iteration) to 50 minutes (third iteration), making this resin more infusible. A consistent pattern of bubbles or voids occurred at the intersection of the fiber tows when infusing this resin into a 3D glass 96-oz fabric.



Figure 8. Second prototype part.

This project helped to shed light on the mechanisms of infusion and the importance of fabric orientation. It was noticed that orienting the fiber parallel to the infusion line produced a slower infusion than orienting the main fiber perpendicular to the infusion line. In one case, when the 3D glass 96-oz fabric was oriented parallel to the infusion line, the total infusion time was 20 minutes; but when the main fiber was oriented perpendicular to the infusion line, the infusion time was only 4 minutes.

A second important point for infusion is the effect of changing the layup schedule. For this trial, the stitched 17.8-oz fabric was used with five layers per panel. Two sequences were used: Panel A: $[0-90^\circ, 0-90^\circ]_{2s}$ and Panel B: $[0-90^\circ, 90-0^\circ]_{2s}$.

Panel A infused faster than panel B. The reason is that in panel A, the infusion speed tended to be constant; meanwhile, in panel B, the fiber perpendicular to the resin line (0° direction) flowed faster than the fibers parallel to the infusion line (90° direction), which flowed at half the speed of the zero fiber orientation. In panel A, the resin that flowed along the 0° fibers also was able to transfer to the 90° fibers on both sides. However, in Panel B, a 'dead' zone was created between each of the two 90° layers and resin infusion was impeded.

Material Characterization

Molding

It was found that the initial composite specimens made were performing unacceptably in fatigue. This was found to be the result of having too much clay in the formulation, incomplete cure, and high void content. The elimination of clay in the formulation was easily accomplished, and a post-cure schedule was added to each panel to ensure completion of the polymerization. The thrust of this investigation was the cause and elimination of voids. Voids are detrimental to fatigue properties of composites.

By degassing the resin before infusion and using vertical infusion, the void content was successfully minimized. Figure 9 shows a comparison between an initial plaque (10 to 13% voids) and one of the latest plaques (2% voids).

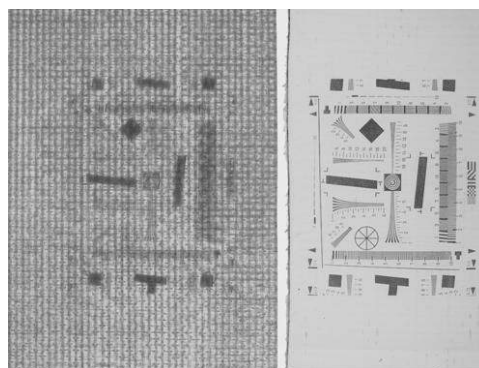


Figure 9. Side-by-side comparison of 10% void plaque and 2% void plaque.

It was necessary to generate and test neat resin samples for input into the PFA database. The resins were characterized under a dynamic mechanical analyzer. This unit, used to measure the glass transition temperature, showed that all the samples needed a post-cure to obtain a saturated cross-link density.

Fracture Toughness

Another method of obtaining material data to support PFA was the use of fracture mechanics. Mode I fracture toughness testing initially gave mixed results, but the testing technique has now been improved. A fixture for Mode II has been fabricated.

The results include an interesting observation of the stitched or z-fibers in the 3D fiber architecture. The fibers not only prevent catastrophic crack growth but also actually impede it to the point of rerouting the crack through the thickness of the specimen. Possibly, the fracture toughness could be increased by decreasing the proportion of z fibers.

Testing with the neat resin showed a continuous fracture toughness (~ 590 J/m) regardless of crack length, thereby providing a noncatastrophic Mode I failure.

Conclusions

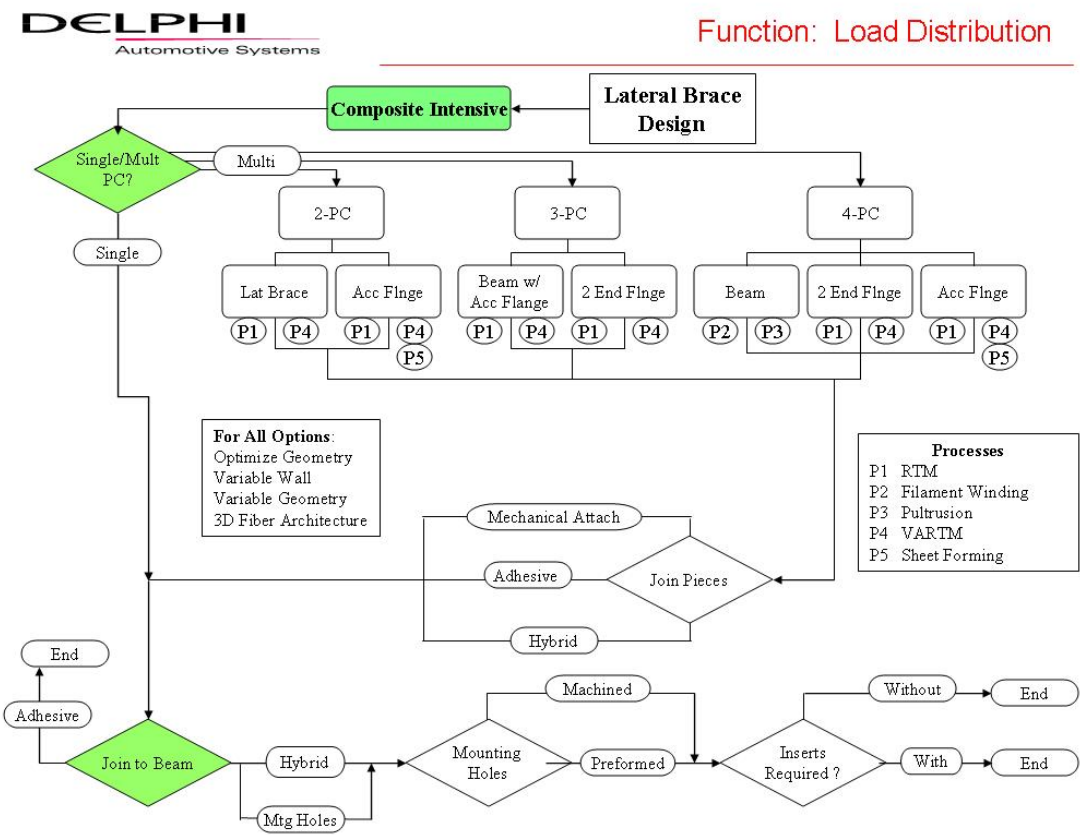
Accomplishments in FY 2004 include the following:

- Integrated PFA to help design composite parts in durability and fatigue environments.
- Successfully predicted S/N curves of composite plaques with varied levels of void content.
- Successfully predicted elastic constants of 3D fabric composites.
- Brought an optimized design close to completion on the lateral brace using 3D fabrics. FEA was used to generate the designs.
- Achieved weight savings of more than 50%.
- Integrated a cost model into the optimization program.
- Considered all-carbon, all-glass, and hybrid materials.

- Successfully designed a manufacturable prototype.
- Successfully fabricated a prototype using aluminum tooling and displayed it at the August VAVE workshop. Design to fabrication took 4 weeks.
- Determined that the aluminum tool can fabricate up to 500 parts.
- Employed both vacuum infusion and RTM to mold plaques for the process development (elimination of voids) and fatigue and durability testing for input into the PFA database, and for the “Attachment Techniques for Heavy Truck Composite Chassis Members” project.
- Successfully measured the mode I fracture toughness for the 3D fabric. It has been determined that the frequency and placement of the ‘z’ fibers can have a major effect on this value.

Future Direction

Results from the VAVE workshop produced the functional analysis system technique model shown in the following chart. The chart envelopes several paths for the design, processing, and attachment of the lateral braces in the tractor suspension. Once design validation is successful, a new application will be pursued.



F. Hybrid Composite Materials for Weight-Critical Structures

Principal Investigator: Mark T. Smith

Pacific Northwest National Laboratory

P.O. Box 999 Richland, Washington 99352

(509) 375-4478; fax: (509) 375-4448; e-mail: mark.smith@pnl.gov

Principal Investigator: Bill Roberts

PACCAR Technical Center

12479 Farm to Market Road, Mount Vernon, Washington 98273

(360) 757-5286; fax: (360) 757-5370; e-mail: broberts@paccar.com

Technology Development Area Specialist: Sidney Diamond

(202) 586-8032; fax: (202) 586-1600; e-mail: sid.diamond@ee.doe.gov

Field Technical Manager: Philip S. Sklad

(865) 574-5069; fax: (865) 576-4963; e-mail: skladps@ornl.gov

Contractor: Pacific Northwest National Laboratory

Contract No.: DE-AC06-76RLO1830

Objective

- Develop and demonstrate (1) the application of hybrid composites and composite/metal hybrids to heavy-duty vehicles and (2) the capability to integrate these materials choices into moderate-volume production.
 - Develop and demonstrate the potential for major weight savings (>50% on a component basis) in critical structures applicable to truck cabs and support components.
 - Demonstrate the basis for use of hybrid metal-composite systems to reduce weight via proof-of-principle experimentation.

Approach

- Investigate the potential of new materials and manufacturing technologies to effect major weight reductions for heavy-duty vehicles.
- Assist in demonstrating the applicability of composites and composite/metal hybrids to operational vehicles with little or no cost impact.
- Provide the experience base to develop the design and analysis tools, as well as the scientific understanding of the factors affecting molding and materials performance.
- Provide the materials suppliers with a market that can stimulate demand, leading to an increase in their production capacity. This will help reduce materials costs by creating higher volumes.

Accomplishments

- Completed three sets of prototype hybrid door components, which were delivered to Pacific Northwest National Laboratory (PNNL) by the subcontractors. The key components include sand cast magnesium door inners (Style and Tech) and molded hybrid glass/carbon fiber upper door frames (Profile Composites).
- Initiated door hardware fitting and assembly tasks at PACCAR and PNNL. These include dimensional inspection and fitting of the magnesium lowers to the hybrid composite uppers, as well as initiation of material adhesive bonding tests at the PACCAR Tech Center.

- Completed bonding adhesion testing of composite and metal systems at PACCAR Tech Center and demonstrated excellent bond strengths and desired bond failure behavior.
- Received fitted hardware at the PACCAR Tech Center for final prototype assembly and bonding. Assembled prototype doors will be placed in the PACCAR cab shaker test system for simulated durability testing. The assembly and testing milestone has been delayed until early 2005 in order to successfully complete bonding adhesion development tests.

Future Direction

- Assemble three prototype hybrid material doors for testing by PACCAR. Plans call for cab shaker tests to be conducted in the first half of 2005.
 - Based on component design and assembly tasks, update door manufacturing cost models for PACCAR (PNNL and Mercia).
 - Compile a final report at the conclusion of the prototype demonstration phase.
-

Introduction

Current materials and manufacturing technologies used for heavy vehicle door systems are often dictated by the high cost of tooling and the relatively low production volumes for Class 8 trucks. Automotive-style stamped door designs, whether of steel or aluminum, require multistage stamping dies that are generally cost-prohibitive at lower production volumes (<50,000 units per year). Alternate materials, such as glass-reinforced sheet molding compound (SMC), require less expensive tooling and can provide a Class A finish; but the relatively poor specific properties of SMC tend to compromise design and result in a heavier door system. For many production truck cabs, a simple aluminum extrusion frame is used with a flat aluminum sheet riveted to the frame. Although this approach does not require expensive tooling, the use of constant cross-section extrusions in the frame is less than optimum, and it requires more assembly labor than other approaches. PACCAR, a world leader in Class 8 truck design and manufacturing, teamed with PNNL to explore alternate “hybrid” door system designs that minimize tooling cost and per/part door cost, while providing a lightweight, structurally stiff, automotive-style door.

Project Approach

The initial approach to development of the hybrid door system was to perform a structural analysis of an existing PACCAR door design and determine what the design and performance goals should be for new-generation door systems.

PACCAR provided a number of weight, cost, and performance parameters that it considered important for future door designs. PNNL was tasked to survey existing and emerging materials and manufacturing approaches that could be applied to a new door design. Following completion of this survey and analysis of existing door designs, PNNL, with design assistance from Mercia, Ltd., developed a series of five door design concepts that included combinations of large die castings, extrusions, carbon- and glass-reinforced composites, and conventional SMC and stamped aluminum exterior panels.

Following a concept review meeting with PACCAR, an optimized hybrid door design concept was selected. The door concept was then defined using computer-aided-design tools and analyzed with finite element models to validate performance, weight, and cost. After determining that the prototype design met or exceeded all performance and projected cost targets, PNNL and PACCAR selected methods to produce prototype components for the full-scale assembly and testing phase of the project. The finite element model of the prototype door system is shown in Figure 1.

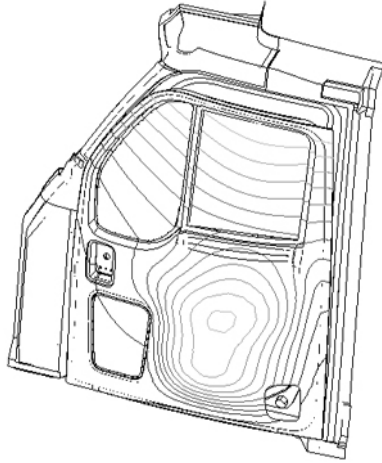


Figure 1. Finite element model of prototype door system under simulated loading conditions.

Conclusions

The prototype development of hybrid materials components for an advanced heavy truck door was completed by the team and its selected subcontractors. Initial prototype assembly has been initiated by the team, including inspection and assembly fitting, as well as adhesive bonding development. Three prototype doors will be assembled by the team for cab testing and evaluation during the first half of 2005. The hybrid door design that will be prototype-tested reduces door weight by 37%. If the hybrid design were to move into production, the use of a stamped aluminum outer panel (cost-prohibitive during the prototype stage) would improve structural performance, reduce cost to project goals, and increase weight savings to 55%.

G. Application of Carbon Fiber for Large Structural Components

Principal Investigator: Kevin L. Simmons

Pacific Northwest National Laboratory

P.O. Box 999, MSIN: K2-44, Richland, WA 99352

(509) 375-3651; fax: (509) 375-2186; e-mail: kl.simmons@pnl.gov

Technology Development Area Specialist: Sidney Diamond

(202) 586-8032; fax: (202) 586-1600; e-mail: sid.diamond@ee.doe.gov

Field Technical Manager: Philip S. Sklad

(865) 574-5069; fax: (865) 576-4963; e-mail: skladps@ornl.gov

Contractor: Pacific Northwest National Laboratory

Contract No.: DE-AC06-76RLO1830

Objective

- Develop selective reinforcement technology that can be applied to large cab components to improve specific stiffness and strength, while reducing overall component weight.

Approach

- Determine the capability of low-cost carbon fibers to be hybridized with glass fibers to provide substantial weight and cost reductions in large cab components.
- Develop a system for preforming carbon and glass fibers together that will allow components to take maximum advantage of the capabilities of selective reinforcement alignment and property contribution.
- Develop models for the analysis of hybrid chopped-fiber preforms and composites that allow the thermal and structural properties to be developed and compared with experimental analysis.
- Perform structural testing to define the limits of the applicability of the carbon/glass hybrid reinforcement materials to the large structures and develop guidelines for applications that may be used by original equipment manufacturers (OEMs).
- Design and develop critical subsection components of large structures to use in correlation with the predictive models and to validate the structural application criteria. Determine the capability of the materials to be fabricated in full-scale components and determine the performance of these full-scale components in real application scenarios.

Accomplishments

- Developed the first Class A structural carbon composite panels for truck applications.
- Showed impact performance that is 2–3 times higher than performance values of standard structural composites.
- Developed hybrid carbon composite with improved impact performance over fiberglass composites.
- Demonstrated thin (2.5 mm) panel fabrication and resin transfer molding capability.
- Demonstrated panel molding with varying cross-sections from 2.5 to 7 mm in a single component.
- Performed panel molding with various filler types and loading, and selected optimum fillers for achieving Class A surface.

- Performed mechanical and impact tests on a range of panels.
- Developed and performed process trials with a new tooling system that allowed the system to work together, including improving thermodynamic control necessary for achieving mechanical and impact properties.

Future Direction

- Scale up to test a production component selected by the cooperative research and development agreement (CRADA) partner.
 - Optimize the resin system using different fillers.
 - Test and validate thickness constraints on panels to achieve structural performance on surface-coated thin hybrid panels.
 - Fabricate test tooling for production-level component.
 - Test and validate barrier coat and optimize for surface profile.
 - Verify tooling performance and long-term viability.
-

Introduction

Selective reinforcements with stiffer fibers have the potential to reduce both costs and weight simultaneously even at current price points. Their introduction is hindered by a lack of understanding of the fibers in existing processes and the need to develop robust methods of preforming glass and carbon fiber materials together. In addition, the capability to attain Class A surface finish is required; and potential development of bonding agents and the ability to model thermal and structural performance of the materials in a hybrid system are needed. The recent development of composite systems combining carbon fiber reinforcement with low-cost automotive and marine resin systems provides the opportunity for selective reinforcement of a broad range of structural composite components.

The purpose of this project is to develop the design and materials processing technology that will facilitate the application of low-cost hybrid glass fiber and carbon fiber reinforcements in large composite components, resulting in reduced weight and improved structural performance. This project will also seek to advance low-cost carbon fiber materials developed by industry by advancing the introduction of low-cost resin systems that are compatible with current heavy vehicle structural composites.

Fiber Preform Development and Evaluation

The requirement for a discontinuous fiber preform that can accommodate multiple project objectives was a key issue in the project. Critical aspects included allowable loft and compressibility, capability to achieve Class A surface, ease of fiber placement, ability to tailor for placement of local additional carbon fiber reinforcement, minimum processing cost, and repeatability of processing. The approach calls for a given amount of loft to be available but for both compressibility and the capability to provide a high-permeability resin flow path. The method and application of the surface fibers have provided benefits in tailoring fiber content and have assisted in achieving success in the Class A arena.

To supply the various molding trial requirements, different core densities and fiber surface densities were evaluated. Packing levels were from net to 60% compaction, which varied fiber loading in the composite from effective values of 25% to well over 45%. Fiber loading in the carbon fraction was approximately 50% and allowed excellent surface density and allowed fabrication of a thin, high-stiffness panel. This is clearly seen in the test results for flexural properties versus the results for tensile properties. Figure 1 shows the surface available from the sample panel.



Figure 1. Molded preform indicating discontinuous fiber surface.

Hybrid Resin Evaluation

The development effort has remained focused on using a carbon- and fiberglass-compatible resin system. This has proved to be a valid selection based on impact test data that indicate excellent performance with carbon fiber systems as well as glass and other systems (Figure 2). The resin is tailored for use in a resin transfer molding (RTM) process. Several features of the development project have been mentioned by the resin supplier as being unique and beneficial based on the project. The capabilities to develop a truck-quality Class A surface without low-profile additives (which compromise toughness) and to achieve consistent molding are both new to the industry. The excellent toughness seen in carbon hybrid composites is also an industry first, described with enthusiasm by the resin supplier as “ballistic performance.” One significant issue with carbon composites is their lack of toughness and brittle failure nature. The team had concerns about the minimum achievable panel thickness because of this issue. Limiting panel thickness would have severely hindered capability to be cost-competitive and provide the weight savings desirable. Resin and process evaluation indicated a need for a system with close temperature control, which required development of tight tolerances on the process and equipment.

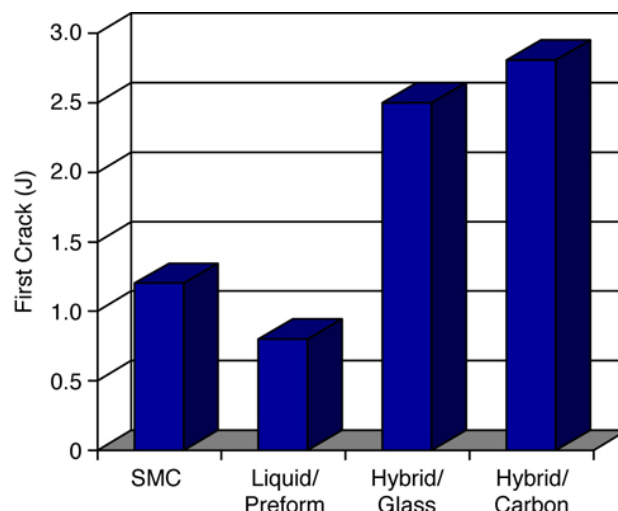


Figure 2. Resin system allowing excellent impact energy.

Molding Trials

Molding trials have consisted of flat panels and large test tool molding trials. Flat plaques were made primarily at Pacific Northwest National Laboratory to develop and verify resin and additive processing conditions as well as to determine the flow rates achievable through preforms of different thicknesses and compaction. Full-scale test tools (approximately 3 × 5 ft mold) were fabricated (Figure 1) to translate these results into a size and form that could demonstrate the effects of different geometries, fiber loadings, and resin flow paths. Experimental results for each provided a process map for the CRADA partner’s confidence in molding actual on-vehicle test components to be provided later this fiscal year. Local condition variability was a key issue in the process control and development efforts, especially as the resin rheometry effects varied with time as reactions occurred.

Several different conditions had to be addressed in order to achieve consistent and reproducible moldings. These included density and compressibility of the pre-form, wettability of the surface fibers, surface energy of the mold’s A and B sides (provided by the particular mold releases), flow-rate into the mold and lag between flow front and fiber wetting front, vacuum level, injection pressures, and mold and materials temperatures. Their effects were often interrelated as regards quality of the components produced. Studies were developed to evaluate common mold release agents and to determine the level of “slip” required to

effectively de-mold parts without causing pre-release at the part surface. This surface requirement proved difficult to achieve, since the materials with medium slip would build up on the tooling and degrade the surface finish. High-slip materials almost always resulted in pre-release at the tool surface, resulting in degradation of the Class A finish capability. Systems evaluated included primarily semi-permanent films. A combination of materials was developed to provide excellent release off the B-side tool and limited release off the A-side to achieve the Class A finish required. Testing is continuing with newly developed formulations for decreased buildup and with internal glyceride-based fatty acid release agents. Surface wettability also impacted the molding quality and the surface pin-holes and voids based on wetting of the fibers in direct contact with the surface.

Four different fabric carriers were evaluated to provide control of resin-injection back-pressure and to determine effective properties with different compressibilities. The best surface finishes achieved were provided by materials that had lower-than-desired permeability and restricted resin flow on the thinner areas (2.7–3.5 mm) of the test parts. After analysis of flow rate and injection pressure parametric studies, vendors have been approached to modify their materials for optimum functionality. New materials to achieve both flow rates required at optimum process pressures and required compressibility of the preforms should be available to us in early FY 2005.

Although temperature has a very significant effect on resin viscosity, cure times, and fiber wetting, it was determined in studies that a very limited temperature range was feasible for this system, based on resin off-gassing and void formation, catalyst selection, and flow. To achieve viable system performance, equipment specifically designed for these resin systems will need to be developed. Pump and feed/storage system customization was required for the experimental trials, which was not an optimal solution.

Gel-coats from several different manufacturers were tested for performance against the A-side tool. Although all performed adequately, a clear choice emerged out of the five tested to meet the CRADA partner's guidelines. The partner desired a system that needed no post-molding sanding and one that could be scuffed with Scotch-Brite™ or a similar

material and sent straight to paint. A study of gel-coat thicknesses and optimum application parameters was initiated, but it had to be stopped because of environmental concerns. A new air handling system is being installed to mitigate this problem and to allow completion of the study. This system should be operational by early November 2004.

Experimental Testing

Mechanical and impact tests were performed on the panels, and excellent translation of properties for all fiber systems was noted. In an unusual departure from common practice, the impact performance of the carbon fiber panels was better than that of the glass fiber panels. The somewhat brittle nature of the fibers in failure was suppressed by a combination of materials and design. The improvements seen were dramatic and bode well for the usefulness of ultra-thin panels.

Specimens were machined and finished on diamond tools and tested with combination extensometers. Results and failure modes were consistent with previously reported testing on the hybrid system that had used different resin systems, except that the performance was significantly better and reflected the improved adhesion to both material phases.

Flexural fatigue testing was performed on several sets of data to determine the durability. The CRADA partner suggested that the material must be able to endure at least one million cycles. Figure 3

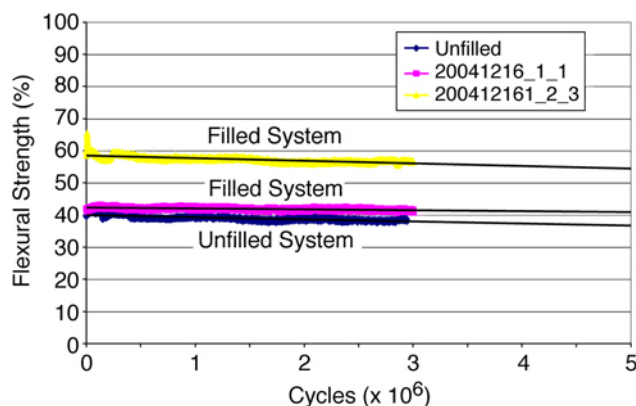


Figure 3. Flexural fatigue comparison at both 40 and 60% of flexural strength. illustrates the fatigue resistance of the developed system at both 40% and 60% of flexural strength. Most specimens were stopped at three million

cycles, but there are data for up to seven million cycles. It was decided to stop the testing at three million cycles so that more samples could be tested.

Fatigue testing on the tooling skin was also conducted to determine the durability of flexing large tooling skins. The material was determined to be suitable, but a more durable surface coating will continue to be investigated.

Rheology measurements were taken on different solids loading of the filler. An optimum range of filler content and particle size was studied and is the basis of future work.

Flow testing under a glass top tooling was accomplished on the four different preform materials. Data showing the different preform materials and the optimized rheology were combined to enhance the understanding of needs and upper limitations.

Cost Analysis

A cost analysis of a large (proprietary) component was performed to determine the break-even points for materials and processes in a typical truck production environment. The effects of a much reduced tooling budget were not factored in because the CRADA partner could not define exactly how and over how many components its internal costing amortized up-front tooling costs.

Tool cost factors would generally sway the costing option in favor of the carbon composite approach. This is because a typical fiberglass injection/compression mold is 4 to 7 times the cost of the RTM tools used in this process. Cost analysis indicated cost parity if carbon fiber is available for approximately \$5/pound and allows for equivalent costing of process ancillaries. The weight savings amounts to 53% over a traditional wet/preform component in production currently.

With tooling cost differentials amortized over two years of production, the break-even point for cost parity is with carbon fiber at just under \$6/pound. Although carbon fiber prices have risen substantially in the past year because of materials shortages, several options for low-cost carbon are being developed. One manufacturer is starting several moth-balled production lines that will ease supply pressures. Aerospace sector supply should increase significantly in 2006 to meet the demand, and these factors will bring pricing back to pre-shortage levels. Long-term pricing for large-volume

orders in FY 2003 was near \$6.10/lb, which is in line with cost parity for this technology given appropriate tool amortization models.

Large Evaluation Tool

In order to evaluate the capability of the process and materials to meet the demands of industry, a proof test component tool was developed. This tool has all the features anticipated in designs, and it was used to evaluate the hybrid process for achieving performance given the requirements of these features. It is not expected that all features can be molded and perform as expected, since the goal of the development is to determine the limitations of the hybrid fiber system as well as provide designers and OEMs with guidelines as to where lightweight materials will be applicable and how to design and manufacture them accordingly.

A new cell was set up for R&D purposes with preforming modifications and resin modification possible in a more appropriate environment. Also, several options for molding were built in that were not possible in the existing production environment but that could easily be implemented once proven. Running this cell, several successful test panel runs were made late in the year using hybrid preforms while meeting requirements of the overall process. Figure 4 illustrates the flexibility of the molding cell and the capability to rotate the position of the mold to change the flow behavior throughout the tool. Samples were provided to be tested early in the next phase. Development of parameters has been much more controllable; and several advanced options for preforming, molding, and materials are being investigated.

A unique proprietary development in a low-cost tooling approach is being used in the test tool. The new technology will be transferred in the scaled-up prototype runs for the client's proprietary component.

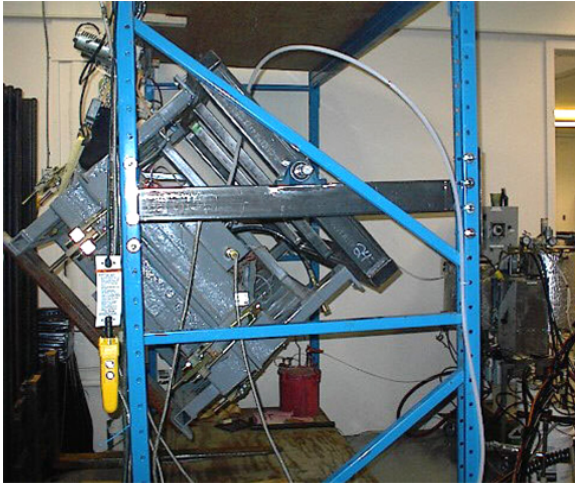


Figure 4. Mold cell for test tool setup for large part molding.

Summary

Highlights of progress during FY 2004:

- Molded structural carbon-fiber-based Class A components with a cost-effective hybrid fiber system.
- Achieved significant structural performance in fatigue and impact resistance not previously seen with these composites.
- Achieved molding of very thin section panels and demonstrated weight savings.
- Filed several inventions and potential patents on the process and technology.
- Proved the performance of the tooling approach.
- Demonstrated a system meeting requirements for no sanding prior to paint (all of the partners' current components go through a 100% sanding operation prior to paint.)
- Published results in peer-reviewed compilation and presentation at American Composites Manufacturers Association Annual Meeting.

Conclusions

Initial work has provided some very specific process and product molding parameter goals that

needed to be addressed to make a system with proven capability to move toward commercialization. A series of factors associated with optimizing details of the process technology are being addressed; the CRADA partner is developing an approach to mold full-scale parts that will ultimately go on over-the-road trials. These parts have been chosen to demonstrate the most challenging aspects of the process capability: namely, highly structural, Class A surfaces in direct line-of-sight, with some complex process details required for success. Tooling quotes and negotiations are ongoing, and several aspects of the process are anticipated to go forward for patent protection. Alternative U.S. government applications have been identified that can benefit significantly from this technology. These will be investigated over the coming fiscal year.

Presentations

K. L. Simmons, G. G. Jones, S. P. Walsh, and G. M. Wood, "High-Performance Laminates Using Blended Urethane Resin Chemistry," Composites 2004 Convention and Trade Show, American Composites Manufacturers Association, Tampa, Florida; October 6–8, 2004.

"Application of Carbon Fiber for Large Structural Components," Pacific Northwest National Laboratory On-site Review, April 21, 2004.

Invention Disclosures

"Development of Improved Carbon Fiber Based Hybrid Fiber Structures," IPID 14431-E, submitted May 21, 2004.

"Tooling Method for Application in Rapid Fabrication of Thin-walled Composite Structures," IPID #14430-E, submitted May 21, 2004.

"A Method for Reducing Inter-laminar Stresses in Chopped Fiber Hybrid Composites," IPID #14421-E, submitted May 21, 2004.